Remote sensing of Groundwater-Dependent Ecosystems in the Kruger National Park, South Africa

Final Report to Water Research Commission

Timothy Dube[1], Tatenda Dalu[2], Mbulisi Sibanda[3]

[1] Institute for Water Studies, University of the Western Cape, Cape Town, South Africa.

[2] Aquatic Systems Research Group, School of Biology and Environmental Sciences, University of Mpumalanga, Nelspruit 1200, South Africa

[3] Department of Geography, Environmental Studies, and Tourism, University of the Western Cape

WRC Report No. 3214/1/25
ISBN 978-0-6392-0724-7

Obtainable from

Water Research Commission
Bloukrans Building, Lynnwood Bridge Office Park
4 Daventry Street
Lynnwood Manor
PRETORIA

hendrickm@wrc.org.za or download from www.wrc.org.za

This is the final report of WRC project no. C2022/2023-00902

EXECUTIVE SUMMARY

Groundwater is a vital source of freshwater, essential for socio-economic development and the sustainability of groundwater-dependent ecosystems (GDEs). These ecosystems play a crucial role in preserving biodiversity and enhancing resilience against the impacts of global environmental change. Recently, GDEs have become increasingly at risk due to anthropogenic and climatic stressors, including hydrological alterations, rising temperatures, and land-use transformations.

The effective management and conservation of these ecologically significant systems are hindered by a lack of comprehensive data on their condition, structure, function, and resilience. Addressing these knowledge gaps is critical for developing scientifically informed conservation strategies that ensure the long-term sustainability of GDEs and their associated biodiversity. The spatial distribution, vegetation composition, soil moisture dynamics, and water quality of GDEs remain poorly understood, particularly in Africa. In the southern regions of Kruger National Park (KNP), groundwater serves as a critical resource for sustaining ecosystems due to significantly lower rainfall when compared to other areas of the park. Keystone phreatophyte species, such as *Boscia albitrunca* (Shepherd's tree), play a vital ecological role by accessing deep groundwater reserves and redistributing moisture to the upper soil layers, thereby supporting the survival of other key plant species in these water-limited environments. Similarly, the groundwater-dependent thorny thickets and grasslands support several species, such as the endangered *Ceratotherium simum* (White Rhino). Characterising these ecosystems in these pristine areas is essential for enabling resource managers to implement timely interventions and mitigate environmental stressors, such as salinisation, before they propagate to other parts. However, these ecosystems remain poorly understood due to a lack of comprehensive data on their spatial distribution, vegetation species diversity, soil moisture dynamics, and water quality. As a result, GDEs in this region are understudied, limiting the ability to develop effective conservation and management strategies.

Traditionally, field-based techniques have been widely employed to map and assess GDEs across different environments. While these methods provide valuable on-the-ground insights, they are often constrained by limited spatial coverage, high costs, and time-intensive data collection processes. In contrast, advancements in Earth observation technologies offer significant advantages over conventional field-based approaches. Remote sensing enables the monitoring of large spatial areas, facilitates regular temporal assessments of ecosystem changes, reduces the costs associated with extensive fieldwork, and provides access to remote or otherwise inaccessible locations. Furthermore, Earth observation techniques allow for the integration of diverse environmental datasets, offering a more comprehensive understanding of GDEs.

When combined with hydrogeological approaches, these advanced geospatial techniques enhance the ability of resource managers and policymakers to make data-driven decisions regarding biodiversity conservation in GDEs. Considering this, the present study aims to develop a geospatial framework for monitoring GDEs in the southern regions of the KNP. This framework will leverage satellite-based spatiotemporal models to support effective ecosystem management and decision-making. To achieve this overarching goal, the study has outlined the following specific objectives:

1. To conduct a comprehensive and state-of-the-art literature review and potential use of remote sensing-based models for GDE monitoring in the light of climate change.
2. To develop remote sensing-based methods for delineating GDEs specifically in vulnerable areas such as KNP, South Africa.

3. To assess the use of spatial explicit techniques in measuring species diversity in GDE.
4. To assess the soil moisture potential of GDEs in the southern tip of KNP, South Africa.
5. To assess water quality and chlorophyll variability in the selected GDEs in the southern tip of KNP, South Africa.

To effectively achieve the contractual objectives, the project was structured into four distinct work packages, each addressing specific research components. The first work package focused on addressing Contractual Objective No. 1 through two comprehensive narrative literature reviews. These reviews provided a theoretical foundation for the study by synthesising existing knowledge on GDEs, remote sensing applications, and associated environmental parameters. The second work package aimed at delineating GDEs, using advanced remote sensing techniques, directly addressing Contractual Objectives No. 2 and 3. This phase involved the development and application of geospatial methodologies to accurately map the extent and distribution of GDEs within the study area. The third work package was dedicated to the in-situ measurement of plant species diversity, soil moisture, and water parameters within GDEs, corresponding to Contractual Objectives No. 3, 4, and 5. This component integrated field-based data collection with remote sensing-derived insights to enhance the characterisation of these ecosystems. The final work package focused on research dissemination, ensuring that key findings are translated into actionable knowledge for stakeholders. This package emphasised the communication of research outputs through scientific publications, policy briefs, and stakeholder engagement activities. Additionally, it included a report on capacity development, highlighting efforts to enhance expertise in GDE monitoring and conservation. To systematically address these work packages and fulfil the overarching contractual goals, the following specific objectives were established:

1. To conduct a detailed synthesis of the progress and advancements in remote sensing integrated with geospatial techniques for assessing groundwater-dependent vegetation (GDV) at fine spatial and temporal scales.
2. To provide a comprehensive review of the applications of groundwater flow models coupled with advanced geospatial tools in understanding the ecohydrology of GDEs and their connectivity to underlying aquifers.
3. To evaluate the effectiveness of machine learning (ML) classifiers in predicting groundwater-dependent vegetation potential zones (GDVpz) within the KNP, South Africa;
4. To accurately characterise groundwater flow systems in the southern region of KNP and enhance hydrogeological modelling of groundwater-dependent ecosystems;
5. To assess (i) spatial and temporal variations in water and sediment chemistry in pan wetlands across different geological formations and hydroperiods (low and high), and (ii) the diversity and abundance of macroinvertebrate communities across geological regions, geological types, and hydroperiods in relation to water and sediment chemistry;
6. To develop and evaluate predictive models for Alpha and Beta diversity in potential groundwater-dependent vegetation zones using spectral coefficient of variation (CV), topographic features, and soil moisture data.
7. To integrate soil moisture data from the Soil Moisture Active Passive (SMAP) satellite with machine learning models based on Sentinel-1 Synthetic Aperture Radar (SAR) data

to analyse temporal and spatial trends in soil moisture and vegetation productivity in GDEs, thereby supporting informed environmental management strategies in KNP.

The project aimed to leverage action research methodologies to facilitate active participation and maximise the benefits for the community of practice in the targeted locations. The project team worked in close collaboration with scientific teams from the KNP, which played a crucial role in fostering strong social capital both within and surrounding the park. As part of this partnership, certain datasets were provided by the authorities of the KNP, enhancing the project's data-driven approach. For example, the project's spatial data for the study area was sourced from KNP. Various studies then derived their sampling points using the shapefiles of the southern region of KNP. These GIS datasets were integrated with satellite imagery, including data from the Sentinel-2 Multispectral Instrument (MSI), Shuttle Radar Topography Mission (SRTM), Soil Moisture Active Passive (SMAP), and Soil Moisture and Ocean Salinity (SMOS) missions. These datasets were accessed and utilised through the widely available big data cloud platform, Google Earth Engine, in combination with various machine learning algorithms for analysis.

In addition, to ensure a rigorous and comprehensive approach to literature review, the project employed the Preferred Reporting Items for Systematic Reviews and Meta-Analyses (PRISMA) guidelines. The PRISMA checklist was used to generate key search terms for retrieving relevant literature from major databases, including Web of Science, Scopus, and ScienceDirect. The first comprehensive state-of-the-art literature review on the use of Earth observation data for the assessment and monitoring of GDEs examined a total of 200 peer-reviewed studies published between 2000 and 2021. The findings revealed significant advancements in remote sensing technologies that have enhanced the monitoring capabilities of GDEs. The reviewed literature emphasised the potential for future studies to explore the utility of cloud computing platforms, particularly Google Earth Engine, which facilitates rapid data processing and integration across extensive spatial and temporal scales. These technologies were identified as critical tools for addressing the challenges posed by climate change, offering researchers valuable insights into ecosystem dynamics. This section of the project underscored how remote sensing methods can improve the detection of changes in GDEs, enabling more timely and precise responses for conservation planning.

The second review assessed groundwater modelling applications coupled with space-based observations in groundwater-dependent assessments. The reviewed literature highlighted concerns regarding the mismatch in spatial and temporal scales between remotely sensed data and groundwater models, which makes it difficult to integrate them in the delineation of GDEs. Additionally, it noted that there is a lack of ground truth data, particularly in remote areas, which further complicates GDE validation efforts. This review then identified the need to integrate spatial data with groundwater numerical modelling to improve the accuracy of the model results by providing more detailed information about the area's geology and hydrogeology. In addition, the review demonstrated the ecological significance of understanding GDE-aquifer connectivity and its critical role in conservation efforts within these ecosystems.

The study examined vegetation diversity using the Shannon-Wiener and Simpson Diversity Indices, finding a negative correlation between environmental variability (measured by the coefficient of variation) and species richness. This suggests that increased environmental fluctuations may reduce vegetation diversity. The findings highlight the need for further exploration of plant phenology's role in diversity and emphasise the importance of understanding

these dynamics for developing effective conservation strategies that account for seasonal and phenological changes.

Concerning the water quality component, a comprehensive water quality assessment and macroinvertebrate sampling, focusing on the influence of hydroperiod (the duration and frequency of water presence) and geological characteristics, was conducted. The first study noted that hydroperiod significantly influences chlorophyll-*a* concentrations more than geological type, with higher levels observed during the low hydroperiod. Benthic chlorophyll-a was positively linked to salinity and TDS but was negatively affected by high pH and large pan surface areas due to nutrient binding and sediment resuspension. Results of the second study on water quality showed that lower hydroperiods correlated with reduced biodiversity, emphasising the critical role of hydrological stability in sustaining diverse invertebrate communities. Furthermore, variations in sediment chemistry, influenced by underlying geological formations, were found to impact nutrient availability, directly affecting invertebrate diversity. These findings underscore the need for nuanced, site-specific conservation approaches that consider both hydroperiod dynamics and geological factors in preserving GDE biodiversity.

In assessing the soil moisture potential within Kruger's GDEs, the study utilised SMAP and Sentinel-1 Synthetic Aperture Radar (SAR) data. Satellite-derived soil moisture measurements correlated strongly with field data, with R^2 values between 0.51 and 0.59. The findings demonstrated the potential of these remotely sensed products in capturing eco-hydrological dynamics in GDE-dominated environments. This understanding of soil moisture variability is critical for conservation planning, as soil moisture plays a direct role in vegetation productivity and GDEs' Health.

New Knowledge and Innovation

The use of Earth observation technologies to create a Geospatial Framework for Monitoring GDEs is a relatively recent development in the context of their application in South Africa. To the best of our knowledge, no study has mapped GDEs in South Africa using geospatial techniques. The information derived from the Geospatial Framework for Monitoring grassland ecosystems is thus critical in determining the spatial extent, biomass and carbon sequestration potential of GDEs in the KNP. Subsequently, this project contributes to the emerging use of Earth observation facilities for detecting and mapping the spatial extent, biomass, species diversity, and water quality attributes of GDEs. This project is a step toward developing smart technologies that provide essential and timely information for resource managers to make in-field decisions and for scientists to offer recommendations for the sustainable management of conservation areas in South Africa. This is relevant in conserving fauna dependent on the existence of GDEs and in meeting the Paris Climate Agreement targets.

Capacity Building

The project was successful in its capacity-building mandate by recruiting and mentoring two African female Master of Science Students and an African female doctoral student. Additionally, this project mentored a postdoctoral fellow and an early-career researcher transitioning to a mid-career researcher. This effort significantly strengthened both the institutional and individual capabilities. The project is still going to recruit one more Master's student by leveraging other

funding streams to address any other issues lurking in the objectives. In this project, the postdoctoral fellow actively participated in supervising students alongside early, mid-career and established researchers. The early and mid-career researchers benefited from the active mentorship provided by experienced researchers in the project, particularly in developing conceptualisation and project management skills.

Conclusion

This project establishes a comprehensive framework for monitoring Groundwater-Dependent Ecosystems by integrating remote sensing technologies with field-based data to assess ecological health in KNP. By examining the interplay between geological, hydrological, and biological factors, the study provides a robust model for sustainable ecosystem management in climate-sensitive regions. The findings underscore the critical role of spatial data characteristics in accurately delineating GDEs, demonstrating how variations in resolution and sensor capabilities influence detection accuracy. The methodologies and insights developed in this research offer a scalable approach that can be adapted to other vulnerable ecosystems worldwide, supporting conservation efforts and informing data-driven decision-making. Ultimately, this study contributes to the broader understanding of GDE dynamics and enhances strategies for preserving these vital ecosystems in the face of global environmental change.

Recommendations

Several research gaps persist in the utilisation of geospatial technologies and data for mapping and monitoring GDEs, particularly in developing countries where fine spatial resolution data availability is limited.

- There is a need for extending the research efforts combining deep machine learning techniques, multisource spatial datasets and groundwater hydrogeological modelling techniques to enhance the delineation of the spatial extent of GDEs.
- Also, fine spatial resolution remotely sensed data needs to be assessed for mapping soil moisture potential in GDEs to better understand flora and fauna abundance, diversity and distribution within these GDEs.
- Future studies should consider engaging Stable and Radioactive Isotope Tracers in concert with GIS techniques in identifying geological interactions unique to groundwater across the hydrological season to verify GDEs.
- Water quality parameters, including the variability in chlorophyll content and its relationship with species diversity in GDEs, require more comprehensive assessments.

ACKNOWLEDGEMENTS

The project team wishes to thank the following people for their contributions to the project.

Reference Group member	Affiliation
Dr Shafick Adams	Water Research Commission (Chairperson)
Prof Thokozani Kanyerere	University of the Western Cape
Dr Farai Dondofema	University of Venda
Mr Majola Kwazikwakhe	Department of Water and Sanitation
Dr Zahn Munch	Stellenbosch University

Scientific Research Team, Capacity Building, and Support Members

Prof Timothy Dube	University of the Western Cape, Project leader
Dr Tatenda Dalu	University of Mpumalanga, Principal Investigator
Dr Mbulisi Sibanda	University of the Western Cape, Researcher
Prof Dominic Mazvimavi	University of the Western Cape, Mentor
Dr Siyamthanda Gxokwe	University of the Western Cape, Postdoctoral Fellow
Ms Chantel Chiloane	University of the Western Cape, PhD student
Ms Trisha Bhaga	University of the Western Cape, PhD student
Ms Qawekazi Msesane	University of the Western Cape, MSc student
Ms Lebogang Mmasechaba Moropane	University of the Western Cape, MSc student
Ms Sibuyisele S. Pakati	University of the Western Cape, PhD student
Ms Naledi Manyaka	University of the Western Cape, MSc student
Ms Anothando Yono	University of the Western Cape, MSc student
Ms Elsie N. Leshaba	University of Mpumalanga, MSc student

TABLE OF CONTENTS

LIST OF FIGURES

LIST OF TABLES

LIST OF ACRONYMS

AHP	-	Hierarchical Processes
AVHRR	-	Advanced Very High-Resolution Radiometer
CART	-	Classification Regression Tree
CGLS	-	Copernicus Global Land Cover Layers
CHIRPS	-	Climate Hazards Group InfraRed Precipitation with Station data
D	-	Simpson Diversity Index
EVI	-	Enhanced Vegetation Index
FEM	-	Finite Element Method
GDEs	-	Groundwater-Dependent Ecosystems
GDV	-	Groundwater Dependent Vegetation
GDVpz	-	Groundwater-Dependent Vegetation Potential Zones
GEE	-	Google Earth Engine
GIS	-	Geographic Information System
GRACE	-	Gravity Recovery and Climate Experiment
GWD	-	Groundwater Depth
H	-	Shannon-Wiener Diversity Index
KNP	-	Kruger National Park
LAI	-	Leaf Area Index
ML	-	Machine Learning
MODIS	-	Moderate Resolution Spectroradiometer
NDVI	-	Normalised Difference Vegetation Index
OBIA	-	Object-Based Image Analysis
OLI	-	Operational Land Imager
RASA	-	Regional Aquifer System Analysis
RF	-	Random Forest
RFE	-	Feature Eliminator
RS	-	Remote Sensing
SGTB	-	Smile Gradient Tree Boost
SMAP	-	Soil Moisture Active Passive
SRTM	-	Shuttle Radar Topography Mission
SVM	-	Support Vector Machines
WoSCC	-	Web of Science

DATA REPOSITORY

For details related to the project's data, please contact:

Institute for Water Studies (IWS)
Room 3.50, Core 2 Level 3, NLS,
Faculty of Science
University of the Western Cape
Robert Sobukwe Road
Private Bag X17, Bellville 7535
Cape Town
South Africa

Email: tidube@uwc.ac.za

CHAPTER ONE

BACKGROUND

1.1 Introduction and Project Objectives

Groundwater is a vital source of freshwater, supporting both socio-economic development and the needs of groundwater-dependent ecosystems (GDEs). Groundwater ecosystems include rivers, lakes, wetlands, and springs. Groundwater-dependent vegetation (GDV), such as phreatophytes, plays a key role within GDEs. These plants, like the Shepherd's tree (*Boscia albitrunca*) in Africa, are considered keystone species, capable of redistributing groundwater to shallower parts of the soil profile, thereby benefiting other co-existing species (Wang et al. 2013). For example, the thorny thickets (*Albizia versicolor* and *Terminalia sericea*) and grasslands (*Hyparrhenia* spp.) although not nutritious, they support various species, including the Sable Antelope (*Hippotragus niger*) and the White Rhino (*Ceratotherium simum*). Meanwhile, the numerous shallow waters from wetlands and springs support a wide variety of vertebrates. All these GDEs are impacted when the groundwater regime changes and exceeds the natural bounds of natural variation. Unsustainable abstractions and poor groundwater quality also present a threat to the GDEs existence. However, the major challenge with enforcing regulations regarding their preservation is that important information about their carbon sequestration potential, species diversity, and pollution abatement remains largely unknown, particularly in Africa (Turner et al., 2001). Subsequently, an understanding of their distribution, vegetation soil and water quality attributes remains complex. Furthermore, insights on the effects of groundwater variations on GDEs remains largely understudied. The southern parts of Kruger National Park (hereafter Kruger) are no exception to this fate, and the GDEs therein are understudied.

Unlike other parts of Kruger with surplus surface water from preceding precipitation, the southern parts of the park are characterized by deep sandy soils with low precipitation and limited surface water resources. If groundwater is not available in these parts of Kruger, ecosystem structure and function will likely shift, vegetation dieback will increase, and invasive species will become more common. Around the Pretoriuskop area in southern Kruger, groundwater is essential for vegetation and other fauna species. Consequently, characterizing GDEs in the southern parts of Kruger will allow resource managers to timely intervene and control environmental stressors (e.g.,

salinization) from cascading to other parts of Kruger. While field-based techniques have been used in mapping GDEs in different environments, these techniques have limited spatial coverage.

Meanwhile, GIS and remote sensing techniques have been demonstrated to be useful in mapping GDEs even in smaller areas owing to the high spatial resolution offered by most remote sensing products (Eamus et al. 2015a). The advent of remote sensing data from active and passive sensors has availed opportunities for up-to-date synoptic inventories of GDEs, even for inaccessible GDEs. Remote sensing has also allowed for the inquiry into whether GDEs are expanding or shrinking for a particular time series. However, the utility of remote sensing in mapping GDEs depends heavily on both the spatial and spectral resolution of the imagery used, since GDEs can be narrow strips and, more importantly, they can even be less than a hectare in size (e.g., the small wetlands in East Africa). Initially, researchers used low-resolution imagery (>30 m) such as Advanced Very High-Resolution Radiometer (AVHRR) and aerial photographs for monitoring GDEs until the availability of medium spatial resolution data (4 m - 30 m). Medium resolution multispectral sensors then became more common for GDEs mapping, along with a set of band combinations.

Importantly, the effectiveness of GDEs mapping also depends on the delineation techniques employed, such as image classification algorithms (Baker et al., 2006). Commonly used classification algorithms for GDEs include the Maximum Likelihood, Minimum Distance, and Support Vector Machines. These algorithms primarily classify images based on top-of-atmosphere reflectance values. However, more advanced techniques, such as Object-Based Image Analysis (OBIA), incorporate additional factors, including reflectance, shape, structure, and connectivity, in the segmentation process before classification (Duro et al., 2012). Studies that successfully employed OBIA often utilised high-resolution optical sensors such as IKONOS and QuickBird (Wang et al., 2020) but tended to overlook medium-resolution imagery due to concerns about spatial resolution. The recent availability of Sentinel-2 imagery, launched in 2016, offers a new opportunity for resource managers to map GDEs with improved accuracy. Sentinel-2 provides a spatial resolution of 10–60 m and high spectral resolution in the near-infrared region, surpassing previous medium-resolution sensors like Landsat 8 Operational Land Imager (OLI).

By integrating medium-resolution multispectral data with machine learning algorithms, the mapping of GDEs can be significantly enhanced (Dronova, 2015). Additionally, advancements in geospatial cloud computing platforms like Google Earth Engine (GEE) have addressed challenges

related to computational intensity and high costs associated with specialized software. The GEE provides users with powerful computational resources and sophisticated image analysis techniques, making it a valuable tool for understanding the dynamics of GDEs. Remote sensing in concert with hydrogeological approaches can provide water resource managers and policy makers with robust information and knowledge necessary for making informed decisions on biodiversity conservation in GDEs (Munch et al., 2013). This project proposed to develop a geospatial framework and models for monitoring GDEs in the southern parts of KNP. The project utilised the cloud-based Google Earth Engine (GEE) platform to delineate and monitor the spatial distribution of GDEs and their associated ecohydrological status (i.e., water quality, soil moisture variability, vegetation species diversity). In addition, invertebrates associated with different water level regimes were also assessed to infer the interactions between groundwater levels and biodiversity within the study area. The framework provides actionable information services for GDEs assessment and monitoring across key land management areas. Specifically, the assessment and monitoring service will deliver satellite-based Earth observation spatiotemporal models that will assist users in operational GDE management, as well as policy and decision-making in the target areas.

1.2 Project aims and objectives

1. To conduct a comprehensive and state-of-the-art literature review and potential use of remote sensing-based models for GDE monitoring in the light of climate change.
2. To develop remote sensing-based methods for delineating GDEs specifically in vulnerable areas such as KNP, South Africa.
3. To assess the use of spatial explicit techniques in measuring species diversity in GDE.
4. To assess the soil moisture potential of GDEs in the southern tip of KNP, South Africa.
5. To assess water quality and chlorophyll variability in the selected GDEs in the southern tip of KNP, South Africa.

1.2.1 Specific objectives

The outlined contractual objectives of this project were addressed by drawing the following specific objectives:

1. To develop a detailed synthesis on the progress and development of remote sensing integrated with geographic and information systems in assessing GDV over fine spatial and temporal scales.
2. To provide a comprehensive overview of the progress and applications of groundwater flow models coupled with advanced geospatial tools to understand the ecohydrology GDEs and their extent of connectivity to underlying aquifers.
3. To assess the efficacy of machine learning (ML) classifiers in predicting groundwater-dependent vegetation potential zones (GDVpz) within the KNP, South Africa.
4. To accurately characterise groundwater flow systems in southern KNP and improve hydrogeological modelling of groundwater-dependent ecosystems.
5. To assess (i) variations in water and sediment chemistry in pan wetlands across different geological types and hydroperiods (low and high) and (ii) spatiotemporal macroinvertebrate diversity and abundance across geological regions, geological types, and hydroperiods in relation to water and sediment chemistry.
6. To assess water quality and chlorophyll variability in the selected GDEs in the southern tip of Kruger National Park.
7. To evaluate models predicting Alpha and Beta diversity in potential groundwater-dependent vegetation zones using spectral coefficient of variation (CV), topographic features, and soil moisture.
8. To integrate soil moisture data from SMAP with machine learning models based on Sentinel-1 SAR data to evaluate temporal and spatial trends in soil moisture and vegetation productivity in GDEs, thereby supporting informed environmental management strategies in the KNP.

1.3 Scope and the overview of the report

This report is presented in a paper format, with each chapter standing alone as an entity that partially addresses the contractual objectives of the project. The report leverages guidance from the WRC project managers, technical reference group members, and the rigorous international peer-reviewed systems, with some chapters published in scientific journals. In this regard, considering that all the work was conducted in the same study area, the study area description is presented only once in the preceding subsection to avoid repetition. In addition, since stand-alone

chapters addressed the same overarching aim and were from the same study area, there are inevitable overlaps in some of the sections, including the methods sections. This was deemed insignificant, since all these chapters present a seamless flow of methods and principles that underpin the current scientific setting to address the same overarching aim. Furthermore, some of the chapters were adapted from articles already published in internationally peer-reviewed journals. The report is structured to address all the project's contractual objectives in a logical framework.

Specifically, the chapters in this report are as follows:

Chapter 1: Presents a comprehensive introduction, background and motivation of the entire study. It outlines the project's contractual objectives as captured in the contract document. It also presents the specific objectives that were drawn up to address the contractual objectives.

Chapter 2: A comprehensive and state-of-the-art literature review on the progress and applications of groundwater flow models coupled with advanced geospatial tools to understand the ecohydrology GDEs and their extent of connectivity to underlying aquifers. This chapter addresses contractual objective number 1.

Chapter 3: Also, a comprehensive and state-of-the-art literature review on the progress and applications of groundwater flow models coupled with advanced geospatial tools to understand the ecohydrology GDEs and their extent of connectivity to underlying aquifers. This chapter contributes to addressing contractual objective number 1.

Chapter 4: Engages various ML classifiers in predicting GDVpz within KNP, South Africa. This chapter addresses a critical gap by evaluating the applicability of ML classifiers in comparison to AHP in pristine ecohydrological settings. Specifically, this chapter addressed project objective number 2, which sought to develop remote sensing-based methods for delineating GDEs specifically in vulnerable areas such as KNP, South Africa.

Chapter 5: Characterised groundwater flow systems in southern KNP to enhance hydrogeological modelling of groundwater-dependent ecosystems. It assessed preferential groundwater flow paths and defined boundary conditions of the GDEs system by analysing borehole core loggings and examining geological cross sections across the study area. Additionally, this chapter contributed to addressing contractual objective number 2.

Chapter 6: Assessed (i) variations in water and sediment chemistry in pan wetlands across different geological types and hydroperiods (low and high) and (ii) spatiotemporal macroinvertebrate diversity and abundance across geological regions, geological types, and hydroperiods in relation to water and sediment chemistry. This chapter hypothesized that hydroperiod, defined as the duration and frequency of inundation, has a substantial influence on the diversity of macroinvertebrates. Overall, this chapter addressed project objectives number 3 and 5, focusing on species diversity and partially on water quality.

Chapter 7: This chapter assessed chlorophyll-*a* dynamics as a proxy for understanding water quality in the KNP, South Africa.

Chapter 8: Predicted vegetation alpha and beta species diversity in potential groundwater-dependent vegetation zones using spectral coefficient of variation (CV), topographic features, and soil moisture. This chapter contributed to addressing contractual objective number 3, focusing on developing techniques for accurately assessing species diversity in GDEs.

Chapter 9: Presents a conceptual procedure for integrating soil moisture data from SMAP with machine learning models based on Sentinel-1 SAR data to evaluate temporal and spatial trends in soil moisture and vegetation productivity in GDEs, thereby supporting informed environmental management strategies in KNP.

Chapter 10: Presents a comprehensive synthesis and discussion of the entire project's outcomes, connecting all individual studies in addressing the project objectives. This chapter also provides conclusions and suggestions for future research.

1.4 Description of the study area

The study area for this project is the Kruger National Park (KNP). KNP is one of the largest conservation areas in Africa, covering almost 2 million hectares. It is located along the north-eastern boundary of South Africa in the Mpumalanga and Limpopo provinces (Figure 1.1). The KNP lies within the savanna biome, which is characterized by a discontinuous tree canopy and an herbaceous layer dominated by C4 grasses. The KNP interior is drained by five perennial rivers, which flow from the west to the east across the KNP before flowing into Mozambique and the Indian Ocean. Rivers established before the Pliocene erosion phase tend to flow from west to east, and smaller rivers tend to flow from the north to south, following the strike of geology.

The study area is generally semi-arid and experiences warm summers with seasonal rainfall. Winters are mild and dry with little to no rainfall. In summer, temperatures may reach 44°C and seldom fall below freezing point in winter. In the KNP, the mean annual rainfall decreases from south to north and from west to east. The KNP receives an annual rainfall of 650 mm (Smit et al., 2013). In KNP, extreme periods of both inundation and aridity are a common phenomenon. On average, in the dry season (June–October), ephemeral water sources dry up, and only the permanent rivers (Sabie and Crocodile) and artificial waterholes are available for wildlife sustenance. The topography of the KNP is primarily influenced by the different rock resistance to weathering. The park is a gently undulating landscape between 200 m and 400 m above sea level with a gentle gradient to the east, except for the Lebombo Mountains, which have a higher elevation. Within the borders of KNP, lies a diverse assemblage of igneous, sedimentary, and metamorphic rocks as well as unconsolidated sediments deposited over a timespan of more than 300 million years (Ma). The primary litho-stratigraphic units within the KNP are the Basement complex, characterised by ancient granitoid rocks dating back to the Swazian era (>3090 Ma), sedimentary and volcanic rocks of the Soutpansberg Group and the volcanic rocks of the Karoo Supergroup. The KNP is divided roughly in half (north to south) as per the dominant basaltic and granite geological formations.

The south-eastern region of the KNP is underlain by rocks that belong to the Nelspruit Suite (Figure 1.1). The batholith rocks are approximately 3303± Ma and are predominantly composed of coarse-grained porphyritic granodiorites, with high contents of quartz, microcline and biotite. In the KNP, geology is the key controlling factor of how the hydrogeological conditions within the area vary. There are two types of aquifers present in the southern part of the KNP: the shallow weathered aquifer and the deep hard rock granite/gneiss aquifer. Borehole yields will heavily rely on the permeability and porosity of the subsurface geology as different geological units will also have different recharge rates, storage capacities and permeabilities. Generally, groundwater is less likely to flow through the hard rock aquifer than through the weathered rock aquifer. In the KNP, groundwater flow direction is from the 1st order hillslope towards the 3rd order hillslope running parallel to streams.

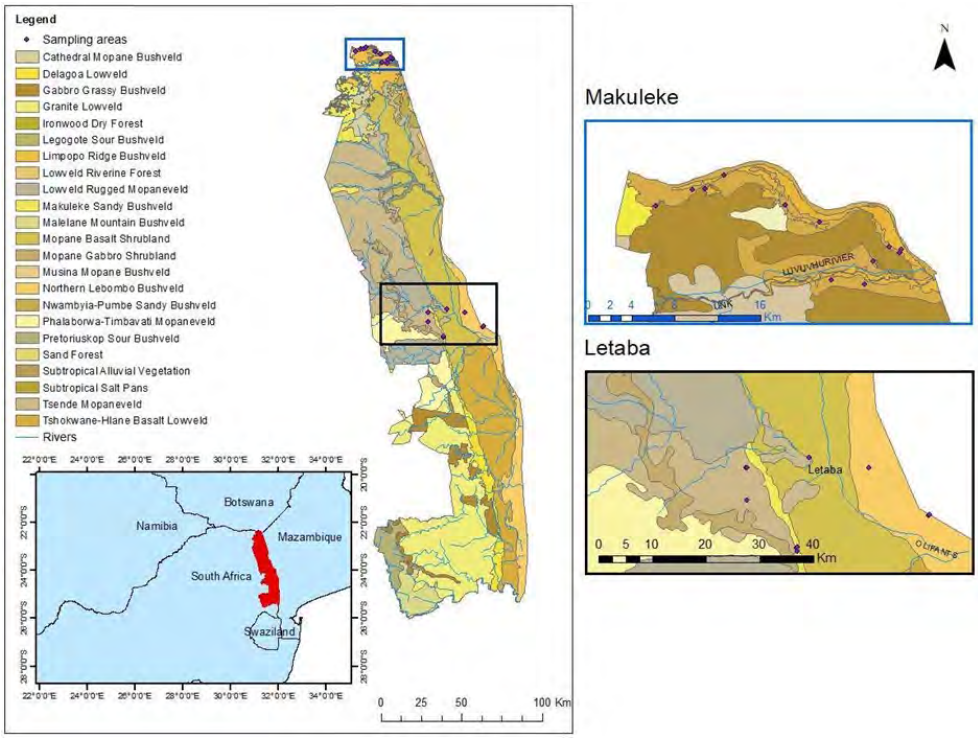

Figure 1.1 Map of the Kruger National Park, South Africa

CHAPTER TWO

THE ROLE OF EARTH OBSERVATION DATA IN GROUNDWATER-DEPENDENT ECOSYSTEMS ASSESSMENT AND MONITORING IN SEMI-ARID ENVIRONMENTS

2.1. Introduction

Vegetation is a major component of terrestrial ecosystems and plays a vital role in energy flow, global carbon circulation, and the hydrological cycle (Zhao et al., 2012). It is estimated that 29% of global carbon emissions are decreased by terrestrial vegetation, thus reducing the accumulation of atmospheric carbon dioxide (Cernusak et al., 2019). Further, desertification processes are buffered by vegetation cover, which maintains healthy natural environmental conditions (Lv et al., 2013). About 25-40 tonnes of the topsoil are eroded annually, due to vegetation clearing and cultivation as well as poor land management practices (FAO and ITPS, 2015; Lv et al., 2013). During this process, 23-42 tonnes of phosphorous and nitrogen are washed away, decreasing the soil's ability to regulate nutrients, carbon, and water (FAO and ITPS, 2015). In addition, the vegetation communities provide other valuable ecosystem services, such as flood control, water purification, pollinator habitats and recreational opportunities (DeFries and Bounoua, 2004; Gerten et al., 2004; Northcote and Atagi, 1997). A study by Blevins and Aldous, (2011) revealed that 17% of terrestrial vegetation in the United States was groundwater dependent and provided habitat for 39% invertebrates. In arid regions, vegetation is a major contributor of soil organic material, which fosters soil aggregation, water attenuation and nutrient accumulation (Lv et al., 2013). Furthermore, vegetation contributes to the economy through ecotourism, as a genetic hub for bioprospecting and in the preservation of biodiversity (Williams., 2018). In 2011, the global economic value of ecosystem services was estimated at 124.8 trillion USD, and the benefits of ecosystem conservation far exceed the costs of conservation (Costanza et al., 2014). Therefore, vegetation must be protected and safeguarded from both natural and anthropogenic threats.

Climate variability affects water availability and temperature which, in turn, affect vegetation distribution, health and productivity (Barron et al., 2014; Kløve et al., 2014). Moreover, a third of the sub-Saharan African landscape consists of arid and semi-arid land, which experiences low rainfall with annual averages below 500mm/yr. Only 2% of the average rainfall replenishes groundwater resources (Wada et al., 2010; Xu and Beekman, 2003). Available surface water for

terrestrial vegetation in these regions is highly limited. Therefore, groundwater is an important resource for growth, species composition and structure as well as the distribution of terrestrial vegetation (Liu, 2011). In addition, some terrestrial vegetation in arid and semi-arid regions is maintained by direct and indirect access to groundwater and is collectively referred to as groundwater-dependent vegetation (GDV) and sometimes as phreatophytes (Richardson and Kruger, 1990). These are a type of GDE.

Global environmental change, infrastructural developments and most importantly, over-exploitation of surface and groundwater resources have largely compromised the ecological integrity of ecosystems (McDowell and Moll, 1992; Rouget et al., 2003). Global change has widespread impacts on the Earth's terrestrial ecosystems, such as habitat loss and fragmentation, biological invasions, pollution, frequent droughts, and climate change, which rapidly erode biodiversity and threaten ecosystem functioning (Lv et al., 2013). For instance, available water for terrestrial vegetation has been compromised due to escalating air temperature, prolonged droughts, as well as over-exploitation of groundwater resources for anthropogenic activities (Williams, 2018; Krogulec, 2018). Subsequently, this compromises the ability of GDV to provide essential ecosystem goods and services (Rouget et al., 2003; Shadwel and Febraury, 2017). Monitoring vegetation conditions and their response to environmental and global changes over time improves our understanding of change processes, and helps identify affected and vulnerable areas (Franklin et al., 2016). Information on the nature and types of vegetation-groundwater interactions will guide policymaking, setting restrictions, and developing strategic mechanisms for groundwater use within the region. In this regard, such information is also critical for supporting agendas on sustainable future development, for example, the United Nations' (UN) Sustainable Development Goal 15 on 'Life on Land' (United Nations, 2017). Vegetation condition and its response to global change are specified in the lists of Essential Climate Variables (Bojinski et al., 2014) and Essential Biodiversity Variables (Pereira et al., 2013).

So far, groundwater-vegetation interaction monitoring has been limited by the trade-off that exists between the costs, efficiency, and level of detail offered by the techniques employed (Hoyos et al., 2016). Water chemistry indicators can give direct evidence of groundwater and vegetation interactions, which helps determine groundwater dependence (Colvin et al., 2007; Orellana et al., 2012). Other indicators are inferential and include: Eddy correlation, Bowen ratio, climatic indices,

sap flow measurements, plant phenology, and leaf area index using ground-based equipment (specialized leaf area meter), to assess the influence of groundwater variability on vegetation (Colvin et al., 2003; Eamus et al., 2015a; Hoyos et al., 2016). While these methods provide highly detailed information, they are limited in that they are costly, resource-intensive, and are unsuitable for catchment-scale assessment of GDV, as they provide site-specific information.

Remote sensing has emerged as an efficient monitoring tool that can provide crucial vegetation information on the status and response to environmental change at the community or landscape scale (Griffiths et al., 2019; Wessels et al., 2008; Zhu, 2017). The success of remote sensing in assessing vegetation response to water availability is well documented in the literature (Colvin et al., 2003; Boulton and Hancock, 2006; Münch and Conrad, 2007; Rohde et al., 2017a; Parker et al., 2018). However, there is a dearth of knowledge on the applicability of satellite and spectral data for determining groundwater-vegetation interactions, especially at the species level. Current research primarily focuses on global groundwater availability and its impact on society, with limited research focusing on ecosystem impacts. The state of knowledge on vegetation and groundwater interactions (Le Maitre et al., 1999; Colvin et al., 2003; Eamus and Froend, 2006; Bertrand et al., 2012) and recent techniques for mapping and assessing GDV (Eamus et al., 2015a; Hoyos et al., 2016; Klausmeyer et al., 2018) is well documented. Therefore, this review chapter aims to develop a detailed synthesis on the progress and development of remote sensing integrated with geographic and information systems in assessing GDV over fine spatial and temporal scales. More specifically, the review objectives are to a) provide a detailed background on GDEs b) Give an overview of groundwater vegetation interactions, assess the effects of climate induced groundwater variability on groundwater dependent vegetation c) exemplify the application of remote sensing (RS) and geographic information systems (GIS) in identifying GDV d) discuss the application potential role of RS and GIS in future applications. The chapter will be a synthesis of the state of knowledge on the physical response patterns and thresholds to acquire a comprehensive understanding of the degree of dependency of GDV in arid environments. The assessment of recent techniques in identifying GDV should prompt research on their potential to acquire information useful for GDV management.

2.2. Literature search on groundwater dependent ecosystems

Relevant literature was acquired from several search engines such as Google Scholar, SCOPUS, and the Web of Science Core Collection (WoSCC). Numerous expressions or topic search keywords were used, and these included: “groundwater”, “groundwater dependent ecosystems”, “remote sensing”, “climate and groundwater”, “semi-arid and arid”, “phreatophytes” and “terrestrial vegetation” were used to source literature from international peer-reviewed journals. These words were selected to retrieve information that provides the background on the interaction of groundwater and the dependent vegetation and highlight the progress in the use of remote sensing approaches. The literature search range was from 2000-2021 with a total of 200 articles from international peer-reviewed journals, theses and reports. An additional source for literature was obtained through a rigorous assessment of references cited by the read papers. Due to the paucity of studies of remote sensing applications, the review was not limited to a specific criterion. Consequently, studies that used remote sensing data for the assessment and monitoring of GDV were considered. The literature search revealed that most publications largely focused on GDEs in general, 52% of those were on GDV, with only 0.06% GDEs incorporating remote sensing approaches. An increase in the number of publications on groundwater-dependent ecosystems and GDV was noted (Figure 2.1).

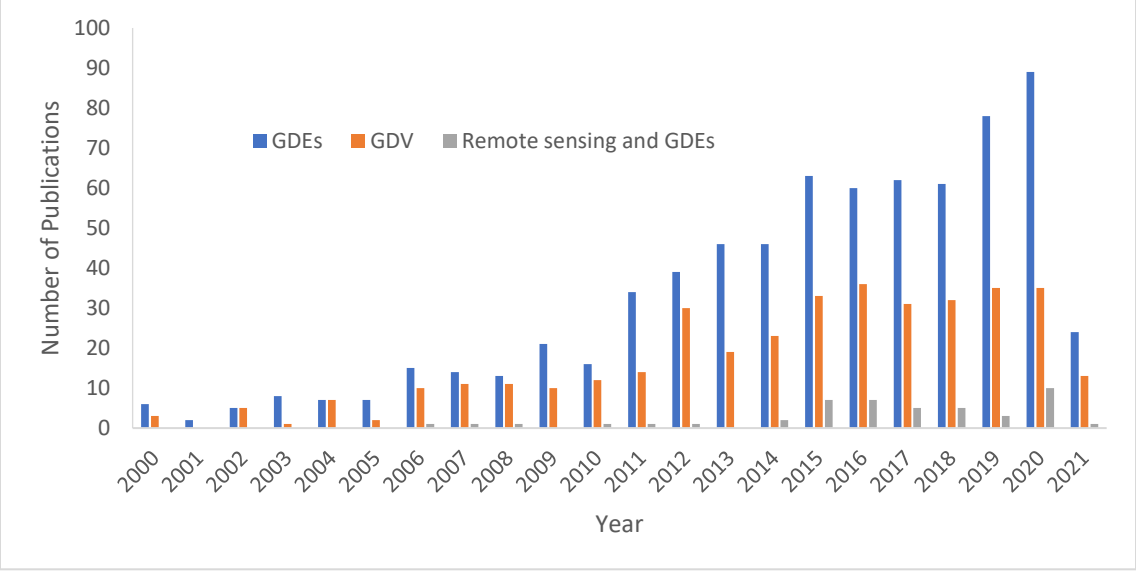

Figure 2.1 Number of publications on GDEs, GDV and remote sensing of GDEs for the period between 2000 and 2021

2.3. Background on groundwater-dependent ecosystems

GDEs are communities of plants, animals and microorganisms that continuously or to some extent rely on the available groundwater to maintain their structure and functioning (Colvin et al., 2003; Kløve et al., 2011). These ecosystems may be maintained by direct or indirect access to groundwater and rely on the flow regime and chemical characteristics of groundwater (Hatton and Evans, 1998). In this regard, when groundwater is limited, the functioning and structure of these ecosystems will be significantly altered. Various classification systems have been introduced based on the geographic setting in which they exist and the type of aquifer-ecosystem interface (Hatton and Evans 2003; Sinclair 2001; Colvin et al., 2007). A classification system with three basic classes based on the type of groundwater reliance was introduced by Eamus et al., (2006). The ecosystem classification method makes distinguishing and identifying groundwater dependence much easier and improves ecological risk assessments. This review focuses on the terrestrial vegetation class, which is referred to as Groundwater Dependent Vegetation and the third class according to Eamus et al., (2006) GDE's classification system (Table 2.1).

Table 2.1 Summary of GDE Classification according to Eamus et al., (2006)

Class	**Ecosystem type**	**Members**
I	Aquifer and cave systems	Stygofauna
II	Ecosystems dependent on the surface expression of Groundwater	wetlands, river base flow, floodplains, riparian vegetation, low lying springs, mound springs
III	Ecosystems dependent on the subsurface expression of Groundwater	Terrestrial vegetation (Phreatophytes) and associated dependent flora and fauna

GDV is vital for biodiversity conservation and provides ecological resources in terrestrial ecosystems. Surface water and groundwater resource quality are maintained by groundwater-dependent vegetation (Hoyos et al., 2016). For example, vegetation aids in the attenuation and infiltration of surface water recharge into the aquifer. Terrestrial vegetation also plays an important role in preventing soil erosion, provides vital habitats, and acts as corridors for migratory species (Kreamer et al., 2015). Terrestrial vegetation dependent on groundwater also acts as nutrient pumps and provides water to shallow-rooted plants through hydraulic lift. In recreational areas such as national parks and fisheries, GDV have economic and aesthetic value and provide

ecosystem services such as runoff interception and carbon capture (Rohde et al., 2017; de Klerk et al., 2012). Therefore, research on GDV has continued to develop and has renewed interest due to increased natural and anthropogenic threats (Chambers et al., 2013; Mawdsley et al., 2009).

2.3.1. Threats to groundwater-dependent vegetation

Groundwater and associated ecosystems are increasingly threatened by global environmental change. These are planetary-scale changes in the Earth's systems, which encompass changes in population, climate, resource use, land use and land cover (Noone et al., 2011). An ever-growing population, agricultural and economic development, coupled with a changing climate, have heightened the pressure on water resources. Climate change has decreased the reliability of surface water resources. As a result, greater consideration has been given to groundwater as a resilient freshwater resource that can augment surface water resources (MacKay, 2006; Kundzewicz and Döll, 2009). Subsequently, groundwater exploitation has drastically increased, with 33% of the global available freshwater supply obtained from groundwater (Vaux, 2011; Richey et al., 2015). Moreover, global groundwater levels and volume have been reported to be on a decline (Richey et al., 2015). Modification of groundwater levels and the deviation of flow patterns from the natural groundwater regime due to anthropogenic influence and climate change have detrimental impacts on the structure and functioning of groundwater-dependent vegetation communities (Kløve et al., 2014; Loomes et al., 2013). Therefore, there is a need to develop management plans and policies which promote the sustainable use of groundwater resources, thereby mitigating negative environmental impacts, such as storage depletion, saltwater intrusion, wetland and riparian habitat loss, land subsidence and reductions in stream flow. The influence of elevated groundwater demand is exacerbated by a rapidly changing climate (IPCC, 2014).

Long-term variability in precipitation, temperature and wind threatens the health and abundance of GDV, which is influenced by the spatial and temporal availability of groundwater (Chambers et al., 2013). Global average surface temperatures have been estimated to increase by 1.5°C from 1880-2014. This rise has been associated with negative impacts on groundwater quantity and quality. Under all climate scenarios, global surface temperatures are expected to rise. Further, drought and flood events are predicted to increase in the 21st century (IPCC, 2014). Reduced precipitation and elevated temperatures are detrimental to groundwater levels because of limited groundwater recharge and increased plant water demand (Noone et al., 2011; Kløve et al., 2014).

There is a large body of literature on anthropogenic impacts on GDV (Muñoz-Reinoso, 2001; Krause et al., 2007; Huang et al., 2020). However, there is little scientific research focusing on the impacts of climate variability on terrestrial vegetation (Barron et al., 2012; Kløve et al., 2011; Taylor and Tindimugaya, 2011). Groundwater and associated ecosystems are particularly vulnerable to climate impacts as the resource is unseen and there exists a time lag before the response is noticed (Morsy et al., 2017). In some instances, inappropriate management policies and strategies have also been linked to the degradation of GDV (Morsy et al., 2017). Therefore, a comprehensive synthesis of knowledge on the interactions and response mechanisms for groundwater and dependent vegetation will ensure the formation of adaptive and holistic management plans.

2.3.2. Groundwater dependent vegetation response to groundwater variability

Groundwater availability affects the spatial distribution and abundance of terrestrial vegetation (Orellana et al., 2012). Numerous studies have been conducted to establish the relationship between groundwater and vegetation (Eamus et al., 2006; Rodriguez-Iturbe and Porporato, 2005; Le Maitre et al., 1999). Vegetation response to fluctuating groundwater levels varies from non-observable changes to alterations of the entire community structure based on their physical and biological properties (Naumburg et al., 2005). Several studies were conducted to characterize phreatophytes according to their relations to groundwater depth (Robinson, 1958; Loheide et al., 2005). They reported that a decreasing water table could result in severe plant water stress when the rate of plant root development is insufficient or when the soil has low water holding capacity. Therefore, a declining water table limits the amount of water available for vegetation, resulting in plant water stress and decreased plant productivity (Loheide et al., 2005; Naumburg et al., 2005). Further, Han and He, (2020) reported a decrease in leaf intensity with a receding water table. Alternatively, a rising water table can flood plant roots, resulting in anoxic stress (Naumburg et al., 2005). In another study, Meinzer, (1929) reviewed GDV species and characterized them according to their rooting depth.

Results revealed that rooting density decreased with an increase in depth to groundwater. The physiological characteristics of GDV included dimorphic roots, which allow them to exploit deep groundwater sources. It was also determined by Laio et al. (2009) that a decline in groundwater level may cause an increase in the plants' rooting zone and an increased aerated soil profile suitable

for new root development. Additionally, Zhang et al. (2020) modelled the spectral vegetation response to depth to the groundwater table using the Tsallis Entropy Theory. It was reported that vegetation response was not uniform; different thresholds exist for grassland, shrubland, and forest vegetation. They found that at depths (>1m), the normalised difference vegetation index (NDVI), which measures the quantity of greenness in vegetation, therefore used as a proxy for vegetation density and health, decreased with increasing depth to the groundwater table. The alternative was also true, whereby NDVI declined with the rising water table at depths (< 1m) (Figure 2.2). Therefore, deeper water tables increase soil volume available for the storage of precipitation and hydraulically lifted water that can drastically increase the water available for plant use and growth. Also, in arid environments, evapotranspiration can result in salt accumulation in soils, and elevated groundwater levels limit the rooting zone to saline soils, resulting in plant stress from access to saline water (Zhang et al., 2020).

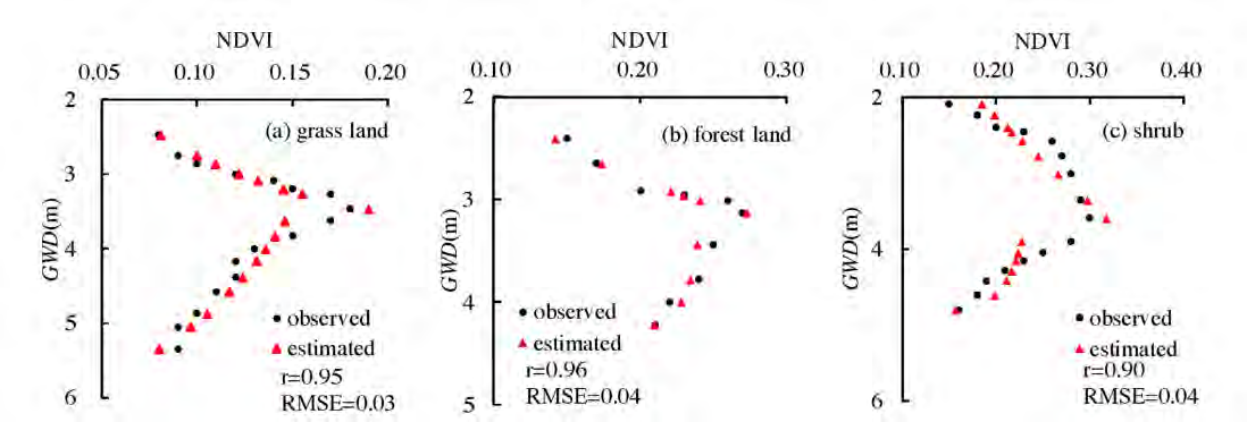

Figure 2.2 The relationship between NDVI of a) grass land b) forest land c) shrub forest and groundwater depth (GWD) based on Tsellis Theory in Ejina oasis in Hei (Source: Zhang et al., 2020)

A declining groundwater table has negative effects on plant physiology (Kath et al., 2014). During transpiration, water from the soil is pulled into the plant roots, then transported through the xylem to the plant leaves. A deficit in soil moisture increases the potential pressure in the xylem to the extent where xylem cavitation occurs. When this threshold is reached, the amount of water transported to plant leaves is decreased, which causes stomatal closure, a reduction in photosynthetic activity and then branch and crown mortality (Le Maitre et al., 1999; Kath et al.,

2014). For instance, Huang et al. (2016) reported the decrease in the ratio of actual evapotranspiration, potential evapotranspiration and a declining groundwater table. Different plant species have different xylem cavitation resistances (Kath et al., 2014; Naumburg et al., 2005). It is reported that riparian vegetation cannot tolerate limited water supply and therefore is vulnerable to xylem cavitation as well as crown and branch mortality (Kath et al., 2014; Hancock et al., 2009; Johansen et al., 2018). On the other hand, xeric phreatophytes are drought-tolerant vegetation species and can survive significant water table declines, despite losing some branches and leaf area. In a different study, Muñoz-Reinoso (2001) examined vegetation changes in Spain and the causal processes. Results revealed species composition change into xerophytic communities, due to a decrease in water availability.

Ecosystems dependent on groundwater show low seasonal variability in vegetation health and transpiration rates when compared to non-GDEs. The effects of groundwater extraction on coastal GDEs in New South Wales were assessed by Adams et al, (2015). Their findings indicated that long-term changes in evapotranspiration from groundwater-dependent vegetation occur seasonally. Evapotranspiration rates had lower variability than those of vegetation dependent on surface water. Further, tree ring analysis has demonstrated that groundwater availability is an important factor in plant growth rates (Xia et al., 2012; Gholami et al., 2015). The hydraulic lift of moisture from deeper soil horizons provides water for shallow-rooted herbaceous vegetation during water stress periods. Increasing groundwater depth has been associated with reduced plant growth rate. In addition, increased growth rates are associated with deeper water tables (Osmond et al., 1987; Sarris et al., 2007). Vegetation response to groundwater variability differs with the plants' anoxic and water stress tolerance, water uptake capacity and the change in the distribution and size of the active rooting zone (Naumburg et al., 2005). The variable plant responses to groundwater variability mean that studies on GDV should not take a generalized approach. However, valuable insights may be attained from long-term understanding of the relationship between groundwater, GDV and climate. Understanding the relationship between how groundwater availability affects vegetation and how that translates in terms of spectral signatures has opened a more cost-effective and robust methodology for the long-term monitoring of GDV (Barron et al., 2014). A detailed summary of recent studies that have exploited the spectral response of DGV to assess their interaction with groundwater is provided in Table 2.2.

Table 2.2 Summary of recent studies on vegetation response to groundwater variability

Application	**Results**	**Reference**
Hydrological controls on vegetation dynamics	The annual correlation between terrestrial water storage and NDVI is greater than that of rainfall and NDVI. The monthly/seasonal correlation between rainfall and NDVI is greater than that of Terrestrial water storage and NDVI.	(Ndehedehe et al., 2019) West and Central Africa
Ecohydrological response	Response to water convergence: 80-day time lag for groundwater, 4-7 years for vegetation	(Liao et al., 2020) China
Groundwater and GDE response to ecological water conveyance	Decrease in depth to water (DT)T ($p<0.05$). Increase in NDVI ($p<0.05$)	(Huang et al., 2020) China
GDE veg Index using Entropy theory	At DT >1m) NDVI declines with increasing DT At DT <1m) veg growth is restricted. NDVI correlation coefficient ($p<0.01$)	(G. Zhang et al., 2020) Northern China
Estimate crop groundwater use	50% of irrigation water from groundwater. Seasonal crops are more reliant on groundwater than perennial crops. Groundwater dependence increases with drying conditions.	(Hunink et al., 2015a) Spain
Effects if Groundwater extraction on Et rates,	Long-term change in Et close to extraction zones. Sig change Et for Facultative communities ($p<0.01$)	(Adams et al., 2015) New South Wales
Role of climate, GW availability and land management on veg vigour	Strong correlation between changes in plant vigour, precipitation, groundwater depth and evaporative demand.	(Huntington et al., 2016) United States
Veg response to groundwater drawdown	Vegetation ecophysiology is negatively affected by groundwater drawdown.	(Antunes et al., 2018) Spain
Quantify groundwater contribution to *Salix psammophila* water use.	Groundwater contribution to evapotranspiration ratio decreases with increasing depth to the groundwater table.	(Huang et al., 2016) China
Demonstrate the role of hydraulic path in determining plant intensity.	Leafing intensity decreases with increasing water table depth and plant height	(Han and He, 2020) China

Effects of groundwater table decline on vegetation transpiration.	Transpiration rates decrease with declining groundwater table, critical depth is at 3.6 and 2.0 m depths. Groundwater depth correlation with evapotranspiration is 0.98	(Wang et al., 2020) China
Relationship between riparian vegetation and groundwater depth	Peak evapotranspiration rates occur at groundwater depths <3m, and evapotranspiration values are significantly lower at depths greater than 3m.	(Lurtz et al., 2020) United States
Assess spatio-temporal evapotranspiration patterns of TGDV	Vegetation in shallow groundwater had high actual evapotranspiration rates as compared to those on deeper groundwater table, during the growth season.	(Sommer et al., 2016)
Influence of water table depth on evapotranspiration rates in the Amazon arc of deforestation	There were no differences in Evapotranspiration (ET), Land surface Temperature (LST) and Enhanced Vegetation Index (EVI) between vegetation and deep and shallow groundwater tables. Higher ET in shallow water table cops than those from deeper water tables during the dry season transition.	(O'connor et al., 2019) Brazil
Show the extent of groundwater-vegetation interaction distribution	Positive relationships (shallow DT with high Plant productivity) for shrubs in mesic regions. Negative relationship (deep DT with high plant productivity) for forests in humid regions. Vegetation primary productivity and groundwater depth are correlated in more than two-thirds of the global vegetated area.	(Koirala et al., 2017) Global

2.3.3. Climate impact on groundwater and dependent ecosystems

Changes in climate on annual or multi-decadal time scales have been seen to impact groundwater recharge and levels, depending on the aquifer size (Huss et al., 2010; Taylor and Tindimugaya, 2011). Groundwater resources and associated vegetation depend on the distribution, amount, timing of precipitation, evaporation loss, and land use/land cover characteristics. An aquifer's recharge potential depends on the groundwater level. A deeper water table increases recharge potential and capture zones. Properties of the aquifer are also vital; smaller shallow unconfined aquifers are more sensitive to climate change, whereas larger confined aquifers are likely to have a more delayed response (Poiani et al., 1996; Scibek and Allen, 2006). Confined non-renewable groundwater will be less sensitive to direct effects of climate change and variability but vulnerable to indirect effects of increased abstractions (Poiani et al., 1996; Scibek and Allen, 2006). Subsequently, the degree at which GDV is affected by climate variability depends on the aquifer

characteristics; therefore, vegetation dependent on groundwater from small and shallow unconfined aquifers is more vulnerable to the effects of climate change (Poiani et al., 1996).

Climate warming can influence the availability and demand for groundwater resources, thus affecting the water available for sustaining ecological functions (Barron et al., 2012; Wattendorf et al., 2010). Further studies on the effects of climate on groundwater and associated vegetation are outlined in Table 2.3. Climate change impacts on general water resources have been widely investigated. Although impacts on groundwater resources have gained increasing attention over the years, there is limited information on how GDVs are impacted. The seasonal distribution of precipitation and the temperature determine global climate zones and consequently the distribution of ecosystems, including GDV (Richards et al., 1975). As they are adapted to specific water regimes, many ecosystems are vulnerable to climate change. For example, the study by Barron et al., (2012) noted that reduced surface water flows and longer dry periods place GDV at high risk, with an estimated 19% decrease in current habitats in Australia. In addition, GDEs are increasingly likely to be threatened by groundwater abstraction. Extreme climate conditions change the hydrological regime, whereas the extent and seasonality of aquatic environments change the environmental conditions of GDV (Kløve et al., 2014).

Table 2.3 Impacts of climate change on groundwater and associated ecosystems

Application	**Key Findings**	**Reference**
Identify key hazards of climate change to develop a DGE risk assessment and decision-making framework	Ecosystem change affected by threshold tolerance of biota. GDV threatened by groundwater decline due to low rainfall, increased water extraction and land use change to pine plantations. The temporal regime of temperature, groundwater depth were significant floristic change drivers.	(Chambers et al., 2013) Australia
Revealing Impacts of Climate Change on GDEs	Temperature and rainfall variability may be the primary threats to groundwater and GDEs. they reduce recharge and possibly increase groundwater withdrawal rates. Climate change further accentuated the degradation of spring biota by causing changes in the precipitation and evapotranspiration regimes.	(Morsy et al., 2017) Kuwait
Impacts of predicted climate change on groundwater flow systems:	Flow systems their hierarchy can change from nested flow systems to a set of single flow cells. Preservation of GDV becomes a challenge under these conditions since long-term climate change could	(Havril et al., 2018) Hungary

Can wetlands disappear due to recharge reduction?	potentially have serious consequences, including wetland disappearance.	
Assessing the role of climate and resource management on groundwater-dependent ecosystem changes in arid environments.	Time series analysis clearly illustrates that there are strong correlations between changes in vegetation vigour, precipitation, evaporative demand, depth to groundwater, and riparian restoration. Trends in summer NDVI and groundwater level changes were found to be statistically significant, and interannual summer NDVI was found to be moderately correlated to interannual water-year precipitation.	(Huntington et al., 2016) United States
Impacts and uncertainties of climate/CO2 change on net primary productivity (NPP) in dryland vegetation.	Simulations showed a consistent temporal pattern of the regional NPP during 2000–2014 that increased during 2008–2011 and decreased during 2005–2006 and 2013–2014. All simulations indicated that ecosystems at high altitudes (> 47°) and were dominated by precipitation change.	(Fang et al., 2019) China

Climate-induced changes in groundwater-surface water interactions will directly and indirectly affect wetlands and GDV. Impacts on GDV will likely result from changes in groundwater and surface water levels and will vary in intensity depending on the location of the landscape, scale of the system and land use changes. Local and intermediate systems are overly sensitive to groundwater level dynamics and increased temperatures lead to significant changes in these systems. Regional-scale systems are less impacted by extreme events, seasonal fluctuations in groundwater level, recharge, and increased evapotranspiration rates. For GDV, a shift in local species composition will occur and decreased leaf density and primary productivity (Mawdsley et al., 2009 ; Naumburg et al., 2005; Shafroth et al., 2000). Additionally, Albano et al., (2020) demonstrated that long-term riparian vegetation response due to climate variability is driven by changes in groundwater and surface water dependence as compared to upland vegetation, which is controlled by the aridity gradient. Other studies also indicated that riparian vegetation had greater potential for groundwater dependence and was therefore sensitive to climate-induced groundwater variability (Barron et al., 2012; Barron et al., 2014; Froend and Sommer, 2010). Further, Kath et al., (2014) demonstrated that climate-induced groundwater decline resulted in the deteriorated tree canopy and a shift in species composition from non-vascular to vascular plants.

Highly variable rainfall could result in fluctuating groundwater levels due to variations in groundwater recharge caused by varying rainfall (Kumar, 2013). Climate warming is predicted to alter the magnitude and timing of recharge (Scanlon et al., 2006; Kløve et al., 2014)). This will result in a shift in the mean seasonal and annual groundwater levels, depending on the rainfall distribution (Liu, 2011; Scanlon et al., 2006). Long-term fluctuations in groundwater levels may also be a result of climate variability, in addition to land-use/landcover and anthropogenically induced alterations (Anderson and Emanuel, 2008; Gurdak et al., 2007). Further, in areas with highly variable vegetation productivity, it is unclear or difficult to determine if climate variability is the main contributor to changes in vegetation productivity since these systems may gain access to precipitation, shallow groundwater, and surface water, varying across temporal and spatial scales. Therefore, discriminating the influence of climate variability from management practices, disturbance and other long-term human activities requires long-term monitoring (Hausner et al., 2018). A review of the literature revealed that there are limited studies that have focused on the impact of climate change (Hancock et al., 2009; Shafroth et al., 2000; Huang et al., 2020). Most studies mainly investigated impacts on surface water, and little work has been done on groundwater. This may be because GDV communities are highly complex and heterogeneous systems that are influenced by multiple factors, which makes it hard to account for their status based on one factor. The integration of scientifically sound methodologies like long-term data handling and cloud-computing techniques with newer approaches that have high processing efficiency has the potential to mitigate these challenges (Hausner et al., 2018; Huntington et al., 2016). The first step for effective management of GDV begins with the knowledge of their location, distribution and areal extent (Rohde et al., 2017a). Groundwater-dependent ecosystems at catchment scale can be identified mainly through field or floristic assessment, numerical modelling and (geospatial) RS and GIS approaches (Eamus et al., 2015; Glanville et al., 2016). The choice of the selected approach is dependent on the temporal and spatial extent of the study as well as available resources.

2.4. Field-based methods for identifying groundwater-dependent ecosystems

Groundwater use by phreatophytes has been assessed using field techniques: isotope analysis (Eamus, 2009; Chapman et al., 2003; Cartwright et al., 2010), water balance methods (Le Maitre and Hughes, 2003), and the assessment of ground-based leaf area index (Eamus, 2006; Hatton & Evans, 1998), vegetation rooting depth (Eamus, 2006; Shafroth et al., 2000), as well as depth to

groundwater models (Hoogland et al., 2010; Eamus, 2009). For instance, water flux measurements were used in determining groundwater use for deciduous black oak trees in California (Miller et al., 2010). The study indicated that black oak trees were obligate phreatophytes, with a groundwater uptake ranging from 4mm/month to 25mm/month. Dependence was most in the dry season, with 80% of evapotranspiration from groundwater (Miller et al., 2010). In Australia, Jones et al. (2019) emphasized the importance of validating ecohydrological conceptual models of GDV. While field techniques offer the most detailed insight on the nature, extent, and degree of groundwater ecosystem dependence, they are resource-intensive, expensive and represent one point in time (Eamus et al., 2015b). Therefore, they are ideal for testing and developing a conceptual understanding of GDV and validating GDV mapping (Glanville et al., 2016a; Gow et al., 2010). However, although these studies demonstrate the importance of field-based methods in GDV characterisation, most of these techniques lack spatial representation, which makes it difficult to upscale to larger areas and is complex in areas characterised by heterogeneous plant species.

2.5. Modelling approach for identifying groundwater-dependent vegetation

Numerical modelling provides simulations on groundwater-vegetation interactions that can be used to infer on ecosystem dependence on groundwater. Model-based methods have been used in conjunction with geospatial techniques (Münch and Conrad, 2007) and field studies (Móricz, 2010; Wu et al., 2015). These methods demonstrate a unique opportunity in understanding GDV as they integrate numerous datasets such as soil water data, groundwater depth and underlying hydrogeological conditions. Due to this ability, it was therefore noted that groundwater contribution and consumption could be modelled with low estimation errors of 0.007 (Wu et al., 2015; Móricz, 2010). However, like any other method, these techniques have their inherent challenges. For example, while numerical models provide innumerable insights, they are not entirely suitable for GDE mapping at catchment scale, especially in data-sparse areas. In addition, the numerical modelling approach can be time-consuming and resource-intensive.

2.5.1 Geospatial approach for identifying and assessing groundwater-dependent vegetation

Remote sensing and GIS techniques are robust methods for mapping GDV at catchment scale. Their implementation, however, requires basic knowledge of groundwater-ecosystem interactions and their spectral signature response (Barron et al., 2014). These approaches relate the presence of

vegetation in unexpected areas and dark soils to high soil moisture content and groundwater availability (Brodie et al., 2002). Remote sensing technologies such as airborne sensors, Light Detection and Ranging (LIDAR), Synthetic Aperture Radar (SAR), and spaceborne satellite sensors provide land surface information used in GDV identification. For example, LIDAR produces high-quality digital elevation models (DEM) used to obtain topographic indicators for locating GDEs such as aspect, slope and topographic wetness index (Hoyos et al., 2016). Based on the assumption that surface water is the surface expression of groundwater, the SAR provides information on seasonal fluctuations of the water table, surface water inundation, vegetation patterns, etc. SAR data can help infer on GDV water balance and hydrological boundaries. Satellite sensors are also widely used to obtain GDV indicators such as vegetation pattern, evapotranspiration, and soil moisture saturation (Table 2.4). Remote sensing equates GDEs to a distinct ecosystem type (green islands); however, groundwater dependence is one factor affecting ecosystem productivity.

Literature search has revealed an increase in the use of remote sensing and GIS approaches in eco-hydrogeology and related environmental studies (Tables 2.2 and 2.4). Remote sensing can offer new applications that can quickly and synoptically monitor and manage areas at different temporal and spatial resolutions. For example, remote sensing supports timely and spatially explicit assessment of groundwater-dependent ecosystems, wetlands, water quality monitoring and aquatic weeds (Zhang et al., 2020; Klausmeyer et al., 2018; Thamaga and Dube, 2018; Lv et al., 2013). Moreover, continual coverage of sensors provides both near-real-time and long-term data required for monitoring GDE response to changing groundwater regimes resulting from climate variability. As such, the use of satellite imagery has provided a reliable source of data that is intensively used in hydrology and ecology (Ali and Alandjani, 2019).

Several satellite sensors are suitable for extracting variables utilized in determining the location of GDV and their probable response to groundwater fluctuations. Sensor suitability has influenced research needs in terms of spatial, temporal, radiometric and spectral resolution. While sensor resolution is an important consideration, the cost of the satellite imagery is usually the major limiting factor. In general, there exists a trade-off between spatial resolution and acquisition; this is also true for spatial and temporal resolution. Very high-resolution sensors such as QuickBird, SPOT, IKONOS and Aerial photography with spatial resolutions < 0.5m are high cost. GDE

potential has been estimated in Portugal, using SPOT 4 and 5 products (Marques et al., 2019). The high spectral resolution sensors were found to be ideal for vegetation mapping and change detection at the species-specific and community level. MODIS, which is a low-cost sensor with low spatial resolution (250m-1000m) and multispectral and multi-date data sets, is therefore useful for global-scale evapotranspiration estimation, monitoring photosynthetic activity, and vegetation mapping (Hoyos et al., 2016). MODIS products have been incorporated with other satellite products for GDV assessments (Gou et al., 2015; Hunink et al., 2015; Doody et al., 2017; Huang et al., 2020; Liao et al., 2020). While MODIS datasets are widely used, they lack the spatial resolution suitable for GDV delineation at scales below the community level. The low spatial resolution has resulted in misclassification errors in heterogeneous environments with mixed vegetation.

Medium spatial resolution (30m) and multispectral sensors such as the LANDSAT series have been extensively used in land cover change detection, vegetation mapping and photosynthetic activity assessments applications at the community level (Roy et al., 2016; Kalbus et al, 2006; Yates et al., 2010; O. Barron et al., 2014; Adams et al., 2015; Doody et al., 2017; Mtengwana et al., 2020; Shoko et al., 2016). Landsat series data are easily accessible and have an archive of historical data, great for applications in developing economies (Dube et al., 2016). An extensive review of literature has revealed that the potential for new generation multispectral remote sensing products, such as Landsat 8 Operational Land Imager (OLI) and Sentinel 2 has yet to be developed in mapping and monitoring GDV. Landsat 8 OLI has improved signal-to-noise characteristics, improved calibration and higher radiometric resolution and spectrally narrower wavebands than the previous Landsat 7 ETM+ (Roy et al., 2016).

The location of potential GDV can be greatly improved through these new features. Sentinel 2 has a high spatial and temporal resolution of 10m and a 5-day revisit time, making it suitable for community-level classification of GDV. In Western Australia, Macintyre et al. (2020) assessed the efficacy of Sentinel 2 imagery for classifying multi-seasonal changes in vegetation for complex areas at fine scales. The classification scheme utilized 24 target classes, and a 60/40 split was used for model building and validation. A comparison of the seasonal variations in vegetation indices, spectral bands, classification trees, and principal component transformations was used as input for machine learning to separate classes. The study findings revealed that Sentinel 2 has a high

potential to determine compositional vegetation characteristics with high accuracy. However, further investigations must be considered to determine the potential for vegetation indices derived from new generation sensors in delineating GDV. Landsat 8 OLI and Sentinel 2 datasets provide spatially and site-specific, timely information on GDEs that may be used in setting management decisions. However, their applicability is limited to the local and community levels. Advancements in remote sensing technological developments have resulted in the introduction of space and airborne hyperspectral sensors with fine spatial resolution (<10m), with strategically positioned spectral bands such as panchromatic and red edge, as well as improved signal-to-noise ratio. For example, Worldview 2 data has been used in assessing arid vegetation health in response to environmental variables such as depth to water, groundwater depletion, and management practices at tree level (Chávez and Clevers, 2012).

Unmanned aerial vehicles (AUVs) is an emerging topic in vegetation studies that has the potential to bridge the gap between expensive satellite remote sensing, fieldwork, and classical manned photographs. AUVs combined with multispectral cameras and hyperspectral remote sensors produce high-quality datasets with user user-determined revisit period, suitable for long-term monitoring of GDV. AUVs have been used in determining vegetation distribution at the plant species level with overall accuracies of 88.9- 94.31% (Zhaoming, 2020; Kaneko and Nohara, 2014). As the field of AUVs is gradually expanding in vegetation studies, there is great potential for AUV application in GDV mapping in complex heterogeneous environments, due to the high spatial resolution (<1cm), and the ability to increase pixel purity by adjusting the flying altitude. Hyperspectral remote sensing data improves GDV investigations, but the datasets are often large. The rapidly increasing archive of data for long-term GDV monitoring has associated challenges such as data storage, computational efficiency, and bandwidth mismatch from multigenerational satellites. The GEE cloud computing environmental platform and Climate Engine have emerged as the solution. GEE stores Petabyte-scale multi-sensor database vector datasets, and parallelised cloud computing. The strength of Cloud-Based computing is that it does not need high computer processing power or the latest software, which opens new research opportunities for resource-poor regions to engage in GDV analysis at the advanced nations (Mutanga and Kumar, 2019; Gxokwe et al., 2020). While there are advancements in remote sensing and vegetation analysis, there remains a gap in assessing their effectiveness in GDV investigations.

Previously employed vegetation indices used for GDVs assessment include the Enhanced Vegetation Index (EVI), Leaf Area Index (LAI), the Tasseled Cap Wetness Index (TCWI) and the Normalized Difference Wetness Index (NDWI). A wide range of studies (Roy et al., 2016; Kalbus et al, 2006; Yates et al., 2010; Barron et al., 2014; Adams et al., 2015; Doody et al., 2017; Gu et al., 2007; Hunink et al., 2015) have demonstrated the capabilities of indices in locating GDV. For example, the study by Gow et al., (2010) collated multiple remotely sensed information from MODIS-EVI, SRT DEM, and water table surface to identify and monitor GDEs within the Hat Head National Park. In Australia, Barron et al., (2014) proposed a method for identifying GDEs from Landsat-TM derived indices. Mapping had high producer accuracy, ranging from 59% to 91% increasing from regional to local scales.

Results showed that GDV with permanent access to groundwater had no significant change in seasonal GDV size. However, a substantial reduction of 26 - 56% in total GDV size is observed over the 10 years. Mapping demonstrated good agreement with field data. GDV was associated with riparian vegetation, terrestrial vegetation with access to shallow groundwater depths (~6m) and found close to springs. Expert knowledge, field techniques and remote sensing techniques were used to develop a catchment-scale mapping method of GDEs in Queensland, Australia (Glanville et al., 2016b). They produced a catchment scale map of GDEs, which can be scaled up or down, and the study emphasized the value in integrating local experts' knowledge with available spatial data and information. While remote sensing data indices are a robust methodology, the literature indicates that GDV identification can be substantially improved by the selection of an appropriate classification technique. Given these indices perform differently in different environments due to pixel mixing, cloud cover, and shadows in mountainous and built-up areas. However, their performance can also be significantly improved by the sensor's spectral characteristics, such as the availability of red edge, near infrared II and panchromatic bands.

Table 2.4 Summary of key research that utilises geospatial techniques to identify potential GDV

Sensor Type	classifier	Key Findings	Limitations	Reference
Landsat 5 TM	NDVI Principal Component	Compared Top of Atmosphere Reflectance and the Atmospherically corrected images (AC) for inflow dependent vegetation. TOA and AC are in good agreement, Kappa = 0.83. Both methods show high accuracies for capturing Known IDV, 85-91%.	Accuracy of the delineated IDV extent may vary due to differences in landscape characteristics and variations in vegetation type.	(Emelyanova et al., 2018a)
Landsat 5 TM MODIS	MODIS (ET, MSSR, Pid) (NDVI, NDWI)	34% of the Australian continent contains GDEs, of which 5% have high potential for GDEs. Emphasized the need to integrate expert knowledge to gain a conceptual understanding for setting rules in identifying potential GDEs.	A broad-scale approach cannot identify GDEs <25X25 m. The method provides a snapshot, and GDEs that may be in decline due to other factors may be missed. The GDE atlas requires regular updating.	(Doody et al., 2017) Australian /continent
WorldView-2 SPOT-7 Landsat 8 OLI	Maximum likelihood Classifier, Object Based Image Classifier	SPOT-7 (Overall Accuracy= 69%) WorldView-2 (Overall Accuracy= 72%) GDEs are likely to occur in lowland areas and break of slope where groundwater is discharged to the surface.	High misclassification (Overestimation) error along the hillslopes during the wet period and higher misclassifications on the riparian zone during the dry season.	(Dlikilili, 2019) South Africa
Landsat MS, TM, ETM, OLI	NDMI, NDVI Parameter-elevation Regressions on Independent Slopes Model	(0.02%) of Landsat data not included. The map constitutes of layers of local datasets for identifying possible locations of GDEs, in a heavily modified environment.	Not all areas included updated landcover layers, gaps in groundwater depth datasets. GDEs are dynamic systems, therefore require regular updating.	(Klausmeyer et al., 2019) United States

	(PRISM) precipitation data			
Landsat 7 ETM MODIS	NDVI LAI K-means Classifier	Not all phreatophytes and wetlands are groundwater dependent, only 9% of phreatophytes had high groundwater use potential. 75% of identified GDEs were at soil depths below 45cm.	The use of vegetation indicators led to overestimations. Cells with mixed vegetation coverage groundwater dependence was not accurately reflected. Resampling of MODIS images may have led to information loss. Lack of previous GDE studies hinders verification of results.	(Gou et al., 2015) Texas, United States
MODIS Terra 7	Standardized NDV K-means cluster classifier	Pixels were likely to be GDV where the groundwater table was shallow.	Standardized NDVI does allow for observing areas with low seasonal variability or interannual variability. No quantitative method to validate results. Areas with low tree density, GDV were not captured.	(Páscoa et al., 2020)

2.5.2. Available groundwater-dependent ecosystems classification algorithms

Spectral discrimination of GDV types in complex environments is challenging, as different vegetation types may have similar spectral characteristics; alternatively, they may show different spectral signatures. Image classification can aid in grouping image pixels into meaningful clusters. Automatic image classification can be done in two ways: unsupervised or supervised, parametric or non-parametric classification. Unsupervised classifiers, such as IsoData and K-means, use clustering mechanisms to group satellite image pixels into unlabelled classes, which are later assigned meaningful labels to produce a well-classified image (Ismail, 2009). Unsupervised classification techniques have been extensively used in mapping and assessing potential GDEs (Barron et al., 2014; Davies et al., 2016; Gou et al., 2015; Münch and Conrad, 2007; Páscoa et al., 2020). Supervised classification requires input from analysts in the form of training datasets. For supervised classifiers, classification accuracy depends on the representativeness of the training sample (Ismail, 2009). When training cannot account for the complex spatial variations, statistically based (unsupervised) clustering can produce better results (Rozenstein and Karnieli, 2011). Common supervised classifiers are Artificial Neural Networks (ANN), Decision Tree (DT), Maximum Likelihood Classifier, K-nearest neighbour, etc. The Maximum Likelihood Classifier (ML) is the most extensively used supervised classification algorithm.

The application of pixel classifiers to mixed pixel images often produces unsatisfactory classification results due to poor spectral and spatial resolutions (Barron et al., 2012; Glanville et al., 2016b; Gow et al., 2010). Increased availability of higher resolution images, coupled with the development of machine learning algorithms, can significantly improve classification accuracies (Hoyos et al., 2016). These include the support vector algorithm (SVM) (Boser et al., 1992), ANN (Paola and Schowengerdt, 1995) and Random Forest (RF) classifiers. The random forest or random decision forest is a learning method for classification operated by the construction of a multitude of decision trees during training, and the output is a class made of the predicted mean of the individual tree (Raczko and Zagajewski, 2017). The advantage to the RF is the short classification time and the method's resistance to overfitting of training datasets (Sabat-Tomala et al., 2020). A previous study by Hoyos et al., (2016) compared the classification and regression tree (CART) and RF for estimating GDV potential. Results revealed that the RF classifier was superior to CART in terms of estimates, accuracy of training data, and sensitivity.

SVM produces significant accuracies with little computation power, they work well on small testing data and noisy datasets (Song et al., 2012). Classes are produced from training data models that transform the space into an optimal hyperplane in the multidimensional feature space, which separates features into classes with the greatest margin of separation (Mountrakis et al., 2011). The SVM classifier has an advantage over ANN in that they are simple to use, reliable, stable and has a faster processing speed (Raczko and Zagajewski, 2017). Reducing training data sample size per sample compromises classification accuracies; however, the SVM seems to be insensitive to this effect (Shafroth et al., 2000; Mountrakis et al., 2011). In South Africa, Cooper (2010) investigated the potential of the SVM recursive feature eliminator (RFE) approach in detecting the presence of *Solamum mauritianum* (Bugweed) alien plant within a forest plantation. The SVM-RFE produced an outstanding classification accuracy of 93% and a skills statistics value of 0.83.

ANNs are complex models that are inspired by biological neural networks to develop classification rules. Raczko and Zagajewski, (2017) studied tree species composition in Poland using the SVM, RF and AAN algorithms for tree species classification. The ANN outperformed the other learning algorithms with 77% overall accuracy, while the SVM and RF produced 68% and 62.5% respectively. Literature reveals that unsupervised classification techniques are reliable and widely developed (Hoyos et al., 2016; Peters et al., 2008) while other studies have indicated the potential for machine learning algorithms in GDE assessment (Peters et al., 2007; Klausmeyer et al., 2019; Páscoa et al., 2020). These methods demonstrate a great potential in retrieving GDE information with reasonable accuracy. However, their performance is also dependent on the scale of application, satellite spectral and spatial data characteristics. Further, the supervised machine learning algorithms produced great results, although significant limitations have been reported. For example, ANN and SVM are not easily automated and require adjustments to several parameters; whereas models such as the RF have been reported to overfit for datasets as small as the size of a tree, which can take up memory. Thus, cloud image processing simplifies the issues related to supervised machine learning algorithms; however, the literature shows that these techniques are underused, especially in GDV assessments (Gxokwe et al., 2020).

2.5.3. Challenges in remote sensing of groundwater-dependent ecosystems

Several studies have noted various limitations in the remote sensing approach for detecting and mapping groundwater-dependent vegetation communities. Remote sensors can detect land surface features such as temperature, vegetation, and land cover; therefore, information on groundwater is only from indirect inferences. Groundwater-vegetation interactions can only be inferred from indicator variables such as vegetation, temperature and surface water (Barron et al., 2014). As such, the information gathered is only estimates that mainly indicate potential GDV. Thus, the results should be validated using field data. Although numerous works have been done in regional GDV mapping, most of the studies have not been validated through ground-truthing. For instance, Jones et al., (2020) investigated GDV communities using stable isotopes and found that 75% of reported GDV sites were using groundwater. Remote sensing offers a snapshot of GDV; those outside the range may not be identified. There is often a lag between changes in water availability and vegetation response (Gow et al., 2010). Further, ecosystems dependent on groundwater affected by a drought may not be identified as GDV if their phenology was in decline at the time. Remote sensing is suitable for places that are minimally modified, in urban or cultivated areas, vegetation greenness may be attributed to the return of irrigation, runoff and dam releases. Also, there is minimal integration between the field, chemical assessment and remote sensing datasets. As a result, remote sensing and GIS-derived information are being undervalued and underutilised. Remote sensing identifies GDV based on the principle that vegetation that is greener than its surroundings during dry periods is likely to be maintained by groundwater; therefore, it is suitable for areas with distinct wet and dry seasons (Barron et al., 2012). This method has been criticized because vegetation greenness may be a result of other factors (Glanville et al., 2016a). For example, wildfires may result in green islands, as resistant forest vegetation is surrounded by fire-prone vegetation (Bowman, 2000; Glanville et al., 2016). Further, remote sensing generates GDV maps with little or no information on how vegetation communities are connected to groundwater within the landscape.

The potential for remote sensing applications in GDV monitoring has not been fully explored. This is attributable to the inaccessibility of high-resolution remotely sensed products. This has been primarily attributed to their high acquisition costs, the low temporal resolution and smaller swath width. The freely available medium resolution products, such as Landsat, are limited in the level of detail that can be achieved for assessing GDV. For instance, some groundwater-dependent communities are at the sub-pixel level (<30m) and may be masked out in mixed

feature pixels. Thus, GDV monitoring, and assessment can benefit from a multidisciplinary approach through the integration of ecohydrological data, geology, soil information, land use and land management practices, soil characteristics, groundwater flux and recharge rates. So far, however, such collaborations are limited. Cloud computing techniques provide access to multi-sensor datasets and computing efficiency that can enhance GDV detection and monitoring, especially in resource-poor regions at low costs. However, challenges due to unreliable network or internet connectivity, unskilled personnel, and the lack of high-performance computing power limit their applicability in underdeveloped countries where it is needed the most.

2.5.4. Possible future direction in remote sensing and GIS applications for groundwater-dependent ecosystems

Several strides have been made in mapping and monitoring GDV and its response to groundwater variability using satellite data. There is still, however, limited information on long-term monitoring of vegetation response to changing groundwater regimes, especially associated with climate change. Investigating the impacts of climate change is limited by the high complexities of GDV, where multiple factors influence the plant's phenology, distribution, and chemical processes. Most of such studies are dominant mainly in Australia, the United States and China; however, there is a dearth in knowledge in resource-poor areas such as the arid regions of Africa. The major limitation is that these methods for GDV identification or delineation are likely to change with differing landscapes, vegetation types and climates; therefore, geospatial techniques need to be evaluated under diverse environmental conditions. Likewise, determining whether changes in groundwater regime and associated vegetation are products of climate change requires long-term (>50 years) monitoring (Kløve et al., 2014). To fully understand these vegetation communities, groundwater-vegetation responses should be monitored seasonally at catchment or species-specific scales. There have been huge developments in geospatial technologies, such as hyperspectral and AUVs datasets, providing new opportunities for species-level vegetation monitoring; however, they have been poorly utilized in GDV assessments. Hyperspectral drones, AUVs and Worldview data potential should be investigated for GDV assessments. Sentinel 1 offers high spatial and spectral resolution datasets that provide valuable information for vegetation mapping and validation. For example, the ground penetrating E-band offers soil moisture data, a valuable variable for GDV mapping. This will provide detailed information useful for decision makers when drawing up strategic catchment management plans.

As groundwater dependence is one characteristic of GDV mapping, there is therefore a need to find the best ancillary (variables) data and predictive models that can be integrated with freely available datasets. Further, Landsat series and MODIS datasets are widely used in GDV mapping; however, the major limitation is their low spatial resolution (>30m). Despite these limitations, the Landsat series has a large historical archive that has not been fully exploited. The introduction of advanced cloud computing methods such as GEE, peta-scale image processing and artificial intelligence (AI) have the potential to overcome limitations of spatial resolution and temporal range through the integration of hyperspectral and coarse-scale multispectral datasets. Cloud computing methods can provide new insight in GDV monitoring and offer new opportunities to resource-poor nations where GDV investigations were hindered by the cost of acquiring these datasets. Further, more studies integrating field methods with remote sensing in assessing GDV should be prioritized, as this will increase the reliability of the derived spatial and thematic GDV maps. When there is a large body of local information on GDV occurrence, geospatial methods can be adequately evaluated and indicate areas of improvement. Further, machine-learning algorithms such as ANN, SVM, and regression tree-based classifiers need to be explored for GDV assessments and distribution mapping.

2.6. Conclusions

Groundwater resources are increasingly deteriorating and constantly under threat due to global change, and increased abstraction impacts vegetation. Literature has revealed the effects of a reduced groundwater table in areas where GDV is dominant. In the context of this review, GDVs were classified as terrestrial vegetation (Phreatophytes) and associated dependent flora and fauna, which are sustained by groundwater. The classification of these systems in this review was based on the classification system of GDEs by Eamus et al. (2006). There is a large body of literature on GDV response to groundwater variability. Most of these studies have shown that GDV has responded variably to groundwater availability based on the plant physiological characteristics, such as the plant rooting depth. Literature shows that the major responses to a declining groundwater table are reduced photosynthetic rates, plant productivity, reduced leaf area and the change in species composition and distribution. However, GDV is also affected by the timing and or groundwater regime. This needs to be explored further, especially with the looming impacts of climate change. Elevated surface temperature and low rainfall are associated with groundwater depth decline, leading to GDV degradation and floristic change. The research reveals the effects of climate variability on GDV are difficult to

isolate. Therefore, further long-term climate-vegetation interaction research is required. Remote sensing has emerged as a popular method for GDV mapping and assessment, because of the efficiency, unique spatial, spectral, and temporal Characteristics that allow GDV assessment at different scales. While readily available datasets (MODIS and Landsat) have provided critical insights on the state of GDV, they are, however limited by the poor (low) spatial and spectral characteristics. There is therefore a need to enhance remote sensing potential by integrating multiple indicator variables in GDV investigations. In addition, new generation sensors (Landsat 8 OLI and Sentinel 2) with improved spatial and temporal resolutions and advances in ML algorithms can further improve the identification and monitoring of GDV. Moreover, the potential of integrating multisource datasets such as drones, AUVs, Worldview and Sentinel 1 to calibrate GDV models should be assessed. Emerging cloud-based image computing techniques such as GEE can significantly improve the long-term monitoring of GDV. The effects of climate change have created a need to adequately delineate vulnerable groundwater-dependent vegetation communities to ensure their sustainability when allocating groundwater resources for anthropogenic activities.

CHAPTER THREE

GROUNDWATER MODELLING APPLICATIONS COUPLED WITH SPACE-BASED OBSERVATIONS IN GROUNDWATER-DEPENDENT ASSESSMENTS: A REVIEW ON APPLICATIONS, CHALLENGES, AND FUTURE RESEARCH DIRECTIONS

3.1. Introduction

Groundwater-dependent ecosystems are complex systems that depend on the consistent or intermittent connection to groundwater for their continued existence and ecological functionality (Klove et al., 2011; Orellana et al., 2012; Pérez Hoyos et al., 2016; Rampheri et al., 2023). These ecosystems encompass a diverse range of habitats, including wetlands, riparian zones, and springs, playing a crucial role in maintaining biodiversity and ecosystem services. The ecological significance of GDEs has gained increasing attention due to their susceptibility to environmental changes (Rohde et al., 2017). Subsequently, research advances have focused on the significant threats to GDEs, including groundwater depletion, impacts of climate change and groundwater contamination (Brown et al., 2011; Eamus et al., 2015). A study by Kidmose et al. (2013) revealed that climate change variations have an impact on groundwater level fluctuations. Long periods of rainfall cause an increase in groundwater levels, while prolonged dry periods and droughts decrease groundwater levels. Considering how GDEs are dependent on groundwater supply, the effects of climate change on groundwater levels are likely to have a considerable impact on the functioning of GDEs. In addition, the impacts of climate change on groundwater level fluctuations are not only influenced by rainfall but also by changes in temperature and land use. Wang et al. (2021) found that increasing temperatures are likely to decrease groundwater levels due to increased evapotranspiration. Furthermore, the overabstraction of groundwater continues to alter the hydrological regimes and aquifer dynamics (Kath et al., 2018). Groundwater levels have been reported to be declining globally (Jasechko & Perrone, 2021), thereby increasing the threat to ecosystem functioning and health of GDEs. Increased groundwater levels offer a reliable source of water, ensuring the long-term viability of GDEs even in arid climates. Additionally, increased groundwater levels strengthen GDEs' resistance to drought and support their function as habitats for species during dry periods. Evaluating the effects of climate change on groundwater and dependent systems is challenging because of the complexity of these systems and the insufficiency of accessible data (Goderniaux et al. 2009).

GDE protection is particularly challenging due to variations in hydrogeological and climatic settings, as well as the variability in groundwater flow paths, discharge patterns, and water quality required for the comprehensive understanding of their functioning at local and regional scale (Tomlinson, 2011; Pérez Hoyos et al., 2016; Rohde et al., 2017; Erostate et al., 2020). However, the study of the relationship between GDEs and groundwater presents a significant stride towards their conservation by improving our understanding of the relationship that exists between GDEs and groundwater, providing information on the vulnerability of GDEs to changes in groundwater levels, which can inform management decisions aimed at protecting these systems. This relationship is referred to as the 'hydrogeological connectivity' in this paper. The hydrogeological connectivity between underlying aquifers and GDEs plays a critical role in determining long-term sustainability and ecological integrity of these delicate ecosystems. This relationship is complex and crucial for the sustainability and functioning of GDEs. It affects important aspects of such as nutrient distribution and water storage. Additionally, the exchange of water between GDEs and aquifers influences local and regional hydrologic cycle, which in turn influences the resilience of ecosystems and contributes to groundwater recharge. To understand the complex relationships between GDEs and groundwater systems, various models and conceptual frameworks have been employed. These frameworks often consider factors such as groundwater recharge, and flow paths as key determinants of hydrogeological connectivity. Understanding these frameworks is essential for understanding how GDEs rely on groundwater for sustainability and how changes in aquifer properties can impact on the ecological integrity of these systems.

While the topic of the relationship between GDEs and groundwater has been widely studied (Bracken & Croke, 2007; Lexartza-Artza & Wainwright, 2009; Lesschen et al., 2009; Bracken et al., 2013; Wei et al., 2023), there are still several challenges identified in existing literature. The process of analysing the relationship between GDEs and the underlying aquifers is limited by the lack of data such as groundwater levels, flow rates, and water quality (Eamus et al., 2015; Doody et al., 2017; Link et al., 2023). In addition, complex hydrogeological systems marked by intricate geological formations and complex flow dynamics pose significant challenges in developing accurate predictive models (Harken et al., 2019). Furthermore, the precise impacts of groundwater abstraction on GDEs are not well understood, especially over long periods. Lastly, human activities such as land use and the abstraction of groundwater can have substantial effects on the connectivity of groundwater and dependent ecosystems (Schirmer et al., 2013). An important first step in studying the hydrogeological relationship

between GDEs and underlying aquifers is the accurate identification and delineation of these systems to comprehensively understand their hydrological connectivity, ecological dependence, and vulnerability to land use and land cover changes. This is usually achieved using field data-based models, which are data-intensive which is very costly to collect for some regions (Gxokwe et al., 2020a).

The availability of remote sensing data and tools offers unprecedented opportunities for the identification and delineation of these GDEs and understanding their eco-hydrological changes and vulnerability to land use and land cover changes over time. With input data from various sources such as Landsat, Sentinel 1 and 2 as well as Moderate Resolution Spectroradiometer (MODIS), among others. However, challenges associated with the spatial resolution of the remote sensing data tend to present inaccuracies during the monitoring of these systems (Gxokwe et al., 2024; Ramperi et., 2020). Moreover, the unavailability of cloud-free images for certain times of the year causes challenges with continuous assessment and monitoring of GDEs from RS data (Gxokwe et al., 2024). Advancements in data analytics tools, such as the introduction of artificial intelligence-based cloud computing platforms, such as Google Earth Engine, offer unprecedented opportunities to address challenges associated with remote sensing applications in GDE assessments and monitoring. With the availability of advanced data handling and processing tools in these platforms, it has become possible to integrate various data types, therefore combining their strengths and improving the delineation and assessment of GDEs over time. In addition, free access to higher resolution remote sensing data such as the Copernicus Sentinel data through these platforms also makes it possible to accurately delineate, assess and monitor ecohydrological changes of the GDEs over time.

Although remote sensing technological advancements have been made, and have the potential of improving the delineation, assessments and monitoring of ecohydrological changes in GDEs over time, these have not been fully explored. Moreover, the potential of coupling geospatial tools to groundwater models for improved groundwater-dependent assessments, according to our knowledge, is not fully understood. Owing to this background, the chapter seeks to provide a comprehensive overview of the progress and applications of groundwater flow models coupled with advanced geospatial tools to understand the ecohydrology GDEs and their extent of connectivity to underlying aquifers. In achieving the main objective, the review firstly provides in broader sense critical background on the science of GDEs and their classification, followed by the progress that has been made in the application of remote sensing and GIS

technologies in the identification and delineation of GDEs. Secondly, the review provides an overview of the application of groundwater modelling techniques and challenges. Lastly, the review presents the potential of integrating geospatial tools into groundwater models and future research prospects. Although other reviews, such as Ramperi et al. (2020), Bertrand et al. (2014) have provided an overview on understanding GDEs and their ecohydrological dynamics over time, however, they did not focus on the progress on coupling groundwater models with geospatial tools to understand these systems. Hence, our review focuses on such, therefore informing the GDEs' monitoring systems in various states about the key priority research areas on these critical ecosystems. Moreover, the review provides an overview of robust methodologies for accurate assessment of GDEs, therefore informing the Sustainable Development Goals (SDG 6.1.1), emphasizing the need to protect and restore aquatic ecosystems.

3.2. Literature search

To achieve the main objectives and relevant literature for this study, an extensive search was conducted on the various search engines like Web of Science (WoSCC, Google Scholar and SCOPUS. During the search of these articles, the following search query was used: (groundwater dependent ecosystems* OR springs*) AND (groundwater modelling OR groundwater simulation) AND (conditions OR contaminant transport OR ecological status OR hydrological connectivity) AND (Finite Difference Methods OR Finite Element Methods OR Remote Sensing OR Earth Observation OR GIS). The search yielded 13900 articles from Google Scholar, 8300 from SCOPUS and 2100 from WoSCC, respectively (n = 29300). Figure 3.1 shows the workflow followed during the literature selection process. The articles included in the review also had to meet the following criteria:

1. The use of remote sensing data to study groundwater and/or GDEs.
2. Integration of remote sensing data and other data sources (e.g. hydrological models, groundwater models, land use data) to study GDEs.
3. The article clearly states the remote sensing and groundwater model used
4. Published in a peer-reviewed, accredited journal.
5. Article written in English
6. Article is freely accessible and available in full text
7. Papers published between 2000 and 2023

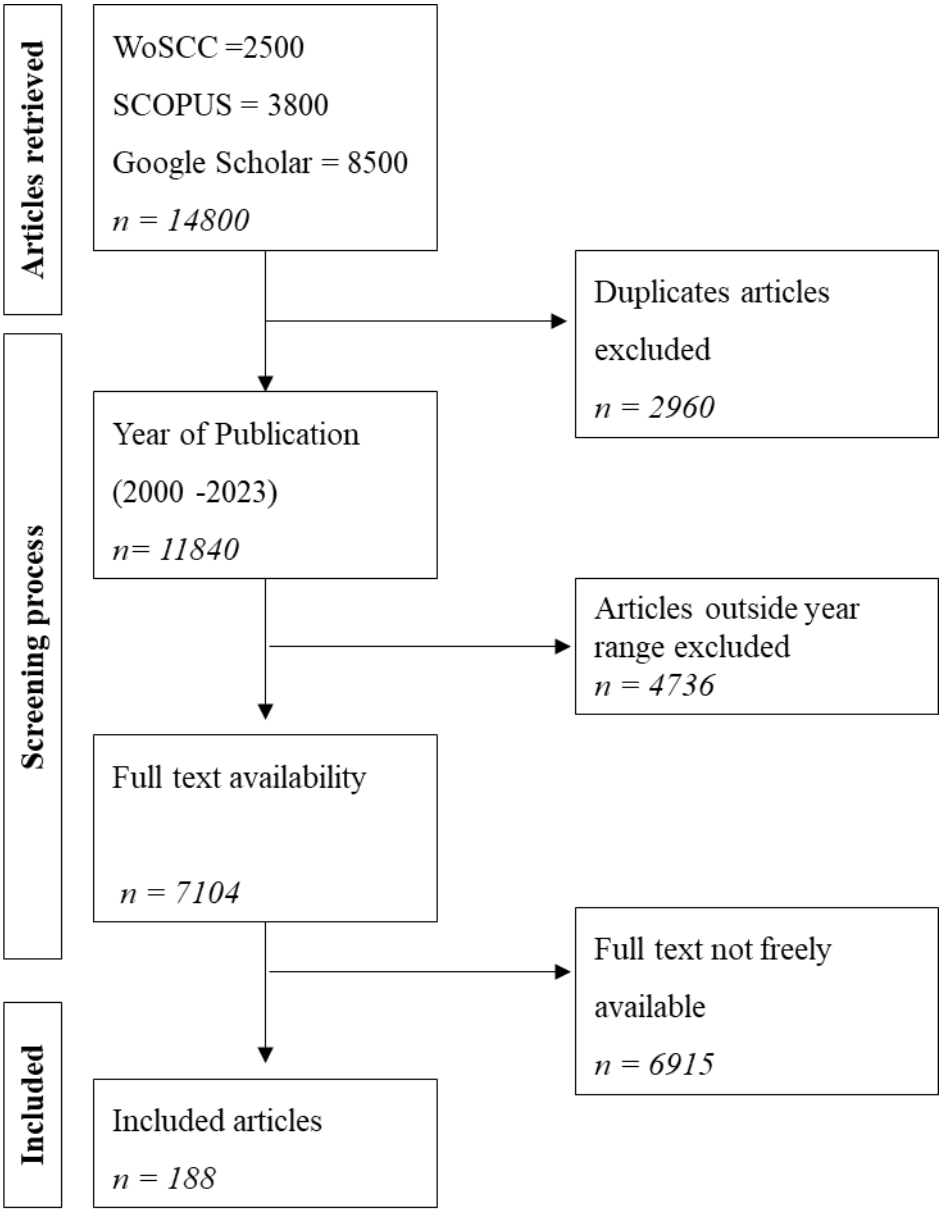

Figure 3.1 Flow diagram showing the selection of articles included in this review

The first stage of the screening process involved the removal of duplicates, given that the search query was the same throughout the databases chosen. After the exclusion of duplicate articles (n = 2960), the articles were screened by the year range (2000 -2023) of the review and a total of 4736 articles were excluded during this process. Further screening was conducted based on free accessibility. Consequently, a total of 6915 articles were excluded due to subscription requirements to access these articles. The remaining articles (n = 188) were downloaded and used in this review. The exclusion of articles based on the full text accessibility would have introduced some bias towards certain studies that have used certain models and remote sensing tools in their analysis.

3.3. Background on groundwater-dependent ecosystems and their classification

For this chapter, GDEs are defined as ecosystems that are maintained by direct or indirect access to groundwater and rely on the flow or chemical characteristics of groundwater for some or all of their water requirements (Rohde et al., 2017). This definition indicates the importance of groundwater in the sustainability and functioning of these ecosystems. During dry seasons, some wetlands in semi-arid and arid regions depend on the supply of groundwater to ensure the provision of ecological services and regulations (Thakur et al., 2012; Rampheri et al., 2023). In addition, when surface water bodies become depleted, phreatophyte vegetation draws water from saturated zones and is also sustained by groundwater when transpiration rates are high (Sommer & Froend, 2014). GDEs support a wide range of ecosystem services and are critical habitats that need to be included in the watershed-level policies and water resources management initiatives to build a sustainable ecosystem with the precise allocation of water resources (Pérez Hoyos et al., 2016; Shukla et al., 2022). However, due to the insufficient supply and over abstraction of groundwater, GDEs are threatened and hence the services they provide. Some of the ecosystem services provided by GDEs include, but are not limited to, water purification, active biodegradation of anthropogenic contaminants and inactivation and elimination of pathogens, carbon sequestration and the mitigation of floods and droughts. GDEs also have an intrinsic value for maintaining biodiversity and ecosystem functioning. As GDEs rely on groundwater to sustain all or some of their water requirements, particularly in arid and semi-arid climates, any alterations in the quality or quantity of groundwater also affect these ecosystems. Due to the growing threat that local and regional anthropogenic changes, together with climate change and variability, pose to aquifers and GDEs, the effects of anthropogenic climate change on groundwater and associated ecosystems have recently attracted a lot of attention (Rampheri et al., 2023).

Over the past century, there have been significant changes in the water cycle (Bierkins & Wada, 2019). Notably, the abstraction of groundwater for various water demands has increased from approximately 500 to over 3500 km^3 yr^{-1} within the past century (Kenikow & Kendy, 2005; Hanasaki et al., 2018; Lall et al., 2020), leading to a depletion of total groundwater available. Consequently, the over abstraction of this resource causes the loss of discharge from groundwater to GDEs, which results in the loss of ecosystem structure and function, resulting in the decline of services provided by these ecosystems (Orellana et al., 2012; Eamus et al., 2015; Chiloane et al., 2022). A study by Pritchett & Manning (2012), revealed that GDEs are vulnerable to water table decline, leading to losses in vegetation cover. Prolonged precipitation

due to climate variations results in groundwater recharge, thus leading to an increase in groundwater levels. Increased groundwater levels offer a reliable source of water, ensuring the long-term viability of GDEs even in arid climates (Rhode et al. 2021). Additionally, increased groundwater levels strengthen GDEs' resistance to drought and support their function as refuges for species during dry periods. Evaluating the effects of climate change on groundwater and dependent systems is challenging because of the complexity of these systems and the insufficiency of accessible data (Goderniaux et al. 2009).

A significant number of studies (Hanock et al., 2009; Serov et al., 2012; Gou et al., 2015; Eamus et al., 2015) highlight the importance of classifying GDEs into different classes to protect and manage them accurately. Several types of GDEs have been acknowledged in literature, and different classification systems have been proposed (Hatton and Evans, 1998; Clifton and Evans, 2001; Sinclair Knight Merz Pty Ltd, 2001; Colvin et al., 2007; Klove et al., 2011). Hatton and Evans (1998) was the first to classify GDEs into five categories namely, (i) obligate GDEs which are entirely groundwater dependent and can lose their complete ecosystem structure and function even due to small changes in groundwater availability, (ii) highly water-dependent GDEs in which small to moderate changes in groundwater availability result in significant changes in ecosystem structure and function, (iii) proportionally dependent GDEs which do not exhibit the threshold-type responses of obligate or highly dependent GDEs, (iv) opportunistic GDEs which are facultative users of groundwater, that is, only in the condition of low surface water flow or droughts, and (v) GDEs that only appear to be groundwater-dependent but are entirely rain fed or dependent only on surface water flows. However, Eamus et al. (2015) and Doody et al. (2017) noted that this classification lacks accuracy in the determination of the degree of dependency, and the presence or absence of threshold response is difficult to establish using this classification. Eamus et al. (2016) further categorised these ecosystems into three classes.

The classes proposed in Eamus et al. (2006) include: Class (i) characterised as aquifers and cave systems, Class (ii) characterised as ecosystems that depend on groundwater seepage to surface water and Class (iii) characterised as ecosystems that depend on the subsurface expression of groundwater. This ecosystem classification approach simplifies the differentiation and recognition of groundwater dependency, thereby enhancing the evaluation of ecological risks (Chiloane et al., 2022). However, Serov & Kuginis (2017) reported that the current available ecosystem classifications do not adequately address GDEs as a whole and are

ineffective in representing the range of GDE types. Additionally, the classification system by Eamus et al. (2006) relied on expert judgement, which makes it difficult to apply consistently.

3.4. Application of space-based observations in groundwater-dependent ecosystems assessment

GDEs assessment mostly relies on inference-based methodologies, which use indicators such as hydrological features, which comprise springs, wetlands, and baseflow, amongst others, as well as vegetation types and conditions of a certain period (Rohde et al., 2024). Such indicators are retrieved from satellite images ranging from coarse, medium to finer resolution datasets based on the sensing characteristics of the satellite sensor collecting a particular dataset (White et al., 2015; Wu, 2018; Bian et al., 2021). The commonly used data types and their characteristics (spatial and temporal resolution are presented in Figure 3.2. These data sources include freely accessible products such as Landsat series, Sentinel, as well as Moderate Resolution Spectroradiometer (MODIS), amongst others, while other commercial products include Quickbird, IKONOS, Aerial photography, and AVIRIS. The commercial satellites are mostly unsuitable for larger-scale and time series monitoring due to cost complexities associated with the acquisition of such data, particularly in resource-scarce regions like sub-Saharan Africa, therefore resulting in the increased use of freely accessible remote sensing products (Thamaga and Dube 2018; Ramperi et al., 2023; Pérez Hoyos et al., 2016a; Castellazzi et al., 2019).

The availability of freely accessible remote sensing data has been the most viable options, resulting in the increased use of these freely accessible satellite products (Doody et al., 2014; Guanter et al., 2015; Dash & Ogutu, 2016; Wu et al., 2021). Although this is the case, there are challenges associated with the use of these data types. These challenges include the spatial resolution of some of the data, which results in challenges with mapping the finest details of the GDEs indicators. For example, earlier studies such as Elmore et al. (2003) monitored vegetation responses to groundwater level changes because of climate variability in eastern California using cloud-free Landsat Thematic Mapper coupled with field-based vegetation surveys and time series groundwater data. Although the study reported acceptable accuracies of the vegetation responses to groundwater level changes derived from the remote sensing data used, there were some inaccuracies observed for some vegetation types attributed to the spatial resolution of the data used.

Advancements in remote sensing data, such as the introduction of new generation satellite products like Sentinel data (1&2) with improved spatial and spectral resolution, offer unprecedented opportunities to address challenges associated with the use of freely accessible remote sensing data in GDEs assessment and monitoring (Chiloane et al., 2020; Liu et al., 2021; Guo et al., 2015; Kiptala et al., 2013; Ndou et al., 2018; Noorduijn et al., 2019). These new generational satellite products have proved to be useful in delineating and assessing changes in the ecohydrological status of GDEs in various climatic zones Gow et al., 2010; Castellazzi et al., 2019; Liu et al., 2021; Rampheri et al., 2023a). However, for the smallest systems (< 10 ha) dominating in certain parts of the world, the use of single-source data products presents some challenges associated with the limitations of a particular product used. Therefore, necessitating, fusion of various data types to improve the delineation and monitoring of GDEs indicators from remote sensing data.

The introduction of advanced geospatial tools and platforms, such as Google Earth Engine cloud computing platforms, offers opportunities to further improve the delineation and monitoring of GDEs, through their specialized data fusion and filtering algorithms, as well as advanced machine learning techniques (Gorelick et al., 2020). Moreover, these platforms provide access to multiple data types and sources, thus simplifying the process of data acquisition (Mahdianpari et al., 2020). These platforms also allow the user to process the data in the cloud, therefore saving on data storage. Some of the studies that have used these platforms include a study by Ramperi et al., (2023), which utilized multisource remote sensing data coupled with an analytical hierarchical process in Google Earth Engine to delineate GDEs in the Khakea-bray transboundary aquifer system. The findings of the study underscored the relevance of these platforms in improving the delineation of the GDEs in the study, although there were noted overestimations in GDEs even in areas with deep groundwater. Another study by Fildes et al. (2023) mapped GDEs in the Leigh Creek area located in the north of Adelaide using multisource remotely sensed data coupled with an analytical hierarchical approach in Google Earth Engine cloud computing platforms. The findings of the study also underscored the relevance of the approach in spatial analysis of GDEs; however, there were some limitations, such as underestimation of GDEs in areas with depth to groundwater closest to the surface. Such limitations require an integration of the quantitative groundwater flow models to improve the representation of these systems, as these models tend to quantitatively assess the exchange of water between groundwater and surface water systems.

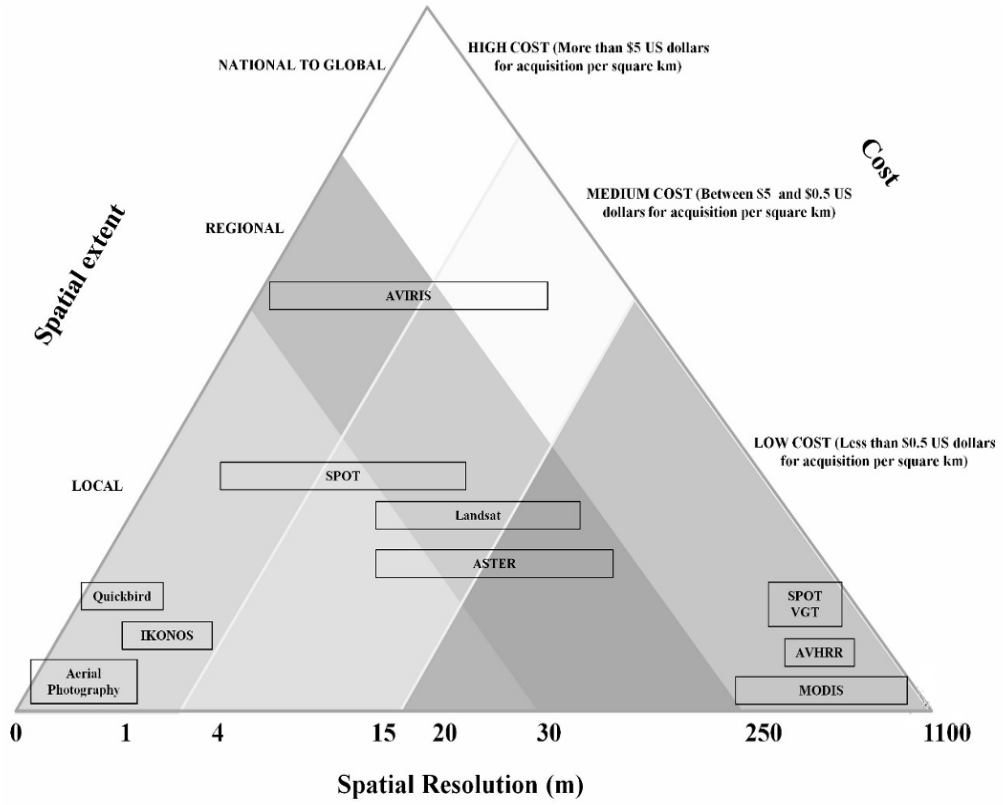

Figure 3.2 Satellite sensors commonly used for mapping and monitoring of GDEs (Pérez Hoyos et al., 2016a)

3.5. Overview of groundwater flow models applied in groundwater-dependent ecosystems assessments

Over the last five decades, many groundwater models have been used for groundwater management by researchers all over the world (Table 3.1). Groundwater flow models can be divided broadly into two categories, i.e., groundwater flow and solute transport models. Solute transport models solve for contaminant movement over time, while groundwater flow models solve for the spatio-temporal values of hydraulic head (Singh, 2014). For complex groundwater flow and contaminant transport systems, numerical models are mostly applied. The selection of a numerical method for a particular field problem depends on several factors, including accuracy, efficiency, and usability. The accuracy and efficiency of a model primarily depend on the availability of data and the scope of the research. Numerical models provide discrete solutions over the entire area that is being modelled, and use direct methods to perform approximations (Gxokwe, 2018). In numerical groundwater modelling, both the finite element and the finite difference approaches have been widely used (Singh, 2014). These approaches

use different sets of equations to solve groundwater flow systems. The dimension of the equations applied depends on the conditions of the aquifer that is being modelled.

3.5.1. Finite Difference Method

The finite difference method (FDM) is one of the oldest methods used in numerical modelling and has been made more useful with the advent of digital computers (Magnus & NJ, 2011). FDM solves the equations of groundwater flow using a grid-based approach, where the groundwater domain is divided into a finite number of rectangular grid cells. Within this model, each rectangle grid cell used has X, Y and Z co-ordinates and the hydraulic head is calculated within the centre of each grid cell (Spitz & Moreno 1996). FDM calculates variables (e.g., hydraulic head or pressure) at discrete grid points by solving algebraic equations derived from the discretised equations. This method is often used for larger-scale simulations, as they can be computationally efficient (Niswonger et al., 2004). MODFLOW is one of the most widely used finite difference models (Kumar, 2002; Zdechlik, 2016), because of its ability to simulate a wide variety of systems, its extensive publicly available documentation, and its rigorous peer review process. Other FDM models include MODPATH and MT3D, which are commonly used in contaminant transport analysis studies (Thoms & Johnson, 2005; Whittier & Maddock, 2006; Fan et al., 2011; Han et al., 2015; Behera et al., 2022; Rafiei et al., 2022). The advantages of FDM include easy data input, numerous facilities for data preparation, extended worldwide experience, availability of source code, and relatively low cost (Kumar, 2002). However, this method has low accuracy in some problems and regular grid (Gxokwe, 2018). Furthermore, it is difficult to apply the FDM when we encounter irregular geometries or an unusual specification of boundary conditions (Anderson and Woessner, 2002).

3.5.2. Finite Element Method

Finite Element Method (FEM) equations are more complex than those of the finite difference method. FEM solves equations by dividing the domain into finite elements that are defined by nodes (Anderson et al., 2015). In this method, the dependent variable (e.g. head) is defined as a continuous solution within elements. A FEM mostly uses triangles to discretize the area being modelled or quadrilaterals in 2D and tetrahedra or hexahedra in 3D. The finite discretisation procedure reduces the problem to one of a finite number of unknowns by dividing the solution region into elements and by expressing the unknown variable in terms of an assumed interpolation function within each element (Hueber et al., 2001). The FEM can formulate solutions for individual elements before putting them together to represent the entire problem.

Other advantages of the FEM include better treatment of thin sections and complex shape, and this method is very versatile, and its versatility can be contained in a single program (Gxokwe, 2018). However, the implementation of the FEM can be more complex, requiring expertise in mesh generation and numerical methods.

3.5.3. Available groundwater models for groundwater-dependent ecosystems assessments and applications

The application of groundwater flow models to large-scale aquifer system simulation began in the late 1970s, with the Regional Aquifer System Analysis (RASA) program of the US Geological Survey (Zhou, & Li, 2011). The use of 3D groundwater flow models has led to significant advances in the understanding of regional groundwater flow systems. Some of the applications of existing groundwater flow models include simulation of water flow and chemical migration in the saturated zone, including river-groundwater relations, assessing the changes of groundwater depth on ecosystems, setting up groundwater protection zones and monitoring networks, and gaining knowledge about the quantitative aspects of the unsaturated zone (Table 3.1). Recently these models have been used in understanding the emerging contaminants such as pesticides and pharmaceuticals in groundwater systems within various aquifer Although these models provided baseline knowledge to groundwater systems for different aquifers and served as an imported tool informing decision making process, they are field data intensive, and such data is scanty to non-existent for some regions due to cost complexities associated with the collection of such data particularly at regional scales (Condol et al., 2021; Ntona et al., 2022). Therefore, introducing data limitations during the implementation of such models. A study by Rodiger et al. (2023) simulated the water table of the Hashemite Kingdom of Jordan using the FEFLOW finite element method. The study reported that scarcity in some of the input data parameters has limited the calibration of the model. Another study by Gxokwe et al. (2020b) modelled the scenarios of water sensitive urban design, including managed aquifer recharge by wetlands and ponds in the Cape Flats Aquifer using the MODFLOW Finite Difference Method. The results demonstrated the potential of managed aquifer recharge during the summer season when the water table is deeper, using wetlands and ponds in the area. Although the study demonstrated such, there were some drawbacks during the calibration of the FDM model caused by the limited availability of water level data in the area.

Table 3.1 Summary of groundwater flow models applied in assessing GDEs

Study focus	Model	Results	Model validation method	Accuracy results	Limitations	Authors
This study used an integral flow modelling approach to simulate surface water-groundwater interactions along a ripple in stream bed.	HYDRUS-2D	The study revealed that surface water flow velocity, bedform geometry, and near-bed pressure significantly influence water exchange between streams and aquifers, with distribution strongly controlled by the hyporheic zone and water table depth.	Visual comparison of simulated and observed heads from other scholars	Good agreement observed between simulated and observed values for the calibrated model	The HYDRUS model was not able to simulate the effects of surface roughness, which can have a significant impact on stream-groundwater interactions.	Broecker et al., (2019)
This study examined the sensitivity of land surface evapotranspiration (ET) to water table depth, soil texture, and two commonly used soil hydraulic parameter datasets using four models with varying levels of complexity.	HYDRUS-1D	The results indicated a strong influence of water table depth on groundwater contributions to ET. Furthermore, the simulated ET was highly dependent on the depth to groundwater.	R^2 determinant	R^2= 0.96 – 0.98	Hydrus-1D consistently predicted a higher ETa/ETp ratio than IBIS. Especially for sand and clay, the difference was as high as a factor of two to three. This difference would have a major impact on regional energy and water balance predictions.	Soylu et al., (2011)
This study used various methods to examine the relationship between the depression wetlands and the underlying groundwater. The study used hydrogeological data, geophysical surveys, dye tracer tests, and water level monitoring to determine the groundwater connectivity of the wetlands.	VS2DI model	The study found that depression wetlands in the study area are hydrologically connected to groundwater, with topographic depressions being more connected than upland slopes, and their connectivity is influenced by geologic properties.	Visual comparison of simulated and observed heads from other scholars	Good agreement observed between simulated and observed values for the calibrated model	The models did not directly model ET, instead, the models used a recharge boundary in upland areas equal to net recharge, defined as precipitation less ET. The study did not simulate spatial heterogeneity in ET.	Neff et al., (2019)
This study used numerical models for predicting two-dimensional groundwater flow in the continental river watersheds based on the water budget in the watershed, and by regarding the effects of groundwater depth on vegetation change as the source/sink factors.	FEFLOW	The study found that groundwater levels decreased in the upper marginal zone of fans and increased in the alluvial-diluvial plains. This led to vegetation deterioration in the upper watersheds and increased soil salinisation in the lower plain	Root Mean Square Error	RMSE = 12 m for Hydraulic head residuals	The model did not account for changes in root water uptake or transpiration rates in response to changing groundwater levels, which may lead to the overestimation of the impact of groundwater level in the ea.	Zhao et al., (2005)

The study modelled future scenarios of the impact of climate change on surface and groundwater and surface water resources in Gareh Bygone Plain, southern Iran.	Runoff-nfall coupled with a MODFLOW-derived roundwater model	The results of the groundwater recharge modelling showed no significant difference between present and future recharge change due to climate change for all scenarios	R^2 determinant	R^2 = 0.82, residual difference between the simulated and observed hydraulic heads for the calibrated model.	Missing Evapotranspiration input data for the period of 1990 and 2021 was a limitation of the study	Hashemi (2015)
This study assessed the changes in important waterfowl habitats - protected wetlands situated in the impact zone of proposed dolomite mining.	FEFLOW	The study found that a decrease in groundwater level in a dolomite quarry wouldn't affect Lake Čedasas or riparian zones. However, combined with predicted climate change, it could impact nearby groundwater levels, affecting Lake Čedasas ecosystems	R^2 determinant	R^2= 0.90 when comparing simulated and observed hydraulic heads for the calibrated model	If lake water level changes are primarily influenced by surface water inflow and outflow, using the FEFLOW 5.0 model alone is inadequate. Instead, other models such as FEFLOW 6.0 or GSLOW versions are necessary to accurately simulate these changes.	Taminskas et al., (2013)
Submarine Groundwater discharge and stream baseflow sustain pesticide and nutrient Fluxes, Faga'Alu Bay, American Samoa	MODFLOW, M3TDMS	Analysis of baseflow contributions revealed that groundwater contributed 41% to the bay and about 9 ± 2 g/d of dichlorodiphenyl-trichloroethane was found in 85% of the samples collected both in Groundwater and the Bay	Root Mean Square Error, R^2 determinant,	RMSE = 12 m for Hydraulic head residuals and R^2 = 0.99	The model worked on a smaller scale, not tested on a larger scale due to field data	Welch et al., (2019)
Assessing the Transport of Pharmaceutical Compounds in a Layered Aquifer Discharging toa Stream	finite element method plemented in COMSOL	The pharmaceutical compounds migrate in both a deep semiconfined aquifer, as well as in the shallow unconfined aquifer, and enter the stream along a 2-km stretch. This contrasted with the chlorinated ethenes, which mainly discharge to the stream as a focused plume from the unconfined aquifer.	Root Mean Square Error, R^2 determinant	RMSE = 10 m for Hydraulic head residuals and R^2 = 0.98	The method relies on the assumption that the compounds migrate with groundwater and are not or only slowly degrading	Balbarini et al., 2024

The increase in availability of numerical models has offered more prospects to improve the assessment and monitoring of GDEs. These models, including amongst others HYDRUS, COSMOL, VS2DI, MIKE SHE and SWAT-MODFLOW have proved to be successful in predicting the extent and changes regarding quality and quantities of these systems over time at acceptable accuracies (Table 3.1). For example, a study by Prucha et al. (2016) developed a physically based MIKE SHE integrated groundwater and surface water model for the Mokolo River basin flow system to simulate key hydraulic and hydrologic indicator inputs to the downstream response to imposed flow transformation for an arid rivers decision support system. Although the study managed to match the observed and simulated hydraulic heads at an acceptable mean error, mean absolute error and root mean square error, calibration for the model presented challenges due to a lack of data on basic subsurface hydrogeologic characterisation. Other studies, such as Qiao et al. (2023); Shah et al. (2007); Soylu et al. (2011); and Balugani et al. (2017), used the HYDRUS model to study plant and soil water interaction in various climatic zones. These studies also reported challenges with model calibrations and simulations due to a lack of data on their input parameters. With the increasing availability of remotely sensed products, there is an opportunity to overcome challenges such as data scarcity, which limits the functionality of groundwater flow models in simulating GDEs.

3.5.4. Geospatial data integration for groundwater modelling and challenges

Groundwater resource management and modelling are hindered by the lack of high-quality data, particularly in arid and semi-arid regions where there are limited monitoring stations (Brunner et al. 2007; Singh 2014). When there is a lack of necessary extensive data required for model processing, the model outputs can either be under- or overestimated, therefore preventing it from being used as a reliable decision support tool (Kasahara & Hill 2006). The integration of remote sensing data with modelling techniques has proved to be an efficient tool in groundwater studies (Saraf and Choudhury 1998; Trabelsi et al. 2013). The integration of such techniques can provide a preliminary spatial distribution of the recharge zone. Large datasets on the hydrogeological framework, hydraulic parameters, hydrological stresses, and measured groundwater heads are required for groundwater basin modelling (Pathak et al. 2018). The amount of time needed for data preparation, processing, and presentation throughout the modelling process can be greatly decreased with a well-designed GIS database (Tsihrintzis et al. 1996). Faults and dikes, lithological changes, and the depth of magnetic features can be identified using airborne geophysical surveys (e.g. Doll et al. 2000; Jorgensen

et al. 2003). Using this knowledge can assist in the accurate conceptualisation of aquifer systems under study, therefore informing the accurate development of a reliable groundwater model. The integration of geospatial data with groundwater models can be achieved through three techniques: loose coupling, tight coupling, and embedded coupling (Ruthy et al. 2003). Most applications of GIS in groundwater modelling use the loose coupling technique (Gogu et al. 2001). This is because this approach allows these two complex systems to be developed and maintained separately, giving users the option to select specific software tools for each domain, improving data transfer, and simplifying model maintenance.

Various studies attest to the suitability of GIS applications in groundwater hydrology (Brunner et al. 2007; Brunner et al. 2008; Singh 2014; Pathak et al. 2018). Chenini and Mammou (2010) demonstrated the potential of GIS and remote sensing in numerical groundwater modelling by coupling a GIS ARCVIEW with MODFLOW in the development of a model for the arid Maknassy basin of Central Tunisia resources. The study found that the extent of groundwater connectivity to GDEs is strongly influenced by the permeability of the aquifer, the size of the groundwater system and the nature of GDEs therefore demonstrating the potential of integrating GIS into groundwater models in improving the monitoring and assessment of GDEs. While integrating GIS and groundwater modelling proved to be useful in GDEs monitoring and assessments, there were still limitations regarding this process of data integrations, and these include, amongst others, changes in the quality of the data fused, which may cause errors in during the modelling development, distortion on the data, particularly remotely sensed images, when merged with other data types (Mahdianpari et al., 2018; Gxokwe et al., 2020b).

The emergence of satellite missions such as Gravity Recovery and Climate Experiment (GRACE) and its advancements over time offer prospects to monitor subsurface water storage changes over time, including the dependency on shallow groundwater systems. The ability of the GRACE Satellite to measure variation in gravitational forces allowed for the determination of large-scale mass distribution, such as large groundwater depletion (Sun et al. 2012; Lakshmi 2016; Ali et al. 2021; Brunner et al. 2006). Data from this satellite mission has been successfully applied in various groundwater modelling studies, such as Rahaman et al. (2019). The study by Rahaman et al. (2019) simulated groundwater flow of the Colorado Basin using GRACE satellite dataset. The results underscored the relevance of GRACE GRACE-derived groundwater flow model to track long-term changes in groundwater storage in the basin; however, the study recommended the inclusion of other field-measured data like climate

variables to enhance the reliability of the model outputs. Another study by Singh et al. (2023) used GRACE data coupled with TerraClimate data to model regional groundwater changes in the Bundelkhand region of Uttar Pradesh, India, between the years 2002 and 2017. The results indicated major fluctuations in groundwater levels, with mostly groundwater depletion occurring around the year 2012. Although the study demonstrated the utility of GRACE imagery coupled with TerraClimate data to model groundwater fluctuations in the area, however, there were some uncertainties with the accuracy of some outputs caused by the coarse spatial resolution of the data used.

Improvements in the newly launched GRACE-FO after the initial GRACE twin satellites have been decommissioned in 2017, offer prospects to improve GDEs monitoring and assessments (Ali et al., 2021). With improved microwave ranging system, and improved resolution, the GRACE-FO has revolutionized the monitoring of groundwater systems, and most recent studies such as Castellazzi et al., (2024); Rohde et al., (2024), have demonstrated the applicability of this satellite data in GDEs assessments and monitoring in larger spatial extent, however its applicability at more localized extent still needs to be investigated. Moreover, the use of GRACE-FO data in the modelling of groundwater dependency still needs to be investigated.

3.6. Limitations of modelling approaches applied in groundwater-dependent ecosystems

Although studies targeted at understanding GDEs have increased, understanding the complex interactions between groundwater and surface water flow remains a challenge. Particularly in arid and semi-arid regions where there is limited surface water availability and high evaporation rates. Understanding the extent of GDEs is important for monitoring and conservation of these ecosystems; however, studies show that understanding the extent of GDEs fully remains a challenge. Modelling the interaction between GDEs and groundwater is a key research area that benefits their management by allowing the prediction of GDE response to different magnitudes, rates and seasons of groundwater drawdown, as well as different climatic scenarios (Eamus & Foen, 2006). An essential first stage in the development of a groundwater model is groundwater system conceptualisation (Anderson et al. 2015). As such, a robust and well-structured conceptual model is essential for ensuring the validity and reliability of a model's results (Gross 2003). However, finding relevant data for model testing remains a challenge (Enemark et al. 2019). GDEs often lack thorough data (Glanville et al. 2016), which makes it challenging to adequately depict the dynamics and components of the

ecosystem. Inadequate data about critical elements like aquifer properties, vegetation characteristics, and ecosystem interactions may significantly limit the level of accuracy of modelling efforts. The absence of detailed data about aquifer properties obstructs the ability to accurately delineate groundwater flow patterns and distribution, while insufficient data on vegetation and ecosystem interactions make it challenging to model the complex relationships between water availability and ecological processes. The relationship between the dynamics of water table levels and vegetation patterns is still being explored (Orellana et al. 2012).

GDEs are linked to the interconnections between groundwater and surface water. Accurately representing these interactions in models may be challenging (Barthel & Banzhaf 2016), particularly considering the changing conditions and variations in the water table. Accounting for varying water levels and their impact on the flow and availability of water in an ecosystem makes accounting for GW-SW interaction in groundwater models more challenging. The modelling process is further complicated by transient variables, such as seasonal changes and human impacts.

3.7. Future research prospects in the application of modelling approaches to groundwater-dependent ecosystems

Current studies conducted groundwater flow modelling rarely take the model's objective into account before creating substitute models for the multi-model strategy (Enemark et al. 2019). The construction of the model and the data applied for model testing should be influenced by the model's objective. Considering the complexity of the hydrogeological characteristics of GDEs, Enemark et al. (2019) suggest that increasing complexity effectively transforms uncertainty in the conceptual model into uncertainty in the parameters by increasing the number of processes in the model and/or the resolution in both space and time. The integration of GIS and remote sensing into groundwater modelling offers the potential to improve the way we study groundwater and dependent ecosystems (Gogu et al. 2001), by enabling the understanding of spatial analysis and visualisation of groundwater dynamics and dependent ecosystems. Technologies like sensor networks have the potential to improve our ability to gather data. These tools can improve our comprehension of the complex interactions between groundwater and ecosystems by providing real-time data. Due to the growing challenges that climate change poses in GDE assessments, future modelling prospects will require the inclusion of scenarios that take changing climate conditions into consideration. These scenarios are expected to involve changes in temperature and precipitation patterns, both of which can have significant impacts on groundwater levels, an essential element of GDEs. We can predict

how GDEs will react and adapt to the changing climate by including these climate change scenarios in the models. Moreover, these models will shed light on the dangers and weaknesses that GDEs can encounter when coping with the effects of climate change.

3.8. Conclusions

Groundwater modelling has become a commonly used tool for hydrogeologists to manage and monitor groundwater. This review highlighted the critical function of GIS-based models in assessing GDEs as their susceptibility to the impacts of climate change. The comprehensive analysis of literature reveals that GIS technology has significantly advanced our ability to understand and predict the responses of GDEs to changing climatic conditions. These models combine environmental variables, hydrological modelling, and spatial data to provide an effective tool for both researchers and decision-makers. However, there remain challenges and areas of improvement. The limitations that have been identified include difficulty with data access, where some of the higher resolution Earth Observation data are commercial and the freely accessible data have limitations in terms of their spatial resolution. However, data integration proves to be a solution to address the limitations of the freely accessible EO data. Although this is a solution, there are still challenges that would result from data integration, and these include, amongst others, image colour distortion, which may result in uncertainties in these model outputs. This study therefore recommends that future studies should focus on improving these EO-based models, which have been revealed to have potential in studying the dynamics of these systems. Such studies will promote the accurate monitoring of GDEs, therefore enhancing the development of policies governing the management and protection of these systems.

CHAPTER FOUR

GEOSPATIAL AND MACHINE LEARNING FRAMEWORK FOR DELINEATING POTENTIAL GROUNDWATER-DEPENDENT VEGETATION ZONES IN KRUGER NATIONAL PARK, SOUTH AFRICA

4.1 Introduction

Groundwater-dependent vegetation, identified as a type of groundwater-dependent ecosystem (Hatton and Evans, 1998), plays a crucial role in maintaining ecological balance. In arid regions, such as the KNP, dryland GDV holds substantial economic, ecological, and social significance. In KNP, GDV sustains wildlife by providing essential resources like water, habitat, and forage during prolonged dry periods. The conservation of these systems not only ensures the survival of wildlife but also supports socio-economic development through activities like eco-tourism (van Aardt *et al.*, 2020). Climate change and increased reliance on groundwater resources threaten groundwater availability for sustaining GDV. Besides research on the changes in groundwater use and availability, research in groundwater-dependent ecosystems, such as GDVs, has intensified over the past 30 years (Chiloane *et al.*, 2021; Link *et al.*, 2023). However, information on GDV ecohydrology is limited and pivotal for integrated resource management and achieving Sustainable Development Goal 15, targeting life on land (Mpakairi *et al.*, 2022). Understanding the distribution of GDV within arid landscapes is the initial step in acquiring information and developing knowledge on GDV species diversity and groundwater use characteristics, such as the extent and timing of their groundwater dependence.

Remote sensing has played a significant role in identifying GDVs in different environments and scales. The geographical information system (GIS) and analytical hierarchical processes (AHP) constitute a proven method for mapping potential GDV. The AHP technique serves as a multi-criteria decision-making tool, integrating various GIS and remotely sensed variables. A notable benefit of the AHP method is its inclusion of expert opinions in the assignment of weights to factors influencing GDV potential. For example, Duran-Llacer *et al.* (2022) indicated that rainfall and land use were the most important contributing parameters for delineating groundwater-dependent ecosystem zones (GDEZ) in Chile. Fildes et al. (2023) highlighted a substantial level of concordance with identified spring locations (77%) and known phreatophytes, as well as groundwater depths (87%) in their assessment of GDE potential through the utilisation of vegetation indices, coefficient of variation statistic, and

other parameters employing AHP. While the integration of GIS and AHP proves to be dependable and effective, the process may entail a considerable amount of time for variable acquisition, occupy storage space, and exhibit inefficiencies (Hoyos *et al*., 2016; Zhaoming, 2020; Chiloane *et al*., 2021; Glanville *et al.*, 2023).

On the other hand, the introduction of machine learning and cloud computing has proven to enhance the delineation of GDV. Notably, the GEE cloud platform stands out by providing an extensive array of readily available geospatial data archives, including Sentinel 2 data, along with tools and advanced technical computing resources. This integration facilitates seamless, rapid, and reproducible classification of GDV (Pekel *et al.*, 2016). Classifiers such as support vector machines (SVM), random forests (RF), and classification regression trees (CART) exhibit significant potential in the delineation of GDV. Hoyos *et al.* (2016) devised a method for mapping GDV potential based on known GDE locations and three influencing factors, employing classification trees (CT) and RF, and found that RF (AUC = 1, accuracy of 0.88, and kappa of 0.96) demonstrated a superior ability to generate GDE probability estimates compared to CT (AUC =0.74, accuracy of 0.99, and kappa of -0.38). The optimal performance of RF could be attributed to its ensemble learning nature, where subsets of trees contribute to the overall prediction, resulting in a more robust and accurate model than a single tree. Additionally, RF introduces randomness in the data, reducing noise and mitigating model overfitting. In a similar study, Al-Fugara *et al.* (2020) compared machine learning models for mapping potential GDEs, and noted optimal accuracies of 83.2% for the mixture discriminant analysis (MDA), 80.6% for the RF, 80.2% for SVM, 78% for the boosted regression trees, and 75.5% for the multivariate adaptive regression spline (MARS). These results underscore the significant potential of machine learning models in delineating GDE potential. Furthermore, it is suggested that an ensemble of machine-learning models could further enhance the mapping of GDV potential.

Machine learning models yield varying outcomes due to their distinct assumptions regarding input data and algorithmic architectures. Consequently, no single classifier is inherently superior. Stacked ensemble models enhance classification performance by integrating the classification strengths of multiple models while mitigating their weaknesses, thereby yielding a superior model (Mudereri *et al.*, 2020; Mtengwana *et al.*, 2021). For instance, in a study by Yao *et al.* (2022), the performance of CatBoost, RF, XGBoost, and a stacked ensemble comprised of these models was evaluated for vegetation mapping. Their findings revealed that the stacked ensemble outperformed the individual models, resulting in an increase in overall

accuracy from 77% to 92%. Similarly, Zhang *et al.*, (2023) classified karst wetland vegetation using four algorithms, including a stacking ensemble. The accuracies of the models ranged from 82% to 93%, with the stacking ensemble demonstrating improved classification results.

Given the significant potential of both machine learning and the traditional AHP method, current studies lack a comprehensive comparison of their capabilities in modelling the potential distribution of GDV zones. Furthermore, no specific suitable model has been applied in different environments exhibiting optimal accuracies. Therefore, there is a need to compare and assess the performance of the traditional AHP and the ensemble stacking machine learning approach in characterising GDV. Thus, this study aimed to address this gap by presenting a detailed exploration of both the AHP and machine learning approaches, followed by a comparison of the results obtained from these two models. Identifying the most efficient and robust methodology for identifying GDV potential areas within the KNP, South Africa, will assist in developing integrated resource management strategies. Furthermore, the identified and proposed method will be adaptable to various semi-arid environments and will have the potential to guide sustainable management practices in conservation areas through the establishment of a continuous monitoring framework for GDV. Ultimately, this method is poised to offer valuable insights into the spatial dynamics of GDV, contributing to a more informed and proactive conservation management strategy.

4.2 Materials and methods

4.2.1 Field data collection

The field survey was conducted in September 2022 (late dry season), when the pans were mostly dry, with a few inundated pans being found in the Makuleke section. The sampling period was selected to easily discriminate vegetation and pans maintained by groundwater from those that are not. Pans with water surrounded by green vegetation during the late dry season are likely to be receiving groundwater. Field plots were randomly sampled within KNP. These sample plots were distributed along natural pans at the Makuleke and Letaba areas within KNP. The centre of the plot was navigated using a handheld Garmin geographic positioning system (GPS) with less than 5m. The north-oriented plots were set to measure 100 m^2 (10 × 10 m), moreover, this corresponds to the Sentinel-2 imagery resolution. Vegetation surveys were conducted in the plots to determine plant species composition and abundance across the GDVpz. A high-resolution image (5 m) matching the date of the site visit was used to obtain additional training points. Overall, 355 points represent two classes, namely, high GDVpz

(green hotspot) and very low GDVpz. These points were separated into two sets, 80% training set and 20% testing set, which was used for model validation.

4.2.2 Identification of potential groundwater-dependent vegetation

To identify potential GDVpz within the study area, the process involved the following sequential steps: conducting a literature review, performing a field survey for data collection and training dataset generation, creating a GIS database, predicting GDVpz, and validating the outcomes. The literature highlighted the importance of geomorphology, vegetation productivity (multi-spectral indices and their derivatives), topography and climate as the major factors influencing the spatial distribution of GDVpz (Rohde *et al.*, 2017; Klausmeyer *et al.*, 2018; Brim Box *et al.*, 2022; Duran-Llacer *et al.*, 2022; Fildes *et al.*, 2023; Rampheri *et al.*, 2023). Thus, the selected GDVpz predictor variables were drainage density, elevation, and lineament density, slope, proximity to water bodies, topographic wetness index, normalised difference vegetation index, normalised difference vegetation index standard deviation, land cover, vertical curvature, and soil texture.

The long-term dry season trend in rainfall for the KNP was acquired to determine which years were dry and suitable for GDVpz delineation. The long-term annual dry season rainfall trends for the area of interest were acquired from the Climate Hazards Group InfraRed Precipitation with Station data (CHIRPS), which is a 30+ year quasi-global rainfall dataset. This dataset incorporates 5.3km spatial resolution satellite data with ground data to produce gridded rainfall time-series data. From this data, a 30-year rainfall mean (1993-2023) was calculated, and the annual dry-season rainfall averages were subtracted from the long-term dry-season mean. This was done to calculate the yearly rainfall deviation trend.

The computation of various topographic and hydrological parameters was conducted within the ArcMap environment utilising the 30m Shuttle Radar Topography Mission (SRTM) imagery sourced from the GEE repository, with the designated path (ee. Image((USGS/SRTMGL1_003)). Drainage density, indicative of groundwater availability, was derived by calculating the total stream length divided by the overall area. Areas exhibiting high drainage density are presumed to undergo groundwater recharge. Lineament density, associated with fractures and fault zones, reflecting enhanced secondary porosity and permeability, and consequently greater groundwater availability, was determined through visual and manual analysis of variable hillshade images in ArcGIS. Proximity to water bodies (Pwb) was assessed to gauge groundwater availability, wherein water areas, likely recharged

by groundwater, were identified. The Euclidean distance tool in ArcGIS was employed to ascertain the proximity of vegetation to these water bodies. The topographic wetness index (TWI) was used to discern water availability based on terrain profiles, with areas prone to water accumulation inferred as likely recipients of groundwater recharge. The TWI was calculated according to Beven and Kirkby (1979) in ArcMap.

Slope, elevation, vertical curvature and Gaussian curvature were derived from a 30m SRTM image in the GEE repository with the path (ee. Image((USGS/SRTMGL1_003)). These parameters were derived on the GEE platform according to the code by Safanelli *et al.* (2020). Areas with gentle slopes (< 3m) at low elevations are low-flow zones with high groundwater availability. Vertical curvature is a form attribute indicating groundwater availability for water bodies and vegetation, as depressions are accumulation zones.

Landcover features were obtained from the Copernicus Global Land Cover Layers: CGLS-LC100 Collection 3, with a 100m spatial resolution and 80% accuracy. The layer was derived from Sentinel-2 images (2015-2019) accessed through the GEE path, ee. ImageCollection ("COPERNICUS/Landcover/100m/Proba-V-C3/Global"). The built-in function for the selection of images in GEE to select the “discrete classification” to obtain the final landcover layer. Landcover affects hydrological features such as runoff and, percolation, subsequently, groundwater availability and provides information on the spatial distribution of surface features such as vegetation, wetlands, and rivers, hence included in this study.

Soil characteristics such as soil texture affect water percolation and soil permeability, subsequently influencing groundwater availability for GDVpz. Therefore, soil texture was also considered as a predictor variable for GDVpz. The iSDAsoil USDA Texture Class dataset provided soil USDA texture class information at depths of 0-20 cm and 20-50 cm, which was obtained and utilised as a predictor variable. The soil texture was derived at 30m pixel size using machine learning techniques coupled with remotely sensed data (Sentinel 2 and Landsat 7/8 images) and a training set of over 100,000 analysed soil samples.

The Sentinel-2 dataset from years 2018, 2019, and 2022 was acquired from the GEE repository. These years were chosen because of the low annual rainfall, which was below the annual mean precipitation for the area over the past 30 years. A total of twenty-one (21) cloud-free images were obtained and averaged using the mean reducer function to produce a single image with 23 bands. The Near Infrared (NIR), and Red bands were then selected to calculate the NDVI).

The standard deviations were also derived by applying the in-built function for computing standard deviation in GEE. These were computed on the previously computed NDVI layer.

4.2.3 A classification framework for delineating groundwater-dependent vegetation potential zones

To delineate GDVs potential zones, the remotely sensed images were first re-projected to the WSGS 1984 coordinate reference system and resampled to 20 m using the in-built reprojection function as well as the Nearest Neighbour approach in GEE. This was done to ensure that all layers had the same pixel size and coordinate system before creating an image stack. The 20m pixel size was used instead of 10m because of the computational limitations on the number of pixels when exporting an image on GEE. The composite image was created using the add bands function in the GEE. After that, three machine learning classifiers were employed for modelling the GDVpz; these included Random Forest (RF), Support Vector Machine (SVM) and Stochastic Gradient Tree Boosting (SGTB) (Figure 4.1). These classifiers were trained using the training function in GEE, and these were then used to classify the composite image in GEE. The SRF and SGTB classification models had 300 trees. Subsequently, a stacked ensemble comprising three models (SRF, SVM, and SGTB) was generated to create a robust model for GDVpz, enabling comparison with the AHP model. The binary classification results were converted into probabilities, using then the probability maps were further reclassified into five classes of probabilities, namely, very Low, low, medium, high and very high. The area of each probability was also calculated during this process.

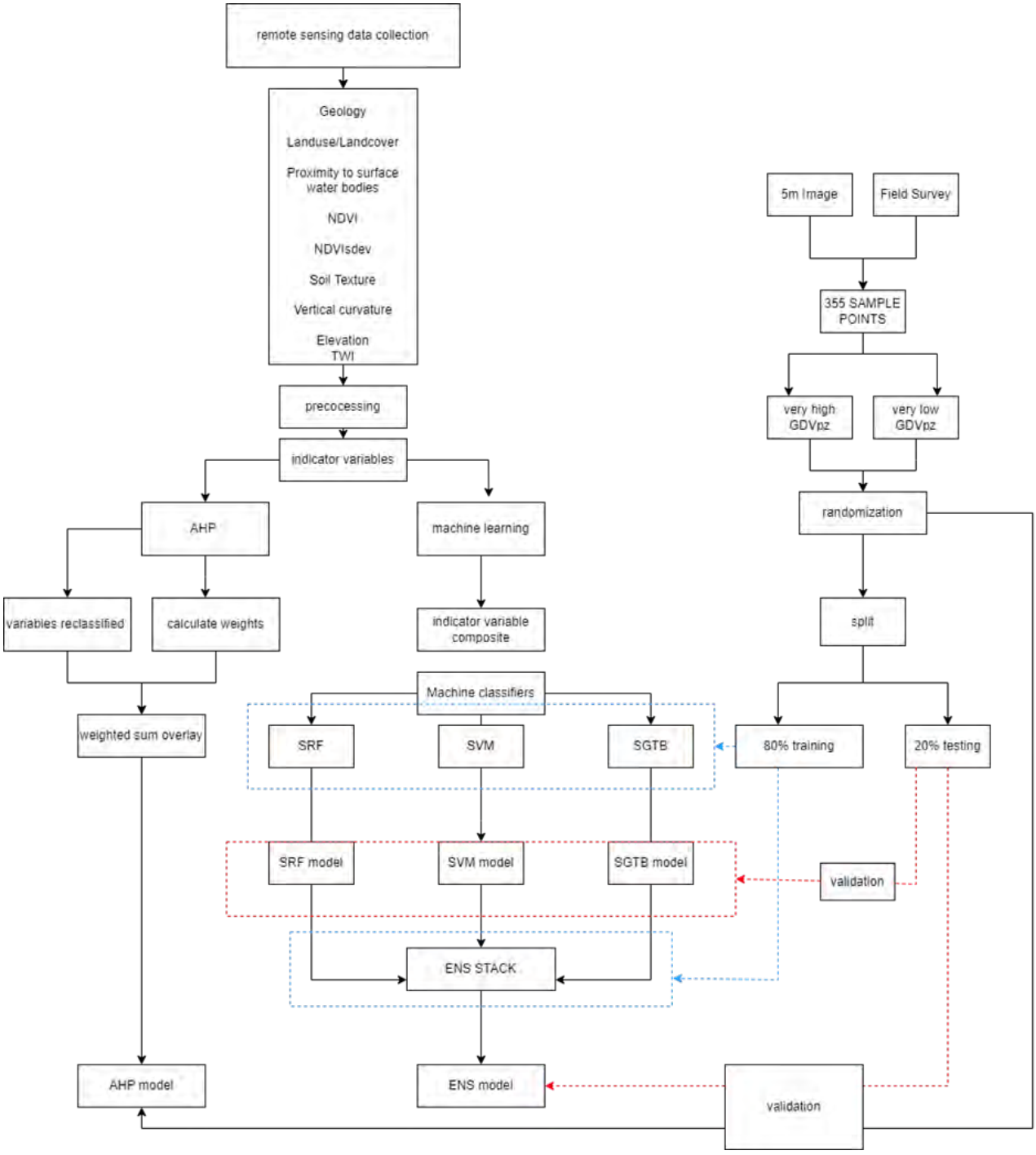

Figure 4.1 Process flowchart for mapping GDVpz within the Makuleke and Letaba regions of KNP

4.2.4 Analytical hierarchy process classification framework

To implement the AHP approach, the eleven variables (i.e. NDVI, NDVIsdev, vertical curvature, slope, elevation, TWI, drainage density, lineament density, soil texture, proximity to water bodies, and land cover) were employed in the machine learning models for

reclassification into five classes using natural breaks in the ArcGIS environment. Weights were then assigned to these predictor variables based on their respective degrees of influence on the potential for an area to be GDV, utilising the AHP. The AHP method was chosen due to its reliability as a multi-criteria decision-making tool, particularly in GDE research. The AHP scale, ranging from 1 to 9 according to Rampheri *et al.* (2023), was applied. The weights were modified and allocated in a manner that ensures an appropriate consistency ratio. A pairwise comparison was conducted between variables to assess their influence on GDV potential zones (GDVpz). Subsequently, all thirteen explanatory variables were amalgamated into a weighted sum overlay and each variable was assigned a weight (Table 4.1).

Table 4.1 Pairwise comparison matrix for assigning variable weights

Factors	NDVIsdev	DD	VC	ST	PwB	LC	LD	TWI	S	E	MeanNVDI
NDVIsdev	1.00	1.00	1.00	1.00	1.00	1.00	7.00	1.00	1.00	1.00	1.00
DD	1.00	1.00	1.00	2.00	1.00	1.00	5.00	1.00	2.00	2.00	1.00
VC	0.50	1.00	1.00	1.00	1.00	0.50	7.00	1.00	2.00	0.50	0.50
ST	1.00	1.00	1.00	1.00	0.33	1.00	5.00	1.00	2.00	5.00	1.00
PwB	1.00	1.00	1.00	3.00	1.00	1.00	7.00	1.00	3.00	2.00	1.00
LC	0.33	1.00	2.00	1.00	1.00	1.00	5.00	1.00	2.00	1.00	1.00
LD	0.14	0.20	0.14	0.14	0.14	0.11	1.00	0.14	0.33	0.20	0.14
TWI	1.00	1.00	1.00	1.00	1.00	1.00	5.00	1.00	1.00	2.00	1.00
S	0.50	0.50	0.50	0.50	0.20	0.50	3.00	1.00	1.00	1.00	1.00
E	0.50	0.50	2.00	0.20	0.20	1.00	5.00	0.50	1.00	1.00	1.00
MeanNDVI	1.00	3.00	2.00	1.00	1.00	3.00	7.00	1.00	2.00	2.00	1.00
Criteria weight (%)	**9.00**	**11.00**	**8.00**	**11.00**	**13.00**	**10.00**	**1.00**	**10.00**	**6.00**	**7.00**	**14.00**

Principle Eigen value (L.max) =11.74
Number of variables (n) =12
L.max - n = 0.74
n - 1 = 10
Consistency Index (CI) = 0.07
Consistency Ratio (CR) = 0.049

Random Index (RI) = 1.51

** E: elevation, LC, landcover, S; slope, VC: vertical curvature, DD: drainage density; S: soil texture, TWI: topographic wetness index, PwB; proximity to water bodies

4.2.5 Model accuracy assessment for the groundwater-dependent vegetation potential zones

To evaluate the performance of the classifiers, four accuracy assessment measures were quantified. These are the Overall Accuracy (OA), Kappa coefficient of agreement, F-Score, producers', as well as users' accuracy. The OA is quantified as the ratio of correctly classified points to the total number of test sample points. The producer's accuracy illustrates the probability that the reference sample is correctly classified on the map, while the user's accuracy indicates the probability of the reference sample being true on the ground. The Kappa coefficient indicates the level of agreement between the classification and the reference data. The accuracy assessments were executed on the GEE code editor using the ground control points representing GDVs zones from field analysis were used to extract regions corresponding to the locations of those points, and these were then used to compute the confusion matrix in GEE. The confusion matrix was then used to calculate the producers' and users' accuracies, Kappa coefficient, as well as F-Scores.

4.3 Results

4.3.1 Annual dry season rainfall trends from 1993 to 2023

The mean annual rainfall during the dry seasons from 1993 to 2023 was 39.67mm per year. Therefore, years with annual rainfall averages below the observed mean were considered dry years suitable for predicting GDVpz. Specifically, the years 2018 (with 38.9mm per year), 2019 (with 27.7mm per year), and 2022 (with 32.3mm per year) experienced rainfall below

this long-term mean and fell within the range of Sentinel 2 data (Figure 4.2). This period of ow rainfall coincided with the 2016-2022 drought, which was induced by the El Niño phenomenon.

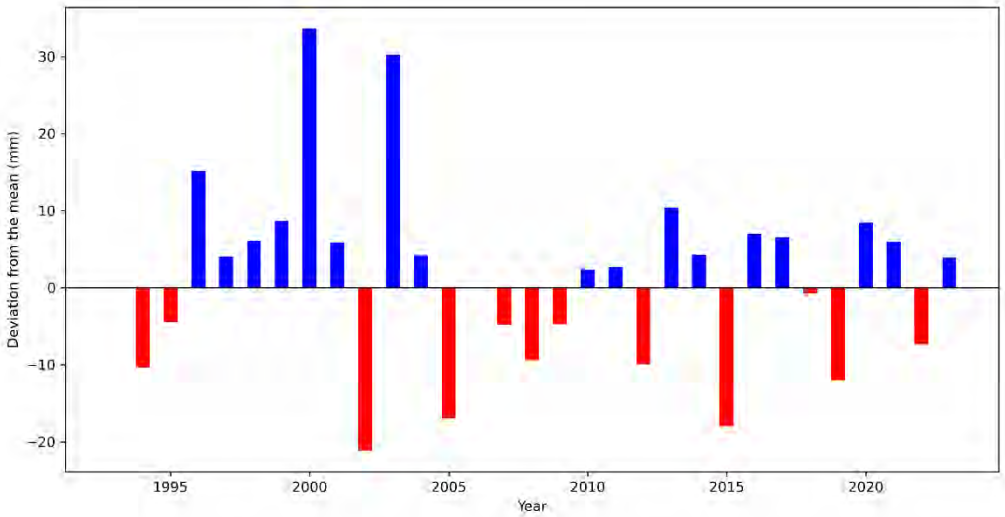

Figure 4.2 Long-term dry season rainfall trend in the Makuleke and Letaba regions of the KNP, South Africa

4.3.2 Classification accuracy results

The overall classification accuracy results ranged from 97% to 99%. The ensemble stack (ENS-stack) model performed the best with an overall accuracy of 99% followed by the SRF and SGTB models, which obtained an OA of 98%. The NB produced the lowest OA of 97%. In terms of the Kappa coefficient (Figure 4.3). The SGBT and ENS-stack models showed the highest level of agreement with a kappa of 97%, followed by the SRF (96%), and SVM model (93%). The F-score, producers and consumers classification accuracies were also computed for the GDVpz models; these were based on the two classes: very low GDVpz, and very high GDVpz. In terms of the producer's accuracy, all four models performed the same, with 96% accuracy for predicting the very high GDVpz and 100% accuracy for very low GDVpz (Table 4.2). Consumer accuracies for the very low GDVpz differed, with the ENS-stack model performing the best (98%), followed by both the SGTB and SRF models (97%), and then the SVM model (95%). Users' accuracies were 100% for the GDVpz classes across all the models. F-scores were similar for the SGT, SRF and ENS-stack models, with 98% for the very high GDVpz class and 99% for the very low GDVpz class. The SVM model had different results with an F-score of 96% and 97% for the very high and very low GDVpz models, respectively (Table 4.2).

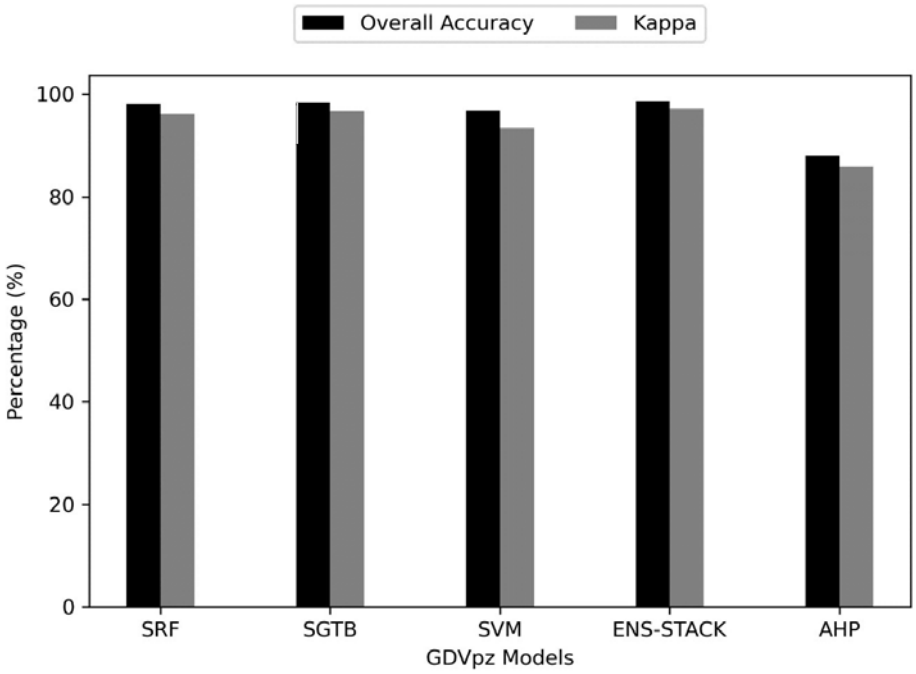

Figure 4.3 Overall accuracy, and Kappa for the GDVpz classifications. SRF- Smile random forest, SGTB- smile gradient tree boosting, SVM- support vector machines, ENS-STACK-ensemble stack, AHP- analytical hierarchal processing

Table 4.2 Producers' and users' accuracy for the groundwater-dependent vegetation potential zone classifications

		Producers' accuracy	Consumers' accuracy
SRF	Very high GDVpz	96	100
	Very low GDVp	100	97
SGTB	Very high GDVpz	96	100
	Very low GDVpz	100	97
SVM	Very high GDVpz	92	100
	Very low GDVpz	100	95
ENS- stack	Very high GDVpz	96	100
	Very low GDVpz	100	98
AHP	Very high GDVpz	97	78
	Very low GDVpz	82	97

4.3.3 Variable Importance

The SGBT and SRF algorithms provide valuable information highlighting variable contributions to the GDVpz model (Figure 4.4). For the SGBT model, the top three important variables were NDVI (26%) and PWB (17%) and DD (11%). The important variables for the SRF model were NDVI (28%), LC (11%) and NDVIsdev (12%). The mean NDVI emerges as the primary variable across all three models, likely due to the training data being obtained from green areas. Conversely, soil texture appears to have minimal impact on the machine learning models but significantly influences the AHP model. The overall assessment of variable importance reveals distinctions and similarities that impact the output of the models.

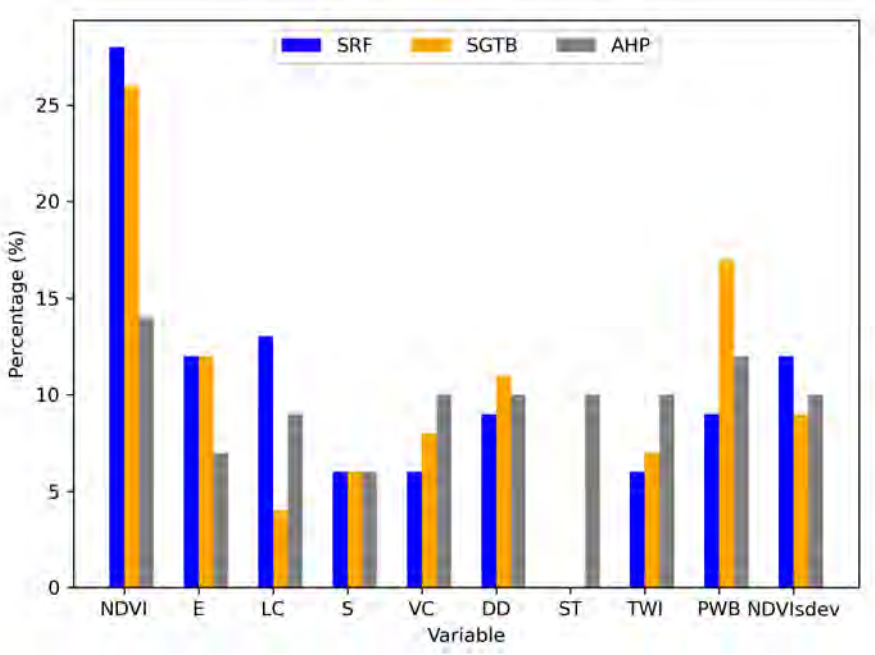

Figure 4.4 Classification variable importance for the GTB and RF classifications. Were, E: elevation, LC, landcover, S; slope, VC: vertical curvature, DD: drainage density; S: soil texture, TWI: topographic wetness index, PwB; proximity to water bodies

4.3.4 Spatial extent and distribution of groundwater-dependent vegetation potential zone

The very low GDVpz class is dominant for all the models. The very high GDVpz areas cover 6.9-9.5% of the study area. The ENS-stack model predicted high GDVpz area coverage compared to the other three models. Indicating that the model favoured the extreme classes of very low GDVpz and very high GDVpz. This is attributed to that the ENS-stack model integrates the outputs from all three machine-learning models. The four models indicate a similar trend in class distribution, with the very low GDVpz class dominating, followed by the

low GDVpz class, then the very high GDVpz class, the medium GDVpz class and lastly the high GDVpz class (Table 4.3).

Table 4.3 The spatial extent of different groundwater-dependent vegetation potential zone probability classes

	SRF	SGTB	SVM	ENS	AHP
Area (km2)					
Very Low	1407	1594	1214	1887	295
Low	360	295	518	64	607
Medium	174	78	202	24	700
High	96	65	105	7	446
Very High	151	157	150	207	136
Total Area	2189	2189	2189	2189	2184

Variations exist in the spatial distribution of GDVpz across different spatial class categories for the SRF, SGTB, and SVM models (Figure 4.5). For instance, in the central-eastern area of the Mahuluke region, zones categorised as low GDVpz by the SGTB model are classified as moderate GDVpz according to the SFR model and fluctuate between very low and moderate GDVpz based on the SVM model. These differences stem from variations in the importance of variables used in each model. In the Makuleke region, areas with very high GDVpz are concentrated along the riparian zones. Conversely, in the Letaba region, very high GDVpz zones are situated in the southeastern and central northern regions. The class distribution indicated by the SRF model suggests a gradual decrease in GDVpz probability as it extends from the areas with very high GDVpz. On the other hand, the SVM model displays less distinct class discrimination for both the Letaba and Makulule areas, appearing to be vaguer in its classification.

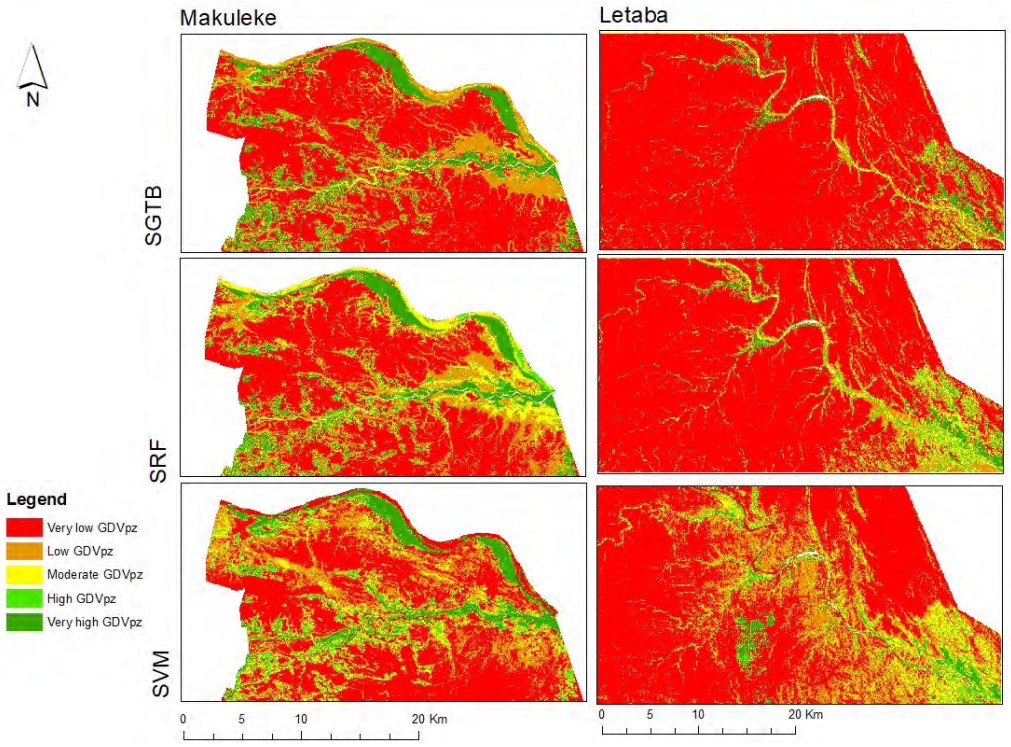

Figure 4.5 Machine Learning predictions of groundwater-dependent vegetation potential zones along the Makuleke and Letaba region of KNP

Visually, noticeable distinctions are apparent in how the AHP and ensemble stack models depict the spatial distribution of GDVpz (Figure 4.6). The ensemble stack model determined the very low GDVpz class as dominant, whereas the AHP model emphasises the dominance of the moderate GDVpz class. In general, the AHP model overestimated areas with very high to high GDVpz when compared to the ensemble model. According to the ensemble model, regions with very high GDVpz are primarily situated along riparian areas, with sporadic patches in the southwestern region of Makuleke. In contrast, the AHP model places very high GDVpz along riparian zones, and the GDVpz probability decreases with distance from rivers in both the Letaba and Makuleke regions situated along riparian areas, with sporadic patches in the

southwestern region of Makuleke. In the Letaba region, very high GDVpz are concentrated along riparian zones in the southeastern region.

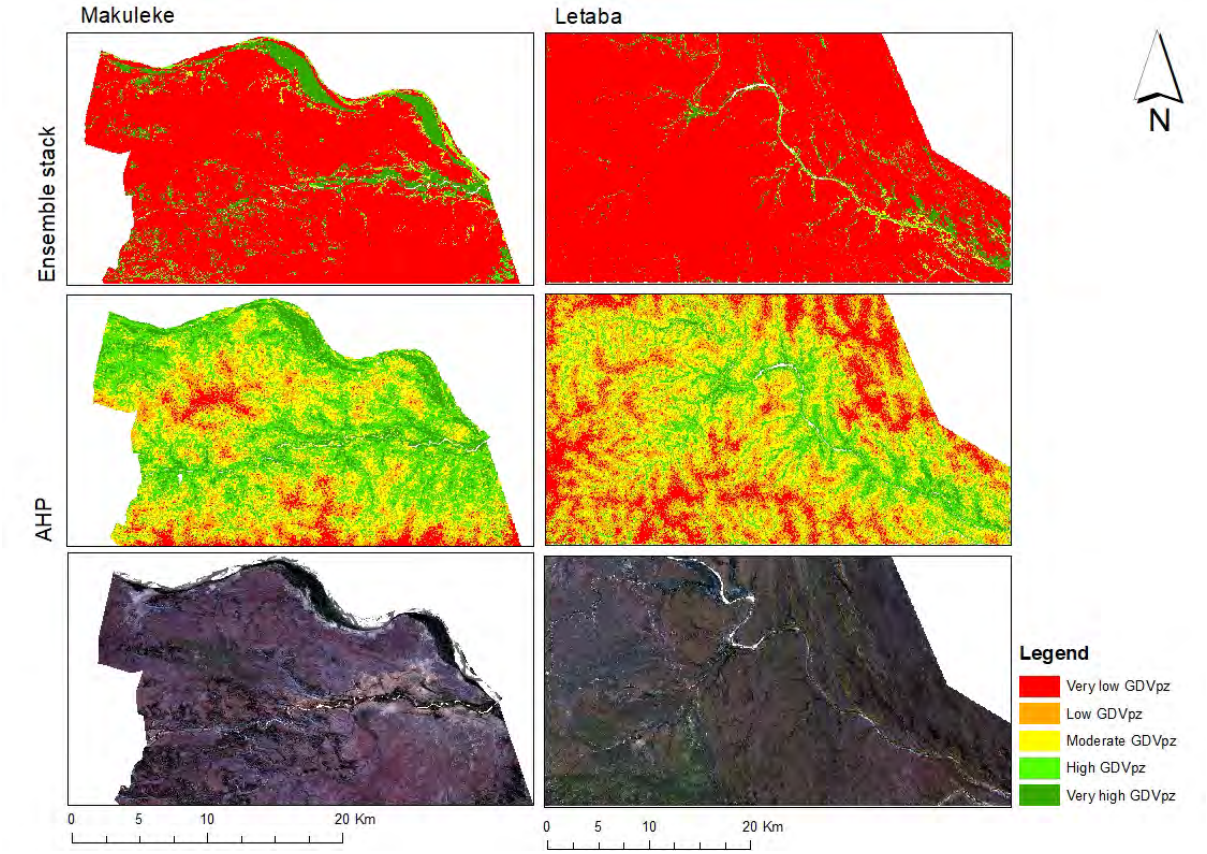

Figure 4.6 Comparison of the analytical hierarchal and process and ensemble stack probabilities of GDV potential zones along the Makuleke and Letaba regions of KNP

4.4 Discussion

4.4.1 Groundwater-dependent vegetation potential zones classification accuracy

This study aimed to assess the potential for GEE machine learning algorithms for modelling groundwater-dependent vegetation potential zones. In addition, the study evaluated the ensemble stacked machine learning model against the more subjective multicriteria decision-making tool, the AHP technique. The model performance for predicting the spatial distribution of GDVpz was high for all three ML models, with overall accuracies above 95%, with limited differences in terms of the producers' and consumers' accuracies, and kappa results. Among the three individual ML classifiers, the SVM model performed the least in terms of all the accuracy tests. This is also illustrated by higher errors of omissions (8%) for the very high GDVpz class exhibited by SVM in comparison to the 4% of the SRF and SGTB classifiers.

The errors of omission are easily observed in the southeastern regions of the Makuleke wetland system as well as the eastern region of the Letaba area. This may be because SRF and SGTB can capture complex, non-linear relationships in the data. They can handle intricate interactions and dependencies among various features, which is essential when dealing with the nuanced and multifaceted nature of GDV. Moreover, the GDV data is imbalanced; SRF and SGTB handle imbalanced data better than SVMs, which may require additional techniques like class weighting or resampling to address the imbalance. The machine learning stacked ensemble has been proven to improve classifications by merging models from primary classifiers into a more accurate secondary classifier (Adede *et al.*, 2019). Thus, the ensemble model of the SRF, SGTB and SVM models was produced and compared against the AHP classification model. The ensemble model performed better than the primary classifiers in terms of the overall accuracy and consumer accuracy; however, in terms of the kappa coefficient and producer accuracy, the ensemble models had similar results to the SRF and SGTB models. These model results are in line with previous research. As an example, the outcomes of the AHP model align with findings in the study conducted by Fildes *et al.*, (2023), demonstrating an 87% agreement between the modelled groundwater-dependent vegetation (GDV) and identified phreatophytes. The AHP classification results were the lowest when compared to the primary ML classifiers and the ensemble classifier. This may be attributed to that the model was based on the weighted variables with no input from the training data, while the ML classifiers incorporated the variables as well as model training. In general, all the models exhibited strong performance, however, the results suggest that machine learning represents a superior option for delineating potential groundwater-dependent vegetation.

4.4.2 Groundwater-dependent vegetation potential zones spatial distribution and areal coverage

The very low GDVpz class dominates the ML classifications, while the AHP classifier distributes the area between the low, moderate and high GDVpz classes. Differences in model areal distribution may be attributed to the classification technique employed. The ML models were based on binary training data (very high GDVpz and very low GDVpz) based on vegetation greenness during the dry season, as well as GDVpz indicator variables. The AHP method, however, relied on the weight of the GDVpz indicator variables, which allowed the GDVpz prediction to be varied between classes, while the ML classifications are likely to favour the two extremes. The spatial distribution of very high GDVpz is concentrated along the rivers, suggesting that groundwater-dependent vegetation may be riparian. The ML models

were also able to capture some isolated GDVpz scattered along the eastern side of the Letaba River. This shows that the models may be efficient in mapping GDVpz in extremely dry areas. In the Makuleke wetland system, GDVpz are of the Lowveld riverine forest, Subtropical alluvial Vegetation and Limpopo Ridge Bushveld vegetation types. Vegetation diversity was high within the GDVpz with *Phragmites mauritianus, Vachellia xanthophloea*, *Hyphaene coriacea, Eragrostis* observed along the Nhlangaluwe natural pan and *Hyphaene coriacea, Eragrostis, Philenoptera violacea, Acacia nigrescens, Boscia mossambicensis, Cyperus, Adansonia digitata* observed along the Makwadzi natural pan in the Makuleke wetland system.

For the Letaba regions, GDVpz are of the Northern Lebombo Bushveld, Tsende Mopaneveld, Makuleke sandy bushveld and Mopane Basalt Shrubland vegetation types. The vegetation was not as diverse as that of the Makuleke vegetation, with Mopane (*Colophospermum*) dominating. Sedges and grasses: *Panicum deustum*, *P. maximum*, and other wetland species trees and shrubs: *Acacia albida*, *A. karoo*, *A. nigrescens, Combretum*, *Diospyros* species, *Euclea* species are plant species indicating a groundwater-dependent ecosystem within a savannah landscape (Colvin et al., 2003). In a study conducted by Taylor (2003), stable water isotopes were employed to evaluate the depth of water utilisation by various sizes of savannah trees in KNP. The findings revealed that distinct savannah plant species accessed water at different depths, a pattern influenced by factors such as growth stage and physiological characteristics, including rooting depth. Thus, further research on the physiological characteristics of vegetation and isotope studies could validate the results of the GDVpz models. These vegetation species provide vital ecosystems supporting wildlife and socio-economic development through wildlife tourism. Thus, it is important to understand the ecohydrology of dryland environments. Holistic management efforts that are well-informed will ensure the sustainability of vital ecosystems and achieve the sustainable development goals, more specifically 15, 6, and 8, which are linked in terms of wildlife conservation.

4.4.3 Limitations of the findings

However, limitations to the study were observed. Firstly, Sentinel 2 images were used because of the moderate spectral resolution (10m) to discriminate smaller isolated clusters of GDVpz. This limited the dry NDVI data to 2018, 2019 and 2022, which were not as dry as previous years. Moreover, since data acquisition and analysis were conducted on the GEE platform, the 20m spatial resolution was used instead because of the pixel size limitations when exporting data for analysis in ArcMap. It is recommended that Landsat data should be utilised to capture extremely dry periods to easily discriminate green islands that may be GDVpz. Furthermore,

indicator variables had coarser spatial resolutions, which may have increased generalisations of the models and contributed to the commission and omission errors. It would be interesting to see how machine learning single-criterion models perform against multiple-criterion models. The main limitation is that training data was produced from a high-resolution image matching the dry period and field survey, based on the green islands. Thus, there is a need for further ground studies that may be used to validate the GDVpz model.

4.5 Conclusion

Remote sensing techniques have shown great efficiency in delineating and assessing groundwater-dependent vegetation globally. This chapter assessed the performance of various machine learning techniques and AHP in predicting the potential zones in the Kruger National Park using Sentinel-2 remotely sensed data coupled with other ancillary data such as Digital Elevation Model, as well as field vegetation survey data, amongst others. The key findings of the chapter revealed that amongst all the machine learning models used in the study, the ENS approach outperformed the AHP approaches in delineating GDV zones in the area with an acceptable accuracy. The results further revealed that the very low GDVpz class dominated the ML classifications, while the AHP classifier distributed the area between the low, moderate and high GDVpz classes. These underscored the relevance of machine learning techniques and multi-source remote sensing data in delineating groundwater potential zones. This finding is critical as it provides robust methodologies to geolocate these systems, therefore enhancing the protection of GDEs in semi-arid regions.

CHAPTER FIVE

AQUIFER CHARACTERIZATION FOR IMPROVED HYDROGEOLOGICAL MODELLING OF GROUNDWATER DEPENDENT ECOSYSTEMS IN THE KRUGER NATIONAL PARK, SOUTH AFRICA

5.1 Introduction

Groundwater serves as a reliable source of water to the ecosystems that depend on it (Eamus et al., 2015; Perez Hoyos et al., 2016; Rampheri et al., 2023). However, reports show that due to climate change and poor management, groundwater levels continue to decline, which may in turn affect the dependent ecosystems (Shadwell & February 2017; Holloway, 2022; Sappa et al., 2023). Ecosystems that depend on the consistent or intermittent connection to groundwater for their continued existence and functioning are referred to as GDEs (Klove et al., Orellana et al., 2012; Perez Hoyos et al., 2016; Rampheri et al., 2023). GDEs provide several socio-ecological benefits, including carbon sequestration, mitigation of floods, droughts and water purification. However, GDEs are threatened due to the over-abstraction of groundwater and hence the services they provide (Khorrami & Malekmohammadi, 2021, Dyring et al., 2023; Fildes et al., 2023). It is therefore important to manage groundwater resources to obtain the maximum value from this resource and to ensure sustainable characteristics. To effectively manage groundwater, there is still much that needs to be studied in understanding aquifer recharge dynamics due to climate variations and the long-term impacts of anthropogenic activities on aquifer sustainability.

Large parts of sub-Saharan Africa are underlain by crystalline basement aquifers, which are distributed extensively in the semi-arid KNP, South Africa (Holland, 2011). Groundwater occurrence in crystalline aquifers is spatially highly variable because of their complex geological, structural and geomorphological features (Holland, 2011; Akanbi, 2018), thereby making it important to identify high-yielding hydrogeological zones that can be targeted for water supply in areas where there are limited water sources. Understanding aquifer characteristics is crucial as it forms the initial stage in comprehending various aspects such as groundwater quantity, yield capacity, storage capacity, and transmission properties within an aquifer system (Gomo, 2018). This knowledge provides valuable insights into the intricate hydrogeological processes governing groundwater movement and storage. It involves determining groundwater flow, groundwater productivity and sustainability of aquifers, using

satellite imagery, pumping tests, geophysics and modelling (Zahid et al., 2018; Ndubuisi, 2021).

For complex aquifer systems, the hydrogeological investigation needs all available data and the use of different investigation techniques, especially geological, geophysical, piezometric, and hydrochemical methods (Kamel et al. 2005; Moral et al. 2008; Ayenew et al. 2008; Mjemah et al. 2011; Jellalia et al. 2015). The ability of an aquifer to transmit and store water is influenced by hydraulic properties, which include Transmissivity, Storativity, and specific capacity. These hydraulic properties are important in developing a groundwater flow model to predict available groundwater for future use (Mjemah et al., 2011). Pumping tests are the most effective method available to assess the hydraulic properties of an aquifer (Cardiff et al., 2013; Moharir et al., 2017). Pumping tests can also highlight other features disturbing groundwater flow, like lateral flow boundaries, hydraulic continuity, constraints of fracture flow, and recharge. All these features are essential in understanding the nature of the aquifer and will enable effective management of groundwater.

The study sought to accurately characterise the groundwater flow systems within the southern region of KNP, aiming to significantly enhance the precision of hydrogeological modelling pertaining to groundwater-dependent ecosystems within this specific geographical area. To achieve this goal, the study delineated several key objectives. Firstly, it sought to establish the preferential groundwater flow paths and comprehensively define the boundary conditions of the investigated system. This was accomplished through the analysis of borehole core loggings and the detailed examination of geological cross sections across the study area. Subsequently, the study aimed to accurately estimate essential aquifer properties, including Transmissivity and Storativity, by utilising sophisticated analytical solutions in conjunction with constant-rate aquifer test data. Finally, the study assessed groundwater recharge dynamics within the study area utilizing the Rainfall Infiltration Breakthrough method. Through the systematic pursuit of these objectives, the study aimed to significantly contribute to the advancement of hydrogeological understanding and modelling precision in the context of the Southern region of KNP.

5.2 Materials and methods

5.2.1 Borehole lithological core-logging

To achieve the objectives of this study, pre-existing boreholes that were drilled by the Department of Water Affairs (now referred to as the Department of Water and Sanitation) drilling rigs from May to October 2012 were used. Boreholes were drilled into both the shallow

weathered material and the consolidated hard rock, each of which was characterized by constant discharge tests, recovery tests, and slug tests to determine aquifer properties. To understand the lithological conformation of the boreholes, the sub-surface material was drilled every meter and brought to the surface by means of compressed air and placed in rows (Riddell et al., 2014; Van Niekerk, 2014). Once the drilled logs were brought to the surface, grab sub-samples were collected and transported to the Geology department laboratory at the University of Pretoria for identification and analysis. The analysis process involved using the Guidelines for Soil and Rock Logging in South Africa, which followed the methodology outlined in the South African National Standard (SANS) 633 profiling and percussion, as well as core borehole logging for engineering purposes (Brink and Bruin, 1990). These guidelines considered properties such as texture, soil, colour, and mineral composition of the lithological log samples, to categorize both weathered and hard rock material.

The location of the boreholes and the geological cross sections of the KNP area are shown below (Figure 5.1). The cross sections were constructed to understand the subsurface geology thus identifying groundwater preferential flow paths, establishing thickness of the hydrogeological units found in the area, potential groundwater recharge zones and potential groundwater discharge zones which were assumed to represent potential GDE zones as well as lithological conformation for the area to establish hydraulic conductivities (K) of the lithological units found in the area and boundary conditions.

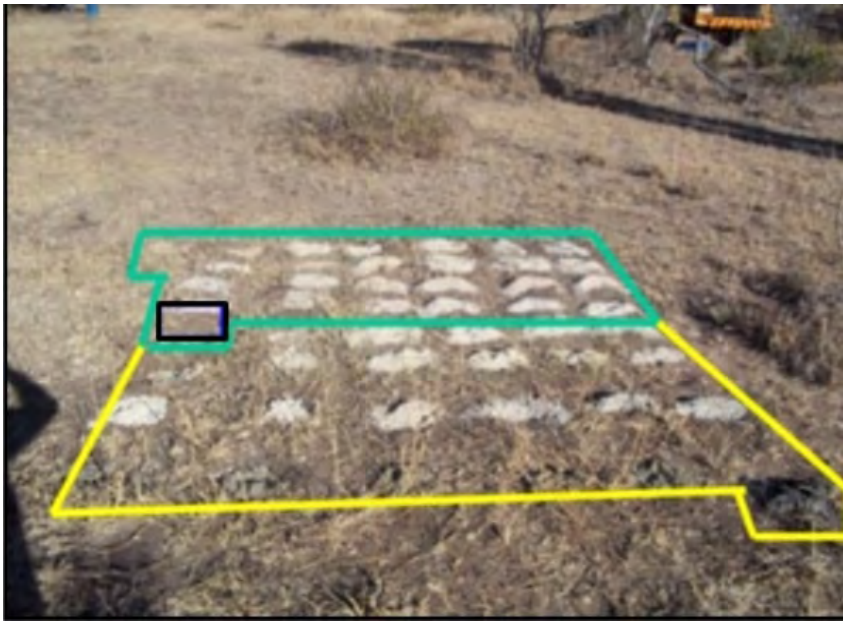

Figure 5.1 Borehole lithology log of weathered material (green highlighted section) and hard rock material (yellow highlighted section) (van Niekerk, 2014)

5.2.2 Estimating aquifer properties

Pre-existing data from the pumping test that was conducted in the boreholes within the lower KNP were used to characterize the aquifers in the area to gain insights on groundwater flow and aquifer hydraulic properties (Transmissivity, Storativity, and hydraulic conductivity). The boreholes were drilled by the Department of Water Affairs using the air percussion drilling approach, and the borehole sites were determined using the electrical resistivity geophysical traverses. This method permitted the collection of detailed information on each subsurface material, and data collected included depth to weathering, hard rock and water strikes amongst others (Van Niekerk, 2014). Lithological characteristics of the KNP were also established from these methods. After the drilling of boreholes, a single-well pumping test was conducted through the application of stress to the aquifer by pumping water at a controlled rate of …l/s and for … hours and subsequently monitoring changes in depth to water in intervals during pumping and after the pump has been switched off. Before the pumping, static water levels were also measured, and these were used to calculate drawdown, which was used in an appropriate analytical solution to derive aquifer properties such as Transmissivity (T), Storativity (S), and Hydraulic Conductivity (K).

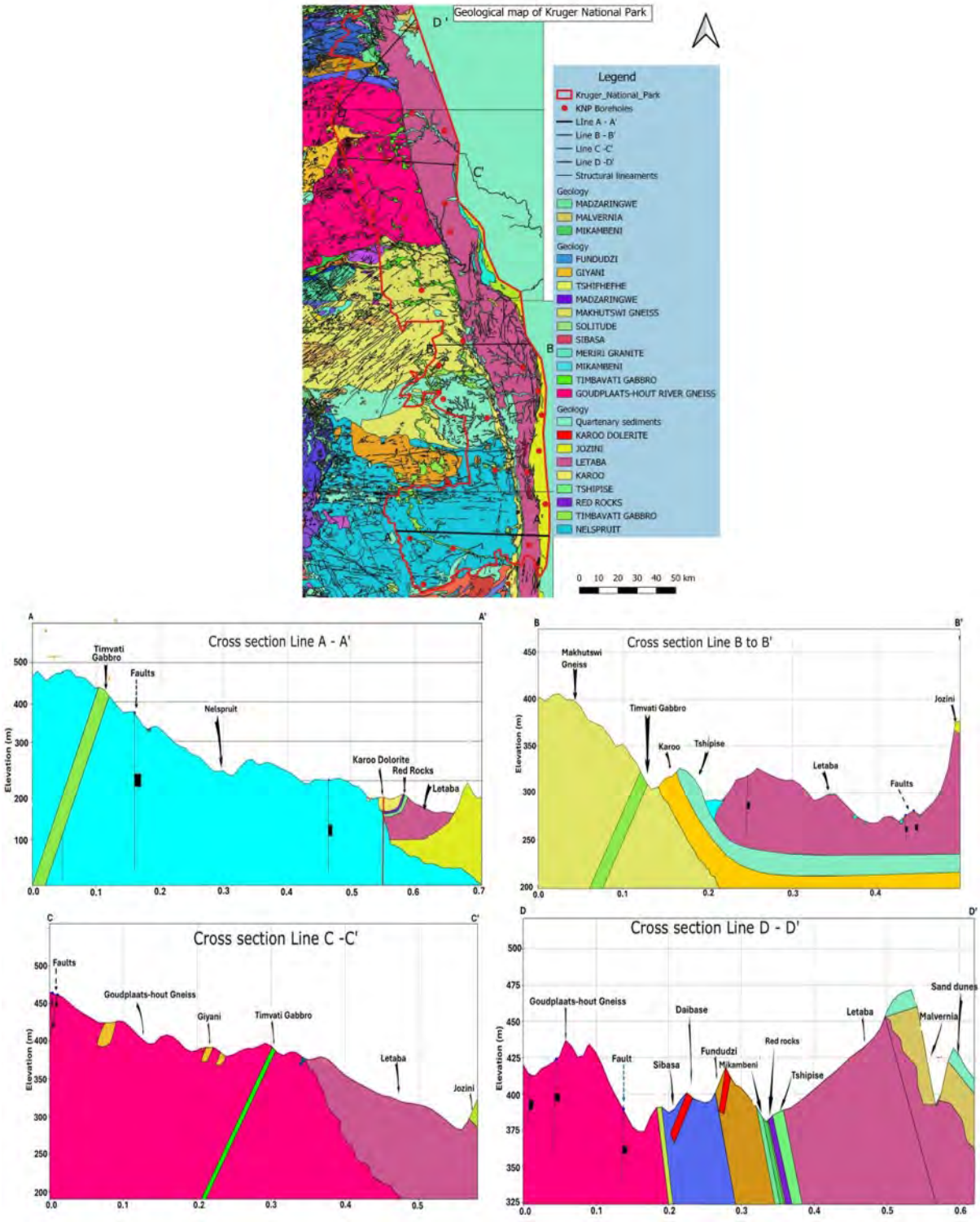

Figure 5.2 Surface and subsurface geology of the KNP

After the conductance of the aquifer test, the data collected was used to calculate drawdown, which is the difference between the static water levels and the depth to water measured during the pumping and recovery period. The calculated drawdown was then used in Theis and Cooper Jacobs Analytical solutions within the Flow Characteristic (FC) platform by Van Tonder et al.

(2001) to derive Transmissivity (T) and Storativity (S). These parameters were derived using equations (5.1, 5.2 and 5.3) in this platform. The Cooper-Jacob analysis was used for the constant drawdown test analysis, while the Theis analytical solution was used for the analysis of the recovery test data. The use of the Theis or Cooper-Jacob solutions are limited to confined aquifer conditions and homogeneous systems. In this study, the Cooper-Jacob analytical solution was selected, provided that the correction factor was applied for the determination of T values for a pumping test.

$$\boldsymbol{S(r,t) = S(r,t) - \frac{S2(r,t)}{2D}} \qquad \textbf{(5.1)}$$

Where, Sc(r, t) is the corrected drawdown in meters, S(rat) is the observed drawdown in meters, and 2D is the saturated thickness in meters prior to pumping.

$$\boldsymbol{T = \frac{2.3Q}{4\pi\Delta s}} \qquad \textbf{(5.2)}$$

Where T= Transmissivity (m2 d^{-1}), Q = Discharge (m3 d^{-1}), and Δs= Change in drawdown per log cycle.

$$\boldsymbol{S = \frac{2.25Tt0}{r2}} \qquad \textbf{(5.3)}$$

Where S= Storativity, T =Transmissivity (m2 d^{-1}), t0 =Time at which the straight-line intercepts zero drawdown, and r = Distance (m) between the pumping borehole and observation borehole.

5.2.3 Estimating Evapotranspiration

The actual evapotranspiration for KNP was estimated based on the water productivity through open access of remotely sensed derived data (WaPOR) developed by the Food and Agriculture Organization of the United Nations (FAO). WaPOR actual evapotranspiration and interception are estimated by the ET_{Look} algorithm (Bastiaanssen et al., 2012). In the ET_{Look} algorithm, with some changes in the Penman-Monteith equation, including (I) using remote sensing data such as precipitation, humidity, wind speed, temperature, NDVI, surface albedo, soil moisture, ground cover and digital elevation model (DEM) and (II) calculating evaporation, transpiration and interception separately (FAO, 2020), ETIa is estimated and the results are available through open access (Blatchford et al., 2020; Geshnigani et al., 2021).

5.2.4 Recharge Estimation

This study assumes that groundwater recharge is only occurring naturally in the aquifer systems of the study area. This study utilized daily rainfall data obtained from the South African Weather Services (SAWS) from 2015-2020. SAWS rainfall stations report 24-h accumulated rainfall in the morning (0800 South African Standard Time). All the rainfall stations in the Southern region of the KNP were investigated for their suitability for use in this study. Firstly, the rainfall stations that were considered were the stations near the boreholes that have been used in this study and only stations where data were available for at least 75 % of the period were considered. The groundwater level data were obtained from the Department of Water and Sanitation (DWS) for the selected southern granite boreholes within KNP for a period of 8 years (2007-2017). The selected boreholes for the study were selected based on the length of the monitoring period and the availability of the study. Data gaps in monitoring records were also considered. Where there were gaps, the mean groundwater level for the selected period was used. The study used the Rainfall Infiltration Breakthrough (RIB) method Id by Xu and van Tonder (2001) to estimate naturally occurring recharge. This method utilizes the relationship between the water level fluctuations and the cumulative rainfall departure (CRD) from the mean rainfall of the preceding times. Groundwater recharge using RIB method is computed using equation 5.4:

$$RIB(i)_m^n = r\left(\sum_{i=m}^{n} P_i - (2 - \frac{1}{P_{av}(n-m)}\sum_{i=m}^{n} P_i)\sum_{i=m}^{n} P_t\right) \quad (5.4)$$

$$(i= 1,2,3,\ldots\ldots I)$$

$$(n= i, n-1, n-2, \ldots\ldots N)$$

$$(m= i, m-1, m-2,\ldots\ldots M)$$

$$m<n<I$$

Where: $RIB(i)_m^n$ Cumulative recharge from rainfall event of m to n, I = total length of the rainfall series, r = is the fraction of cumulative rainfall departure, P_i = rainfall amount at the i_{nth} time scale (daily, monthly or annually), P_{av} = mean precipitation of the whole time series and P_t = is a threshold value representing the boundary conditions (P_t ranges from 0 to P_{av}).

Value of 0 represents a closed aquifer system, which means that the recharge at i_{th} time scale only depends on preceding rainfall events from P_m to P_n ; while value of P_{av} represents an open

system, which means that the recharge at the *80har* time scale depends on the difference between the average rainfall of preceding rainfall events from P_m to P_n and the average rainfall of the whole time series. Both r and P_t values are determined during the simulation process. The RIB method assumes that groundwater recharge has a linear relationship with water level fluctuations under natural conditions.

5.3 Results

5.3.1 Stratigraphic analysis

Figure 5.3 shows the lithological correlation between the 5 selected boreholes. The SG_1st_C_61m and SG_1st_c_103m boreholes form part of the southern Nelspruit formation, characterised by granite first-order boreholes, which exhibit a low permeability weathered granite aquifer and relatively high permeability hard granite rock aquifer at the crest. This is evident in the lithological logs shown in Figure 5.3. In particular, the SG_1st_C_103m borehole comprises two distinct layers of granite, highly weathered granite, and hard rock granite. The uppermost unit of the borehole, with a thickness of 1m is the clayey fine-medium grained sand. This type of soil is associated with low porosity. Underlying is the highly weathered granite with a thickness of 79 m, followed by the hard rock granite. Two water strikes are observed in this borehole at 55 m and 75 m, which indicate high high-yielding borehole. The uppermost part of the SG_1st_C_61m borehole consists of silty clay, fine-medium grained sand, colluvium and residual granite with a thickness of 2m. Underlying is the hard rock granite with a thickness of 55 m, followed by the closely jointed, slightly weathered granite with a thickness of 4m. The water strike in this borehole is observed at a depth of 55m. The water strikes observed at the boreholes may be an indication of the presence of a fracture or a flow/recharge zone. The SG_3rd_R_43m, SG_3rd_M_49m and SG_3rd_C_55m form part of the southern granite third order. The SG_3rd_R_43m borehole consists of dark brown, medium-coarse-grained sand with scattered gravel, with a thickness of 2m. Underlying is the highly weathered micaceous granite with a thickness of 30m, followed by the highly porphyritic granite. The lower part of this borehole consists of gneiss with a thickness of 4m. All the boreholes in the southern granite third-order hillslope have similar lithological structures, with SG_3rd_C_55m having a thick layer of highly weathered granite.

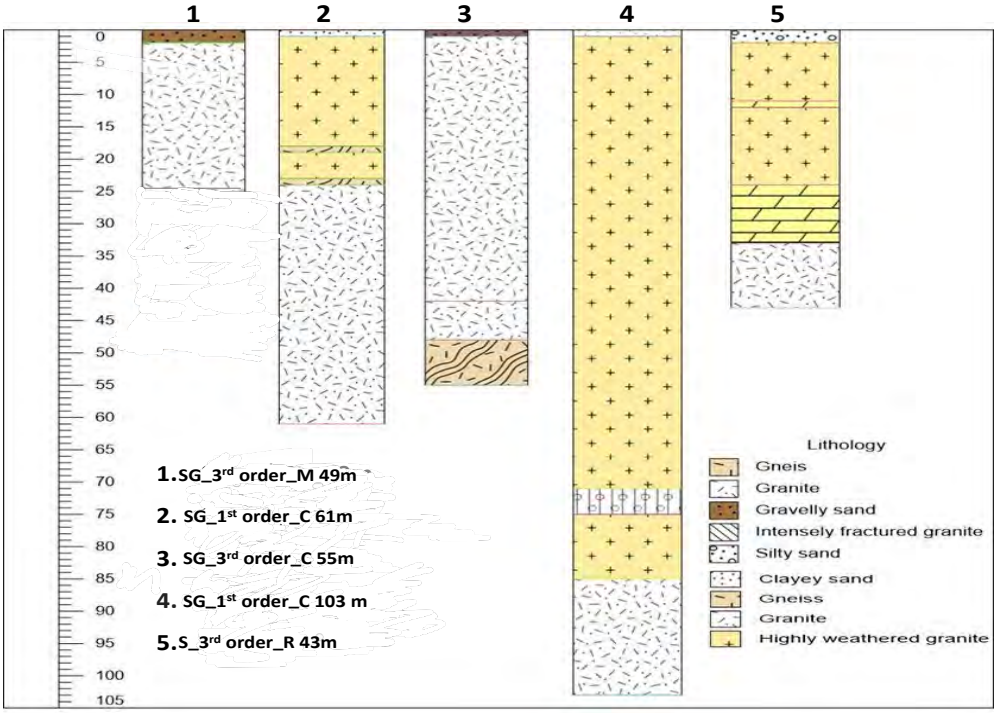

Figure 5.3 Lithological logs for boreholes located within the southern granite formation of KNP

5.3.2 Aquifer properties results

The constant discharge and recovery test results are presented in Tables 5.1 and 5.2, respectively. It is evident from the results below that the aquifers in the KNP have low hydraulic conductivities, which may be due to the soil being impermeable and hence water will move slowly through it. The results in the tables below also show that Transmissivity and Storativity values were obtained from boreholes drilled in sites with variable geological features.

Table 5.1 Transmissivity and Storativity results obtained from Cooper-Jacob time drawdown for the constant discharge test

Borehole	**Formation**	**Analytical Model**	**Transmissivity (m^2/day)**	**Storativity**
SG_1st_C_103m	Nelspruit	Basic FC	11.2	2.22×10^{-3}
SG.1st_R_61m	Nelspruit	Cooper Jacob	0.5	2.56×10^{-1}
SG_3rd_R_43m	Nelspruit	Cooper Jacob	4.8×10^{-3}	4.12×10^{-8}
SG_3rd_M_49m	Nelspruit	Cooper Jacob	3.3	3.10×10^{-3}
SG_3rd_C_55m	Nelspruit	Basic FC	9	1.28×10^{-3}

The results in Table 5.1 show that SG_1st_C_103m yielded T and S values of 11.6 m^2 d^{-1} and 2.22×10^{-3}, respectively. SG.1st_R_61m yielded T and S values of 0.5 m^2 d^{-1} and 2.56×10^{-1}, respectively. The SG_3rd_R_43m yielded T and S values of 4.80×10^{-3} m^2 d^{-1} and 4.12×10^{-8}, respectively. The SG_3rd_M_49m yielded T and S values of 3.3 m^2 d^{-1} and 3.10 $\times^{-4}$, respectively. SG_3rd_C_55m yielded T and S values of 9 m^2 d^{-1} and 1.28×10^{-6}, respectively. The drawdown plots of these boreholes are presented in Figure 5.4 below. Most of these boreholes have a low Transmissivity with only a few comprising slightly higher Transmissivity, which are boreholes drilled into the fractured and highly weathered granite/gneiss aquifer.

Figure 5.4 shows the drawdown versus time curve resulting from the observed boreholes. As shown in figure 5.4a (SG_1st_C_103m), the drawdown increased from around 1 m in 4 minutes after the onset of the pumping test. The borehole did not reach a steady-state drawdown; this may be an indication of the pumping rate exceeding the natural groundwater rate of the aquifer. Figure 5.4b (SG.1st_R_61m) and 5d (SG_3rd_M_49m) portrays a linear flow regime aquifer behaviour. A linear flow indicates fractured and horizontal wells. Figure 5.4c (SG_3rd_C_55m) shows that the drawdown increased around 1 m in 4 minutes after the onset of the pumping test. When the pumping of groundwater had been undertaken for 75 minutes, the drawdown showed little change leading to a steady-state drawdown of 3.5m.

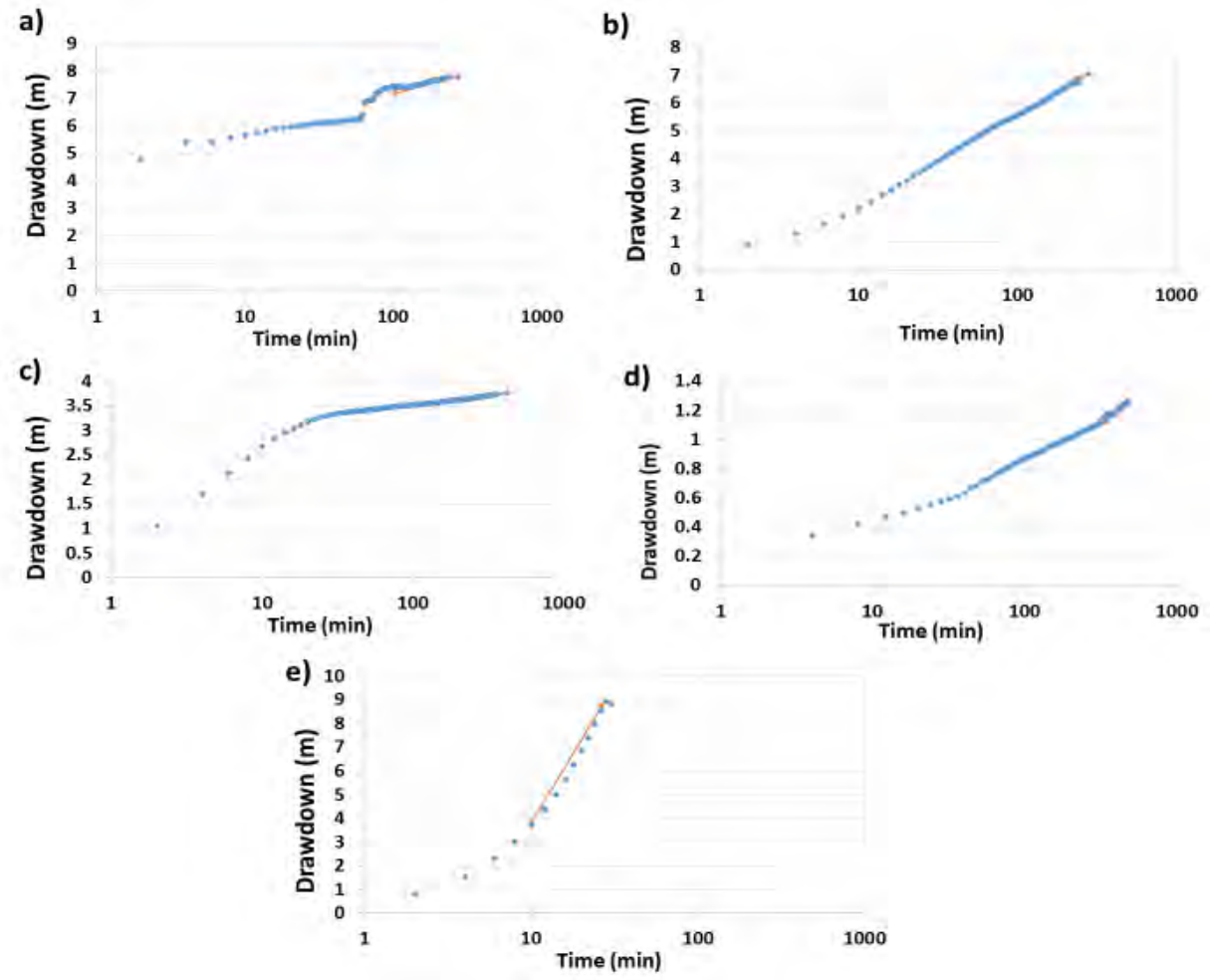

Figure 5.4 Cooper-Jacob plots showing line of best fit for, a) SG_1st_C_103m, b) SG_1st_R_61m, c) SG_3rd_55m, d) SG_3rd_M_49m, and e) SG_3rd_R_43m

Table 5.2 Transmissivity and Storativity obtained from Theis's recovery test for constant discharge test

Borehole	**Formation**	**Transmissivity (m^2/day)**	**Storativity**
SG_1st_C_103m	Nelspruit	9	1.6×10^{-2}
SG.1st_R_61m	Nelspruit	1	8.03×10^{-3}
SG_3rd_R_43m	Nelspruit	1	1×10^{-6}
SG_3rd_M_49m	Nelspruit	3	4.83×10^{-4}
SG_3rd_C_55m	Nelspruit	9	1×10^{-6}

The Theis Recovery method was applied to evaluate the adequacy of the results obtained from the constant rate pumping test. Figure 5.5 shows the shows the recovery of water level versus time plots resulting from the observed boreholes. Figure 5.5a (SG_1st_C_103m) shows early-time recovery, where drawdown is rapidly decreasing as water flows back into the borehole. The residual drawdown from 65-1000 minutes suggests that the water level has stabilised and is no longer rising significantly. This shows that the borehole has reached a near-equilibrium state, where the rate of water inflow into the borehole equals the rate of any residual outflow. Figure 5.5b (SG.1st_R_61m) shows no recovery in water level from 0-10 minutes immediately after pumping has stopped this may be due to low permeability and resistance to water flow near the borehole. The constant residual drawdown from 11 to 1000 minutes suggests that the water level has stabilized and is not recovering further. This indicates that the borehole has reached a state of equilibrium very quickly and that the aquifer is not contributing additional water to the well. Figure 5.5d (SG_3rd_M_49m) shows similar results to figure 5.5b. Figure 5.5e (SG_3rd_R_43m) shows a linear recovery, which suggests moderate permeability, allowing water to flow back into the borehole steadily but not rapidly. The recovery starts after 9 minutes, which might suggest an initial delay due to delayed response in the recharge process.

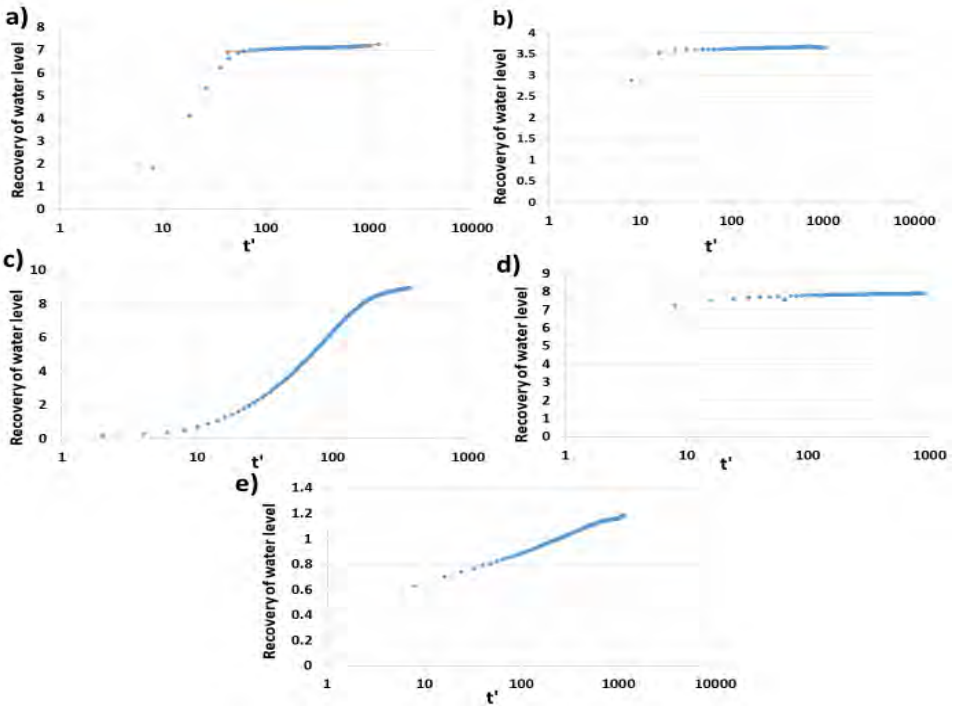

Figure 5.5 Recovery plots for, a) SG_1st_C_103m, b) SG.1st¬¬_R_61m, c) SG_3rd_C_55m, d) SG_3rd_M_49m and e) SG_3rd_R_43m

5.3.3 Evapotranspiration estimation

Actual evapotranspiration per catena unit, derived from the WAPOR product for the 2014 to 2015 hydrological year, is shown in Figure 5.6. The results show that there is a varying demand for water in the different southern granite catena units for water due to differences in soil moisture and proximity to water sources. The southern granite riparian (SG_R) catena shows greatest demand with actual ET up to 815mm. The maximum estimated actual ET for the mid-slope and crest catena units is 788 mm and 765 mm, respectively. During the wet season (October – November), there was no distinct difference in the mid-slope and the crest catena units. Actual ET rises mostly from mid-summer till the autumn season (January to May) as shown in the Figure below. This may be due to the residual soil moisture from the wet season and active vegetation growth.

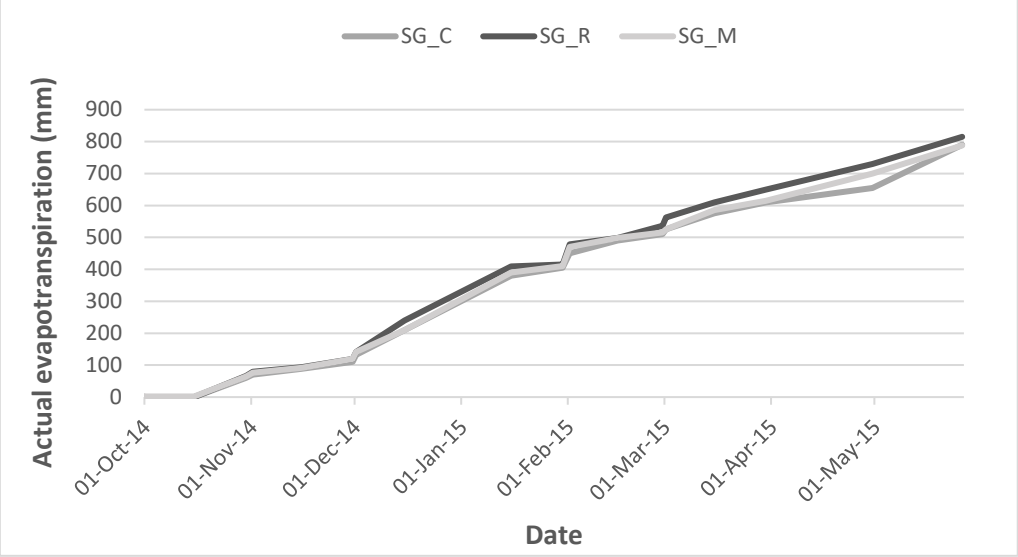

Figure 5.6 Actual evapotranspiration derived from WAPOR for the southern granite cres, riparian, and mid-slope catena unit

5.3.4 Groundwater Recharge results

The total monthly recharge estimates for the year 2007 up to 2015 are presented in Table 5.3. The results indicate that the recharge rate for the study site ranges between 20,55 mm/a (2,3 % of annual rainfall) and 29,4 mm/a (4,8% of annual rainfall) in 2007 to 2015. The results in table 5.3 suggest that most of the rainfall is lost through evapotranspiration due to the warm climate and extensive vegetation in the area. From Table 5.3, it can also be observed that a sporadic recharge pattern is evident in the area.

Table 5.3 Groundwater recharge from July 2007- May 2015

Borehole	Rainfall (mm/a)	Recharge (mm/a)	Recharge (% of annual rainfall)
SG_1st_C_103m	579	1,4	0,2
SG.1st_R_61m	537	10,6	2,0
SG_3rd_R_43m	579	11,6	2,0
SG_3rd_M_49m	447	21,4	4,79
SG_3rd_C_55m	537	3,8	0,7

The results shown in Figure 5.7 of groundwater levels against the simulated CRD and RIB groundwater head, show that groundwater levels respond to a one-month cumulative series of preceding rainfall events. There are several periods where groundwater head does not respond to high rainfall events, suggesting a delay in groundwater infiltration. As a result, a poor correlation was observed between groundwater fluctuations/recharge and rainfall. SG_3rd_M_49m (Figure 5.7b) borehole groundwater levels experience rapid response to rainfall events, which may be caused by the fractures and coarse grain material found in the area where the borehole was drilled. Another possibility would be the geological intrusion of the Timbavati Gabbro to the Nelspruit formation which is 4m away from where the borehole was drilled. The intrusion may create new groundwater flow paths within the Nelspruit formation, which may potentially increase or decrease the rate of recharge, causing fluctuations in water levels. The simulated groundwater levels at SG_3rd_C_55m (Figure 5.7d) borehole are relatively stable.

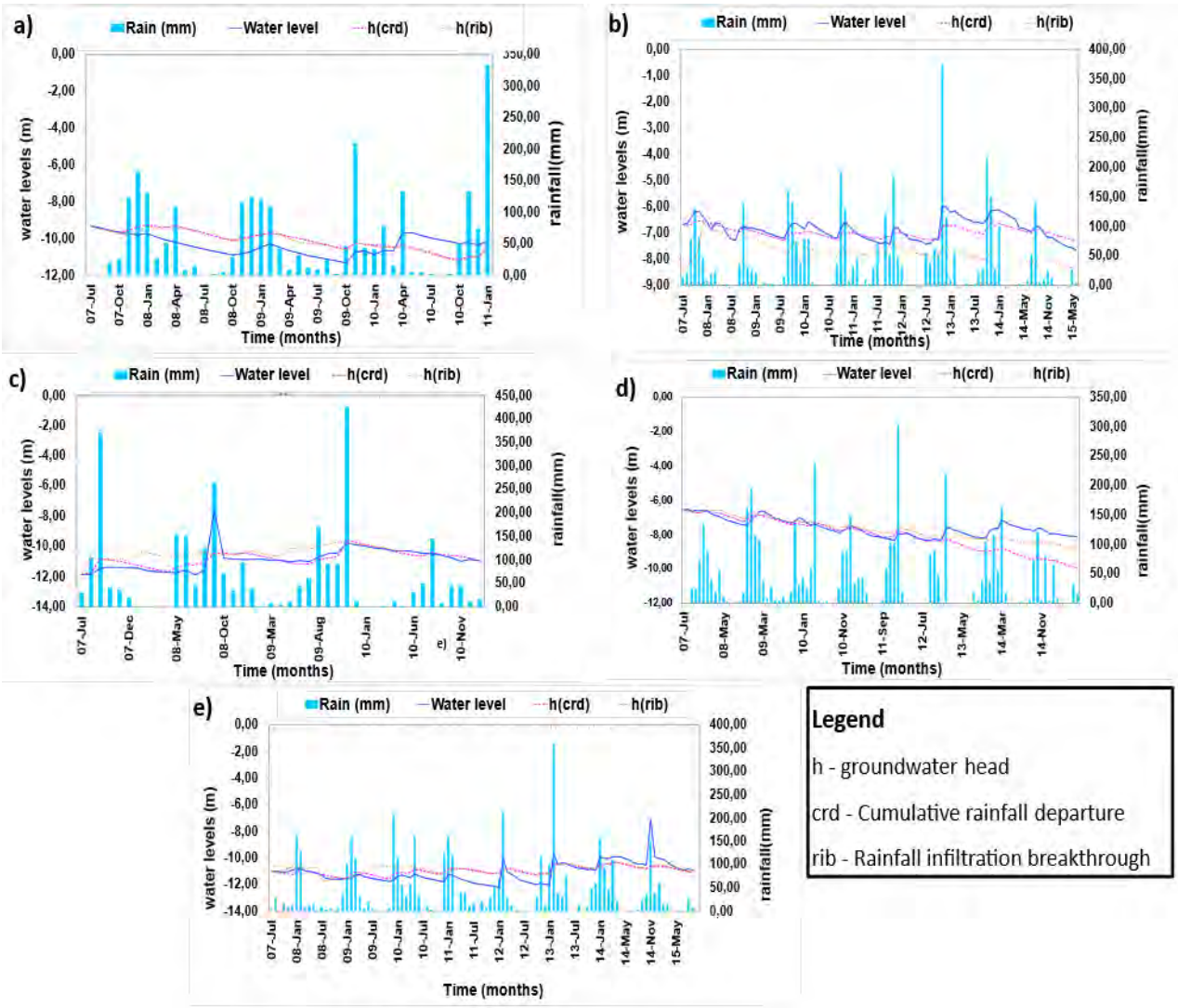

Figure 5.7 Monthly observed water level and groundwater recharge obtained from the RIB model and CRD method for a) SG_3rd_R_43, b) SG_3rd_M_49m, c) SG_1st_c_103m, d) SG_3rd_C_55m and e) SG_1st_C_61m

The groundwater level responds to a cumulative 12-month series of preceding rainfall events, as shown by the CRD interpretation. SG_1st_C_61m (Figure 5.7e) and SG_1st_c_103m (Figure 5.7c) show similar trends and response to rainfall. The SG_1st_c_103m borehole has a 2-month lag in response to rainfall events in September 2012, while SG_1st_C_61m showed no response to rainfall events. The water levels observed in these boreholes show direct response to rainfall for the first two months of the rainy season and then show gradual response thereafter. These trends in water level indicate a piston recharge process as a sequence of rainfall events is required for the water levels to rise.

5.4 Discussion

According to Vivier and Van Tonder, (1997), fractures have high Transmissivity and low Storativity while matrices have low Transmissivity and high Storativity. The geological analysis and pumping test results in the KNP indicate a fractured and unconfined aquifer. The Transmissivity here is greatly influenced by the density and connectivity of fractures. Borehole SG_1st_C_103m had the highest Transmissivity value which could be due to the dominant weathered granite in the area, while SG_3rd_R_43m had the lowest Transmissivity. This may be caused by the fact that this borehole is dominated with fine-grained clayey sand with low permeability that restricts the flow of water, which results in the borehole having the lowest Transmissivity. Fischer et al. (2009) stated that crystalline rocks are likely to be characterized by low Transmissivity or hydraulic conductivity (K) values, which is evident in the results presented above. The acquired Transmissivity values also correlate with the recovery Transmissivity values hence the constant discharge test results can be considered reliable. These results also correlate with the findings by Van Niekerk (2014), which stated that the southern granite supersite is characterized by low to moderate storage capacity, due to the presence of fractured bedrock, which is why the Storativity in these boreholes is relatively low. Fractured aquifers have complex hydrogeological characteristics (Krásny & Sharp, 2007), which make modelling GDEs occurring within these aquifers difficult. Fractured aquifers display high heterogeneity in hydraulic conductivity, Storativity, and groundwater flow paths (Comte et al., 2019). This heterogeneity further complicates the accurate representation of groundwater flow and its interaction with GDEs. The spatial distribution of GDEs in fractured aquifers follow groundwater preferential flow paths determined by the fractures. Based on groundwater levels within the southern granite supersite, groundwater will not follow the topography and flow down gradient but rather run parallel to the surface drainage network with groundwater flow (Ridell et al., 2014). Additionally, groundwater occurrence/storage is mainly in water filled joints, faults, zones of weathering and structures such as dyke intrusions. The hydrogeological conceptual model of the KNP is presented in Figure 5.8.

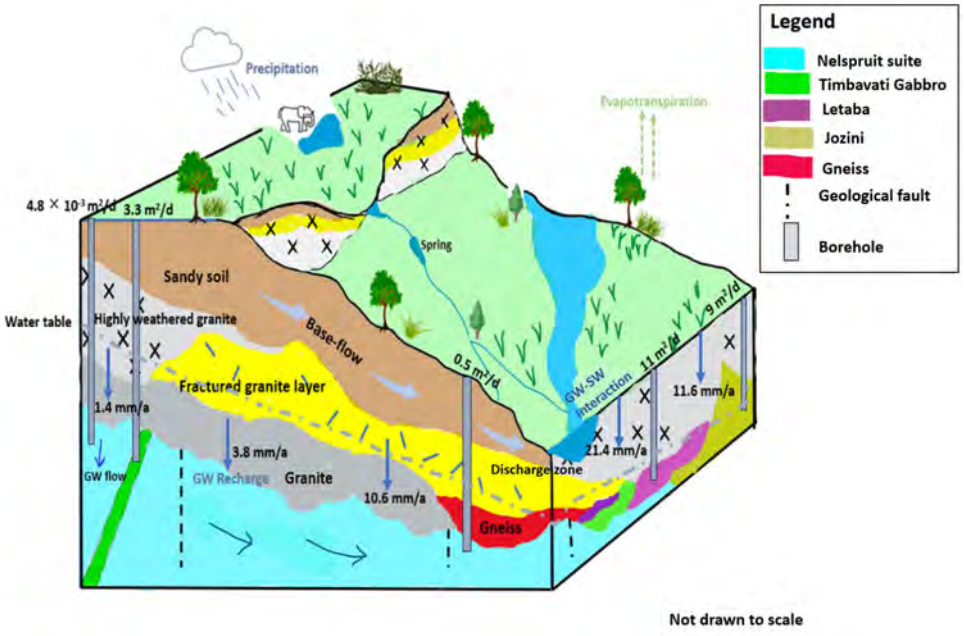

Figure 5.8 A hydrogeological conceptual model of the southern granite supersite in KNP

Recharge is an important parameter for any hydrological model, especially in groundwater modelling (Suryanarayana & Mahammood, 2019). Groundwater recharge in KNP primarily occurs through the infiltration of rainfall and surface water interactions, with most recharge occurring during periods of heavy rain. Recharge occurs both in the vertical and horizontal direction (Petersen, 2012). The RIB and CRD analysis of groundwater level fluctuations in the southern KNP shows that recharge to the aquifers responds to dry and wet cycles that last for over several years. The simulated groundwater level shows delayed response to increases in water levels due to rainfall, this is due to the very low Transmissivities and Storativity inherent in basement aquifers, which slows down the infiltration of water. Therefore, the water levels observed at SG_3rd_M_49m, SG_1st_C_103m and SG_3rd_R_43m suggest that these boreholes are situated in discharge zones and SG.1st_R_61m and SG_3rd_C_55m are potential recharge areas.

5.4.1 Implications and limitations of the study

This study holds significant prospects for groundwater management and modelling GDEs. The study provides detailed information on aquifer parameters, recharge rates and geological formation of aquifers, which enhances the accuracy of groundwater models used to assess GDEs and understand their connectivity to aquifers. This improved understanding of the hydrogeological processes allows for precise groundwater flow paths, which can be used to

assess potential impacts of groundwater abstraction to GDEs. Moreover, the identification of high groundwater recharge zones assists in prioritizing conservation efforts and guide the monitoring and management of GDEs to ensure long-term sustainability. However, this study only focused on the southern region of the KNP, and therefore the interpretations of this study may not be applicable to the other regions of the park. Additionally, this study only focused on Transmissivity and Storativity aquifer parameters to characterize the aquifers in the study site and does not provide a full characterization of aquifers.

5.5 Conclusion

The current chapter aimed at characterizing the aquifers at the KNP for improved hydrogeological modelling of groundwater-dependent ecosystems. This was done by establishing preferential groundwater flow paths of the studied system using borehole core loggings and geological cross sections of the area, estimating aquifer parameters from pre-existing pumping test data using the Cooper-Jacobs analysis and estimating recharge in the studied area. Results show that the aquifers in the KNP have low hydraulic conductivities, with groundwater mostly occurring in dykes and fault zones. Groundwater flow in the Southern KNP flows downslope from the first order hillslope down to the third order hillslope. However, this study was only conducted on a small scale and more research at a larger scale is needed to effectively characterise aquifers in KNP and effectively manage the groundwater resource. This study showed that aquifer characterisation can be useful in the management of groundwater resources by identifying areas where groundwater is likely to occur and how much groundwater is available at a given area. To manage GDEs much still needed to be achieved, however aquifer characterisation results can be useful in informing hydrogeological models for improved results and accuracy.

CHAPTER SIX

MACROINVERTEBRATE DIVERSITY WITHIN PAN WETLANDS IN RELATION TO GEOLOGICAL TYPE AND HYDROPERIOD

6.1 Introduction

Ephemeral wetlands or pan ecosystems are an important but poorly understood component of the natural world, particularly within tropical regions (Dube et al., 2017; de Necker et al., 2023; Munyai et al., 2023a). Despite being vital to aquatic life, it was not until the last two decades that they were recognized as significant habitats (Mabidi et al., 2017; Dalu et al., 2022). While wetlands provide numerous ecological benefits, they have historically been undervalued and subjected to widespread destruction due to a lack of conservation and protection (Matlala, 2010). Pérez et al. (2016) state that increased knowledge about their location, size, ecohydrological condition and biodiversity is critical before robust protection can be afforded to these ecosystems (Perez et al. 2016). Furthermore, notwithstanding their small size, wetland pan systems play a crucial role as natural water purifiers, effectively filtering and absorbing numerous pollutants from surface water. They provide essential ecosystem services such as phytoremediation and bioremediation, while also serving as habitats of considerable diversity for flora and fauna, thereby attracting tourism (Helson, 2012; Dube et al., 2020).

Aquatic macroinvertebrates refer to a diverse group of larger invertebrates, measuring over 500 μm, that inhabit various brackish, saline, and freshwater environments such as oceans, rivers, lakes and reservoirs, wetlands, and estuaries (Bonacina et al., 2023). They are highly diverse and locally abundant organisms, that play a crucial role in the functioning of aquatic ecosystems (Hendrey, 2001; Dalu et al., 2017; Hauer and Resh, 2017). These organisms are essential to the proper functioning of aquatic ecosystems as they regulate primary production, decomposition, and nutrient cycling (Allan et al., 2021; Stephenson et al., 2020; Dalu and Wasserman, 2022). They are widely acknowledged as a crucial food source for amphibians, fish, and other macroinvertebrates, making them indispensable elements of aquatic food webs (Colnurn et al., 2008; Hölker et al., 2015; Dalu et al., 2017; de Necker et al., 2023). Additionally, macroinvertebrate diversity flourishes in pan ecosystems because many of the taxa are opportunistic and possess specific adaptations that enable them to withstand seasonal drying every year (Necker et al., 2016).

Freshwater macroinvertebrates can be categorised as either semi aquatic or fully aquatic, meaning they complete their entire life cycle within the water (Wasserman et al., 2018; Dube et al., 2020). Their restricted mobility in freshwater habitats constrains their dispersal, making them suitable taxa for biomonitoring activities (Ollis et al., 2006; Chi et al., 2022). Following this, Dalu and Wasserman (2022) showed that macroinvertebrates are one of the most regularly employed biological indicators when assessing aquatic habitats, especially temporary pans. Despite being key indicators of ecological integrity and ecosystem health within wetland ecosystems they are among the most vulnerable animals in aquatic ecosystems (Ferreira et al., 2012; Dalu et al., 2021; Kafula et al., 2023). Aquatic macroinvertebrates are specialized to certain habitats, substrate types, temperatures, and dissolved oxygen concentrations, and can serve as indicators of disturbance (Victor, 2013). In wetland systems, their abundance and diversity are highly influenced by hydroperiod, water and sediment chemistry variables (Dalu and Wasserman, 2022, Munyai et al., 2023). Several studies (e.g., Schäfer, 2019; Dalu et al., 2021; Bonacina et al., 2023) have shown that macroinvertebrate taxa can respond to changes in water levels and quality, which alters community composition and impacts aquatic ecosystem functioning. Fluctuations in water levels can also have a direct impact on macroinvertebrate communities causing changes in water and sediment chemistry properties including physical factors (Rosenberg and Resh, 1993).

The current study aimed to assess (i) water and sediment chemistry variation in pan wetlands across different geological types and hydroperiods (i.e., low and high hydroperiod), and (ii) spatiotemporal macroinvertebrate diversity and abundances across geological regions, geological types and hydroperiods in pan wetlands in relation to water and sediment chemistry variables. We hypothesized that pans' (i) water and sediment chemistry concentrations will vary spatially and temporally, with high concentrations associated with low hydroperiod. (ii) macroinvertebrate diversity and abundances will be higher during the high hydroperiod than the low hydroperiod due to increased habitat availability.

6.2 Materials and Methods

In situ measurements were taken for the following parameters at each pan and hydroperiods: electrical conductivity (µS cm^{-1}), salinity (ppt), pH, water temperature (°C), salinity (ppt), resistivity (Ω) and total dissolved solids (TDS) (mg L^{-1}) from two distinct locations on either

side of the pan, using a Cyberscan Series portable handheld multiparameter meter (Eutech Instruments, Singapore). Without disturbing the sediment, two 250 mL polyethylene bottles were used to collect water from each site and hydroperiods for nutrient (i.e., phosphate, nitrate and ammonium) analysis and chlorophyll–*a* concentration determination in the laboratory. The 250 mL water samples collected from each pan were placed on ice until further processing. Water depth (m) and area (m^2) were measured using a graduated measuring rod and a handheld Garmin GPS (GPSMAP 64), respectively.

In the laboratory, the water samples were vacuum filtered (vacuum < 5 cm Hg) through 0.7 µm (diameter 47 mm) GIC Scientific glass fibre filters for total pelagic chlorophyll–*a* (chl–*a*) concentration, with the resultant filtered water being used for nutrient analysis. The ammonium concentration was determined using a HANNA freshwater ammonia high-range test kit (HI3824) with a range of 0–100 mg L^{-1} and a resolution of 0.1 mg L^{-1} based on the adaptation of the American Society for Testing and Materials (ASTM) Manual of Water and Environmental Technology D1426, Nessler method. Phosphate concentration was measured using the HANNA phosphate high range (HI717) test kit, with a range of 0–30 mg L^{-1} and resolution of 0.1 mg L^{-1} based on the adaptation of the ammonia acid method for the Standards Methods for the Examination of Water and Wastewater, 18th edition. Nitrate concentration was measured using nitrate test kit with range of 0–30 mg L^{-1} and resolution of 0.1 mg L^{-1} based on the adaptation of the cadmium reduction method. All nutrients were analysed using a HANNA HI83300 multiparameter photometer (HANNA Instruments Inc., Rhode Island).

The pelagic chl–*a* concentrations were determined as a proxy for quantifying phytoplankton biomass by filtering the water samples through a 0.7 µm GIC Scientific glass fibre filters. After filtration, the filters were placed individually in 15 mL centrifuge tubes containing 10 mL of 90 % acetone solution and then stored in a freezer for at least 24 hours to allow for chl–*a* extraction (see Lorenzen, 1967 methodology). After 24 hours, the samples were removed from the freezer and centrifuged at 3000 rpm for 10 minutes before 2 mL was extracted from each sample to measure absorbance at the wavelength of 665 nm and 750 nm before and after acidification by 0.01 M hydrochloric acid using a SPECTRO star NANO (BMG LabTech GmbH, Ortenberg).

6.2.1 Sediment chemistry variables

At each pan and hydroperiods, two sediment samples were collected randomly, using a plastic hand shovel and then carefully transferred into labelled Ziplock bags. The bags were then packed on ice in a cooler box to maintain their integrity during transportation to the laboratory for subsequent analysis. In the laboratory, the sediment samples were oven-dried at 70 °C for 72 hours. The sediment samples were then subjected to disaggregation using a porcelain mortar, followed by straining through a sieve (mesh 0.05 mm) to remove plant roots and other debris from the samples. The sediment samples were then sent to BEMLAB, a South African National Accreditation System (SANAS) accredited laboratory for pH, resistivity, H^+, stone proportion (%), sediment organic carbon (SOC) nutrient (P), non–metals (K, Ca, Na, Mg, B, S) and metals (Mn, Zn, Cu, Fe) analysis.

Benthic algal core samples (volume = 16.1 cm^3) were collected from each pan (n = 2) per hydroperiod, using a Perspex sediment corer of 20 mm internal diameter inserted by hand into the sediment. About 20 mL of 90 % acetone was introduced into the container with the sediment sample, swirled in the vortex, and the container with the sample was put in a freezer for 24 h for chl–*a* extraction. After 24 hours, samples were removed from the freezer and centrifuged at 3000 rpm for 10 minutes before 2 mL was extracted from each sample to measure absorbance at the wavelength of 665 nm and 750 nm before and after acidification by 0.01 M hydrochloric acid using a SPECTRO star NANO (BMG LabTech GmbH, Ortenberg) following Sartory and Grobbelaar (1984) and Human et al. (2018).

6.2.2 Macroinvertebrate sampling

Two macroinvertebrate samples were obtained at each pan and hydroperiod, using handheld net aluminium rim (30 × 30 cm dimensions, mesh 500 µm) and 1.5 m length. The net was fully immersed in the pan, and the collection of macroinvertebrates was conducted by systematically sweeping a defined transect measuring 10 m in length by disturbing any available vegetation, substratum, and rocks. This action was undertaken to displace macroinvertebrates that attached to any substratum. The net was expeditiously retrieved from the aquatic environment to minimise the potential loss of live and agile organisms before the sample was transferred into a tray to remove any organic material. The macroinvertebrates were then transferred into 500 mL plastic containers and preserved in 70 % ethanol. In the laboratory, an Olympus dissecting microscope (up to ×200 magnification) was used to identify macroinvertebrates to at least

genus or species level for most taxa according to Gerber and Gabriel (2002) and Fry (2021). The relative percentage abundances of each taxon were determined, and macroinvertebrate metrics were evaluated for each hydroperiod.

6.2.3 Data analysis

Before multivariate analysis, sediment metal and non–metal concentrations and water physics–chemical variables (except for pH) were log–transformed to meet two basic assumptions of an ANOVA (i.e., homogeneity and normality). The differences in sediment metal and non–metal concentrations, environmental variables, and macroinvertebrate diversity metrices between hydroperiods (i.e., high and low) and geological types (i.e., sandstone, granite, basalt and rhyolite) were assessed using a two–way ANOVA analysis, after testing for homogeneity of variance and normality of distribution using SPSS version 25. Tukey's post–hoc analysis was employed to assess the significant values that were different for water and sediment chemistry variables.

A distance–based permutational analysis of variance (PERMANOVA; Anderson, 2001) was conducted, using Bray–Curtis and Euclidean distance dissimilarities based on 9 999 permutations with Monte Carlo tests to examine differences in macroinvertebrate community structure across geological types and hydroperiods. Furthermore, the differences in macroinvertebrate community structure between hydroperiods and geological types were analysed using a two–way analysis of similarity (ANOSIM; Clarke, 1993). The ANOSIM statistic R is derived from comparing mean ranks between groups and within groups. The range of values for this variable is between –1 and +1, with a value of 0 indicating random grouping. SIMPER analysis was conducted to assess the key taxa driving community differences among hydroperiods and geological types. PERMANOVA+ for PRIMER version 6 software (Anderson et al., 2008) was used for these analyses.

Macroinvertebrate community data was used to calculate diversity matrices (i.e., Evenness, Abundance, Simpson, Shannon–Weiner) to assess for differences in species diversity among pans and hydroperiods in PAST version 2.0 (Dalu et al., 2020). Furthermore, the following metrices were determined; the Ephemeroptera, Plecoptera, and Trichoptera (%EPT), Ephemeroptera, Trichoptera, Odonata, and Coleoptera (%ETOC), Diptera (%Diptera), and Chironomidae + Oligochaeta (%Chironomidae + Oligochaeta).

An initial detrended canonical correspondence analysis (DCCA) was conducted to investigate the potential relationship between water and sediment chemistry variables on macroinvertebrate communities. This analysis aimed to determine whether linear or unimodal analysis methods should be utilised, following the approach outlined by Šmilauer and Leps (2014). The gradient lengths obtained from the DCCA output were analysed, and the longest gradient exceeded 4; hence, a linear canonical correspondence analysis (CCA) model was chosen (Šmilauer and Leps, 2014). A CCA was implemented to show how the significant variables jointly influenced macroinvertebrate community structure across pans in different geological types and hydroperiods. The macroinvertebrate and water and sediment chemistry variables data were square–root and log (x + 1) transformed, respectively, to reduce the effects of extreme values, (pH was excluded from this). Monte Carlo permutation tests (9 999 unrestricted permutations, $p < 0.05$) were used to test the significance of the axis.

6.3 Results

6.3.1 Water chemistry

Chlorophyll–*a* concentration during the high hydroperiod was similar (mean 0.1 mg m^{-3}) across the geological types (Table 6.1). The water temperature varied across geological types. In granite and basalt pans, the temperatures measured were relatively similar between low and high hydroperiod while in the sandstone and rhyolite pans, the temperature varied greatly between the low and high hydroperiod (Table 6.1). The pH levels across the various geological types were relatively consistent, falling within a mean range of 6.7 to 7.1 during the high hydroperiod, while the low hydroperiod showed more variation between geological types with a high mean range of 5.9–7.4 (Table 6.1). The total dissolved solids (TDS) levels showed significant variations across geological types and hydroperiods, with elevated values during the low hydroperiod (Table 6.1). Conductivity levels were relatively similar across geological types during the low hydroperiod (mean range: 281.8 - 312.8 µS cm^{-1}) with substantially higher conductivity means in the low hydroperiods in both the Granite and Rhyolite pans. Salinity levels varied widely across geological types and hydroperiod (Table 6.1). While ammonium concentrations were relatively similar across geological types in the high hydroperiod, they varied greatly in the low hydroperiod with a substantially higher concentration of ammonium in the rhyolite pans during this period. A similar pattern was observed when analysing the phosphates, but with more variation among geological types in the hydroperiod (Table 6.1).

Water temperature, pH, TDS, conductivity, phosphates, and salinity showed significant differences (ANOVA, $p < 0.05$) among hydroperiods (Table 6.2), with significant differences (ANOVA, $p < 0.050$) among geological types being observed for water temperature and ammonium (Table 6.2). Based on the Tukey's posthoc analysis, only water temperature was found to be significantly different ($p < 0.001$) among sandstone *vs* granite, sandstone *vs* basalt, granite *vs* sandstone, granite *vs* rhyolite and basalt *vs* rhyolite (Table 6.3).

6.3.2 Sediment chemistry

During the high hydroperiod, most of the sediment chemistry variables had high values in the rhyolite (i.e., H^+, stone, K, Ca, Mg, Na, Zn, Mn, B, Fe, SOC, S) and granite (i.e., benthic chl–*a*, pH, resistivity, P, Cu) pan systems (Table 6.1). Whereas during the low hydroperiod, the rhyolite pan systems had high values for H^+, stone, K, Na, Zn, B and Fe (Table 6.1). Most of the sediment variables were found to be statistically significant (ANOVA; $p < 0.05$) across hydroperiods and geological types (Table 6.2). Benthic chl–*a*, K, B, Fe, S, stone and resistivity, SOC, Cu, Zn, Mn and P concentrations were found be significantly different among hydroperiods (Table 6.2). However, only pH, H^+, P, Na, Mn, and B, C, S, Zn, stone and resistivity were statistically significant (ANOVA, $p < 0.05$) among geological types (Table 6.2). Based on Tukey's posthoc analysis, most of the sediment variables, pH, resistivity, H^+, stone, P, Na, Zn, Mn, B, SOC and S were found to be significantly different among the geological pan types (Table 6.3).

Table 6.1 Mean (± standard deviation) for water and sediment variables recorded from 12 pan wetlands across four geological types (sandstone, granite, basalt, and rhyolite) during high and low hydroperiods in the central KNP, South Africa. Abbreviations: chl–*a* – chlorophyll–*a*, TDS – total dissolved solids

Variables	**Units**	**High water period**				**Low water period**			
		Sandstone	**Granite**	**Basalt**	**Rhyolite**	**Sandstone**	**Granite**	**Basalt**	**Rhyolite**
Water									
Pelagic chl–*a*	mg m^{-3}	0.1 ± 0	0.1± 0	0.1 ± 0.1	0.1 ± 0	0.2 ± 0.1	0.2 ± 0.2	0.1 ± 0	0.4 ± 0.4
Ammonium	mg L^{-1}	1.8 ± 0.5	2.0 ± 0.6	1.8 ± 0.4	1.8 ± 0.3	1.3 ± 0.4	2.2 ± 0.5	1.4 ± 0.4	3.1 ± 0.2
Phosphates	mg L^{-1}	1.1 ± 0.2	0.8 ± 0.8	1.4 ± 1.4	0.6 ± 0.8	2.0 ± 0.6	1.6 ± 0.6	4.1 ± 2.2	2.7 ± 0.9
Nitrate	mg L^{-1}	2.2 ± 1.7	1.9 ± 1.2	2.3 ± 1.1	1.6 ± 0.6	3.7 ± 3.7	4.9 ± 5.7	2.4 ± 1.7	1 ± 0.2
Temperature	°C	26.3 ± 1.3	28.3 ± 0.7	27.2 ± 0.8	26.0 ± 1.3	21.9 ± 1.2	27.7 ± 2.2	28.1 ± 2.3	20.9 ± 0.3
pH		6.8 ± 0.1	7.1 ± 0.2	6.9 ± 0.2	6.7 ± 0.6	5.9 ± 0	5.9 ± 0.1	6.0 ± 0.1	7.4 ± 2.1
TDS	mg m^{-2}	200.7 ± 17.5	160.8 ± 108.9	148.5 ± 126.7	262.9 ± 226.5	331.3 ± 217.9	410.5 ± 76.8	185.5 ± 29.2	341.3 ± 19
Conductivity	µS cm^{-1}	287.8 ± 29.7	281.8 ± 188.9	287.8 ± 250.7	312.8 ± 329	228.8 ± 103.2	743.6 ± 131.5	334.3 ± 73.5	774.1 ± 2.8
Salinity	ppm	188.2 ± 13.9	138.3 ± 93.4	139.8 ± 125.8	229.7 ± 209.1	372.2 ± 239.7	427.9 ± 169.4	171.0 ± 28.3	401.6 ± 31.7
Resistivity	Ω	4135.0 ± 477.8	3979.0 ± 1654.6	5374 ± 3078.1	3767.1 ± 3407.3	2507.5 ± 1326.7	3499.5 ± 4474.8	2682.0 ± 629.5	1478.5 ± 75.6
Area	m^2	8975.4 ± 1012.6	867.4 ± 1203.3	2120.2 ± 2005.7	25817.2 ± 54917.7	2227.7 ± 3589.8	455.3 ± 267.7	233.5 ± 157	797.5 ± 662.5
Sediment									

Benthic chl–*a*	mg m^{-2}	115.0 ± 23.0	131.9 ± 164.5	29.2 ± 27.1	11.1 ± 4.6	413.1 ± 234.3	101.5 ± 107.3	509.3 ± 520.3	185.5 ± 113.8
pH	KCl	5.0 ± 0.5	5.1 ± 0.1	5.0 ± 0.3	4.8 ± 0.4	5.4 ± 0.1	5.3 ± 0.2	4.9 ± 0.2	4.2 ± 0.1
Resistivity	Ω	1573.8 ± 560.6	2316.7 ± 1266.1	1358.3 ± 484.1	926.7 ± 245.4	1522.5 ± 1038.1	1005.0 ± 173.6	1002.5 ± 282	650 ± 0
H+	cmol kg^{-1}	1.0 ± 0.2	0.7 ± 0.2	0.8 ± 0.3	1.7 ± 1.4	0.7 ± 0.3	0.7 ± 0.2	1.0 ± 0.1	2.7 ± 0.3
Stone	%	6.9 ± 0.7	5.1 ± 3.2	6.4 ± 13.2	11.7 ± 11.9	1.6 ± 1	8.8 ± 0.8	21.8 ± 17.5	22.2 ± 0.8
P	mg kg^{-1}	36.3 ± 39.1	44.5 ± 10.1	18.9 ± 15.6	13.4 ± 10.7	112.4 ± 26.5	54.2 ± 3	46.8 ± 5.5	10.8 ± 1.2
K	mg kg^{-1}	302.6 ± 85.1	286.0 ± 100.1	249.2 ± 65.5	325.5 ± 36.4	440.5 ± 355.6	535.8 ± 138.5	531.3 ± 91	878.5 ± 6.3
Ca	cmol kg^{-1}	4.7 ± 2.3	4.5 ± 2.4	4.5 ± 1.4	5.5 ± 1.3	4.8 ± 4.2	5.1 ± 1.3	7.4 ± 2	5.4 ± 0.1
Mg	cmol kg^{-1}	3.0 ± 1.9	2.3 ± 1.3	2.9 ± 1	4.4 ± 3.2	2.3 ± 1.6	2.6 ± 0.6	5.6 ± 1.2	3.0 ± 0.1
Na	cmol kg^{-1}	0.3 ± 0.1	0.2 ± 0.1	0.3 ± 0.2	0.5 ± 0.2	0.3 ± 0.1	0.2 ± 0.1	0.2 ± 0.1	0.7 ± 0.1
Cu	mg kg^{-1}	6.2 ± 3.4	7.7 ± 5.4	4.4 ± 1.6	5.6 ± 0.3	8.6 ± 6.7	12.2 ± 6.7	10.3 ± 1.3	11.1 ± 1.4
Zn	mg kg^{-1}	1.6 ± 0.2	1.3 ± 0.6	0.8 ± 0.6	2.7 ± 3.1	2.1 ± 1.1	2.6 ± 0.5	1.1 ± 0.2	5.3 ± 0.8
Mn	mg kg^{-1}	155.5 ± 40.7	171.4 ± 67.5	103.2 ± 53.7	211.9 ± 147.9	125.4 ± 107.1	306.5 ± 96.2	130.0 ± 20	298.5 ± 0.7
B	mg kg^{-1}	0.3 ± 0.1	0.2 ± 0.1	0.3 ± 0.1	0.4 ± 0	0.2 ± 0.1	0.3 ± 0.1	0.6 ± 0.1	0.7 ± 0.1
Fe	mg kg^{-1}	453.3 ± 180.1	284.5 ± 147.8	185.3 ± 78.5	534.4 ± 649.7	1358.5 ± 754.5	1079.2 ± 246.2	878.5 ± 162.7	1390 ± 183.8
C	%	0.8 ± 0.3	0.5 ± 0.1	0.7 ± 0.1	1.3 ± 1.1	0.7 ± 0.4	0.8 ± 0.2	0.8 ± 0.1	2.1 ± 0

S	mg kg^{-1}	7.7 ± 0.7	4.3 ± 1	5.6 ± 2	12.1 ± 9.6	12.7 ± 7.3	17.3 ± 2.7	7.4 ± 1.8	19.8 ± 6.5

Table 6.2 Two–way analysis of variance (ANOVA) results for water and sediment variables across geological types (i.e., granite, sandstone, basalt, rhyolite) and hydroperiods (i.e., high, and low) measured from 12 pan wetlands located in the central KNP. The bold values emphasise significant differences at $p < 0.05$

Variables	Hydroperiods			Geological type			Hydroperiods × Geological type		
	df	**F**	***p***	***df***	**F**	***p***	***df***	**F**	***p***
Water									
Pelagic chl–*a*	**1**	**4.220**	**0.049**	3	0.553	0.650	3	1.501	0.234
Ammonium	1	0.717	0.404	3	**3.326**	**0.033**	**3**	**8.514**	**<0.001**
Phosphate	**1**	**26.834**	**<0.001**	3	2.738	0.061	3	0.611	0.613
Nitrate	1	0.440	0.512	3	0.866	0.469	3	0.689	0.566
Temperature	**1**	**32.383**	**<0.001**	**3**	**23.242**	**<0.001**	**3**	**12.051**	**<0.001**
pH	**1**	**14.261**	**0.001**	3	2.640	0.068	**3**	**5.467**	**0.004**
TDS	**1**	**11.102**	**0.002**	3	1.451	0.248	3	0.401	0.753
Conductivity	**1**	**5.471**	**0.026**	3	0.648	0.590	3	1.542	0.224
Salinity	**1**	**16.808**	**<0.001**	3	1.747	0.179	3	0.545	0.655
Restivity	1	0.292	0.593	3	0.681	0.571	3	0.162	0.921
Area	1	1.787	0.191	3	1.121	0.356	3	0.595	0.623
Sediment									
Benthic chl–*a*	**1**	**29.556**	**<0.001**	3	0.734	0.540	3	2.681	0.065
pH	1	2.578	0.119	**3**	**12.314**	**<0.001**	3	1.849	0.160
Resistivity	1	**6.422**	**0.017**	**3**	**3.059**	**0.043**	3	0.921	0.443
H+	1	3.869	0.058	**3**	**10.184**	**<0.001**	3	0.769	0.520
Stone	**1**	**6.372**	**0.017**	**3**	**4.546**	**0.010**	3	1.530	0.227
P	**1**	**4.487**	**0.043**	**3**	**15.855**	**<0.001**	3	1.560	0.220
K	**1**	**23.562**	**<0.001**	3	2.543	0.075	3	2.136	0.116
Ca	1	1.342	0.256	3	1.358	0.274	3	0.562	0.644
Mg	1	0.693	0.412	3	2.736	0.061	3	1.287	0.297
Na	1	1.174	0.287	**3**	**8.634**	**<0.001**	3	0.429	0.734
Cu	**1**	**11.300**	**0.002**	3	0.960	0.424	3	0.329	0.805
Zn	**1**	**10.804**	**0.003**	**3**	**5.258**	**0.005**	3	0.872	0.466
Mn	**1**	**5.508**	**0.026**	**3**	**8.005**	**<0.001**	3	0.195	0.899
B	**1**	**18.603**	**<0.001**	**3**	**11.726**	**<0.001**	3	2.900	0.051
Fe	**1**	**38.230**	**<0.001**	3	1.246	0.310	3	0.359	0.783
C	**1**	**4.592**	**0.040**	**3**	**7.679**	**0.001**	3	0.766	0.522
S	**1**	**26.120**	**<0.001**	**3**	**4.281**	**0.013**	3	2.858	0.054
Taxa richness	**1**	**4.155**	**0.050**	3	2.094	0.122	**3**	**7.801**	**0.001**
Abundances	**1**	**10.539**	**0.003**	**3**	**4.305**	**0.012**	**3**	**4.777**	**0.008**
Shannon–Wiener	1	0.001	0.976	3	0.328	0.805	3	2.310	0.096

Simpson	1	0.042	0.839	3	0.362	0.781	3	0.754	0.529
Evenness	1	2.872	0.101	3	1.196	0.328	3	2.415	0.086
%Ephemeroptera	1	1.304	0.262	3	1.448	0.248	3	1.448	0.248
%Trichoptera	**1**	**15.433**	**<0.001**	3	2.013	0.133	3	2.013	0.133
%Diptera	**1**	**8.297**	**0.007**	3	2.366	0.091	3	2.464	0.082
%EPT	**1**	**9.556**	**0.004**	**3**	**2.977**	**0.047**	3	0.852	0.477

Table 6.3 Tukey's post–hoc results highlighting environmental variables that were found to be significant ($p < 0.05$) across four geological types (sandstone, granite, basalt and rhyolite) in pan wetlands located in KNP, South Africa

Variable	**Geology**	***p***
Temperature	Sandstone vs Granite	<0.001
	Sandstone vs Basalt	0.001
	Granite vs Sandstone	<0.001
	Granite vs Rhyolite	<0.001
	Basalt vs Rhyolite	0.001
Sed–pH	Sandstone vs Basalt	0.001
	Sandstone vs Rhyolite	<0.001
	Rhyolite vs Granite	0.016
Sed–Resistivity	Granite vs Rhyolite	0.020
H+	Basalt vs Rhyolite	0.023
	Rhyolite vs Sandstone	<0.001
	Rhyolite vs Granite	0.002
	Rhyolite vs Basalt	0.023
Stone	Sandstone vs Rhyolite	0.023
P	Sandstone vs Basalt	<0.001
	Sandstone vs Rhyolite	<0.001
	Granite vs Basalt	0.050
	Granite vs Rhyolite	<0.001
Na	Granite vs Rhyolite	<0.001
	Basalt vs Rhyolite	0.001
	Rhyolite vs Sandstone	0.002
Zn	Basalt vs Rhyolite	0.015
Mn	Sandstone vs Granite	0.002
	Sandstone vs Rhyolite	0.004
B	Sandstone vs Basalt	0.020
	Sandstone vs Rhyolite	0.001
	Granite vs Basalt	0.024

	Granite vs Rhyolite	0.001
SOC	Sandstone vs Rhyolite	0.002
	Granite vs Rhyolite	0.003
	Basalt vs Rhyolite	0.018
S	Basalt vs Rhyolite	0.017

6.3.3 Macroinvertebrate community structure

Based on PERMANOVA analysis, significant differences in macroinvertebrate community structure among geological types (Pseudo–F = 11.925, $df = 1$, $p < 0.001$) and hydroperiods (Pseudo–F = 1750 $df = 3$, $p = 0.027$) were observed. However, no significant ($p > 0.05$) pairwise combinations were observed for the geological types of macroinvertebrate communities. A total of 5 145 individual macroinvertebrates belonging to 41 genera/taxa and 9 orders (i.e., Hemiptera, Coleoptera, Crustacea, Mollusca, Annelida, Diptera, Odonata, Trichoptera, Ephemeroptera) were identified from the 12 pan wetlands across both hydroperiods (29 taxa–high hydroperiod, 12 taxa – low hydroperiod). The Annelida, Crustacea, Hemiptera, Mollusca and Trichoptera represented most of the taxa during the high hydroperiod, and Crustacea, Diptera, Hemiptera, Odonata and Mollusca were among the most dominant groups in the low hydroperiod.

Two–way ANOSIM results indicated significant differences among hydroperiods (Global R = 0.80, $p < 0.001$) and geological types (Global R = 0.39, $p < 0.001$). The SIMPER analysis indicated the main drivers for the dissimilarity (86.9 %) between high and low hydroperiod were *Anisops* sp. (16.4 %), *Enithares* sp. (15.0 %) and Cypridoidea (12.9 %). These drivers were similar between high (42.0 %) and low (42.1 %) hydroperiods. For the high hydroperiod, Cypridoidea (28.3 %), *Enithares* sp. (18.7 %), *Ecnomus* sp. (16.9 %) and *Laccotrephes* sp. (10.2 %) were the dominant taxa, whereas for the low hydroperiod, *Enithares* sp. (32.2 %), *Anisops* sp. (29.3 %) and Chironominae (10.9 %) were the dominant taxa contributing to differences in community structure.

For the different geological types, the dominant taxa were *Laccotrephes* sp. (28.5 %), *Enithares* sp. (25.0 %), Cypridoidea (22.0 %) and Branchiopodidae (11.7 %) in sandstone, *Enithares* sp. (34.7 %), Cypridoidea (22.8 %), *Ecnomus* sp. (15.9 %) in granite,, Cypridoidea (30.8 %), *Ecnomus* sp. (20.2 %), *Enithares* sp. (15.3 %), *Anisops* sp. (12.6 %) and *Lymnaea truncatula*

(10.2 %) in basalt, and *Potamonautes* sp. (32.1 %) and *Lepidurus apus* (21.0 %) in rhyolite pans. The ANOSIM analysis indicated significant ($p < 0.05$) pairwise comparisons for all geological types of combinations, with SIMPER analysis highlighting important taxa driving the dissimilarities (Table 6.5).

In general, the %EPT were high during the high hydroperiod (Table 6.4). Species abundance was high during the low hydroperiod, with the granite pans having high particularly high abundance when compared to the other geological types. Two–way ANOVA analysis indicated significant differences ($p < 0.05$) among hydroperiods for taxa richness, abundances, %Trichoptera, %Diptera and %EPT and significant differences ($p < 0.05$) among the geological types for abundances and %EPT (Table 6.5). Tukey's posthoc analysis highlighted significant differences ($p = 0.015$) in %EPT between sandstone *and* basalt pans.

Table 6.4 Mean (± standard deviation) of macroinvertebrate abundances and community metrices observed in high and low hydroperiods across pan wetlands with different geological types (sandstone, granite, basalt and rhyolite) located in the central KNP, South Africa

Taxa	**Abbreviations**	**High hydroperiod**				**Low hydroperiod**			
		Sandstone	**Granite**	**Basalt**	**Rhyolite**	**Sandstone**	**Granite**	**Basalt**	**Rhyolite**
Annelida									
Salifidae	Salifida	8.4 ± 16.6		1.6 ± 2.5					
Aliolimnatis sp.	AliolSp	1.2 ± 2.5	5.1 ± 12.5			0.5 ± 1.1	0.5 ± 0.9	3.8 ± 2.9	0.3 ± 0.4
Oligochaeta	Oligocha								2.1 ± 0.3
Crustacea									
Streptocephalus sp.	Branchio	15.5 ± 26.6	3.7 ± 9.2	11.5 ± 16.6	22.2 ± 35.8	24.3 ± 28.1	2 ± 4		
Cypridoidea	Cyprid	31.2 ± 30.1	39.2 ± 32.8	42.9 ± 28.2	18.1 ± 28.5	31.1 ± 23.6	4.2 ± 8.2		18.7 ± 10.8
Lepidurus apus	LepiApus		1.2 ± 3.1	0.8 ± 2.1	13.7 ± 16.1				
Triops sp.	PotamSp				25.8 ± 28.4				
Coleoptera									
Acidocerinae	Acidocer		0.6 ± 1.5	0.2 ± 0.5					

Hydrocanthus sp.	HydrcSp			0.4 ± 1.0					
Hydrochus sp.	HydroSp	0.5 ± 0.8	1.2 ± 3.1						
Rhantus sp.	RhantSp	1.1 ± 2.2	2.9 ± 3.3	1.4 ± 2.2		0.3 ± 0.6	0.6 ± 0.5		0.3 ± 0.5
Regimbartia sp.	RegimSp		3.0 ± 4.8	0.4 ± 0.9	1.2 ± 2.1	0.5 ± 1.1	0 ± 0.1		
Copelatus sp.	CopelSp				0.1 ± 0.3				
Hydrophilus aculeatus	HydrAcul		0.4 ± 1	0.4 ± 1.1					
Berosus sp.	BerosSp			0.8 ± 1.2					
Stenelmus sp	SteneSp			0.2 ± 0.5					
Spercheus sp.	SpercSp			0.2 ± 0.4					
Cybester sp.	CybesSp								
Hydaticus exclamations	HydrExcSp							2.1 ± 4.1	
Diptera									
Ochthera sp	OchthSp				0.8 ± 2.1				0.3 ± 0.5
Culex sp.	CulexSp							0.3 ± 0.6	
Chrysops sp.	ChrysSp					9.5 ± 19			
Chironominae	Chironom					9.7 ± 12.9	36.4 ± 41.7	2.1 ± 3.7	3.2 ± 0.9
Ephemeroptera									
Afroptilum sudafricanum	AtrpSudf							5.2 ± 10.4	
Hemiptera									
Appasus sp.	AppasSp		1.3 ± 1.6		0.3 ± 0.7	0.1 ± 0.2	0.1 ± 0.1		
Enithares sp.	EnithSp	14.2 ± 12.1	24.6 ± 22.2	1.6 ± 1.3	6.7 ± 13.2	9.7 ± 12.2	33.4 ± 26.6	37.9 ± 8.3	14.1 ± 15.5

Hydrometra sp.	HydrmSp		0.5 ± 1.3						
Laccotrephes sp.	LacctSp	20.6 ± 21.2	1.6 ± 1.8						
Ranatra sp.	Ranatra	0.6 ± 1.5							0.3 ± 0.4
Sigara sp.	Sigara	0.5 ± 1.3					1.1 ± 0.7	0.3 ± 0.6	1.2 ± 1.8
Anisops sp.	AnispSp					10.2 ± 9.4	17.7 ± 19.7	48.2 ± 13.2	38.6 ± 47.4
Neomecrocons sp.	Neomecrc								0.6 ± 0.9
Mollusca									
Galba truncatula	LymnTrun		2.1 ± 5.1	18.1 ± 19.1	1.8 ± 2.9				
Pisidium sp.	PisidSp	3.1 ± 7.6			1.0 ± 2.5				
Pseudosuccinea columella	PseuColm			0.4 ± 1.1		2.6 ± 4.3	3.6 ± 4.5		
Melanoides tubercullata	MelnTubr								9.8 ± 11.6
Bellamya capillata	BellCapl					0.2 ± 0.4			
Trichoptera									
Ecnomus sp.	EcnomSp	2.4 ± 5.1	11.6 ± 8.3	17.9 ± 9.4	6.8 ± 11				
Odonata									
Anax speratus	AnxSprSp		0.3 ± 0.8	0.2 ± 0.5	0.9 ± 2.2				
Pseudogrion sp.	PseudSp			0.4 ± 0.9		0.7 ± 1.5			8.6 ± 7.7
Pinheyschna sp.	PinheSp								1.0 ± 0.3
Metrices									
Taxa richness		5.7 ± 1.6	6.0 ± 1.7	6.8 ± 2.0	4.5 ± 1.8	5.8 ± 2.4	6.8 ± 1.5	4.5 ± 0.6	11.0 ± 1.4
Abundances		45.3 ± 37.9	37.2 ± 15.0	59.8 ± 21.7	38.8 ± 37.1	205.5 ± 242.9	682.3 ± 580.8	56.8 ± 45.6	140.5 ± 20.5

Shannon–Wiener		1.19 ± 0.31	1.23 ± 0.31	1.27 ± 0.42	0.97 ± 0.33	1.21 ± 0.16	0.93 ± 0.12	1.04 ± 0.28	1.49 ± 0.55
Simpson		0.58 ± 0.15	0.59 ± 0.13	0.6 ± 0.19	0.52 ± 0.15	0.64 ± 0.03	0.50 ± 0.08	0.59 ± 0.11	0.64 ± 0.24
Evenness		0.62 ± 0.16	0.61 ± 0.14	0.55 ± 0.08	0.67 ± 0.23	0.63 ± 0.13	0.39 ± 0.08	0.65 ± 0.16	0.42 ± 0.17
%Trichoptera		2.4 ± 5.1	11.6 ± 8.3	17.9 ± 9.4	6.8 ± 11				
%Ephemeroptera								5.2 ± 10.4	
%EPT		2.4 ± 5.1	11.6 ± 8.3	17.9 ± 9.4	6.8 ± 11			5.2 ± 10.4	
%Diptera					0.8 ± 2.1	19.3 ± 31.9	36.4 ± 41.7	2.4 ± 4.3	3.6 ± 1.5

Table 6.4 Two–way ANOSIM and SIMPER testing groups on macroinvertebrates communities during high and low hydroperiods in pan wetlands across four geological types located in the central KNP

Groups	**Global Test R**	**Pairwise test R**	***p***	**Dissimilarity distance**	**Main dissimilarity contributes taxa**
+-Hydroperiods	**0.80**		**<0.001**		
High water × Low water		0.8	**<0.001**	86.9	*Anisops* sp. (16.4 %), *Enithares* sp. (15.0 %), Cypridoidea (12.9 %)
Geological types	**0.39**		**<0.001**		
Sandstone × Granite		**0.2**	**0.032**	66.1	Cypridoidea (15.2 %), *Enithares* sp. (14.1 %), Branchiopodidae (11.0 %)
Sandstone × Basalt		0.62	**<0.001**	70.6	Cypridoidea (16.2 %), Branchiopodidae (12.4 %), *Enithares* sp. (10.7 %),
Sandstone × Rhyolite		0.41	**0.004**	78.9	Cypridoidea (15.0 %), Branchiopodidae (13.0 %), *Laccotrephes* sp. (11.11 %), *Potamonautes* sp. 10.7 %)
Basalt × Granite		0.36	**0.001**	62.2	*Enithares* sp. (16.5 %), Cypridoidea (11.9 %)

Rhyolite × Granite		0.3	**0.009**	74.9	Cypridiodea (16.2 %), *Enithares* sp. (13.9 %), *Potamonautes* sp. (11.1 %)
Rhyolite × Basalt		0.53	**<0.001**	72.8	Cypridoidea (20.4 %), *Lymnaea truncatula* (10.3 %), Branchiopodidae (10.0 %)

6.3.4 Relationship between macroinvertebrate community structure and environmental variables

The canonical correspondence analysis (CCA) axes 1 and 2 explained 35.8 % of the fitted cumulative variation in the macroinvertebrate community structure and environmental variables across different hydroperiods and geological types. The macroinvertebrate communities were distinguished between high and low hydroperiods across axis 2 (Figure 6.1). About nineteen sediment (i.e., resistivity, pH, nitrate, Mn, Zn, S, Fe, stone, K, Cu, benthic chl–*a*, B, SOC, H^+) and water (i.e., temperature, nitrate, TDS, salinity, P, phosphate) variables were significant in structuring macroinvertebrate community (Figure 6.1a). The low hydroperiod pans were negatively associated with CCA axis 1. They were characterised by benthic chl–*a*, phosphate, stone, Cu, Fe, C, B, P, and H^+, and associated taxa such as Oligochaeta, *Hyditicus exclamationis*, *Cybester* sp., *Ranatra* sp., *Atroptilum Sudafricanum*, *Pinheyschna* sp., *Enithares* sp., and *Melanoids tubarcellata* (Figure 6.1a). Macroinvertebrate taxa from the different geological type pans did not show clear separation patterns and had substantial overlaps (Figure 6.1b). High hydroperiod pans were associated with CCA axis 1 and were characterised by sediment–pH, temperature, nitrate, salinity, TDS, Mn, Zn and S (Figure 6.1a). These pans were associated with taxa such as *Ecnomus* sp., *Anax speratus*, *Pseudosuccinea columella*, *Sigara* sp., *Laccotrephes* sp., *Appasus* sp., *Hydrochus* sp., Cypridoidea, *Hydrometra* sp., and *Galba truncatula* (Figure 6.1b). During the high hydroperiod, macroinvertebrate taxa showed substantial overlaps in the sandstone, granite and basalt pans, with the rhyolite pans clearly separating from the other geological types (Figure 6.1b).

Using Pearson correlations, a significant and weak negative relationship between macroinvertebrate abundances and water pH (r = –0.34, p = 0.040) was observed. In contrast, a weak positive relationship was observed between macroinvertebrate abundances and conductivity (r = 0.32, p = 0.049), salinity (r = 0.33, p = 0.044), Cu (r = 0.32, p = 0.050), Fe (r = 0.35, p = 0.033) and S (r = 0.40, p = 0.012).

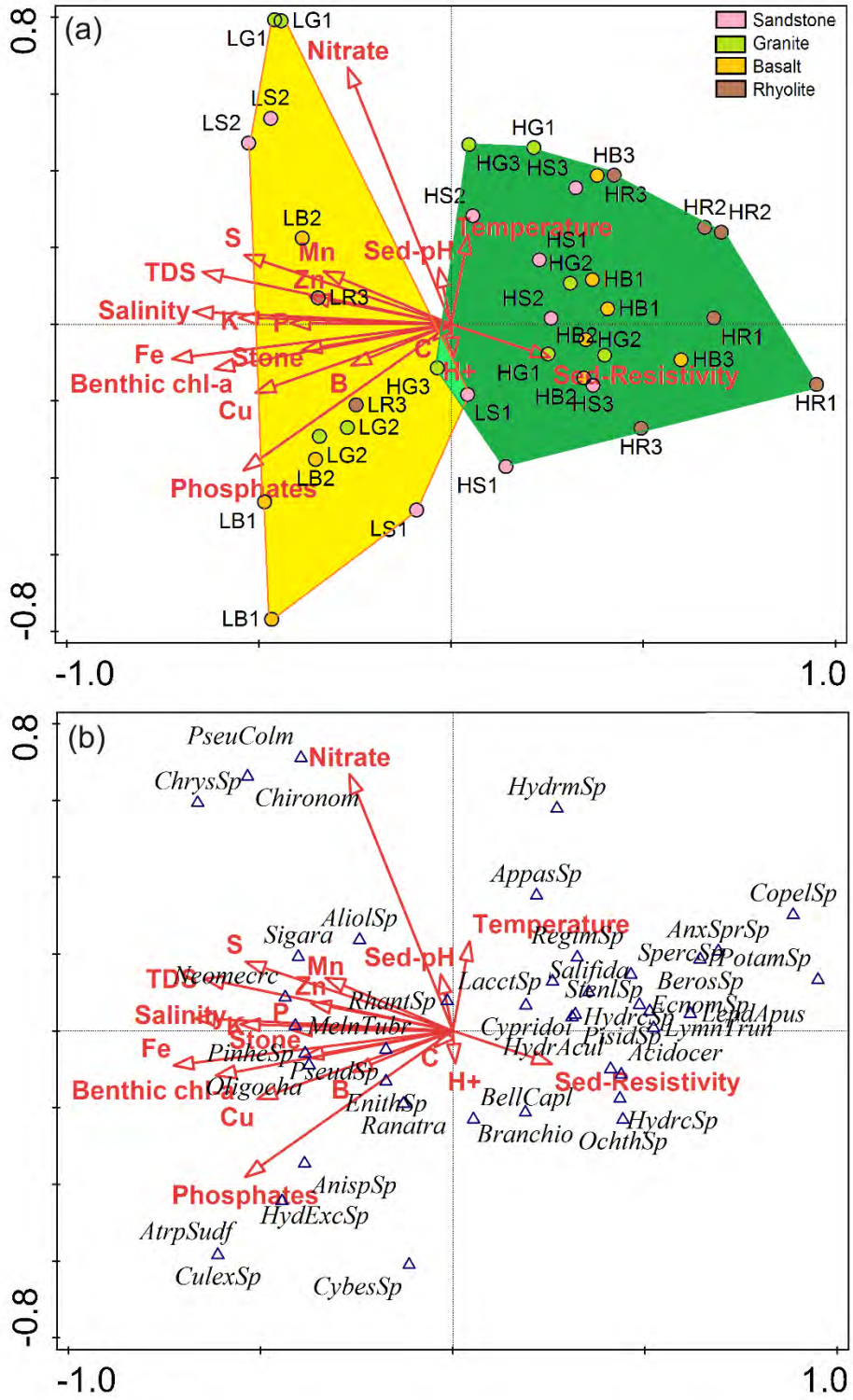

Figure 6.1 Canonical correspondence analysis of macroinvertebrate community structure with sediment and water variables across hydroperiods and geological types for pan wetlands found within the central KNP: (a) samples, water, and sediment variables, and (b) taxa, water and sediment variables. Abbreviations: L – low hydroperiod, H – high hydroperiod and the letters next to L and H indicates the geological types i.e., G – granite, B – basalt, S – sandstone and R – rhyolite, sed – sediment, TDS – total dissolved solids, chl–a – chlorophyll–*a*, and taxa abbreviations are highlighted in Table 6.4

6.4. Discussion

The study showed that hydroperiod played a significant role in structuring or determining the macroinvertebrate diversity and abundances within the different pan systems. Macroinvertebrates were more diverse during high hydroperiod except for rhyolite pans, and more abundant during the low hydroperiod. These results partly supported the study's hypothesis, because while macroinvertebrate diversity was higher in the high hydroperiod, macroinvertebrate abundances was found to be higher during the low hydroperiod. This may be the result of reduced habitat suitability and increased reproductive rates, in response to limited water. Furthermore, increased reproduction rates may result in the production of resting eggs or propagules that will disperse to new environments/habitats (Wasserman et al., 2018). The findings of this study are supported by previous research indicating that changes in water and sediment quality can have a significant impact on the macroinvertebrate composition and community (Dalu and Chauke, 2020; Halabowski and Lewin, 2021; Dalu et al., 2022; Munyai et al., 2023). According to Masina et al. (2023), various macroinvertebrate taxa exhibit distinct preferences for specific ranges of environmental variable characteristics.

Several water and sediment variables during both the low and high hydroperiod were found to have influenced macroinvertebrate community structuring. This supports the findings of Masina et al. (2023), which found that water (i.e., temperature, dissolved oxygen, pH, salinity, conductivity), physical (i.e., stone composition) and sediment (i.e., sulphur, Na) parameters were found to have a significant impact on the macroinvertebrate communities. Moreover, Dalu and Chauke (2020) found that variables such pH, phosphate, temperature, ammonium, macrophyte cover, conductivity and water depth were significant in structuring macroinvertebrate communities in a subtropical wetland system.

Significant differences in macroinvertebrate community metrices were observed across different geological types, and across hydroperiods. Both Shannon–Wiener and Simpson diversity index values were higher during high hydroperiod. The EPT metric index refers to Ephemeroptera, Plecoptera, and Trichoptera, three distinct orders that have been demonstrated to have a heightened susceptibility to environmental changes within the habitat (Hickey and Clements, 1998; Girgin et al., 2010; Masina et al., 2023). According to Ab–Hamid and Rawi (2017), the presence of EPT species denotes that water and sediment parameters in the habitat are within the tolerance limit of the taxa. In our study EPT values could be calculated at all

geological types during high hydroperiod, whereas in the low hydroperiod, the EPT values were only recorded in the basalt pans. This suggest that's the water quality is comparatively better in the high hydro period when compared to the low hydro period.

The diversity of Diptera was found to be low in this study, with Chironominae being only identified during the low hydroperiod. These results correspond with Masina et al. (2023) who observed Diptera during low hydroperiods in the Khakhea Bray pan wetlands, South Africa. However, they contrast with the findings of Odume and Muller (2011) and Dalu and Chauke (2020), who found Chironomidae in the summer months (i.e., high hydroperiod). Macroinvertebrate diversity was significantly different between the high and low hydroperiod, potentially due to each taxa's response to environmental change (Ferreira et al., 2014; Aschalew and Moog, 2015).

Although a weak negative relationship between macroinvertebrate abundances and water pH was observed, a weak positive relationship was observed between macroinvertebrate abundances and conductivity and salinity. The pH sensitivity of macroinvertebrates was taxon-specific, with certain taxa such as the Afroptilum sudafricanum (Ephemeroptera) and Ecnomus sp (Trichoptera) being adversely affected by acidic conditions. These results are consistent with Courtney and Clements (1998) who found that the primary cause of decline in mayflies (Ephemeroptera) abundances was due to their sensitivity towards highest acid concentration.

The high benthic chl–*a* concentration observed during the low hydroperiod may be a result of eutrophication, as was alluded to by Dalu and Chauke (2020). This could potential harm aquatic biota resulting in the reduction biodiversity. Although these chl-*a* concentrations were high during the low hydroperiod, there were generally low when compared to other studies in the region (e.g., Nhiwatiwa et al., 2019; Dalu et al., 2022; de Necker et al., 2023). Moreover, high nutrient concentration (i.e., ammonium, phosphate, nitrate) was observed in the low water period and these results were consistent with the findings by Dalu and Chauke (2020) indicating an increase of chl–*a* concentration along a nutrient gradient.

Based on the findings, it is apparent that a uniform strategy for wetland protection may not yield desired outcomes. Hence, an understanding that macroinvertebrate diversity is influenced by various geological types and hydroperiods might provide valuable insights for informing policy decisions to optimise the preservation of biodiversity by formulating conservation

strategies that are tailored to the unique requirements of individual wetland types. Moreover, policy makers may incorporate the research findings of the impact of geological type and hydroperiod on macroinvertebrate diversity into land use planning procedures. This approach will consider the of protection of various wetland habitats in zoning restrictions as well as in development plans. However, despite the influence the study may have on policy development. It only considered the geological type and hydroperiod, were other significant environmental factors such as vegetation cover, and anthropogenic influences may have a great influence on the variety of macroinvertebrates. Moreover, the accuracy of the results may have been compromised due to limitations in the sample duration. A study conducted over a long period of time may have the potential to yield more accurate results and a better understanding of the seasonal shifts in macroinvertebrate diversity.

6.5 Conclusion

The findings of the study revealed that macroinvertebrate communities were influenced by hydroperiod and geological types in pans. Moreover, the results indicated that hydroperiod, which refers to the duration and frequency of inundation, has a substantial influence on the diversity of macroinvertebrates. Specifically, low hydroperiods tend to result in a decline in biodiversity within pan wetlands. With sediments having a crucial role in providing sustenance and habitat, particularly for organisms such as chironomids and other benthic invertebrates. Sediment chemistry being influenced by geological types, had an impact on the nutrient content and substrate features that were essential for the habitats of macroinvertebrates. Furthermore, the quality of water was a crucial factor, with parameters such as pH, DO, and nutrient concentrations having a direct impact on the diversity, abundance, and health of macroinvertebrates. The research underscores the necessity of implementing conservation approaches that are not a one-size fit all. An understanding of these complex interconnections between geological type, hydroperiod, sediment chemistry, and water chemistry necessitates the implementation of site and hydroperiod specific conservation and management strategies, providing wetland managers proactive solutions to proficiently safeguard these ecological systems, guaranteeing the enduring existence of varied macroinvertebrate populations and the overall well-being of pan wetlands.

CHAPTER SEVEN

CHLOROPHYLL-*A* CONCENTRATION DYNAMICS IN THE LETABA SECTION, KRUGER NATIONAL PARK, SOUTH AFRICA

7.1 Introduction

Phytoplankton is a critical component of primary production in wetlands (Molinari et al., 2021) as it contributes to aquatic foodweb dynamics (Thuy et al., 2018). Phytoplankton dynamics using chlorophyll-*a* concentration as a proxy for biomass within wetland systems are a critical indicator of primary productivity and overall ecosystem health (Dalu et al., 2020). As the primary pigment in phytoplankton, chlorophyll-*a* reflects the abundance of photosynthetic organisms, which form the base of aquatic food webs. In groundwater-dependent wetlands, these dynamics are influenced by a complex interplay of factors, including nutrient availability, light penetration, water temperature, and hydrological fluctuations. Seasonal variations, anthropogenic impacts, and climatic changes further modulate these patterns. Additionally, chlorophyll variations in groundwater-dependent wetlands have not been extensively researched, yet they are critical proxies of productivity.

Phytoplankton also play important roles in the biogeochemical cycles of many elements in these systems through uptake, incorporation, or production during photosynthesis and nitrogen fixation. (Basu and Mackey, 2018). As unicellular photosynthetic organisms, phytoplankton growth is primarily driven by light and nutrients (Dalu and Wasserman, 2018; Hopkins et al., 2021). One of the primary reasons for measuring phytoplanktonic biomass is to estimate primary production rates. The total chlorophyll-*a* (chl-*a*) concentration is the most widely used proxy of phytoplankton biomass because it is coloured, specific to, and shared by all primary producers (Huot et al., 2007). The study of chl-*a* in relation to sediment chemistry dynamics in floodplain wetlands is important because sediments can potentially indicate the status of contamination in various floodplain pans across different hydroperiods (Dalu et al., 2020). Sediments can also provide information about different human activities that are taking or have taken place in a particular catchment where floodplain wetlands are located (Taylor and Owens, 2009). In natural aquatic environments, sediments are the main sink for various metals, but due to changes on environmental conditions such as pH, water temperature, and oxygen redox potential, sediments can potentially act as a source of metals (Chon et al., 2012; Li et al., 2020).

Metal elements entering the aquatic systems can be accumulated at the bottom, subject to the absorptive capacity and textural composition of sediments (Kuriata-Potasznik et al., 2016).

Therefore, understanding chlorophyll-*a* dynamics is essential for assessing water quality, managing wetland resources, and predicting responses to environmental stressors, making it a key focus in ecological and conservation studies.

7.2 Materials and methods

7.2.1 Pelagic chlorophyll-a concentration

Without disturbing the sediment, two 250 mL polyethylene bottles were used to collect water from each site and hydroperiods for and chlorophyll–*a* (chl–*a*) concentration determination in the laboratory. The pelagic chl–*a* concentrations were determined as a proxy for quantifying phytoplankton biomass by filtering the water samples through a 0.7 µm GIC Scientific glass fibre filters. After filtration, the filters were placed individually in 15 mL centrifuge tubes containing 10 mL of 90 % acetone solution and then stored in a freezer for at least 24 hours to allow for chl–*a* extraction (see Lorenzen, 1967 methodology). After 24 hours, the samples were removed from the freezer and centrifuged at 3000 rpm for 10 minutes before 2 mL was extracted from each sample to measure absorbance at the wavelength of 665 nm and 750 nm before and after acidification by 0.01 M hydrochloric acid using a SPECTRO star NANO (BMG LabTech GmbH, Ortenberg).

7.2.2 Benthic chlorophyll-a concentration

Benthic algal core samples (volume = 16.1 cm^3) were collected from each pan (n = 2) per hydroperiod, using a Perspex sediment corer of 20 mm internal diameter inserted by hand into the sediment. About 20 mL of 90 % acetone was introduced into the container with the sediment sample, swirled in the vortex, and the container with the sample was put in a freezer for 24 h for chl–*a* extraction. After 24 hours, samples were removed from the freezer and centrifuged at 3000 rpm for 10 minutes before 2 mL was extracted from each sample to measure absorbance at the wavelength of 665 nm and 750 nm before and after acidification by 0.01 M hydrochloric acid using a SPECTRO star NANO (BMG LabTech GmbH, Ortenberg) following Sartory and Grobbelaar (1984) and Human et al. (2018).

7.2.3 Data analysis

Before multivariate analysis, pelagic and benthic chlorophyll-*a* concentrations were log–transformed to meet two basic assumptions of an ANOVA (i.e., homogeneity and normality). The differences in pelagic and benthic chlorophyll-*a* concentrations between hydroperiods (i.e., high and low) and geological types (i.e., sandstone, granite, basalt and rhyolite) were assessed using a two–way ANOVA analysis, after testing for homogeneity of variance and normality of distribution using SPSS version 25. Tukey's post–hoc analysis was employed to assess the significant values that were different for water and sediment chemistry variables.

7.3 Results

Pelagic chlorophyll–*a* concentration during the high hydroperiod was almost similar (mean 0.1 mg m^{-3}) across the geological types, with the basalt pans having a pelagic chlorophyll-*a* concentration (Figure 7.1a). The low hydroperiod had high chlorophyll-*a* concentrations compared to the high hydroperiod with the rhyolite pans having high chlorophyll-*a* concentrations (Figure 7.1a). No significant differences (ANOVA, $F = 0.553$, $df = 3$, $p = 0.650$) were observed for geology types, however, hydroperiods were found to be significantly (ANOVA, $F = 4.220$, $df = 1$, $p = 0.049$) different in terms of chlorophyll-*a* concentrations.

Benthic chlorophyll–*a* concentrations were significantly high during the low hydroperiod in the sandstone, rhyolite and basalt pans, with almost similar concentrations being found in the granite pans (Figure 7.1b). We found be significantly different (ANOVA, $F = 29.556$, $df = 1$, $p < 0.001$) chlorophyll-*a* concentrations among hydroperiods, with similarities being observed for geological types (ANOVA, $F = 0.540$, $df = 3$, $p = 0.065$).

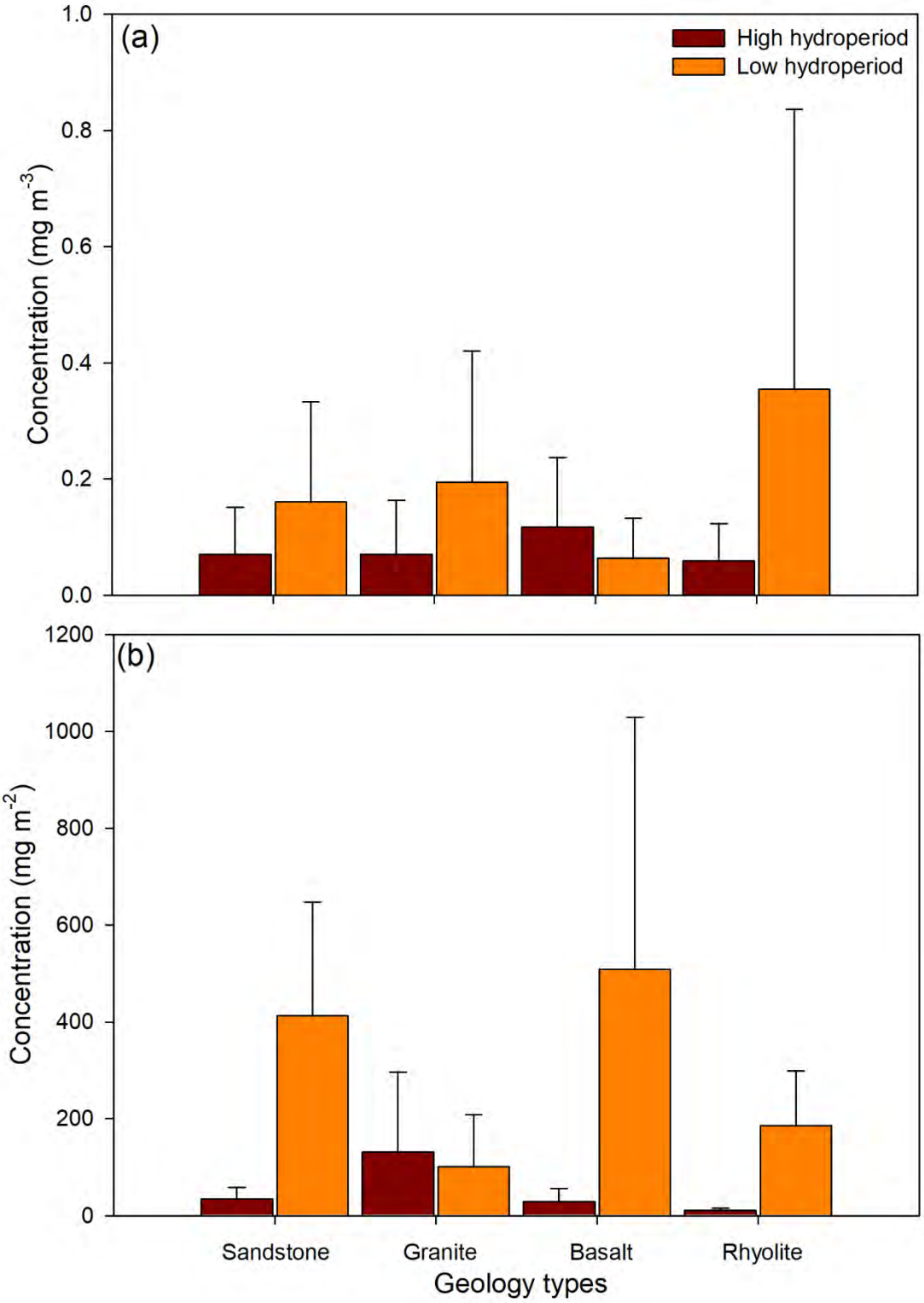

Figure 7.1 (a) Pelagic and (b) benthic chlorophyll-a concentration recorded in pans across different geological types during the low and high hydroperiod

Using Pearson correlations, we found significant and positive relationship between pelagic chlorophyll-*a* concentration with Zn (r = 0.44, p = 0.006), Fe (r = 0.37, p = 0.024), C (r = 0.38,

p = 0.020) and S (r = 0.35, p = 0.031) (Figure 7.2). Pelagic chlorophyll-*a* concentration is a key indicator of phytoplankton biomass, is critically influenced by the availability of trace metals such as Zn and Fe, as well as elements such as C and S as indicated by the study results. These relationships underpin aquatic primary productivity and biogeochemical cycles, shaping freshwater ecosystems and carbon sequestration. Zinc (Zn) and Fe act as micronutrients essential for phytoplankton physiology. Iron is a cofactor in enzymes involved in photosynthesis (e.g., cytochrome complexes) and nitrogen assimilation, often limiting productivity in high-nutrient, low-chlorophyll regions such as pan systems. Zinc though less studied, is crucial for carbonic anhydrase, an enzyme facilitating CO_2 hydration, thereby enhancing carbon fixation (Sunda, 2012). Similarly, Zn and Fe can alleviate co-limitation, boosting chlorophyll-*a* concentrations when both are available (Twining and Baines, 2013). Carbon (C) forms the structural backbone of organic matter. Phytoplankton assimilate dissolved inorganic carbon via photosynthesis, directly linking C availability to chlorophyll-*a* production. Elevated CO_2 levels can stimulate growth, particularly under nutrient-replete conditions, though responses vary by species (Riebesell, 2004). Organic carbon exudates also foster microbial loops, indirectly supporting phytoplankton communities.

Sulphur (S) contributes to amino acids (cysteine, methionine) and dimethylsulfoniopropionate, a compound implicated in osmoregulation and antioxidant defence. DMSP breakdown products influence cloud formation and climate feedback, while intracellular S availability supports protein synthesis and cellular integrity, enhancing phytoplankton resilience and biomass (Stefels et al., 2007). Collectively, these elements drive phytoplankton dynamics. Fe and Zn enable metabolic functions, C provides energy and structure, and S supports stress adaptation. Their interplay underscores the sensitivity of pelagic chlorophyll-*a* concentrations to biogeochemical cycles, with implications for ocean productivity and climate regulation. Understanding these relationships aids in predicting responses to anthropogenic changes, such as trace metal deposition or ocean acidification.

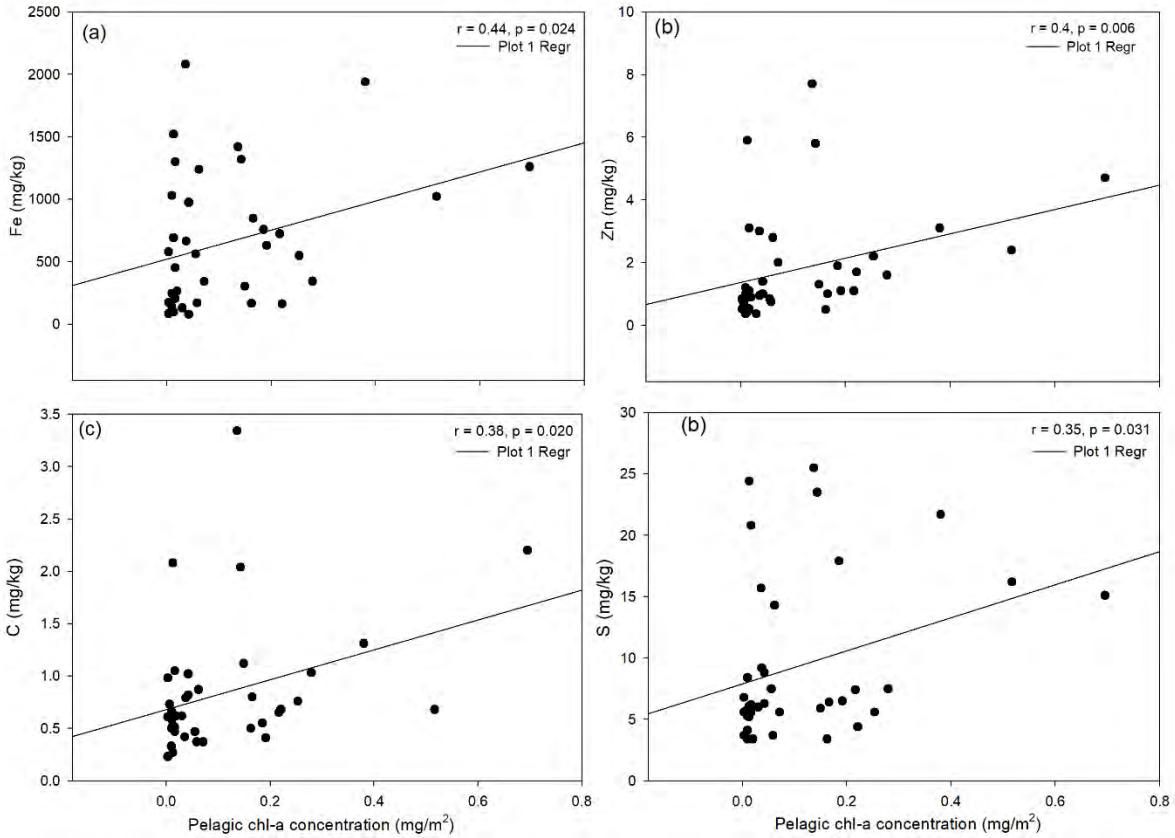

Figure 7.2 Relationship between pelagic chlorophyll-*a* concentration with selected environmental variables among pans

Based on Pearson correlation, water phosphate (r = 0.50, p = 0.002), total dissolved solids (r = 0.36, p = 0.027), salinity (r = 0.40, p = 0.014), sediment phosphorus (r = 0.41, p = 0.010), K (r = 0.32, p = 0.050) and Fe (r = 0.43, p = 0.008) were found to significant and positively related to benthic chlorophyll-*a* concentration (Figure 7.3a, c, d, f, g, h). However, pH (r = -0.33, p = 0.042) and pan surface area (r = -0.37, p = 0.023) were found to be significantly negatively correlated with benthic chlorophyll-*a* concentration (Figure 7.3b, e).

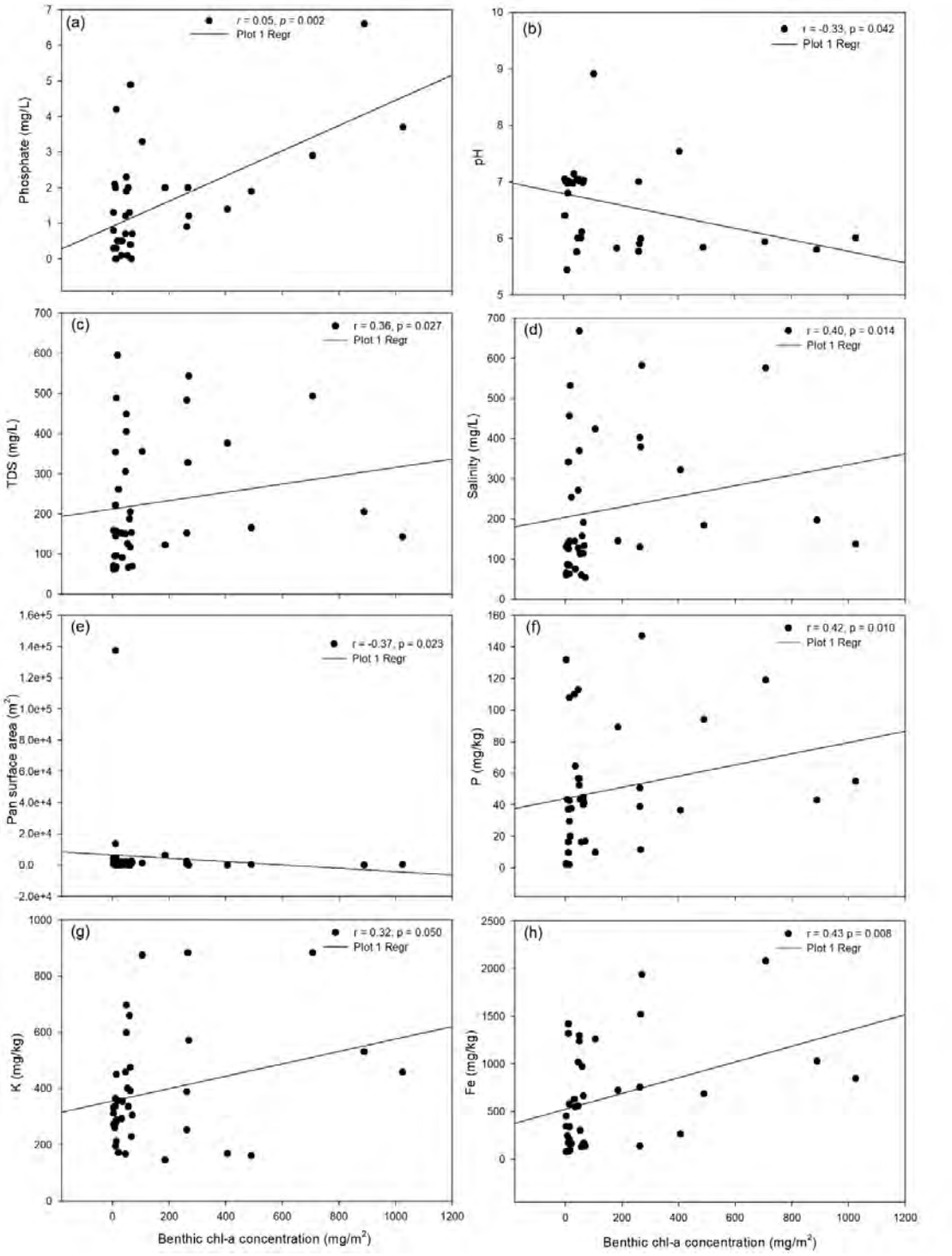

Figure 7.3 Relationship between pelagic chlorophyll-a concentration with selected environmental variables among pans

Benthic chlorophyll-*a* concentration is a key indicator of phytoplankton biomass in wetland sediments and is influenced by multiple physicochemical factors that enhance primary productivity. Phosphorus availability, particularly water phosphates are a critical driver and are

often considered to be a limiting nutrient for phytoplankton growth (Smith and Schindler, 2009). Elevated phosphate concentrations directly stimulate benthic algal proliferation, increasing chlorophyll-a synthesis. Similarly, sediment phosphorus acts as a reservoir, releasing soluble reactive phosphorus into the water column under anoxic conditions, further fuelling phytoplankton biomass (Reddy et al., 1999).

Total dissolved solids (TDS) and salinity also exhibit positive correlations with benthic chlorophyll-*a* concentration. The TDS encompasses ions such as calcium and magnesium, which can enhance nutrient bioavailability. In wetlands, moderate salinity (a component of TDS) supports halotolerant phytoplankton species, fostering community shifts that boost productivity (Wetzel, 2001). Salinity-driven ion gradients may additionally stabilise cell metabolism, optimising photosynthetic efficiency. Sediment-derived K and Fe further contribute to chlorophyll-*a* dynamics. Potassium is a macronutrient which regulates enzyme activation and osmotic balance in phytoplankton, promoting growth under high sediment concentrations. Iron is integral to chlorophyll synthesis and electron transport in photosynthesis (Sunda and Huntsman, 1995). Moreover, Fe mediates phosphorus cycling; under reducing conditions, Fe (III) oxides dissolve, releasing adsorbed phosphate into the water column, indirectly stimulating phytoplankton biomass (Reddy et al., 1999). These interlinked factors underscore the synergistic role of nutrients and ions in sustaining benthic phytoplankton. Wetlands, as dynamic interfaces, thus rely on sediment-water exchanges and ionic composition to modulate primary production. Understanding these relationships aids in managing eutrophication and conserving wetland ecosystems.

In freshwater wetlands, benthic chlorophyll-*a* concentration exhibits negative relationships with both pH and pan surface area, influenced by ecological and physicochemical dynamics. Elevated pH often correlates with reduced benthic chlorophyll-*a* concentration, potentially due to nutrient limitation. In alkaline conditions, phosphorus (P) binds to calcium and/or magnesium, forming insoluble complexes (Wetzel, 2001), thereby limiting bioavailability for benthic phytoplankton. Additionally, high pH may favour submerged macrophytes over phytoplankton, intensifying competition for light and nutrients (Vadeboncoeur et al., 2002). In contrast, in lower pH environments, organic matter decomposition releases dissolved organic carbon and nutrients, potentially enhancing benthic phytoplankton growth (Stevenson et al., 1996). Pan surface area, representing open water extent, also inversely relates to benthic chlorophyll-*a* concentration. Large pans experience greater wind-driven turbulence, resuspending sediments and reducing benthic phytoplankton stability (Smith et al., 2015).

Increased surface area may dilute nutrient concentrations, limiting phytoplakton proliferation, while expanded photic zones favour phytoplankton over benthic communities (Vadeboncoeur et al., 2018). Small, vegetated pans reduce wind disturbance and provide organic substrates, fostering benthic phytoplankton growth. Furthermore, larger pans often undergo fluctuating water levels, disrupting benthic habitat continuity (Coops et al., 2003). Thus, these relationships underscore the sensitivity of benthic phytoplankton to abiotic factors. Management strategies aiming to preserve wetland biodiversity or regulate phytoplankton biomass should consider pH moderation through buffering and maintaining heterogeneous wetland morphometry to balance open water and vegetated areas. Future research should explore the interactive effects of pH, hydrology, and nutrient fluxes to refine predictive models for wetland ecosystems.

7.4 Conclusion

Sediment quality variables were found to be significant drivers of both the pelagic and benthic chlorophyll-a concentrations within the pans. The chlorophyll-a concentration tended to vary across hydroperiods, highlighting the importance of seasonal changes in the water as important drivers for chlorophyll-a concentration. Hydroperiod significantly influences chlorophyll-*a* concentrations more than geological type, with higher levels observed during the low hydroperiod. Trace elements (Zn, Fe) and nutrients (C, S, P, K) play a crucial role in phytoplankton productivity. Benthic chlorophyll-*a* is positively linked to salinity and TDS but negatively affected by high pH and large pan surface areas due to nutrient binding and sediment resuspension. Effective wetland management should focus on maintaining nutrient balance, stable hydrology, and optimal pH conditions to support productivity and prevent eutrophication. Further studies using GIS/remote sensing are required to quantify and map chlorophyll-a concentration over large spatiotemporal scales.

CHAPTER EIGHT

MAPPING AND MONITORING OF VEGETATION SPECIES DIVERSITY, STRUCTURAL, AND PHENOTYPICAL TRAITS IN GROUNDWATER-DEPENDENT ECOSYSTEMS

8.1. Introduction

Vegetation biodiversity in dryland ecosystems is crucial for ecological integrity, human well-being, and global sustainability. Drylands account for 41% of the Earth's land area (UNCCD, 2019) and provide habitat to 35% and 20% of the global diversity hotspots, respectively, underscoring the significance of vegetation biodiversity in sustaining essential ecosystem functions. Dryland areas are defined by their aridity index (AI < 0.65), consisting of low and unpredictable precipitation and high evapotranspiration rates (Zhang et al., 2023). The significance of diverse vegetation in arid regions extends to vital aspects such as soil fertility, water regulation, adaptation to climate variability, and the provision of essential resources for local communities facing environmental challenges spurred by global changes (Díaz et al., 2019). In conservation areas like the KNP, the ecological value of varied vegetation is amplified, as these areas serve as biodiversity hotspots offering forage, water, and habitat to wildlife, particularly during prolonged dry periods (Mpakairi et al., 2022; Rampheri et al., 2022). These vegetation hotspots usually form part of GDEs (Alaibakhsh et al., 2017), sources of sustenance for regionally confined species and endangered wildlife (Mpakairi et al., 2022). Apart from the implementation of hydrological surveys, identifying GDEs poses challenges, especially when assessing the vegetation reliant on groundwater, which further complicates the process (Pérez Hoyos et al., 2016). In dryland areas, natural pans rely on groundwater; thus, the vegetation surrounding them is likely dependent on groundwater (Mpakairi et al., 2022). The presence of a high-water table around these natural pans replenishes them and supplies soil water, supporting the ecological functions of the surrounding vegetation (Albano et al., 2020; Lamontagne et al., 2005; Mpakairi et al., 2022).

Vegetation near natural pans tends to exhibit high density and diversity, which may decrease as the distance from the pans increases. Climate change and groundwater pollution are increasing the reliance on groundwater, posing threats to the quantity and quality of available water essential for maintaining the ecological functions of GDEs (Hultine et al., 2020). This could result in the degradation of GDEs, leading to biodiversity loss, bush encroachment, and

deforestation (Rampheri et al., 2022). Landscape alterations such as disturbance, fragmentation, and changes in land cover influence the abundance of rare and endangered species, consequently impacting biodiversity (Liu et al., 2021). Indicators such as functional diversity loss, habitat loss, population declines, and species invasions highlight the challenges in preserving vegetation diversity. To mitigate biodiversity loss, effective management plans should rely on comprehensive and timely information regarding the status and trends of vegetation diversity within these conservation hotspots (Glanville et al., 2023; Link et al., 2023; Liu et al., 2021). This includes an assessment of vegetation species diversity, alpha diversity (local species richness), beta diversity (community difference), and gamma diversity (regional diversity) (Baldeck and Asner, 2013; Lausch et al., 2020; Luz de la Maza et al., 2002; Rocchini et al., 2010). In this regard, robust methodologies suitable for monitoring and assessing vegetation biodiversity in GDEs across various scales are essential.

Generally, vegetation biodiversity studies heavily rely on field survey techniques, which offer detailed insights into species richness, abundance, and phenological characteristics of plants. While these field surveys accurately quantify alpha diversity (species diversity at local scales), works that demonstrate their utility in quantifying beta diversity (differences between two sites) are limited even in relation to the quantification of gamma diversity over a broader geographic area (Andermann et al., 2022). Furthermore, field survey techniques are time-consuming, expensive, and prone to biases when scaled up. Notably, vegetation species sampling in the field can often be impacted by observer bias, spatial errors, and historical biases in species distribution records (Wang and Gamon, 2019). Alternative methods for estimating diversity, such as using occurrence records, floras, and checklists to tally the total number of species within large biogeographic regions, exist. Although these approaches do not entail modelling distributions of individual species, they are susceptible to biases in data collection. Certain taxa may be disproportionately represented in specific checklists and biodiversity repositories, potentially skewing estimates. Moreover, this method assumes a uniform diversity value within each analysed region, overlooking potential diversity variations within these extensive areas (Andermann et al., 2022).

Estimates of vegetation diversity using remote sensing, particularly those based on the spectral variation hypothesis (SVH), offer a rapid and precise means to evaluate vegetation diversity across vast and complex landscapes. The SVH suggests that the spectral patterns of diversity across extensive landscapes are indicative of vegetation diversity. In landscapes characterised by spectral heterogeneity, diverse ecological niches are expected, indicating a correlation

between environmental variability and ecological diversity (Rocchini et al., 2004). Based on this hypothesis, diversity is inferred from spectral variation, requiring datasets capable of capturing subtle differences in spectral patterns. Consequently, data from high spatial and hyperspectral sensors have been successful in accurately estimating spectral diversity, whereas data from coarse sensors like MODIS have shown poorer performance in this regard (Cleemput et al., 2018; Anand et al., 2022). Zhang et al. (2023) demonstrated that datasets from moderate spatial resolution (<30m) could effectively estimate alpha and beta diversity in drylands. The applicability of spectral variation in diversity still lacks attention is still limited in drylands. However, multispectral sensors such as Sentinel 2 MSI have helped bridge this gap by accurately discerning spectral variations due to their moderate spatial resolution and inclusion of unique spectral bands like the red edge band, renowned for its optimal influence in vegetation mapping applications. Sentinel 2 has displayed considerable promise in mapping forest diversity by capturing phenology-related information of tree species through Multi-Temporal and Spectral-Temporal-Metric data, thereby substantially enhancing the accuracy of plant diversity predictions (R2 ranging from 0.37 to 0,68) (Liu et al., 2023; Chrysafis et al., 2020; Kumar et al., 2022). Nevertheless, computation of gamma diversity at large scales is constrained by the computational and financial costs involved.

Various techniques are commonly used to measure vegetation diversity based on the SVH. These include (i) distance from the spectral centroid in spectral space (Rocchini, 2007), (ii) variation in NDVI (Gould, 2000), (iii) convex hull volume in principal component space (Dahlin, 2016), and (iv) Rao's Q (Torresani et al., 2019). However, there is still no consensus on which SVH technique is superior. Additionally, studies suggest that the spectral coefficient of variation is a reliable predictor of vegetation biodiversity. While each technique for estimating vegetation diversity has its advantages and limitations, combining multiple approaches and fostering interdisciplinary collaboration can enhance the accuracy and comprehensiveness of vegetation diversity assessments. Therefore, this study aims to evaluate models of vegetation species diversity derived from spectral CV, topographic features, and soil moisture to predict Alpha and Beta diversity in potential groundwater-dependent vegetation zones. The study also seeks to investigate the effects of distance from pans on vegetation diversity and examine temporal trends in vegetation diversity during dry years in the KNP, South Africa.

8.2 Materials and Methods

8.2.1 Data collection methods

Twelve of the Makuleke wetland system natural pans located in the Pafuri area were sampled, and the second set of sample plots was within the Letaba region of KNP. The field survey was conducted in September 2022 (late dry season), when the pans were mostly dry with a few inundated from the Makuleke area. The sampling period was selected to easily discriminate vegetation species and pans maintained by groundwater from those that are not. Pans with water and green vegetation surrounded by dry vegetation late dry season are likely to be receiving groundwater, and thus the green vegetation was groundwater dependent. During the field survey, dominant vegetation was identified by a biologist, and pictures were taken to validate with information from the iNaturalist plant identification programme. Field plots were randomly sampled within the identified potential groundwater-dependent ecosystem zones (pGDEZ). These sample plots were distributed along natural pans at the Makuleke area and Letaba area within the KNP. The centre of the plot was navigated using a handheld GPS with less than 5m. The north-oriented plots were set to measure 100m2 (10m × 10m), moreover, this corresponds to the Sentinel-2 imagery. Vegetation surveys were conducted in the plots to determine plant species composition and abundance across the pGDEZ and note the phenological characteristics. During the field surveys, a total of 23 plots were considered in this study for sampling vegetation data in the Maluleke and Letaba regions. The different vegetation species at each plot were identified and recorded at each plot location to prepare the data matrix for computing alpha and beta diversity. The species were further grouped into genera. The spectral Coefficient of variation (CV) was used to calculate vegetation diversity.

8.2.2 Predicting vegetation diversity

During the prediction of vegetation diversity, the spectral coefficients of variations were used, and these were derived for a harmonised Sentinel-2 data available in the Google Earth Engine catalogue. The data was selected because of its improved spatial and temporal resolutions. During the analysis, the data were initially filtered by the KNP boundary, and then by date and cloud cover. The images selected were collected during the dry season (May-September 2022) and had a cloud cover proportion of less than 5%. A total of 7 images were collected, and these were composited using the median composite approach to reduce the image stack rather than selecting a single date image, which is prone to atmospheric influences. The resulting composite image was then used to create a cloud mask at 0.1 as well as a built-up area mask at 0.5 to eliminate features such as built-up areas as well as water features, amongst others. The

thresholds were based on literature and an understanding of the landscape (Mpakairi et al., 2022). Vegetation diversity has been shown to correlate with CV (Madonsela et al., 2021; Oldeland et al., 2010). The coefficient of variation was calculated as the mean CV for each wavelength from all the bands within the Sentinel 2 image in GEE using equation 7.1.

$$CV=\sum 2200\lambda=442(\sigma(\rho\lambda)\mu(\rho\lambda))/ \text{ number of bands} \quad 7.1$$

Where $\rho\lambda$ represents the reflectance at wavelength λm and $\sigma(\rho\lambda)$ and $\mu(\rho\lambda)$ denote the standard deviation and average value of reflectance at wavelength λ across all the pixels in the image.

Topographical data, including slope and elevation, were retrieved from a 30m SRTM image sourced from the Google Earth Engine (GEE) repository using the specified path (ee. Image((USGS/SRTMGL1_003)). These parameters were computed on the GEE platform following the methodology outlined by Safanelli et al. (2020). Areas characterised by gentle slopes (<3m) and lower elevations are identified as low-flow zones with increased groundwater availability.

Subsurface soil moisture (SUSM) served as an input indicator for vegetation diversity. The *SUSM* data were obtained from the Google Earth Engine repository (*ee. ImageCollection("NASA_USDA/HSL/SMAP10KM_soil_moisture"*)). The SUSM was extracted for the 2018, 2019 and 2022 dry periods. The SUSM data has a spatial resolution of 10 km and was resampled to 20m to match that of the CV dataset. This dataset integrates soil moisture observations from the satellite-derived Soil Moisture Active Passive (SMAP) Level 3 into the adapted two-layer Palmer model using a 1-D Ensemble Kalman Filter (EnKF) data assimilation method. This assimilation of SMAP soil moisture observations enhances the accuracy of model-based soil moisture predictions, particularly in regions with insufficient precipitation data and limited instrumentation. The spatial resolution of the SUSM data is originally 10 km, but it was resampled to 20m to align with the resolution of the CV dataset. The CV was later used to compute alpha and beta vegetation diversity.

8.2.3 Calculating alpha and beta vegetation diversity and spatial regression

During the computation of alpha and beta vegetation diversity, the Shannon-Weiner Diversity Index (H') was used for each plot. H' is a qualitative measure that reflects different types of species within a sample or community and their frequency of occurrence. The H' ranges between 0 and 5. This index was chosen because it accurately measures species richness when the frequency of occurrence is standardised. Each species was given an abundance value of 1.

$$H = -\sum i=1\ pi \ln pi \qquad (7.2)$$

Where S is the total number of species in the window, and pi is the proportion of species i to S. Another diversity measure observed was beta diversity, the measure of species difference/similarity between neighbouring plots. The Sorensen similarity index measures the overlap in species composition between two populations, relative to the number of species in both populations. The index varies between zero (no overlap) and one (perfect overlap). The equation follows.

$$\text{Sørensen-similarity} = 2\times(A\times B)/(A)+(B) \qquad (7.3)$$

Where A×B represents the number of species common to both sites A and B, A represents the number of species in A, and B represents the number of species.

Further, the Hellinger method was used to calculate species' contribution to vegetation diversity, local beta, richness, and diversity for each plot. The Hellinger distance between the probability distributions of species composition at different sites was calculated using this formula (Hellinger, 2012).

$$D_{\mathrm{H}}(P_1, P_2) = \frac{1}{\sqrt{2}}\sqrt{\sum_{i=1}^{k}(\sqrt{p_i} - \sqrt{q_i})^2} \qquad (7.4)$$

Where the summation is over all the elements in the probability space, pi are the probabilities under distribution P, and qi are the probabilities under distribution Q.

The multicollinearity test was conducted to determine appropriate variables for predicting alpha and beta diversity for the plots. The spectral indices, spectral bands, CV, slope, elevation and subsurface soil moisture vegetation indices were used as predictor variables for the diversity regressions. However, the results indicated high perfect collinearity between the variables. However, models with low multicollinearity included CV, slope, elevation, SUSM, thus, these variables were used to model alpha and beta diversity in the KNP. The relationship between the predictor variables and species diversity as the response variable was further evaluated by the multi-linear regression analysis techniques. Multi-linear regression results determined the corrected Akaike's Information Criterion (cAIC), Spearman correlation and Coefficient of determination (R^2), adjusted R^2 and f-statistic, which were used to determine the strength of the relationship between each predictor variable and the field diversity values. First, the Shapiro-Wilk test was computed to determine the normality of the datasets. The datasets

were not normally distributed; thus, the non-parametric, Pearson correlation was computed to evaluate the linear relationship between alpha and beta diversity and the predictor variables.

To model the 2022 distribution of alpha and beta diversity, the linear regression function in GEE with four predictor variables and one response variable was used. The predicted alpha and beta values were then extrapolated across the KNP. The framework for modelling vegetation diversity within the KNP is outlined in Figure 8.1. This method was repeated for the 2018 and 2022 datasets to account for the temporal dynamics of alpha and beta diversity. From the 2022 extrapolated alpha and beta images, the predicted alpha and beta values were extracted to compute and plot the correlation between field alpha and predicted alpha using the Scipy stats functions and seaborn in Jupiter Notebook.

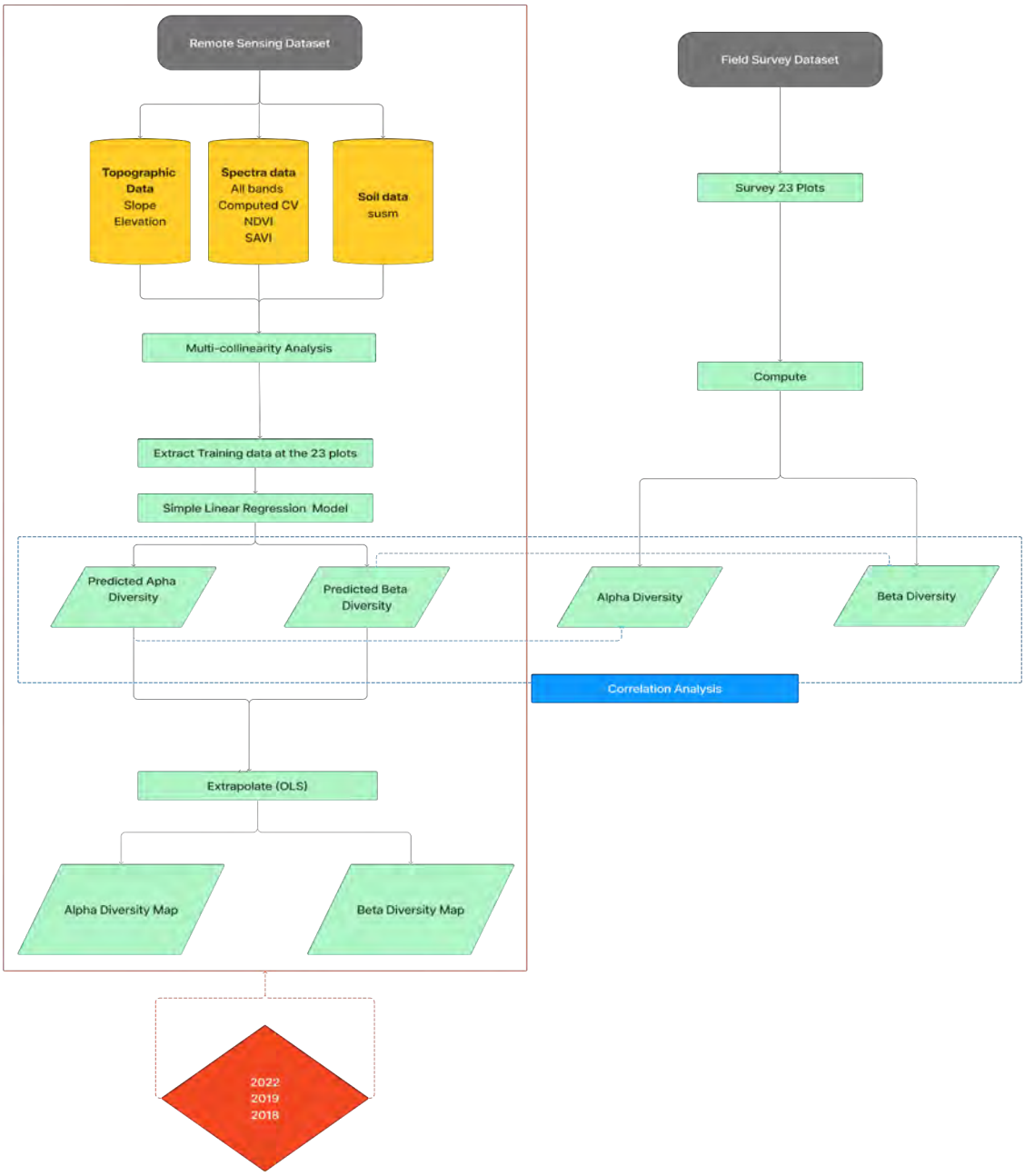

Figure 8.1 Framework for modelling alpha and beta diversity in KNP

8.3 Results

8.3.1 Alpha (species richness) and beta diversity (differences in species composition) for the selected sites

Vegetation alpha diversity ranged between 0.69 to 1.95 for both the Makuleke and Letaba regions. In terms of beta diversity, the Makuleke region has greater total beta biodiversity than the Letaba Region of KNP (Table 7.1). The beta diversity at the Makuleke (75%) and Letaba (51%) sites is related to species turnover between the different windows, as opposed to nestedness (variation in composition).

Table 7.1 Beta diversity partitioning for the Makuleke and Letaba vegetation

	Beta diversity	Replacement	Richness difference	Replacement/beta total	Richness difference/beta total
Makuleke	0.33	0.24	0.08	0.75	0.25
Letaba	0.28	0.14	0.14	0.51	0.49

8.3.2 Macroinvertebrate contribution to beta diversity at the Letaba and Makuleke sites

The identified vegetation genera and their contribution to beta diversity at the Makuleke and Letaba sites are displayed in Figure 8.2. For the Makuleke sites, *Diospyros*, *Eragrostis*, and *Hyphaene* were the three most contributors to beta diversity. For the Letaba area, beta diversity was mostly contributed by *Combretum*, *Eragrostis*, and *Philenoptera*.

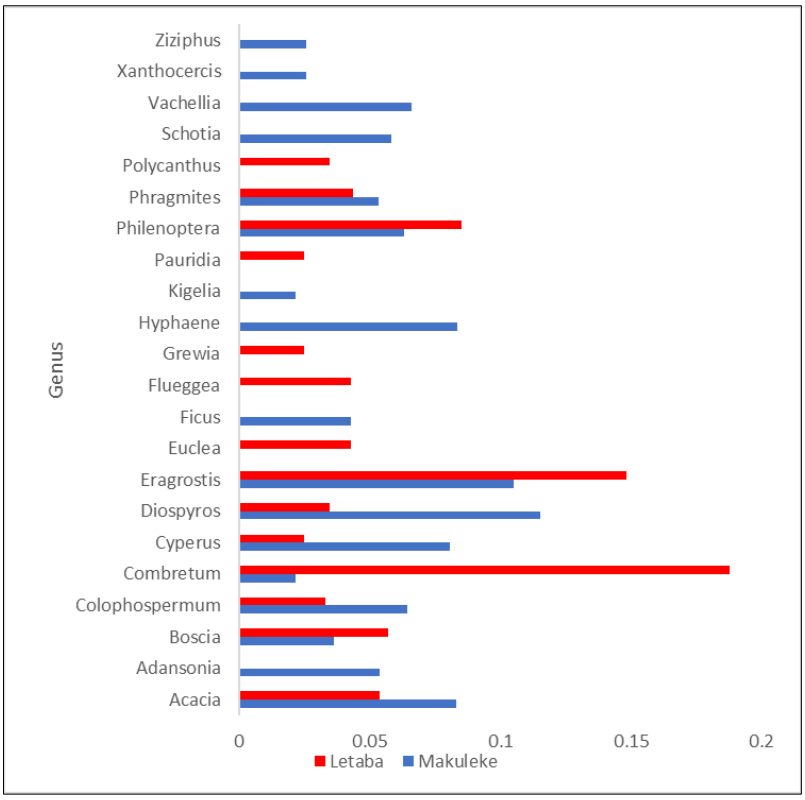

Figure 8.2 Genus contributions to beta diversity for the Makuleke and Letaba regions of the KNP

8.3.3 Predicting alpha and beta diversity using multiple linear regression

In examining the association between vegetation diversity and the predictor variables, Pearson correlation results showed a negative correlation between alpha diversity and the variables CV, slope, elevation, and SUSM, while a positive correlation was observed between beta diversity and elevation as well as SUSM (Table 7.2). Specifically, alpha diversity showed a moderate negative relationship with slope (-0.37) and CV (-0.17). On the other hand, beta diversity exhibited a stronger negative correlation with CV (-0.44) and moderate positive correlations with elevation (0.28) and SUSM (0.20).

Based on the Ordinary Least Squares (OLS) regression analysis, approximately 15.1% of the variability in alpha diversity and 30.9% of the variability in beta diversity could be attributed to the variations of predictor variables considered in this study, as indicated by the R-squared values. However, the low adjusted R-squared values suggest that the models explain very little of the variability in both alpha and beta diversity. Additionally, the F-statistics indicated that the results of the beta diversity model were more statistically significant than those of the alpha diversity model. Furthermore, the lower value of the Akaike Information Criterion (AIC) in

the beta model suggests that it was a better-fitting model when compared to the alpha diversity model.

Table 7.2 Details Person correlation between predictor variables the estimated alpha and beta diversity. Model performance is also evaluated using r^2. adjusted r^2, f-statistic and AIC

Pearson's Correlation with Alpha:	Alpha	Beta
CV	-0.17	-0.44
Slope	-0.37	-0.29
Elevation	-0.07	0.28
SUSM	-0.10	0.20
OLS Regression Results:		
R-squared:	0.16	0.31
Adjusted R-squared	0.02	0.15
F-statistic	1.12	1.90
AIC	19.30	-97.95

8.3.4 Correlation between field-based and predicted alpha and beta diversity

The correlation analysis between field-based and predicted alpha and beta diversity yielded a value of -0.07 (Figure 8.3a). This indicated that the association between field-based and predicted alpha and beta diversity was negative and very weak. However, this correlation was not statistically significant, as indicated by a p-value of 0.75. Meanwhile, the correlation analysis between the observed and predicted beta diversity exhibited a significant ($p = 0.041$) coefficient value of -0.44, indicating a moderate negative correlation between the observed beta diversity and the predicted beta diversity. An R-squared value of 0.19 suggested that approximately 19% of the variance in the observed beta diversity could be explained by the predicted beta diversity (Figure 8.3b).

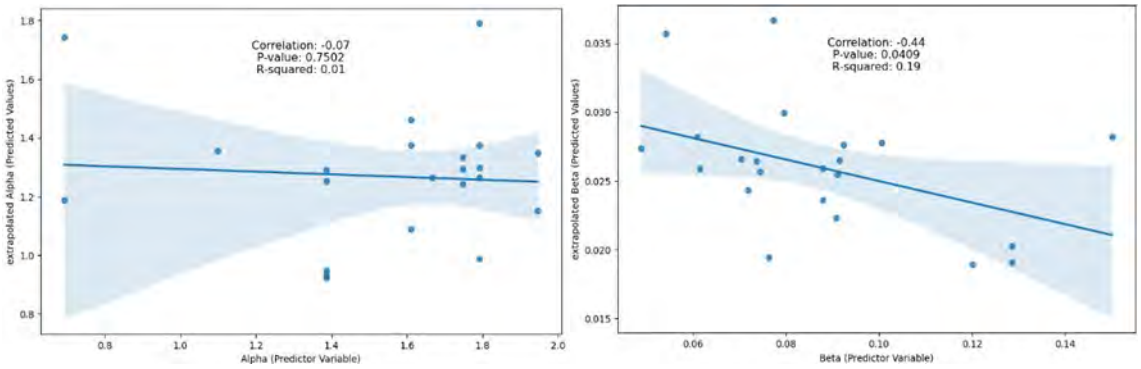

Figure 8.3 (a) Plot of the correlation between alpha diversity and the predicted alpha diversity, and (b) correlation between beta diversity and the predicted beta diversity

8.3.5 Spatial variation of alpha and beta diversity

Vegetation alpha diversity was notably elevated in the Maluleke woodlands forest situated along the floodplains of the Limpopo and Luvhuvhu rivers. The Makuleke region is predominantly marked by areas exhibiting moderate levels of alpha diversity. Comparatively, the Letaba area demonstrated moderate to high levels of alpha diversity in contrast to the Makuleke region. Furthermore, vegetation diversity was prominently heightened in the western sector of the Letaba area, extending beyond the confines of riparian zones. Additionally, the southeastern segment of the KNP showcased notably high alpha diversity. Alpha diversity ranges from 0-2.96, which is moderate compared to the general range of 0-5 (Figure 8.4)

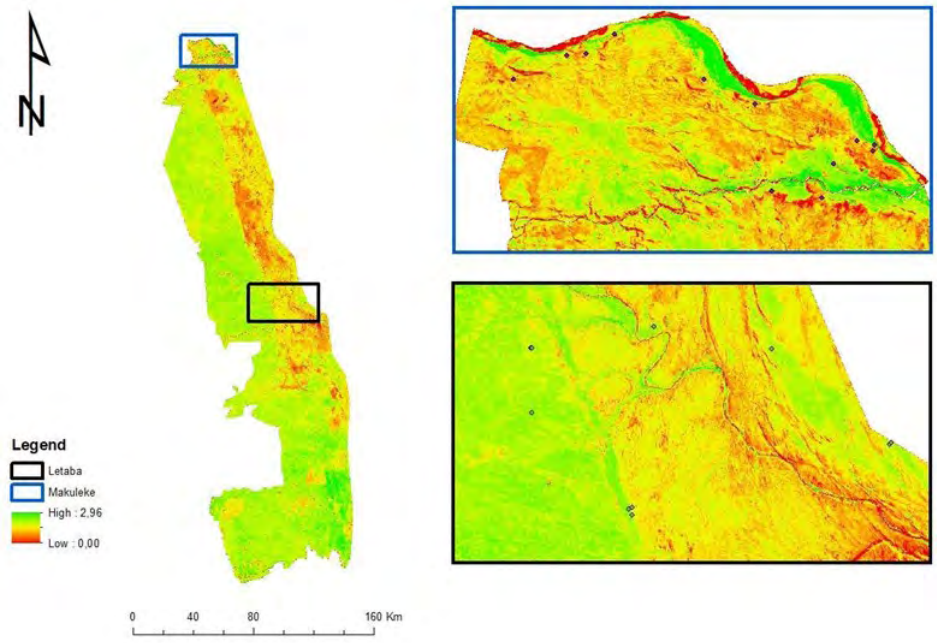

Figure 8.4 Alpha Diversity within the Kruger National Park

Meanwhile, the spatial distribution of vegetation beta diversity was noted to align with the spatial patterns of alpha diversity. The highest levels of beta diversity were observed in the southeastern part of the KNP and along the floodplains of the Limpopo and Luvhuvhu rivers within the Makuleke conservation area. In the Letaba section, vegetation diversity was moderately high and extended beyond riparian areas. The beta diversity values ranged from 6.24 x 10-^{5} to 0.06, indicating a notable reduction in diversity compared to the general spectrum of 0-1 (Figure 8.5). Additionally, beta diversity is moderately high in the vicinity of the sampled pans.

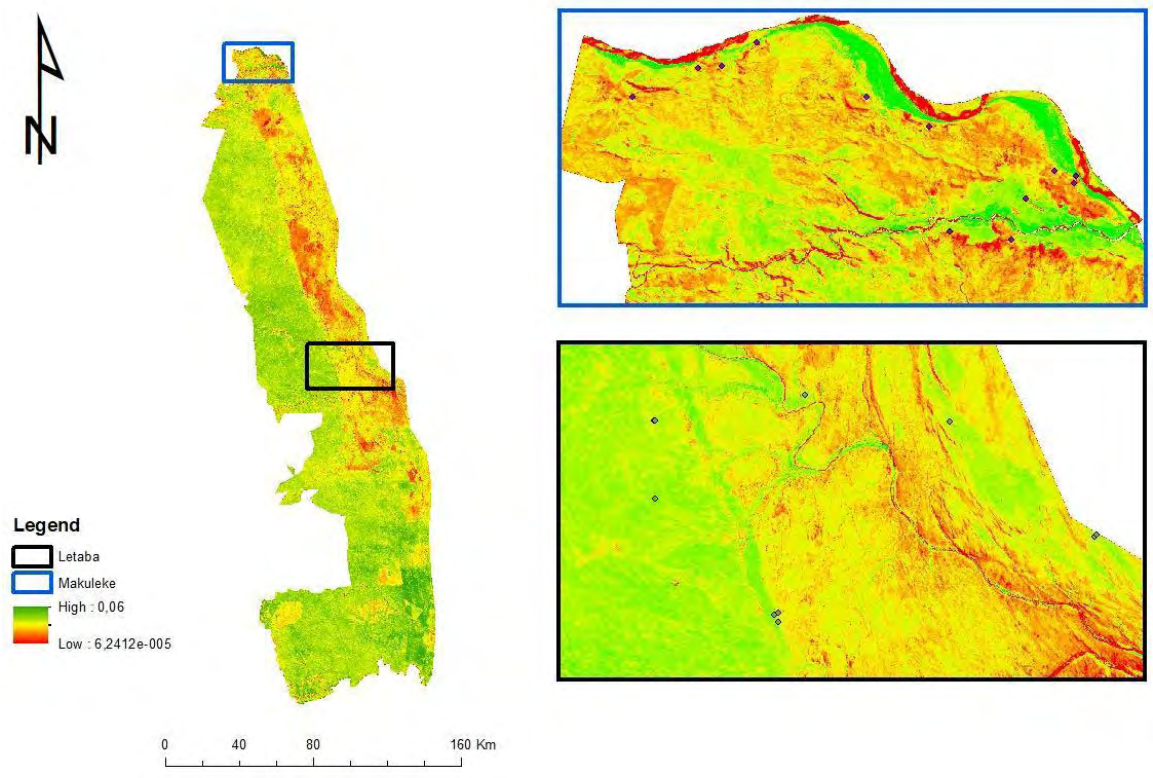

Figure 8.5 Beta Diversity within the Kruger National Park

8.3.6 Relationship between alpha and beta diversity and distance from wet and dry pans

The inverse AICc curves were found to be more suitable for modelling the relationship between alpha diversity and the distance from wet pans, while polynomial AICc curves effectively captured the relationship between dry pans and both alpha and beta diversity. This suitability is evidenced by the low AICc values of the curve estimates (Table 7.3).

Table 7.3 The estimated values from the six AICc curve estimates

	Alpha Wet	Beta Wet	Alpha Dry	Beta Dry
Linear AICc:	-65,56	-143,33	-75,78	-153,55
Cubic AICc	-63,49	-141,26	-77,88	-155,65
Quadratic AICc	-64,18	-141,95	-77,03	-154,80
Logarithmic AICc	-68,43	-146,20	-75,07	-152,84
Polynomial AICc	-63,07	-140,84	**-78,24**	**-156,01**
Inverse AICc	**-72,56**	**-150,33**	-75,88	-153,64

The polynomial fit was used to estimate the relationship between vegetation diversity and distance from dry pan. Alpha diversity is estimated to increase with the increase in distance from the dry pans (Figure 8.6). The increase is exponential around 350m from dry pans.

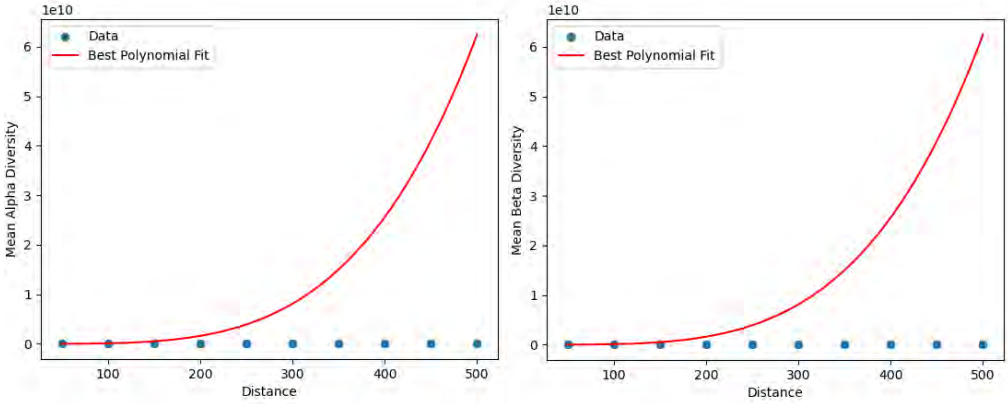

Figure 8.6 Alpha and beta relationship between diversity and distance from dry pans

Inverse curves were employed to analyse the relationship between distance from wet pans and both alpha and beta diversity. Alpha diversity declined with an increase in distance away from the wet pans. The highest alpha diversity was observed within a 100-meter radius of the wet pan. Similarly, beta diversity decreased with the increase in distance away from the pan. A notable decline in diversity was observed within the 150-meter range before levelling off. Peak diversity values are observed near the pans (Figure 8.6).

8.3.7 Changes in the spatial distribution of alpha and beta vegetation diversity within the KNP, South Africa

Figure 8.7 illustrates the time series of alpha and beta diversity for the years 2018, 2019, and 2022. Alpha diversity ranged from 1.0 to 1.31 across the three years. The highest mean annual alpha diversity was observed in 2019 (1.31), followed by 2018 (1.07), while 2022 had the lowest (1.01). Regarding beta diversity, the highest value was observed in 2022 (0.03), followed by 2018 (0.02), with the lowest recorded in 2018 (0.01). An inverse relationship between annual alpha and beta diversity is evident across the observed three years.

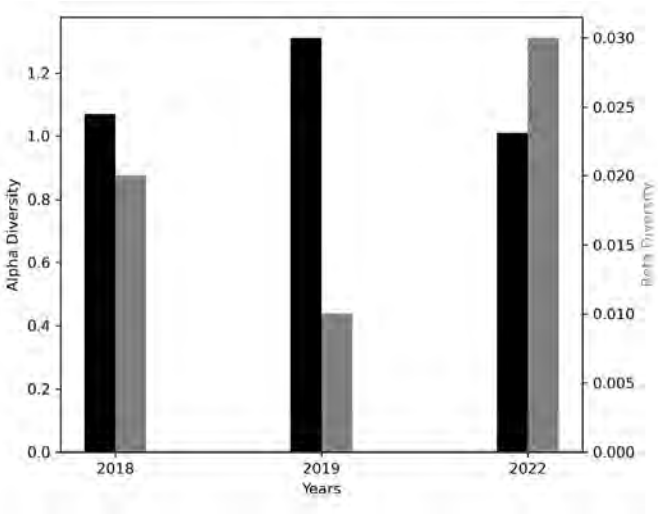

Figure 8.7 Annual dry year alpha and beta diversity means for the KNP, South Africa

It was observed that the spatial patterns of beta diversity closely resembled those of alpha diversity. Minimal changes in the spatial distribution of both alpha and beta diversity were observed between 2018 and 2019. However, notable changes in the spatial patterns of alpha and beta diversity were noted in 2022, particularly with an intensified diversity observed in the southern regions of the KNP (Figure 8.8).

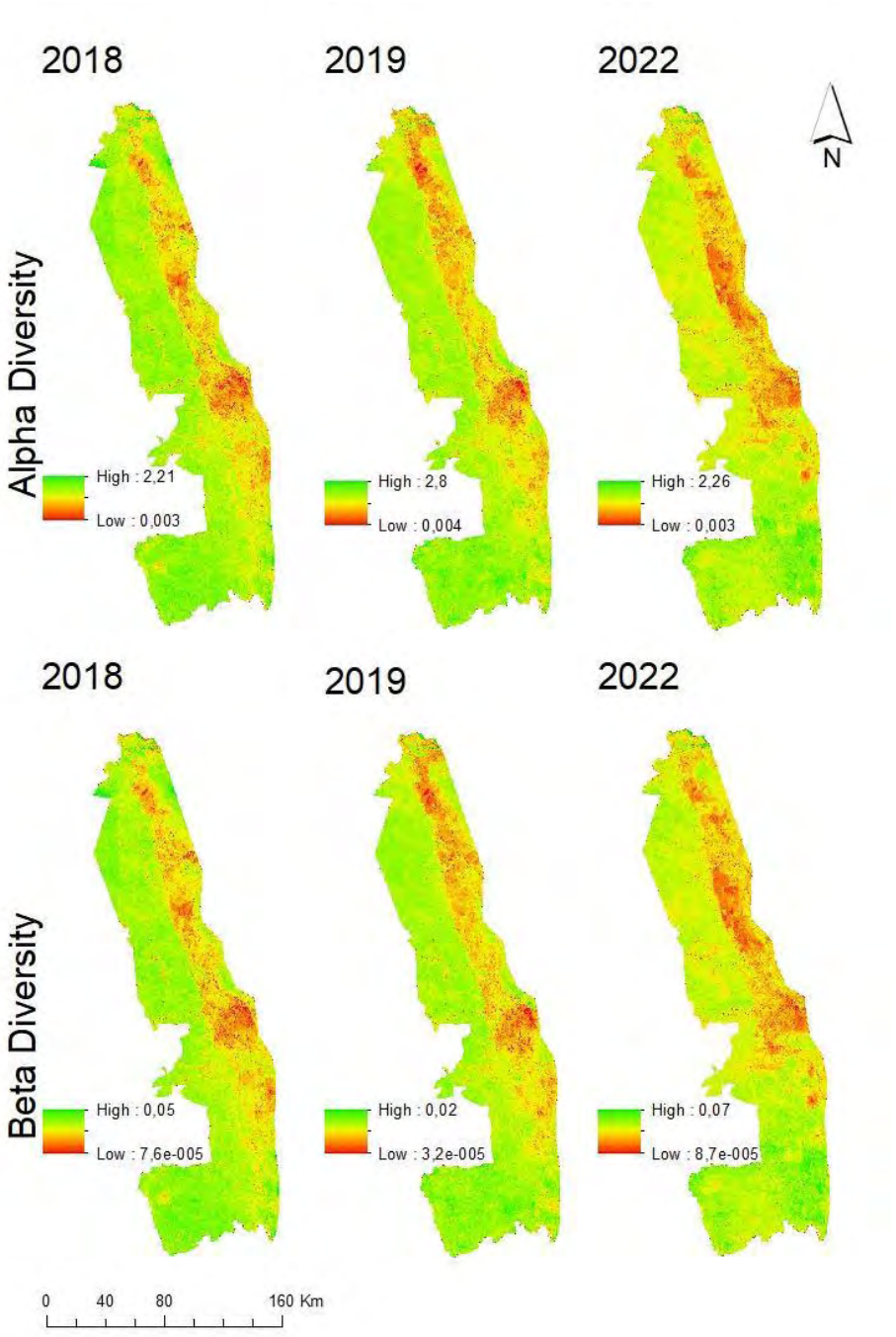

Figure 8.8 Temporal changes in the spatial extent of alpha and beta diversity in the KNP for the years 2018, 2019 and 2022

8.4 Discussion

The KNP stands as a vital conservation area in South Africa, playing a pivotal role in the country's economic and social development due to its exceptional floral and faunal diversity (Fynn and Bonyongo, 2011). It is imperative to conduct regular assessments and monitoring of

vegetation diversity to uphold sustainable conservation practices (van der Mescht and Codron, 2023). Therefore, the objective of this study was to map the multi-temporal diversity of vegetation and determine dominant vegetation types within GDEs.

8.4.1 Alpha and beta diversity predictions

The combination of CV, slope, elevation, and SUSM model proved to be more effective in predicting beta diversity when compared to alpha diversity. This is attributed to these variables providing insights into the spatial distribution patterns and environmental gradients that drive variations in beta diversity across different habitats or locations. However, their utility in predicting alpha diversity may be limited due to the intricate interplay of various factors influencing species richness at finer spatial scales linked to alpha diversity. In a study conducted by Hejda et al. (2022), it was found that local factors significantly influenced species richness within the KNP. Factors such as bedrock type, proximity to seasonal rivers influencing water availability, and grazing pressure were identified as key determinants affecting species diversity and composition. For instance, areas situated on granite bedrock exhibited higher herbaceous shrub species richness when compared to those on basalt bedrock. Furthermore, disturbance events such as drought and fire were identified as additional factors impacting species richness within the KNP (Trotter, 2022). As a result, species richness in the KNP may be closely associated with and influenced by localised factors.

8.4.2 Alpha and beta diversity along the pans

Species richness indicated by the alpha diversity ranged from 0.80 – 1.95, suggesting that the sites had low to moderate diversity. Environmental and biogeographic determinants, such as slope, elevation and soil moisture, influence community alpha diversity. For instance, Sabatini et al. (2022) determined that alpha diversity was mostly influenced by plot size, warmest mean temperature, temperature at the warmest, wettest quarter, type of ecoregions and percentage of soil fragments. Soil moisture was determined to be significantly and positively correlated with vegetation diversity and productivity in semi-arid regions like the KNP (Deng et al., 2016; Wang et al., 2021). Madonsela et al. (2021) also indicated that species richness is mostly influenced by precipitation and water availability in arid regions such as the KNP. In terms of beta diversity, the similarity between vegetation communities, the Makuleke sites had a higher similarity index (shared species between sites) when compared to the Letaba sites. Richness differences contribute the most to the observed beta diversity for both the Letaba and Makuleke

sites. High species turnover in vegetation communities indicates dynamic ecological processes and environmental heterogeneity between the vegetation sites, especially for the Makuleke sites. High species turnover suggests that the vegetation community is responding to spatial and temporal variations in environmental conditions such as climate change, elevation and moisture gradients, intense competition, facilitation, or other biotic interactions may contribute to species turnover as different species thrive under varying conditions (Chase and Myers, 2011; Theron et al., 2020). Based on the simple regression results, CV, slope, SUSM, and elevation model for beta diversity was better than that of alpha diversity. This could be because beta diversity is at a community level, aligning with the moderate resolution of the predictor variables utilised in this study. Conversely, alpha diversity could be better modelled using detailed, finer-resolution data. Overall, the models successfully captured the spatial distribution of alpha and beta diversity within the KNP.

8.4.3 Analysis of alpha and beta diversity spatiotemporal dynamics

The western part of the park exhibited the highest alpha and beta diversities, while the western portions consistently display lower diversity levels during the years 2018, 2019 and 2022. The favourable conditions contributing to high alpha and beta diversity in certain areas may be linked to factors such as humid conditions, warm temperatures, proximity to water bodies, and access to groundwater (Gillson and Ekblom, 2009; Madonsela et al., 2021; Rampheri et al., 2022). The interannual variations observed in alpha and beta diversity trends suggest potential associations with various climatic influences such as temperature, evapotranspiration, and precipitation (Santini et al., 2017). Areas exhibiting high alpha diversity are critical zones. The areas of high species diversity contribute to ecosystem stability and resilience from disturbances such as invasive species, habitat degradation and climate change. Moreover, they support the conservation of wildlife and endemic species and provide ecosystem services such as forage, habitat, nutrient cycling, and soil formation. Thus, they should be continuously monitored and managed. The inverse model demonstrates the relationship between alpha and beta diversity with the increase in distance from dry pans. Alpha and beta diversity were highest close to wet pans and decreased with increasing distance from the wet pans.

8.4.4 Dominant vegetation genera observed at the Letaba and Makuleke sites

The dominant vegetation genera at the Letaba area are *Combretum*, *Eragrostis*, and *Philonoptera* while for the Makuleke region, the *Diospyros, Eragrostis* and *Hyphaene.* The genera *Combretum, Eragrostis, Philonoptera, Diospyros,* and *Hyphaene* play significant roles in the ecological dynamics of the KNP. They provide habitat and food for various wildlife species, including browsing mammals. These genera collectively contribute to the biodiversity, habitat structure, and ecological balance within the KNP. The park's diverse plant life supports a variety of herbivores, contributes to soil stability, and plays a vital role in maintaining overall ecosystem health. Understanding the importance of these genera is crucial for effective conservation and management strategies within the park (van Aardt et al., 2020). For instance, *Combretum* and *Hyphaene* species, such as the Ilala palm *(Hyphaene petersiana),* are iconic in the park. They provide food and nesting sites for various animals, and their presence contributes to the unique landscape. *Eragrostis* species, commonly known as lovegrasses, are crucial components of the grass layer. They contribute to the diet of grazers and provide cover for smaller fauna (Theron et al., 2020; van Aardt et al., 2020). Moreover, other observed genera such as *Boscia* and *Combretum* are listed as priority species in the park. *Philonoptera* and *Diospyros* species are woody plants, with deep tap roots that may reach into groundwater and their reliance on groundwater can vary depending on species and local environmental conditions (Dzikiti et al., 2017). *Hyphaene* species, particularly palms like the Ilala palm, are generally adapted to a variety of moisture conditions. Palms can have extensive root systems, but their reliance on groundwater may depend on factors such as soil type and the availability of surface water. Groundwater use can be influenced by factors such as soil characteristics, seasonal variations, and the overall hydrological context of the region in the water limited park (Antunes et al., 2018).

8.5 Conclusions and study limitations

The objective of this study was to assess the utility of remotely sensed data in mapping vegetation species diversity, assessing their spatial and temporal dynamics, and dominant vegetation species within potential groundwater-dependent vegetation zones. The findings reveal a negative correlation between alpha and beta diversity measured in the field and those extrapolated through regression models, indicating that more variables should be further investigated to determine if they could improve the models; however, these techniques can

effectively estimate both beta and alpha diversity. A limitation of the study lies in its reliance on a limited number of sampling points; the spatial resolution of predictor variables was higher than that of the Sentinel 2 image and sampling plots. To enhance understanding, future research could investigate how plant phenology, based on the growth stages of vegetation, influences the correlation between predictor variables and vegetation diversity. The study outcomes could facilitate the identification of priority conservation areas within the KNP, providing resource managers with a strategic pathway to meet national and regional biodiversity targets, including Sustainable Development Goal (SDG) 15. Consequently, the methodology developed in this work holds promise for future studies seeking a priori knowledge applicable to various global ecosystems, including groundwater-dependent ecosystems.

CHAPTER NINE

DEVELOPMENT OF SOIL MOISTURE PRODUCTS FOR GROUNDWATER DEPENDENT ECOSYSTEMS

9.1 Introduction

Soil moisture variability is crucial in GDEs, influencing hydrological dynamics, vegetation composition, and overall ecosystem health. It affects the water cycle by controlling processes such as infiltration, runoff, and plant transpiration, while also impacting nutrient cycling, microbial activity, and carbon sequestration rates. Although traditional methods for measuring soil moisture, such as ground-based sensors and remote sensing, provide valuable data, challenges arise due to the complex interactions of ecohydrological and geological factors. The Soil Moisture Active Passive (SMAP) and Soil Moisture and Ocean Salinity (SMOS) missions offer global soil moisture data at coarse scales, but Sentinel-1 Synthetic Aperture Radar (SAR) provides higher spatial resolution, making it more suitable for local analysis. Recent studies have shown the effectiveness of machine learning algorithms in predicting soil moisture using Sentinel-1 data, enhancing predictions and enabling the upscaling of values. This chapter aims to integrate soil moisture data from SMAP with machine learning models based on Sentinel-1 SAR data to evaluate temporal and spatial trends in soil moisture and vegetation productivity in GDEs, thereby supporting informed environmental management strategies in KNP.

9.2 Materials and methods

Soil moisture data for the KNP were obtained from the SMAP level (L4) soil moisture product, encompassing surface soil moisture (0–5cm), vertical surface moisture, root zone soil moisture (0–100 cm), and additional research products. The dataset boasts a spatial resolution of 9 km, with a revisit time of 2–3 days, making it suitable for mapping frequently changing soil moisture conditions. Root zone soil moisture data was specifically extracted and reprojected. To interpolate soil moisture dynamics for the years 2020, 2021, and 2022, kriging interpolation functions within the GEE were utilized. These years were selected due to their representation of low rainfall periods within the study areas, thereby shedding light on areas likely to be groundwater dependent.

To establish a correlation between field–measured soil moisture and simulated soil moisture from SMAP, the measured soil moisture values, initially calculated as percentages, were converted to volume fraction (cm^3/cm^3) by dividing the observed soil moisture by 100.

Additionally, given that the root zone soil moisture encompasses depths from 0 to 100 cm, the field–measured values obtained within 20–meter intervals, spanning from 0 to 100 cm, were averaged. Soil moisture values were extracted from the SMAP soil data at the locations of the sampled pans. This normalisation of the data facilitated a direct comparison between the two datasets. A scatter plot of field-based soil moisture vs simulated soil moisture was done to assess the linear relationship between the two datasets. The r^2 was used to assess the strength of the relationship between the two datasets.

In addition to the SMAP product, Sentinel 1 data were also used to compute soil moisture for the GDEs in the KNP. During this process, surface reflectance data were acquired from the GEE repository using the dataset 'COPERNICUS/S1_GRD'. This data was filtered for the period from September 1, 2022, to September 30, 2022, to match the timeframe when soil moisture samples were taken at KNP. The Sentinel-1 mission provides data from a dual-polarization C–band SAR instrument at 5.405 GHz (C band). This collection includes Sentinel-1 Ground Range Detected (GRD) scenes, processed using the Sentinel-1 Toolbox to generate a calibrated, ortho–corrected product. The collection is updated daily, with new assets ingested within two days of availability.

The VV and VH bands were selected as predictor variables for estimating soil moisture at the pans. Ground estimates of soil moisture were imported and divided into 70% training and 30% testing datasets. A Smiple Random Forest regression model with tuned hyperparameters was then trained. This model consisted of 100 trees, with two variables per split, a minimum leaf population of 1, and no maximum nodes. The correlation between the observed and predicted soil moisture values was evaluated using a scatter plot and the R^2. The spatial trend in predicted soil moisture on the pans was analysed using a linear plot.

To assess the spatial and temporal variations in response to soil moisture, satellite images from the COPERNICUS/S2 collection were acquired for the wet seasons (October–May) of 2020–2022 and the dry seasons (May–September) of 2020–2022. The Sentinel dataset provides imagery with a spatial resolution ranging from 10 to 20 meters and a revisit time of 16 days. Seasonal image collections were processed to obtain average images for each year. NDVI (Normalized Difference Vegetation Index) was computed using the formula developed by Rouse et al. (1974) within the Google Earth Engine platform. NDVI values were then extracted from each pixel to assess changes in vegetation vigour, which is an indicator of moisture

availability. Additionally, the average seasonal NDVI values for each year were extracted to examine the temporal impact of soil moisture within the broader area of the KNP.

9.3 Results

9.3.1 Observed soil moisture versus simulated soil moisture

The surface soil moisture measured in situ data was compared to simulated soil moisture data at 18 natural pans in the KNP. A correlation coefficient of 0.59 suggests a moderate positive correlation between the observed and simulated soil moisture data. This suggested that the simulated soil moisture has predictive capability for in situ soil moisture (Figure 9.1). Soil moisture levels within the measured natural pans varied from 10 % to 17 %. Comparatively, the predicted soil moisture has a weaker negative (0.51) correlation with the observed soil moisture. According to the Sentinel 1 model, soil moisture values within the measured natural pans varied from 9 % to 13 %.

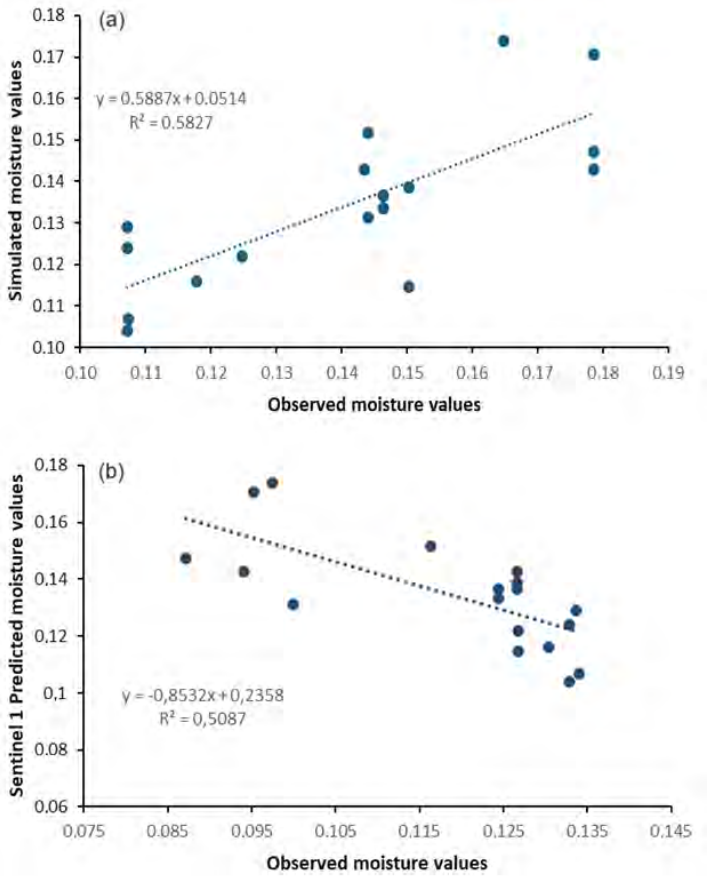

Figure 9.1 (a) Linear correlation between observed and simulated soil moisture values, and (b) Linear correlation between the observed and S1 predicted soil moisture values

9.3.2 Linear temporal dynamics of soil moisture of the natural pans

The simulated soil moisture was utilised to assess the temporal dynamics of soil moisture among the different pans. In comparison, 2021 exhibited high soil moisture values, indicating a wetter year, whereas 2020 experienced the driest conditions with a notable decrease in soil moisture levels across the observed natural pans (Figure 9.2). During the wet year, soil moisture was notably high along the Makuleke riparian pan (13–18) and low along the pans in the Letaba region (1–12). In 2022, classified as a moderate year, the Letaba pans appeared to retain more soil moisture compared to the Makuleke riparian pans. There was no clear distinction in soil moisture trends between the Letaba and Makuleke pans in 2020. The influence of soil types on soil moisture can be observed when comparing the moisture trends of pans 1–12. Transitions between different soil types, such as granite (pans 1–3), sandstone granite (pans 4–6), basalt granite (pans 7–9), and rhyolite granite (pans 10–12), reveal observable changes in soil moisture. An interesting finding is that the granite pans exhibit elevated soil moisture levels during the driest year, despite being associated with soils featuring poorer drainage and fertility. Conversely, these pans demonstrate the highest soil moisture content during the wettest year.

Comparing Sentinel-1 predicted soil moisture with the 2022 simulated soil moisture, both lines indicate similar patterns of moisture distribution across the pans, suggesting that the Sentinel-1 data is capturing the overall trend of soil moisture for 2022. There are some pans (1–3 and 14–18) where the Sentinel-1 predicted values are slightly higher or lower than the simulated values, indicating areas where the Sentinel-1 data either overestimates or underestimates soil moisture compared to the model simulation. The close alignment between the Sentinel-predicted and simulated 2022 soil moisture data highlights that the potential of using Sentinel-1 SAR data for soil moisture estimation at a local scale is comparable to that of the simulated products.

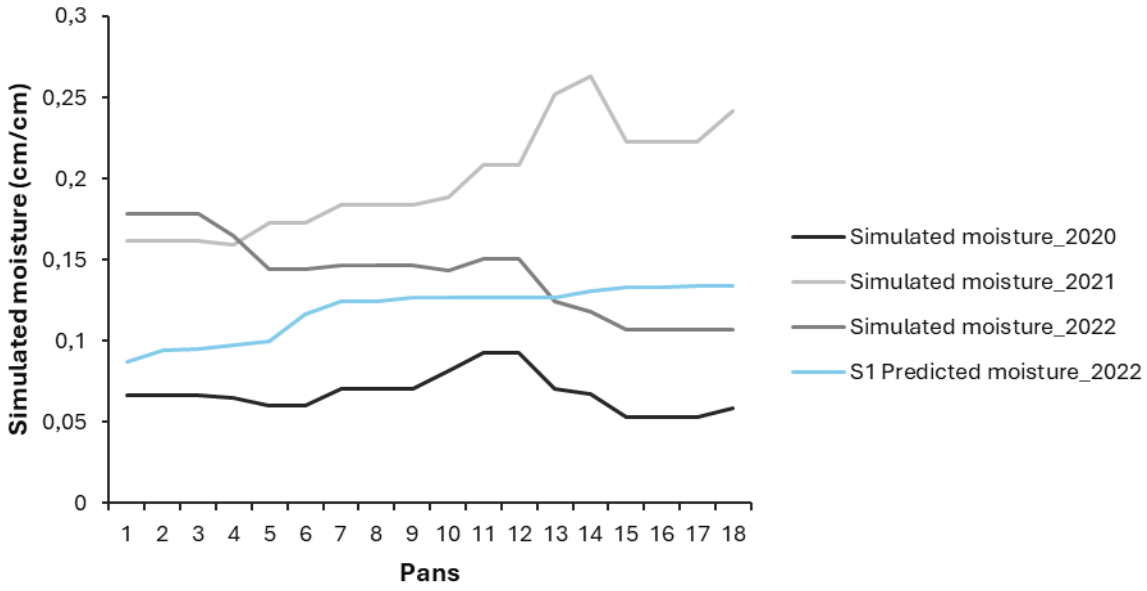

Figure 9.2 Simulated soil moisture values across the observed natural pans in the KNP

9.3.3 Derived temporal and seasonal NDVI trends – a proxy for soil moisture content variability

High NDVI values are observed for the 2021 wet season across the pans (Figure 9.3); these results are in accordance with the observed high soil moisture values (Figure 9.3). Generally, vegetation across pans 14–17 has higher NDVI and is associated with Eutric Leptosols and the Eutric Cambrisols (16 and 17), which are deep, well-drained and have good fertility because of the presence of high organic matter.

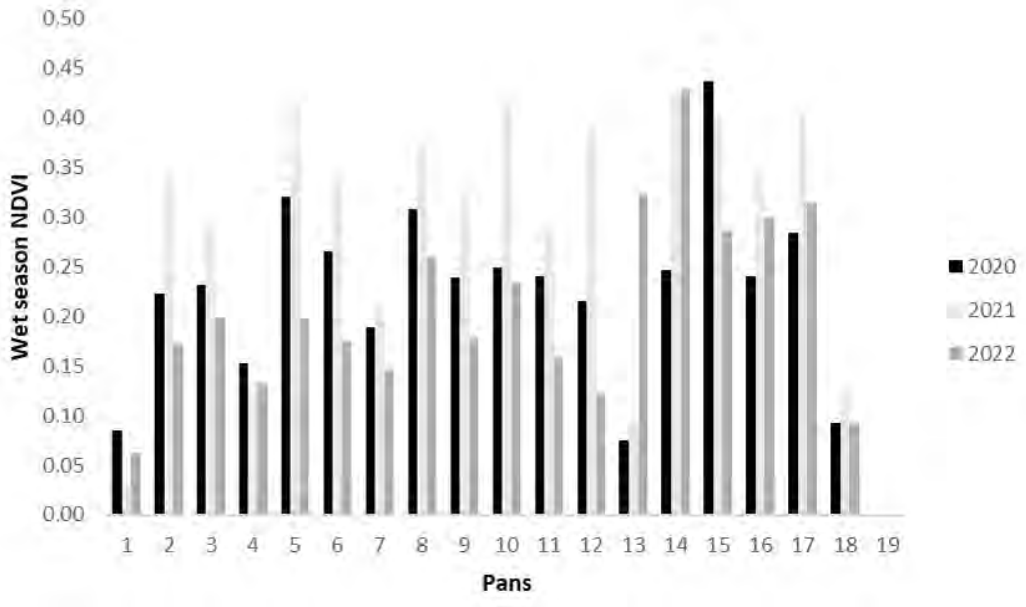

Figure 9.3 NDVI temporal trends across the sampled natural pans

The dry season NDVI trends follow those of the wet season, whereby NDVI values are highest in 2021. Vegetation density is highest across the Makuleke Eutric Leptisols and *Eutric Cambrisols* where the soil moisture was observed to be highest in 2021. Low NDVI values are observed for the 2022 year (Figure 9.4).

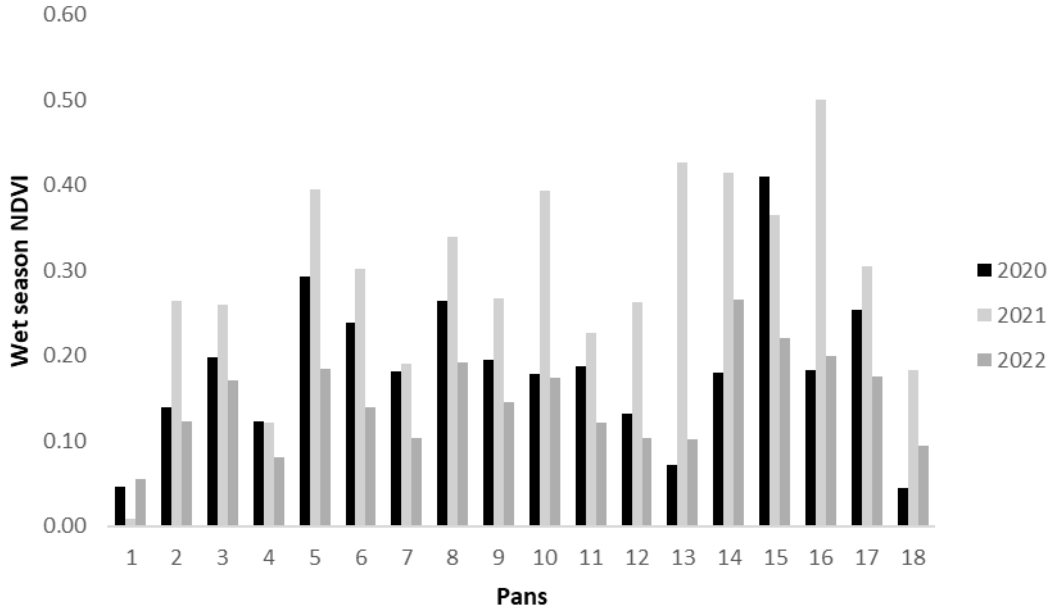

Figure 9.4 NDVI temporal trends across the sampled natural pans

9.3.4 Spatio–temporal dynamics of soil moisture in the KNP

Soil moisture exhibits both temporal and spatial variability annually based on SMAP and Sentinel-1 (Figures 9.5 and 9.6). In 2020, soil moisture levels were generally low, ranging from 0.03 to 0.10, with the southern regions of KNP experiencing the driest conditions. 2021 recorded the highest soil moisture levels, with both southern and northern regions exhibiting higher moisture content, while the central regions displayed moderate levels. In comparison, 2022 saw moderate soil moisture levels, with the central and southern regions showing moderate moisture content. Throughout the study period, the soil moisture trend in KNP fluctuated from dry to wet and then drying.

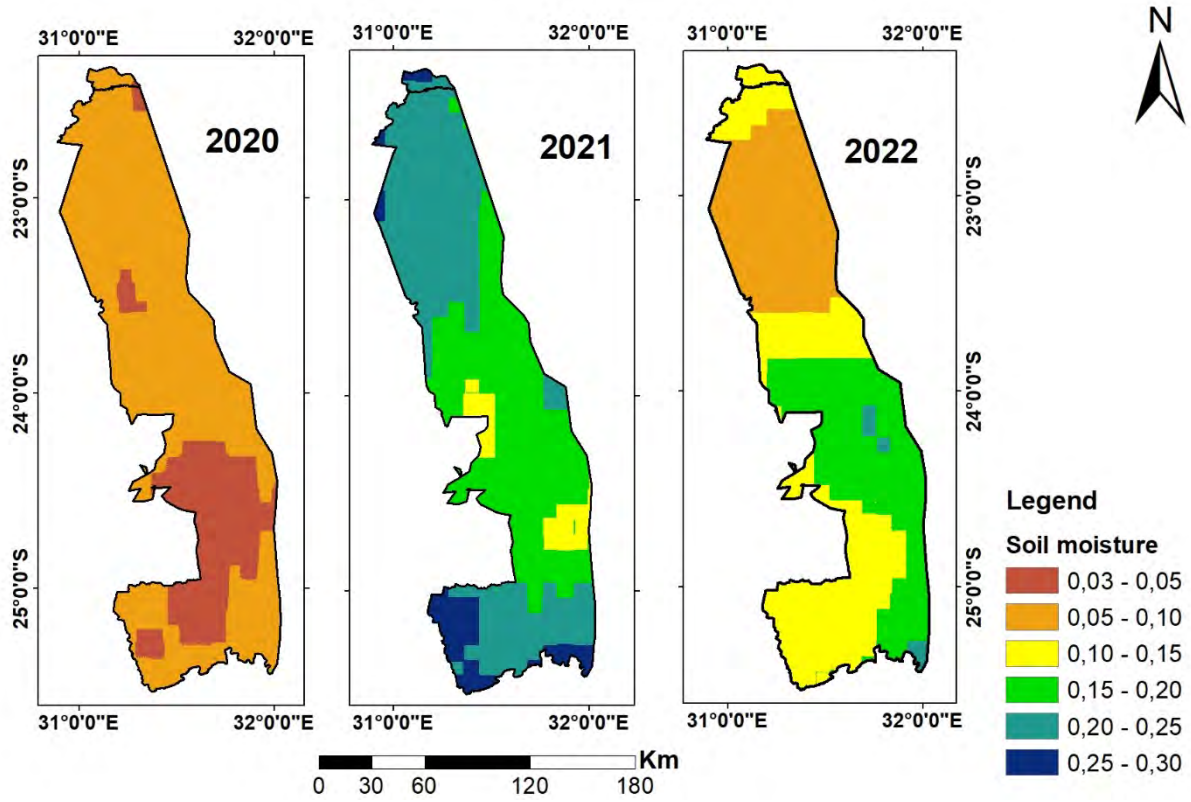

Figure 9.5 Spatial and temporal patterns in soil moisture in the KNP.

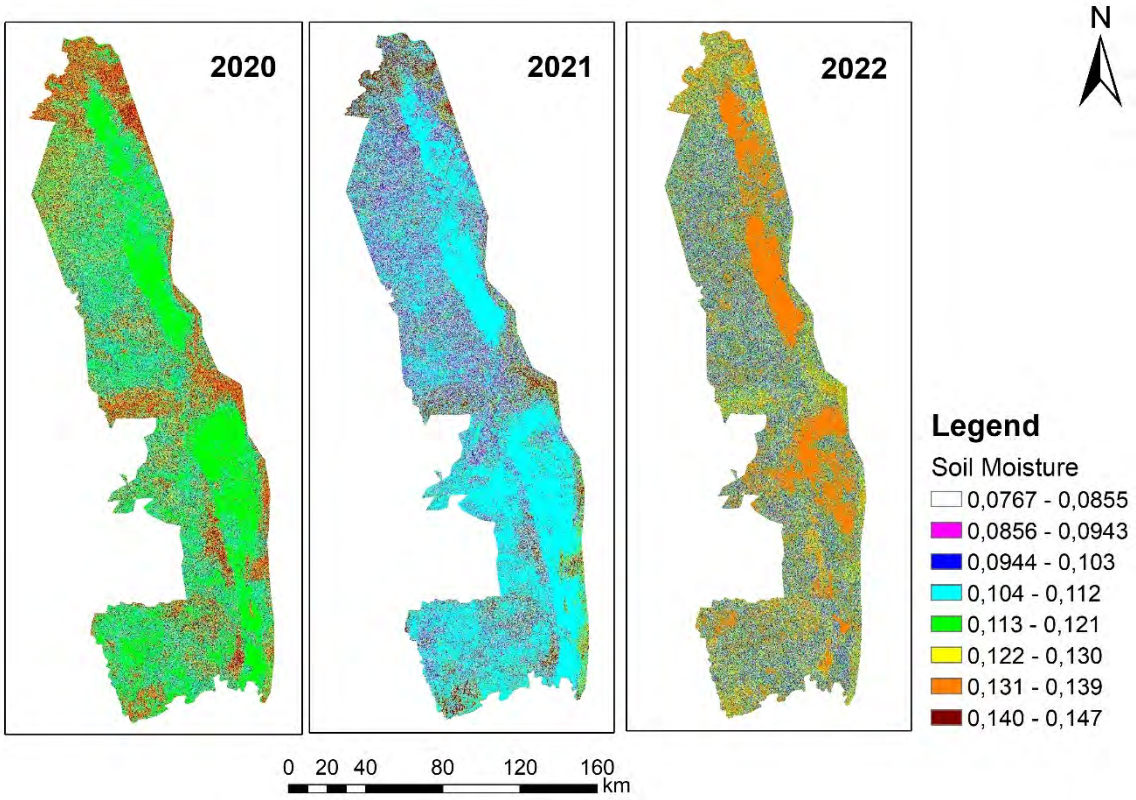

Figure 9.6 Spatial and temporal patterns in soil moisture in the KNP based on the Sentinel–1 data

9.3.5 Seasonal patio–temporal dynamics of NDVI in the KNP

The year 2020 had low vegetation productivity for both the wet and fry seasons (Figure 9.7). An increase in vegetation diversity in 2022 across the KNP was observed, where soil moisture has increased throughout the Park.

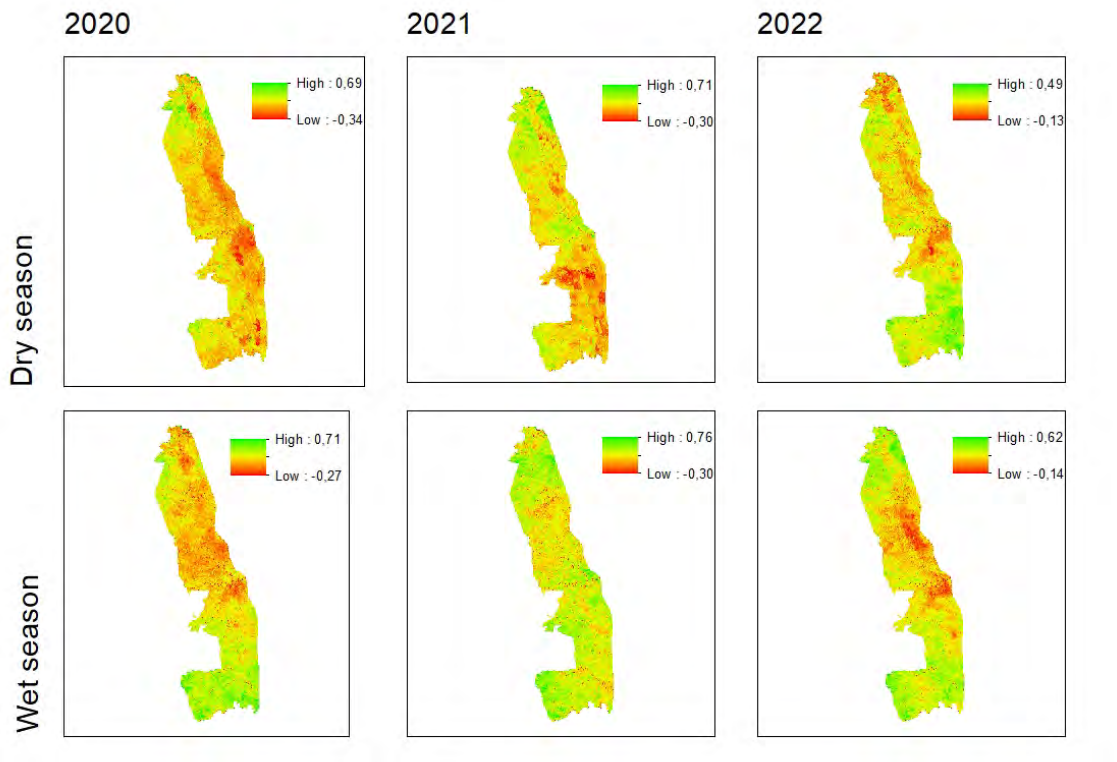

Figure 9.7 Spatio–temporal patterns of NDVI across KNP, South Africa

9.4 Discussion and conclusions

The primary objective of this chapter was to create a soil moisture map of KNP and analyse the spatial and temporal soil moisture patterns during dry years. Comparing Sentinel-1 predicted soil moisture with in situ measurements revealed a moderate correlation ($r^2 = 0.51$). These findings align with those of (Heckel et al., 2021; Urban et al., 2018), who conducted a similar comparison between Sentinel-1 derived soil moisture and field–based observations in KNP. However, limited accessibility to field soil moisture data posed a challenge. Machine Learning algorithms are optimal with a larger training dataset; the limited soil moisture data points resulted in lower model accuracy. While the coarser spatial resolution of the SMAP may lead to generalisations and introduce uncertainties when comparing simulated and observed soil moisture, as noted by Stradiotti et al. (2024) it was a better model. Incorporating a larger in situ soil moisture dataset would enhance the analysis of the agreement between Sentinel-1

predicted and observed soil moisture. Nonetheless, the results affirm the capability of remotely sensed soil moisture in assessing soil moisture patterns within KNP.

The simulated soil moisture effectively captured the interannual changes in pan dynamics, mirroring observed spatial variations in soil moisture throughout KNP. 2021 emerged as the wettest year, followed by 2022, with 2020 being the driest in terms of soil moisture levels. Soil moisture dynamics are associated with precipitation intensity, highlighting that intense rainfall events replenish surface and subsurface soil moisture, whereas low–intensity rainfall events facilitate gradual infiltration and percolation, augmenting subsurface water availability (Berry and Kulmatiski, 2017; Urban et al., 2018). Moreover, areas with dense vegetation tend to exhibit more stable soil moisture compared to regions with sparse vegetation, which display greater variability in soil moisture content (Urban et al., 2018). Soil water content values enable the derivation of soil moisture retention curves, aiding in the estimation of soil water potential. Soil moisture within KNP is influenced by soil types; for instance, soil moisture characteristics of basalt soils differ from those of granite soils (Buitenwerf et al., 2014).

The impacts of climate change are expected to escalate, leading to an increase in the frequency and intensity of extreme droughts and heat waves. These drought events are characterised by a scarcity of soil moisture, stemming from limited water infiltration into the soil and heightened evapotranspiration. For example, Kennenberg et al. (2024) have demonstrated that soil moisture plays a pivotal role in driving carbon and water fluxes in dryland ecosystems. Hence, there is a pressing need to enhance model representations to elucidate how soil moisture constrains ecosystem fluxes and how atmospheric drivers influence vegetation in dryland areas (Hsu and Dirmeyer, 2023; Zhou et al., 2021). The anticipated effects of climate change are poised to induce significant alterations in savannah ecosystems, necessitating the implementation of adaptation management strategies to mitigate impacts on wildlife conservation and socio–economic development. To address these challenges, innovative approaches for monitoring and forecasting soil moisture at higher spatial and temporal resolutions are imperative.

CHAPTER TEN

SYNTHESIS, CONCLUSION AND RECOMMENDATIONS

10.1 Introduction and Project Overview

Groundwater is important for freshwater supply, supporting socio-economic development and GDEs, which are essential for biodiversity and climate resilience. However, GDEs are being significantly threatened by altered hydrological cycles, rising temperature and land-use changes. Effective management of these ecosystems is hindered by limited information on their spatial distribution, vegetation diversity, soil moisture, and water quality, particularly in Africa. The southern Kruger, which relies on groundwater due to low rainfall, illustrates this challenge. Its status and interactions between its GDEs, including vegetation species and water quality, face environmental stressors such as salinisation. Traditional field-based mapping approaches, which were previously utilised to understand them, while they are informative, are limited by cost, time and spatial coverage. Then the advent of Earth observation technologies provided significant advantages, enabling broad spatial coverage, regular monitoring, cost efficiency, access to remote areas and integration of different datasets for comprehensive GDE insights. In concert with hydrogeological methods, these tools offer valuable information for informed biodiversity conservation decisions. In this regard, this project aimed to develop a geospatial framework for monitoring GDEs in southern KNP, using satellite-based spatiotemporal models to support effective management and decision making. Specifically, the project aimed:

1. To conduct a comprehensive and state-of-the-art literature review and the potential use of remote sensing-based models for GDE monitoring in the light of climate change.
2. To develop remote sensing-based methods for delineating GDEs specifically in vulnerable areas such as KNP, South Africa.
3. To assess the use of spatial explicit techniques in measuring species diversity in GDE
4. To assess the soil moisture potential of GDEs in the southern tip of KNP, South Africa
5. To assess water quality and chlorophyll variability in the selected GDEs in the southern tip of KNP, South Africa

To address these contractual objectives, the project was categorised into seven specific objectives. Subsequently, the following specific objectives were established to address the outlined work packages and contractual goals.

1. To develop a detailed synthesis on the progress and development of remote sensing integrated with geographic and information systems in assessing GDV over fine spatial and temporal scales.
2. To provide a comprehensive overview of the progress and applications of groundwater flow models coupled with advanced geospatial tools to understand the ecohydrology GDEs and their extent of connectivity to underlying aquifers.
3. To assess the efficacy of machine learning (ML) classifiers in predicting groundwater-dependent vegetation potential zones (GDVpz) within KNP, South Africa.
4. To accurately characterise groundwater flow systems in southern KNP and improve hydrogeological modelling of groundwater-dependent ecosystems.
5. To assess (i) variations in water and sediment chemistry in pan wetlands across different geological types and hydroperiods (low and high) and (ii) spatiotemporal macroinvertebrate diversity and abundance across geological regions, geological types, and hydroperiods in relation to water and sediment chemistry.
6. To evaluate models predicting Alpha and Beta diversity in potential groundwater-dependent vegetation zones using spectral coefficient of variation (CV), topographic features, and soil moisture.
7. To integrate soil moisture data from SMAP with machine learning models based on Sentinel-1 SAR data to evaluate temporal and spatial trends in soil moisture and vegetation productivity in GDEs, thereby supporting informed environmental management strategies in KNP.

In conducting the state-of-the-art literature review, the findings indicated that, although there were studies that utilised freely available remotely sensed data products in assessing and monitoring GDEs, there were some inaccuracies in these assessments, which were attributed to the sensor characteristics of these utilized missions. The review noted that advancements in data analytics, such as the introduction of cloud computing platforms like Google Earth Engine, could offer an unprecedented opportunity to address issues associated with the gathering and analysis of data in GDEs monitoring from remote sensing data, with their advanced data filtering, integrations and processing tools. The findings of the second review highlighted concerns regarding the mismatch in spatial and temporal scales between remotely sensed data

and groundwater models, which makes it difficult to integrate them in the delineation of GDEs. Additionally, it noted that there is a lack of ground truth data, particularly in remote areas, which further complicates GED validation efforts. This review then identified the need to integrate spatial data with groundwater numerical modelling to improve the accuracy of the model results by providing more detailed information about the area's geology and hydrogeology.

In assessing the utility of remote sensing data in mapping Vegetation Species Diversity, Structural, and Phenotypical Traits in GDEs using the Shannon-Wiener Diversity Index and Simpson Diversity Index coupled with vegetation indices like the NDVI, the findings revealed a negative correlation between the coefficient of variation (CV) and vegetation diversity. Overall, the results highlighted that these techniques can effectively estimate both beta and alpha diversity.

In assessing the variability of chlorophyll-a concentrations in groundwater-dependent wetlands, results demonstrated that hydroperiod influences chlorophyll-a concentrations more than geological type. The low hydroperiod exhibited increased levels, particularly for benthic chlorophyll-a. Additionally, trace elements, including Zn and Fe and nutrients (C, S, P, K), played an important role in sustaining pelagic and benthic phytoplankton communities by enhancing metabolic functions, nutrient cycling, and photosynthesis. Higher TDS and salinity positively contributed to benthic chlorophyll-a concentrations, suggesting that moderate ionic presence supports productivity in groundwater-dependent wetland systems. Finally, pH and pan surface area were demonstrated to negatively affect benthic chlorophyll-a, likely due to nutrient limitation, competition with macrophytes and sediment resuspension in larger pans.

Then, in assessing water quality indicators for the mapped GDEs within the KNP through field surveys of physicochemical as well as biological analysis, the findings highlighted that macroinvertebrate communities were influenced by hydroperiod and geological types in pans. Results particularly implied that the duration and frequency of inundation have a substantial influence on the diversity of macroinvertebrates. Sediment chemistry influenced by geological types had an impact on the nutrient content and substrate features that were essential for the habitats of macroinvertebrates. Furthermore, the quality of water was a crucial factor, with parameters such as pH, DO, and nutrient concentrations having a direct impact on the diversity, abundance, and health of macroinvertebrates, while chlorophyll-a concentrations for the pan varied spatially and temporally, with high concentrations observed during the low hydroperiod.

These findings underscore the necessity of implementing conservation approaches that are not a one-size-fits-all all.

Finally, in assessing the applicability of SMAP and Sentinel-1 SAR coupled with field-measured soil moisture data for monitoring variations in soil moisture within selected GDE pans of the KNP, the study underscored the reliability of satellite-based soil moisture estimates. The findings highlighted the influence of soil moisture on vegetation productivity and its close association with soil type. These insights are crucial for eco-hydrogeologists seeking to understand soil moisture and carbon dynamics within GDEs, thereby contributing to their conservation of GDEs and the sustainability of wildlife.

10.2 Limitation of the Study

The study was more aligned to Earth observation data and did not engage more physical measured data sets and techniques, such as the Stable and Radioactive Isotope Tracers, to confirm the GDEs in this study. Another limitation of the study lies in its reliance on a limited number of sampling points and offering a snapshot of the relationship between CV and vegetation diversity. Regarding the aspects of chlorophyll content variability, there is still a need for robust assessment and mapping to understand its impact on water invertebrates' species diversity.

10.3 Conclusions

This project offered a comprehensive framework for monitoring groundwater-dependent ecosystems by integrating remote sensing technologies with field data, enhancing our understanding of their ecological health. By assessing the interactions among geological, hydrological and biological factors, the project provides a model for sustainable ecosystem management in climate-sensitive regions. These established techniques and insights are anticipated to contribute extensively to conservation efforts, providing a scalable approach applicable to GDEs in other vulnerable ecosystems globally. These outcomes facilitate the identification of priority conservation areas within the KNP, providing resource managers with a strategic pathway to meet national and regional biodiversity targets, including SDG 15. Consequently, the methodology developed in this project holds promise for future studies seeking a priori knowledge applicable to various global ecosystems, including GDEs.

10.4 Recommendations

Several research gaps persist in the utilisation of geospatial technologies and data for mapping and monitoring GDEs, particularly in developing countries where fine spatial resolution data availability is limited.

- There is a need for extending the research efforts combining deep machine learning techniques, multisource spatial datasets and groundwater hydrogeological modelling techniques to enhance the delineation of the spatial extent of GDEs.
- Also, fins spatial resolution of remotely sensed data needs to be assessed for mapping soil moisture potential in GDEs to better understand flora and fauna abundance, diversity and distribution within these GDEs.
- Future studies should consider engaging Stable and Radioactive Isotope Tracers in concert with GIS techniques in identifying geological interactions unique to groundwater across the hydrological season to verify GDEs.
- Water quality parameters, including chlorophyll content variability and its relationship with species diversity in GDES, require more comprehensive assessments.
- Because the findings of this study established the relationship between the species diversity and variations in hydrographs, future studies could consider the potential of utilising waterborne invertebrates in confirming whether certain pools maybe GDEs and in assessing their state at any time.
- To enhance understanding of vegetation species diversity in GDEs, future research could investigate how plant phenology, based on the growth stages of vegetation, influences the correlation between CV and vegetation diversity.
- Future studies should focus on integrating geological type, hydroperiod, sediment chemistry, and water chemistry to develop site-specific conservation and management strategies for GDEs. This approach will provide ecosystem managers with proactive solutions to effectively protect these ecological systems, ensuring the long-term survival of diverse macroinvertebrate populations and the overall health of GDEs.

REFERENCES

Abbas, K., Deroin, J.P. and Bouaziz, S., 2019. Multitemporal Remote Sensing for Monitoring Highly Dynamic Phenomena: Case of the Ephemeral Lakes in the Chott El Jerid, Tunisia. In *Advances in Remote Sensing and Geo Informatics Applications: Proceedings of the 1st Springer Conference of the Arabian Journal of Geosciences (CAJG-1), Tunisia 2018* (pp. 101-103). Springer International Publishing.

Adams, M., Smith, P.L. and Yang, X., 2014. Assessing the effects of groundwater extraction on coastal groundwater-dependent ecosystems using satellite imagery. *Marine and Freshwater Research*, *66*(3), pp.226-232.

Albano, C.M., McGwire, K.C., Hausner, M.B., McEvoy, D.J., Morton, C.G. and Huntington, J.L., 2020. Drought sensitivity and trends of riparian vegetation vigor in Nevada, USA (1985–2018). *Remote Sensing*, *12*(9), p.1362.

Al-Fugara, A.K., Pourghasemi, H.R., Al-Shabeeb, A.R., Habib, M., Al-Adamat, R., Al-Amoush, H. and Collins, A.L., 2020. A comparison of machine learning models for the mapping of groundwater spring potential. *Environmental Earth Sciences*, *79*(10), p.206.

Ali, S. and Alandjan, G., 2019. Mapping land cover damages in mega floods through integration of remote sensing and GIS techniques. *3c Tecnología: glosas de innovación aplicadas a la pyme*, *8*(1), pp.258-275.

Amani, M., Ghorbanian, A., Ahmadi, S.A., Kakooei, M., Moghimi, A., Mirmazloumi, S.M., Moghaddam, S.H.A., Mahdavi, S., Ghahremanloo, M., Parsian, S. and Wu, Q., 2020. Google earth engine cloud computing platform for remote sensing big data applications: A comprehensive review. *IEEE Journal of Selected Topics in Applied Earth Observations and Remote Sensing*, *13*, pp.5326-5350.

Anderson Jr, W.P. and Emanuel, R.E., 2008. Effect of interannual and interdecadal climate oscillations on groundwater in North Carolina. *Geophysical Research Letters*, *35*(23).

Antunes, C., Chozas, S., West, J., Zunzunegui, M., Diaz Barradas, M.C., Vieira, S. and Máguas, C., 2018. Groundwater drawdown drives ecophysiological adjustments of woody vegetation in a semi-arid coastal ecosystem. *Global Change Biology*, *24*(10), pp.4894-4908.

Araya-López, R.A., Lopatin, J., Fassnacht, F.E. and Hernández, H.J., 2018. Monitoring Andean high-altitude wetlands in central Chile with seasonal optical data: A comparison between Worldview-2 and Sentinel-2 imagery. *ISPRS journal of photogrammetry and remote sensing*, *145*, pp.213-224.

Baker, C., Lawrence, R., Montagne, C. and Patten, D., 2006. Mapping wetlands and riparian areas using Landsat ETM+ imagery and decision-tree-based models. *Wetlands*, *26*(2), pp.465-474.

Barbieri, M., Barberio, M.D., Banzato, F., Billi, A., Boschetti, T., Franchini, S., Gori, F. and Petitta, M., 2023. Climate change and its effect on groundwater quality. *Environmental Geochemistry and Health*, *45*(4), pp.1133-1144.

Barron, O., Silberstein, R., Ali, R., Donohue, R., McFarlane, D.J., Davies, P., Hodgson, G., Smart, N. and Donn, M., 2012. Climate change effects on water-dependent ecosystems in south-western Australia. *Journal of Hydrology*, *434*, pp.95-109.

Barron, O.V., Emelyanova, I., Van Niel, T.G., Pollock, D. and Hodgson, G., 2014. Mapping groundwater-dependent ecosystems using remote sensing measures of vegetation and moisture dynamics. *Hydrological Processes*, *28*(2), pp.372-385.

Barron, O.V., Emelyanova, I., Van Niel, T.G., Pollock, D. and Hodgson, G., 2014. Mapping groundwater-dependent ecosystems using remote sensing measures of vegetation and moisture dynamics. *Hydrological Processes*, *28*(2), pp.372-385.

Bertrand, G., Goldscheider, N., Gobat, J.M. and Hunkeler, D., 2012. From multi-scale conceptualization to a classification system for inland groundwater-dependent ecosystems. *Hydrogeology Journal*, *20*(1), pp.5-25.

Bertrand, G., Siergieiev, D., Ala-Aho, P. and Rossi, P.M., 2014. Environmental tracers and indicators bringing together groundwater, surface water and groundwater-dependent ecosystems: importance of scale in choosing relevant tools. *Environmental earth sciences*, *72*, pp.813-827.

Bhaga, T.D., Dube, T., Shekede, M.D. and Shoko, C., 2020. Impacts of climate variability and drought on surface water resources in Sub-Saharan Africa using remote sensing: A review. *Remote Sensing*, *12*(24), p.4184.

Bhaga, T.D., Dube, T., Shekede, M.D. and Shoko, C., 2020. Impacts of climate variability and drought on surface water resources in Sub-Saharan Africa using remote sensing: A review. *Remote Sensing*, *12*(24), p.4184.

Blevins, E. and Aldous, A., 2011. Biodiversity value of groundwater-dependent ecosystems. *The Nature Conservancy, WSP*, pp.18-24.

Bojinski, S., Verstraete, M., Peterson, T.C., Richter, C., Simmons, A. and Zemp, M., 2014. The concept of essential climate variables in support of climate research, applications, and policy. *Bulletin of the American Meteorological Society*, *95*(9), pp.1431-1443.

Boser, B.E., Guyon, I.M. and Vapnik, V.N., 1992, July. A training algorithm for optimal margin classifiers. In *Proceedings of the fifth annual workshop on Computational learning theory* (pp. 144-152).

Boulton, A.J. and Hancock, P.J., 2006. Rivers as groundwater-dependent ecosystems: a review of degrees of dependency, riverine processes and management implications. *australian Journal of Botany*, *54*(2), pp.133-144.

Bowman, D.M.J.S., 2000. Rainforests and flame forests: the great Australian forest dichotomy. *Australian Geographical Studies*, *38*(3), pp.327-331.

Brodie, R.S., Green, R. and Graham, M., 2002. Mapping groundwater-dependent ecosystems: a case study in the fractured basalt aquifers of the Alstonville Plateau, New South Wales, Australia. In *Proceedings of the International Groundwater Conference*.

Brown, J., Bach, L., Aldous, A., Wyers, A. and DeGagné, J., 2011. Groundwater-dependent ecosystems in Oregon: An assessment of their distribution and associated threats. *Frontiers in Ecology and the Environment*, *9*(2), pp.97-102.

Cao, S.K., Chen, K.L., Cao, G.C., Zhang, L., Ma, J., Yang, L., Lu, B.L., Chen, L. and Lu, H., 2011. The analysis of characteristic and spatial variability for soil organic matter and organic carbon around Qinghai Lake. *Procedia Environmental Sciences*, *10*, pp.678-684.

Cartwright, I., Weaver, T., Cendón, D.I. and Swane, I., 2010. Environmental isotopes as indicators of inter-aquifer mixing, Wimmera region, Murray Basin, Southeast Australia. *Chemical Geology*, *277*(3-4), pp.214-226.

Cernusak, L.A., Haverd, V., Brendel, O., Le Thiec, D., Guehl, J.M. and Cuntz, M., 2019. Robust response of terrestrial plants to rising CO2. *Trends in Plant Science*, *24*(7), pp.578-586.

Chambers, J., Nugent, G., Sommer, B., Speldewinde, P., Neville, S., Beatty, S., Chilcott, S., Eberhard, S., Mitchell, N., D'Souza, F. and Barron, O., 2013. Adapting to climate change: A risk assessment and decision-making framework for managing groundwater dependent ecosystems with declining water levels. Guidelines for use, National Climate Change Adaptation Research Facility, Gold Coast, 59 pp.

Chang, C.T., Wang, S.F., Vadeboncoeur, M.A. and Lin, T.C., 2014. Relating vegetation dynamics to temperature and precipitation at monthly and annual timescales in Taiwan using MODIS vegetation indices. *International Journal of Remote Sensing*, *35*(2), pp.598-620.

Chapman, J.B., Lewis, B. and Litus, G., 2003. Chemical and isotopic evaluation of water sources to the fens of South Park, Colorado. *Environmental Geology*, *43*, pp.533-545.

Chávez Oyanadel, R.O. and Clevers, J.G.P.W., 2012. Object-based analysis of 8-bands Worldview2 imagery for assessing health condition of desert trees. Wageningen University. CGI Rep. 2012-001 15.

Chen, C.P. and Zhang, C.Y., 2014. Data-intensive applications, challenges, techniques and technologies: A survey on Big Data. *Information sciences*, *275*, pp.314-347.

Chen, W., Sun, Z., Wang, Y. and Ma, R., 2014. Major scientific issues on water demand studying for groundwater-dependent vegetation ecosystems in inland arid regions. *Earth Science: Journal of China Union of Geosciences*, *39*, pp.1340-1348.

Chiloane, C., Dube, T. and Shoko, C., 2022. Impacts of groundwater and climate variability on terrestrial groundwater dependent ecosystems: A review of geospatial assessment approaches and challenges and possible future research directions. *Geocarto International*, *37*(23), pp.6755-6779.

Coluccio, K. and Morgan, L.K., 2019. A review of methods for measuring groundwater–surface water exchange in braided rivers. *Hydrology and Earth System Sciences*, *23*(10), pp.4397-4417.

Colvin, C., Le Maitre, D., Saayman, I. and Hughes, S., 2007. An introduction to aquifer dependent ecosystems in South Africa. *Pretoria: Natural Resources and the Environment, CSIR*.

Colvin, C., Le Maitre, D.C. and Hughes, S., 2003. *Assessing terrestrial groundwater dependent ecosystems in South Africa* (Vol. 1090). Pretoria: Water Research Commission. 1-77005-038-8

Cooper, M., 2014. *Advanced Bash-scripting Guide: An In-depth Exploration of the Art of Shell Scripting. Volume 1*. Linux Documentation Project.

Corwin, D.L., 1996. GIS applications of deterministic solute transport models for regional-scale assessment of non-point source pollutants in the vadose zone. *Applications of GIS to the Modeling of Non-point Source Pollutants in the Vadose Zone*, *48*, pp.69-100.

Costanza, R., De Groot, R., Sutton, P., Van der Ploeg, S., Anderson, S.J., Kubiszewski, I., Farber, S. and Turner, R.K., 2014. Changes in the global value of ecosystem services. *Global Environmental Change*, *26*, pp.152-158.

Dalu, T., Nhiwatiwa, T. and Clegg, B., 2013. Temporal variation of the plankton communities in a small tropical reservoir (Malilangwe, Zimbabwe). *Transactions of the Royal Society of South Africa*, *68*(2), pp.85-96.

Dalu, T., Wasserman, R.J., Magoro, M.L., Froneman, P.W. and Weyl, O.L., 2019. River nutrient water and sediment measurements inform on nutrient retention, with implications for eutrophication. *Science of the Total Environment*, *684*, pp.296-302.

Dams, J., Salvadore, E., Van Daele, T., Ntegeka, V., Willems, P. and Batelaan, O., 2012. Spatio-temporal impact of climate change on the groundwater system. *Hydrology and Earth System Sciences*, *16*(5), pp.1517-1531.

Davies, T., Everard, M. and Horswell, M., 2016. Community-based groundwater and ecosystem restoration in semi-arid north Rajasthan (3): Evidence from remote sensing. *Ecosystem Services*, *21*, pp.20-30.

De Klerk, A.R., De Klerk, L.P., Chamier, J. and Wepener, V., 2012. Seasonal variations of water and sediment quality parameters in endorheic reed pans on the Mpumalanga Highveld. *Water SA*, *38*(5), pp.663-672.

de Oliveira, M.L., Dos Santos, C.A., de Oliveira, G., Silva, M.T., da Silva, B.B., de BL Cunha, J.E., Ruhoff, A. and Santos, C.A., 2022. Remote sensing-based assessment of land degradation and drought impacts over terrestrial ecosystems in Northeastern Brazil. *Science of the Total Environment*, *835*, p.155490.

DeFries, R. and Bounoua, L., 2004. Consequences of land use change for ecosystem services: A future unlike the past. *GeoJournal*, *61*, pp.345-351.

Dlikilili, S., 2019. Investigating the groundwater dependence and response to rainfall variability of vegetation in the Touws river and catchment using remote sensing.

Doody, T.M., Barron, O.V., Dowsley, K., Emelyanova, I., Fawcett, J., Overton, I.C., Pritchard, J.L., Van Dijk, A.I. and Warren, G., 2017. Continental mapping of groundwater dependent ecosystems: A methodological framework to integrate diverse data and expert opinion. *Journal of Hydrology: Regional Studies*, *10*, pp.61-81.

Dronova, I., 2015. Object-based image analysis in wetland research: A review. *Remote Sensing*, *7*(5), pp.6380-6413.

Dube, T., Pandit, S., Shoko, C., Ramoelo, A., Mazvimavi, D. and Dalu, T., 2019. Numerical assessments of leaf area index in tropical savanna rangelands, South Africa using Landsat 8 OLI derived metrics and in-situ measurements. *Remote Sensing*, *11*(7), p.829.

Duran-Llacer, I., Arumí, J.L., Arriagada, L., Aguayo, M., Rojas, O., González-Rodríguez, L., Rodríguez-López, L., Martínez-Retureta, R., Oyarzún, R. and Singh, S.K., 2022. A new method to map groundwater-dependent ecosystem zones in semi-arid environments: A case study in Chile. *Science of the Total Environment*, *816*, p.151528.

Duro, D.C., Franklin, S.E. and Dubé, M.G., 2012. Multi-scale object-based image analysis and feature selection of multi-sensor earth observation imagery using random forests. *International Journal of Remote Sensing*, *33*(14), pp.4502-4526.

DWAF., 2001. *Guidelines on the establishment and management of catchment forums: in support of integrated water resources management. Integrated water resources management*. Subseries No. MS6.2. Department of Water Affairs and Forestry, Pretoria.

Dwire, K.A., Mellmann-Brown, S. and Gurrieri, J.T., 2018. Potential effects of climate change on riparian areas, wetlands, and groundwater-dependent ecosystems in the Blue Mountains, Oregon, USA. *Climate Services*, *10*, pp.44-52.

Eamus, D. and Froend, R., 2006. Groundwater-dependent ecosystems: the where, what and why of GDEs. *Australian Journal of Botany*, *54*(2), pp.91-96.

Eamus, D., 2009. *Identifying groundwater dependent ecosystems: a guide for land and water managers*. Land & Water Australia.

Eamus, D., Froend, R., Loomes, R., Hose, G. and Murray, B., 2006. A functional methodology for determining the groundwater regime needed to maintain the health of groundwater-dependent vegetation. *Australian Journal of Botany*, *54*(2), pp.97-114.

Eamus, D., Zolfaghar, S., Villalobos-Vega, R., Cleverly, J. and Huete, A., 2015. Groundwater-dependent ecosystems: recent insights, new techniques and an ecosystem-scale threshold response. *Hydrology and Earth System Sciences Discussions*, *12*(5).

Eamus, D., Zolfaghar, S., Villalobos-Vega, R., Cleverly, J. and Huete, A., 2015. Groundwater-dependent ecosystems: Recent insights from satellite and field-based studies. *Hydrology and Earth System Sciences*, *19*(10), pp.4229-4256.

El-Hokayem, L., De Vita, P. and Conrad, C., Identification of Groundwater Dependent Vegetation Using High Resolution Sentinel-2 Data–a Mediterranean Case Study. *Available at SSRN 4132042*.

Emelyanova, I., Barron, O. and Alaibakhsh, M., 2018. A comparative evaluation of arid inflow-dependent vegetation maps derived from LANDSAT top-of-atmosphere and surface reflectances. *International Journal of Remote Sensing*, *39*(20), pp.6607-6630.

Essam, D., Ahmed, M., Abouelmagd, A. and Soliman, F., 2020. Monitoring temporal variations in groundwater levels in urban areas using ground penetrating radar. *Science of the Total Environment*, *703*, p.134986.

Fang, X., Chen, Z., Guo, X., Zhu, S., Liu, T., Li, C. and He, B., 2019. Impacts and uncertainties of climate/CO2 change on net primary productivity in Xinjiang, China (2000–2014): A modelling approach. *Ecological Modelling*, *408*, p.108742.

Fitoka, E., Tompoulidou, M., Hatziiordanou, L., Apostolakis, A., Höfer, R., Weise, K. and Ververis, C., 2020. Water-related ecosystems' mapping and assessment based on remote sensing techniques and geospatial analysis: The SWOS national service case of the Greek Ramsar sites and their catchments. *Remote Sensing of Environment*, *245*, p.111795.

Forkuor, G., Zoungrana, J.B.B., Dimobe, K., Ouattara, B., Vadrevu, K.P. and Tondoh, J.E., 2020. Above-ground biomass mapping in West African dryland forest using Sentinel-1 and 2 datasets-A case study. *Remote Sensing of Environment*, *236*, p.111496.

Franklin, J., Serra-Diaz, J.M., Syphard, A.D. and Regan, H.M., 2016. Global change and terrestrial plant community dynamics. *Proceedings of the National Academy of Sciences*, *113*(14), pp.3725-3734.

Froend, R. and Sommer, B., 2010. Phreatophytic vegetation response to climatic and abstraction-induced groundwater drawdown: examples of long-term spatial and temporal variability in community response. *Ecological Engineering*, *36*(9), pp.1191-1200.

Gerten, D., Schaphoff, S., Haberlandt, U., Lucht, W. and Sitch, S., 2004. Terrestrial vegetation and water balance—hydrological evaluation of a dynamic global vegetation model. *Journal of Hydrology*, *286*(1-4), pp.249-270.

Gholami, V.C.K.W., Chau, K.W., Fadaee, F., Torkaman, J. and Ghaffari, A., 2015. Modeling of groundwater level fluctuations using dendrochronology in alluvial aquifers. *Journal of hydrology*, *529*, pp.1060-1069.

Gillson, L. and Ekblom, A., 2009. Untangling anthropogenic and climatic influence on riverine forest in the Kruger National Park, South Africa. *Vegetation History and Archaeobotany*, *18*, pp.171-185.

Glanville, K., Ryan, T., Tomlinson, M., Muriuki, G., Ronan, M. and Pollett, A., 2016. A method for catchment scale mapping of groundwater-dependent ecosystems to support natural resource management (Queensland, Australia). *Environmental Management*, *57*, pp.432-449.

Gondwe, B. R. (2010). *Exploration, modelling and management of groundwater-dependent ecosystems in karst* (Doctoral dissertation, PhD Thesis, DTU Environment Department of Environmental Engineering Technical University of Denmark).

Gou, S., Gonzales, S. and Miller, G.R., 2015. Mapping potential groundwater-dependent ecosystems for sustainable management. *Groundwater*, *53*(1), pp.99-110.

Gow, L., Brodie, R.S., Green, R., Punthakey, J., Woolley, D., Redpath, P. and Bradburn, A., 2010. Identification and monitoring GDEs using MODIS time series: Hat Head National Park—A case study. *Groundwater 2010: The challenge of sustainable management*.

Graw, V., Ghazaryan, G., Dall, K., Delgado Gómez, A., Abdel-Hamid, A., Jordaan, A., Piroska, R., Post, J., Szarzynski, J., Walz, Y. and Dubovyk, O., 2017. Drought dynamics and vegetation productivity in different land management systems of Eastern Cape, South Africa—A remote sensing perspective. *Sustainability*, *9*(10), p.1728.

Griffiths, P., Nendel, C. and Hostert, P., 2019. Intra-annual reflectance composites from Sentinel-2 and Landsat for national-scale crop and land cover mapping. *Remote Sensing of Environment*, *220*, pp.135-151.

Gu, Y., Brown, J.F., Verdin, J.P. and Wardlow, B., 2007. A five-year analysis of MODIS NDVI and NDWI for grassland drought assessment over the central Great Plains of the United States. *Geophysical research letters*, *34*(6).

Guirado, E., Blanco-Sacristán, J., Rigol-Sánchez, J.P., Alcaraz-Segura, D. and Cabello, J., 2019. A multi-temporal object-based image analysis to detect long-lived shrub cover changes in drylands. *Remote Sensing*, *11*(22), p.2649.

Guirado, E., Blanco-Sacristan, J., Rodriguez-Caballero, E., Tabik, S., Alcaraz-Segura, D., Martinez-Valderrama, J. and Cabello, J., 2021. Mask R-CNN and OBIA fusion improves the segmentation of scattered vegetation in very high-resolution optical sensors. *Sensors*, *21*(1), p.320.

Gurdak, J.J., Hanson, R.T., McMahon, P.B., Bruce, B.W., McCray, J.E., Thyne, G.D. and Reedy, R.C., 2007. Climate variability controls on unsaturated water and chemical movement, High Plains aquifer, USA. *Vadose Zone Journal*, *6*(3), pp.533-547.

Gusha, M.N., Dalu, T. and McQuaid, C.D., 2021. Interaction between small-scale habitat properties and short-term temporal conditions on food web dynamics of a warm temperate intertidal rock pool ecosystem. *Hydrobiologia*, *848*(7), pp.1517-1533.

Gxokwe, S., Dube, T. and Mazvimavi, D., 2020. Multispectral remote sensing of wetlands in semi-arid and arid areas: a review on applications, challenges and possible future research directions. *Remote Sensing*, *12*(24), p.4190.

Gxokwe, S., Dube, T. and Mazvimavi, D., 2022. Leveraging Google Earth Engine platform to characterize and map small seasonal wetlands in the semi-arid environments of South Africa. *Science of the Total Environment*, *803*, p.150139.

Gxokwe, S., Dube, T., Mazvimavi, D. and Grenfell, M., 2022. Using cloud computing techniques to monitor long-term variations in ecohydrological dynamics of small seasonally-flooded wetlands in semi-arid South Africa. *Journal of Hydrology*, *612*, p.128080.

Han, L. and He, D., 2020. Leafing intensity decreases with increasing water table depth and plant height in Populus euphratica, a desert riparian species. *Acta Oecologica*, *109*, p.103672.

Hancock, P.J., Hunt, R.J. and Boulton, A.J., 2009. Preface: hydrogeoecology, the interdisciplinary study of groundwater dependent ecosystems. *Hydrogeology Journal*, *17*(1), pp.1-3.

Hasmadi, M., Pakhriazad, H.Z. and Shahrin, M.F., 2009. Evaluating supervised and unsupervised techniques for land cover mapping using remote sensing data. *Geografia: Malaysian Journal of Society and Space*, *5*(1), pp.1-10.

Hatton, T., Evans, R. and Merz, S.K., 1997. *Dependence of ecosystems on groundwater and its significance to Australia*. Sydney: Sinclair Knight Merz. Land and Water Resources. 12(98):77.

Hausner, M.B., Huntington, J.L., Nash, C., Morton, C., McEvoy, D.J., Pilliod, D.S., Hegewisch, K.C., Daudert, B., Abatzoglou, J.T. and Grant, G., 2018. Assessing the effectiveness of riparian restoration projects using Landsat and precipitation data from the cloud-computing application ClimateEngine. org. *Ecological Engineering*, *120*, pp.432-440.

Havril, T., Tóth, Á., Molson, J.W., Galsa, A. and Mádl-Szőnyi, J., 2018. Impacts of predicted climate change on groundwater flow systems: can wetlands disappear due to recharge reduction?. *Journal of Hydrology*, *563*, pp.1169-1180.

Holm-Hansen, O. and Riemann, B., 1978. Chlorophyll a determination: improvements in methodology. *Oikos*, pp.438-447.

Hoogland, T., Heuvelink, G.B. and Knotters, M., 2010. Mapping water-table depths over time to assess desiccation of groundwater-dependent ecosystems in the Netherlands. *Wetlands*, *30*, pp.137-147.

Howard, J. and Merrifield, M., 2010. Mapping groundwater dependent ecosystems in California. *PLoS One*, *5*(6), p.e11249.

Hoyos, I.C.P., 2016. *Identification of phreatophytic groundwater dependent ecosystems using geospatial technologies* (Doctoral dissertation, The City College of New York).

Hoyos, I.P., Krakauer, N. and Khanbilvardi, R., 2015. Random forest for identification and characterization of groundwater dependent ecosystems. *WIT Transactions on Ecology and the Environment*, *196*, pp.89-100.

Huang, F., Chunyu, X., Zhang, D., Chen, X. and Ochoa, C.G., 2020. A framework to assess the impact of ecological water conveyance on groundwater-dependent terrestrial ecosystems in arid inland river basins. *Science of the Total Environment*, *709*, p.136155.

Huang, F., Zhang, Y., Zhang, D. and Chen, X., 2019. Environmental groundwater depth for groundwater-dependent terrestrial ecosystems in arid/semiarid regions: A review. *International Journal of Environmental Research and Public Health*, *16*(5), p.763.

Huang, J., Zhou, Y., Wenninger, J., Ma, H., Zhang, J. and Zhang, D., 2016. How water use of Salix psammophila bush depends on groundwater depth in a semi-desert area. *Environmental Earth Sciences*, *75*, pp.1-13.

Hunink, J.E., Contreras, S., Soto-García, M., Martin-Gorriz, B., Martinez-Álvarez, V. and Baille, A., 2015. Estimating groundwater use patterns of perennial and seasonal crops in a Mediterranean irrigation scheme, using remote sensing. *Agricultural Water Management*, *162*, pp.47-56.

Huntington, J., McGwire, K., Morton, C., Snyder, K., Peterson, S., Erickson, T., Niswonger, R., Carroll, R., Smith, G. and Allen, R., 2016. Assessing the role of climate and resource management on groundwater dependent ecosystem changes in arid environments with the Landsat archive. *Remote Sensing of Environment*, *185*, pp.186-197.

Huss, M., Hock, R., Bauder, A. and Funk, M., 2010. 100-year mass changes in the Swiss Alps linked to the Atlantic Multidecadal Oscillation. *Geophysical Research Letters*, *37*(10).

IPCC. 2014. *Climate change 2014: impacts, adaptation, and vulnerability*. Summary for policymakers, climate change 2014: impacts, adaptation and vulnerability - contributions of the working group II to the fifth assessment report.

Ismail, M.H., 2009. Evaluating supervised and unsupervised techniques for land cover mapping using remote sensing data. *Geografia: Malaysian Journal of Society and Space*, 5(1), pp. 1–10.

Johansen, O.M., Andersen, D.K., Ejrnæs, R. and Pedersen, M.L., 2018. Relations between vegetation and water level in groundwater dependent terrestrial ecosystems (GWDTEs). *Limnologica*, *68*, pp.130-141.

Jones, C., Stanton, D., Hamer, N., Denner, S., Singh, K., Flook, S. and Dyring, M., 2020. Field investigation of potential terrestrial groundwater-dependent ecosystems within Australia's Great Artesian Basin. *Hydrogeology Journal*, *28*(1), pp.237-261.

Jones, J.W., 2019. Improved automated detection of subpixel-scale inundation—Revised dynamic surface water extent (DSWE) partial surface water tests. *Remote Sensing*, *11*(4), p.374.

Jozdani, S.E., Johnson, B.A. and Chen, D., 2019. Comparing deep neural networks, ensemble classifiers, and support vector machine algorithms for object-based urban land use/land cover classification. *Remote Sensing*, *11*(14), p.1713.

Kalbus, E., Reinstorf, F. and Schirmer, M., 2006. Measuring methods for groundwater–surface water interactions: a review. *Hydrology and Earth System Sciences*, *10*(6), pp.873-887.

Kaneko, K. and Nohara, S., 2014. Review of effective vegetation mapping using the UAV (Unmanned Aerial Vehicle) method. *Journal of Geographic Information System*, *6*(06), p.733.

Kath, J., Reardon-Smith, K., Le Brocque, A.F., Dyer, F.J., Dafny, E., Fritz, L. and Batterham, M., 2014. Groundwater decline and tree change in floodplain landscapes: Identifying non-linear threshold responses in canopy condition. *Global Ecology and Conservation*, *2*, pp.148-160.

Klausmeyer, K., Howard, J., Keeler-Wolf, T., Davis-Fadtke, K., Hull, R. and Lyons, A., 2018. Mapping indicators of groundwater dependent ecosystems in California: methods report. *San Francisco Califonia*. p. 1–35.

Klausmeyer, K.R., Biswas, T., Rohde, M.M., Schuetzenmeister, F., Rindlaub, N., Housman, I. and Howard, J.K., 2019. *GDE pulse: Taking the pulse of groundwater dependent ecosystems with satellite data. San Francisco, California* [online]

Kløve, B., Ala-Aho, P., Bertrand, G., Boukalova, Z., Ertürk, A., Goldscheider, N., Ilmonen, J., Karakaya, N., Kupfersberger, H., Kvœrner, J. and Lundberg, A., 2011. Groundwater dependent ecosystems. Part I: Hydroecological status and trends. *Environmental Science and Policy*, *14*(7), pp.770-781.

Kløve, B., Ala-Aho, P., Bertrand, G., Gurdak, J.J., Kupfersberger, H., Kværner, J., Muotka, T., Mykrä, H., Preda, E., Rossi, P. and Uvo, C.B., 2014. Climate change impacts on groundwater and dependent ecosystems. *Journal of Hydrology*, *518*, pp.250-266.

Koirala, S., Jung, M., Reichstein, M., de Graaf, I.E., Camps-Valls, G., Ichii, K., Papale, D., Ráduly, B., Schwalm, C.R., Tramontana, G. and Carvalhais, N., 2017. Global distribution of groundwater-vegetation spatial covariation. *Geophysical Research Letters*, *44*(9), pp.4134-4142.

Krause, S., Heathwaite, A.L., Miller, F., Hulme, P. and Crowe, A., 2007. Groundwater-dependent wetlands in the UK and Ireland: controls, functioning and assessing the likelihood of damage from human activities. *Water Resources Management*, *21*, pp.2015-2025.

Kreamer, D.K., Stevens, L.E. and Ledbetter, J.D., 2015. Groundwater dependent ecosystems—Science, challenges, and policy directions. *Groundwater*, *205*, p.230.

Krogulec, E., 2018. Evaluating the risk of groundwater drought in groundwater-dependent ecosystems in the central part of the Vistula River Valley, Poland. *Ecohydrology and Hydrobiology*, *18*(1), pp.82-91.

Kumar, C.P., 2013. Recent studies on impact of climate change on groundwater resources. *International Journal of Physical and Social Sciences*, *3*(11), pp.189-221.

Kundzewicz, Z.W. and Doell, P., 2009. Will groundwater ease freshwater stress under climate change?. *Hydrological Sciences Journal*, *54*(4), pp.665-675.

Laio, F., Tamea, S., Ridolfi, L., D'Odorico, P. and Rodriguez-Iturbe, I., 2009. Ecohydrology of groundwater-dependent ecosystems: 1. Stochastic water table dynamics. *Water Resources Research*, *45*(5).

Le Maitre, D.C., Scott, D.F. and Colvin, C., 1999. Review of information on interactions between vegetation and groundwater. *Water South Africa*. 25:137–152.

Liu, C., Liu, H., Yu, Y., Zhao, W., Zhang, Z., Guo, L. and Yetemen, O., 2021. Mapping groundwater-dependent ecosystems in arid Central Asia: Implications for controlling regional land degradation. *Science of the Total Environment*, *797*, p.149027.

Liu, H.H., 2011. Impact of climate change on groundwater recharge in dry areas: An ecohydrology approach. *Journal of Hydrology*, *407*(1-4), pp.175-183.

Liu, Y., Liu, R. and Shang, R., 2022. GLOBMAP SWF: a global annual surface water cover frequency dataset during 2000–2020 for change analysis of inland water bodies. *Earth System Science Data Discussions*, *2022*, pp.1-24.

Loheide, S.P., Butler Jr, J.J. and Gorelick, S.M., 2005. Estimation of groundwater consumption by phreatophytes using diurnal water table fluctuations: A saturated-unsaturated flow assessment. *Water Resources Research*, *41*(7).

Loomes, R., Froend, R. and Sommer, B., 2013. Response of wetland vegetation to climate change and groundwater decline on the Swan Coastal Plain, Western Australia: Implications for management. *Ribeiro L, Stigter TY, Chambel A, Condesso de Melo MT, Monteiro JP, Medeiros A eds.: Groundwater and Ecosystems. CRC Press, Leiden, Netherlands*, pp.207-219.

Lurtz, M.R., Morrison, R.R., Gates, T.K., Senay, G.B., Bhaskar, A.S. and Ketchum, D.G., 2020. Relationships between riparian evapotranspiration and groundwater depth along a semiarid irrigated river valley. *Hydrological Processes*, *34*(8), pp.1714-1727.

Lv, J., Wang, X.S., Zhou, Y., Qian, K., Wan, L., Eamus, D. and Tao, Z., 2013. Groundwater-dependent distribution of vegetation in Hailiutu River catchment, a semi-arid region in China. *Ecohydrology*, *6*(1), pp.142-149.

Macintyre, P., Van Niekerk, A. and Mucina, L., 2020. Efficacy of multi-season Sentinel-2 imagery for compositional vegetation classification. *International Journal of Applied Earth Observation and Geoinformation*, *85*, p.101980.

MacKay, H., 2006. Protection and management of groundwater-dependent ecosystems: emerging challenges and potential approaches for policy and management. *Australian Journal of Botany*, *54*(2), pp.231-237.

Marques, I.G., Nascimento, J., Cardoso, R.M., Miguéns, F., de Melo, M.T.C., Soares, P.M., Gouveia, C.M. and Besson, C.K., 2019. Mapping the suitability of groundwater-dependent vegetation in a semi-arid Mediterranean area. *Hydrology and Earth System Sciences*, *23*(9), pp.3525-3552.

Martarelli, L., Gafà, R.M., La Vigna, F., Monti, G.M. and Silvi, A., 2022. New hydrogeological results on the Groundwater Dependent Ecosystem of the Pilato Lake (Sibillini Mts, Central Italy). *Acque Sotterranee-Italian Journal of Groundwater*, *11*(1), pp.27-35.

Masek, J.G., Wulder, M.A., Markham, B., McCorkel, J., Crawford, C.J., Storey, J. and Jenstrom, D.T., 2020. Landsat 9: Empowering open science and applications through continuity. *Remote Sensing of Environment*, *248*, p.111968.

Massey, R., Sankey, T.T., Yadav, K., Congalton, R.G. and Tilton, J.C., 2018. Integrating cloud-based workflows in continental-scale cropland extent classification. *Remote Sensing of Environment*, *219*, pp.162-179.

Mawdsley, J.R., O'malley, R. and Ojima, D.S., 2009. A review of climate-change adaptation strategies for wildlife management and biodiversity conservation. *Conservation Biology*, *23*(5), pp.1080-1089.

McDowell, C. and Moll, E., 1992. The influence of agriculture on the decline of West Coast Renosterveld, south-western Cape, South Africa. *Journal of Environmental Management*, *35*(3), pp.173-192.

Medeiros A, editors. *Groundwater and ecosystems*. Leiden, Netherlands: CRC Press; p. 207–219.

Meng, X., Gao, X., Li, S., Li, S. and Lei, J., 2021. Monitoring desertification in Mongolia based on Landsat images and Google Earth Engine from 1990 to 2020. *Ecological Indicators*, *129*, p.107908.

Miller, G.R., Chen, X., Rubin, Y., Ma, S. and Baldocchi, D.D., 2010. Groundwater uptake by woody vegetation in a semiarid oak savanna. *Water Resources Research*, *46*(10).

Mo, K., Chen, Q., Chen, C., Zhang, J., Wang, L. and Bao, Z., 2019. Spatiotemporal variation of correlation between vegetation cover and precipitation in an arid mountain-oasis river basin in northwest China. *Journal of Hydrology*, *574*, pp.138-147.

Móricz, N., 2010. Water balance study of a groundwater-dependent oak forest. *Acta Silvatica Et Lignaria Hungarica: An International Journal in Forest, Wood And Environmental Sciences*, *6*, pp.49-66.

Morsy, K.M., Alenezi, A. and AlRukaibi, D.S., 2017. Groundwater and dependent ecosystems: revealing the impacts of climate change. *International Journal of Applied Engineering Research*, *12*(13), pp.3919-3926.

Mountrakis, G., Im, J. and Ogole, C., 2011. Support vector machines in remote sensing: A review. *ISPRS Journal of Photogrammetry and Remote Sensing*, *66*(3), pp.247-259.

Mpakairi, K.S., Dube, T., Dondofema, F. and Dalu, T., 2022. Spatio–temporal variation of vegetation heterogeneity in groundwater dependent ecosystems within arid environments. *Ecological Informatics*, *69*, p.101667.

Mpakairi, K.S., Dube, T., Dondofema, F. and Dalu, T., 2022. Spatial characterisation of vegetation diversity in groundwater-dependent ecosystems Using in-Situ and Sentinel-2 MSI Satellite Data. *Remote Sensing*, *14*(13), p.2995.

Mtengwana, B., Dube, T., Mkunyana, Y.P. and Mazvimavi, D., 2020. Use of multispectral satellite datasets to improve ecological understanding of the distribution of Invasive Alien Plants in a water-limited catchment, South Africa. *African Journal of Ecology*, *58*(4), pp.709-718.

Münch, Z. and Conrad, J., 2007. Remote sensing and GIS based determination of groundwater dependent ecosystems in the Western Cape, South Africa. *Hydrogeology Journal*, *15*, pp.19-28.

Munoz-Reinoso, J.C., 2001. Vegetation changes and groundwater abstraction in SW Doñana, Spain. *Journal of Hydrology*, *242*(3-4), pp.197-209.

Mutanga, O. and Kumar, L., 2019. Google earth engine applications. *Remote Sensing*, *11*(5), p.591.

Naghibi, S.A. and Dashtpagerdi, M.M., 2017. Evaluation of four supervised learning methods for groundwater spring potential mapping in Khalkhal region (Iran) using GIS-based features. *Hydrogeology Journal*, *25*(1), p.169.

Ndehedehe, C.E., Ferreira, V.G. and Agutu, N.O., 2019. Hydrological controls on surface vegetation dynamics over West and Central Africa. *Ecological Indicators*, *103*, pp.494-508.

Nevill, J.C., Hancock, P.J., Murray, B.R., Ponder, W.F., Humphreys, W.F., Phillips, M.L. and Groom, P.K., 2010. Groundwater-dependent ecosystems and the dangers of groundwater overdraft: a review and an Australian perspective. *Pacific Conservation Biology*, *16*(3), pp.187-208.

Nguyen, U., Glenn, E.P., Dang, T.D. and Pham, L.T., 2019. Mapping vegetation types in semi-arid riparian regions using random forest and object-based image approach: A case study of the Colorado River Ecosystem, Grand Canyon, Arizona. *Ecological Informatics*, *50*, pp.43-50.

Nhu, V.H., Rahmati, O., Falah, F., Shojaei, S., Al-Ansari, N., Shahabi, H., Shirzadi, A., Górski, K., Nguyen, H. and Ahmad, B.B., 2020. Mapping of groundwater spring potential in karst aquifer system using novel ensemble bivariate and multivariate models. *Water*, *12*(4), p.985.

Noone, K.J., Nobre, C. and Seitzinger, S., 2011. The International Geosphere-Biosphere Programme's (IGBP) scientific research agenda for coping with global environmental change. *Coping with Global Environmental Change, Disasters and Security: Threats, Challenges, Vulnerabilities and Risks*, pp.1249-1256.

O'connor, J., Santos, M.J., Rebel, K.T. and Dekker, S.C., 2019. The influence of water table depth on evapotranspiration in the Amazon arc of deforestation. *Hydrology and Earth System Sciences*, *23*(9), pp.3917-3931.

Orellana, F., Verma, P., Loheide, S.P. and Daly, E., 2012. Monitoring and modeling water-vegetation interactions in groundwater-dependent ecosystems. *Reviews of Geophysics*, *50*(3).

Osmond, C.B., Austin, M.P., Berry, J.A., Billings, W.D., Boyer, J.S., Dacey, J.W.H., Nobel, P.S., Smith, S.D. and Winner, W.E., 1987. Stress physiology and the distribution of plants. *BioScience*, *37*(1), pp.38-48.

Paola, J.D. and Schowengerdt, R.A., 1995. A review and analysis of backpropagation neural networks for classification of remotely-sensed multi-spectral imagery. *International Journal of Remote Sensing*, *16*(16), pp.3033-3058.

Parker, B.M., Sheldon, F., Phinn, S. and Ward, D., 2018. Changes in foliage projective cover and its implications for mapping groundwater dependent vegetation across a precipitation gradient. *Ecohydrology*, *11*(4), p.e1937.

Páscoa, P., Gouveia, C.M. and Kurz-Besson, C., 2020. A simple method to identify potential groundwater-dependent vegetation using NDVI MODIS. *Forests*, *11*(2), p.147.

Pedzisai, E., Mutanga, O., Odindi, J. and Mushore, T.D., 2022. The use of remote sensing indices to understand flood-recharged soil moisture impacts on trees in semi-arid floodplains: A review. *Ecohydrology*, *15*(7), p.e2460.

Pereira, H.M., Ferrier, S., Walters, M., Geller, G.N., Jongman, R.H.G., Scholes, R.J., Bruford, M.W., Bruford, M.W., Brummitt, N., Butchart, S.H.M. and Cardoso, A.C., 2013. Essential biodiversity variables. *Science*, 339 (6117): 277-278.

Pérez Hoyos, I.C., Krakauer, N.Y., Khanbilvardi, R. and Armstrong, R.A., 2016. A review of advances in the identification and characterization of groundwater dependent ecosystems using geospatial technologies. *Geosciences*, *6*(2), p.17.

Peters, J., De Baets, B., Samson, R. and Verhoest, N.E.C., 2008. Modelling groundwater-dependent vegetation patterns using ensemble learning. *Hydrology and Earth System Sciences*, *12*(2), pp.603-613.

Peters, J., De Baets, B., Verhoest, N.E., Samson, R., Degroeve, S., De Becker, P. and Huybrechts, W., 2007. Random forests as a tool for ecohydrological distribution modelling. *Ecological Modelling*, *207*(2-4), pp.304-318.

Raczko, E. and Zagajewski, B., 2017. Comparison of support vector machine, random forest and neural network classifiers for tree species classification on airborne hyperspectral APEX images. *European Journal of Remote Sensing*, *50*(1), pp.144-154.

Richardson, D.M. and Kruger, F.J., 1990. Water relations and photosynthetic characteristics of selected trees and shrubs of riparian and hillslope habitats in the south-western Cape Province, South Africa. *South African Journal of Botany*, *56*(2), pp.214-225.

Richey, A.S., Thomas, B.F., Lo, M.H., Reager, J.T., Famiglietti, J.S., Voss, K., Swenson, S. and Rodell, M., 2015. Quantifying renewable groundwater stress with GRACE. *Water Resources Research*, *51*(7), pp.5217-5238.

Rodriguez-Iturbe I, Porporato A. 2005. Ecohydrology of water-controlled ecosystems: soil moisture and plant dynamics. *Ecohydrology of Water-controlled Ecosystems: Soil Moisture and Plant Dynamics*. 1:86–101.

Rohde, M.M., Froend, R. and Howard, J., 2017. A global synthesis of managing groundwater dependent ecosystems under sustainable groundwater policy. *Groundwater*, *55*(3), pp.293-301.

Rouget, M., Richardson, D.M., Cowling, R.M., Lloyd, J.W. and Lombard, A.T., 2003. Current patterns of habitat transformation and future threats to biodiversity in terrestrial ecosystems of the Cape Floristic Region, South Africa. *Biological Conservation*, *112*(1-2), pp.63-85.

Roy, D.P., Kovalskyy, V., Zhang, H.K., Vermote, E.F., Yan, L., Kumar, S.S. and Egorov, A., 2016. Characterization of Landsat-7 to Landsat-8 reflective wavelength and normalized difference vegetation index continuity. *Remote Sensing of Environment*, *185*, pp.57-70.

Rozenstein, O. and Karnieli, A., 2011. Comparison of methods for land-use classification incorporating remote sensing and GIS inputs. *Applied Geography*, *31*(2), pp.533-544.

Sabat-Tomala, A., Raczko, E. and Zagajewski, B., 2020. Comparison of support vector machine and random forest algorithms for invasive and expansive species classification using airborne hyperspectral data. *Remote Sensing*, *12*(3), p.516.

Safaee, S. and Wang, J., 2020. Towards global mapping of salt pans and salt playas using Landsat imagery: A case study of western United States. *International Journal of Remote Sensing*, *41*(22), pp.8693-8716.

Sarris, D., Christodoulakis, D. and Körner, C., 2007. Recent decline in precipitation and tree growth in the eastern Mediterranean. *Global Change Biology*, *13*(6), pp.1187-1200.

Scanlon, B.R., Keese, K.E., Flint, A.L., Flint, L.E., Gaye, C.B., Edmunds, W.M. and Simmers, I., 2006. Global synthesis of groundwater recharge in semiarid and arid regions. *Hydrological Processes: An International Journal*, *20*(15), pp.3335-3370.

Scibek, J. and Allen, D.M., 2006. Modeled impacts of predicted climate change on recharge and groundwater levels. *Water Resources Research*, *42*(11).

Shadwell, E. and February, E., 2017. Effects of groundwater abstraction on two keystone tree species in an arid savanna national park. *PeerJ*, *5*, p.e2923.

Shafroth, P.B., Stromberg, J.C. and Patten, D.T., 2000. Woody riparian vegetation response to different alluvial water table regimes. *Western North American Naturalist*, pp.66-76.

Shoko, C., Mutanga, O. and Dube, T., 2016. Progress in the remote sensing of C3 and C4 grass species aboveground biomass over time and space. *ISPRS Journal of Photogrammetry and Remote Sensing*, *120*, pp.13-24.

Sisay, A., 2016. Remote sensing based water surface extraction and change detection in the central rift valley region of ethiopia. *American Journal of Geographic Information System*, *5*(2), pp.33-39.

Smith, G.T., 2016. *Detection and Analysis of Spatiotemporal Changes in Great Basin Groundwater Dependent Vegetation Vigor* (Master's thesis, University of Nevada, Reno).

Sommer, B., Boggs, D.A., Boggs, G.S., van Dijk, A. and Froend, R., 2016. Spatio-temporal patterns of evapotranspiration from groundwater-dependent vegetation. *Ecohydrology*, *9*(8), pp.1620-1629.

Song, X., Duan, Z. and Jiang, X., 2012. Comparison of artificial neural networks and support vector machine classifiers for land cover classification in Northern China using a SPOT-5 HRG image. *International Journal of Remote Sensing*, *33*(10), pp.3301-3320.

Taylor, R. and Tindimugaya, C., 2012. The impacts of climate change and rapid development on weathered crystalline rock aquifer systems in the humid tropics of sub-Saharan Africa: Evidence from south-western Uganda. *Climate change effects on groundwater resources: a global synthesis of findings and recommendations*, pp.17-32.

Thamaga, K.H. and Dube, T., 2018. Remote sensing of invasive water hyacinth (Eichhornia crassipes): A review on applications and challenges. *Remote Sensing Applications: Society and Environment*, *10*, pp.36-46.

Thamaga, K.H., Dube, T. and Shoko, C., 2022. Advances in satellite remote sensing of the wetland ecosystems in Sub-Saharan Africa. *Geocarto International*, *37*(20), pp.5891-5913.

Theron, E.J., van Aardt, A.C. and Du Preez, P.J., 2020. Vegetation distribution along a granite catena, southern Kruger National Park, South Africa. *Koedoe: African Protected Area Conservation and Science*, *62*(2), pp.1-11.

Tsitsi, B., 2016. Remote sensing of aboveground forest biomass: A review. *Tropical Ecology*, *57*(2), pp.125-132.

United Nations. 2017. The sustainable development goal report 2017 [WWW Document]. https://sustainabledevelopment.un.org/aboutmajorgroups.html.https://unstats.un.org/s

dgs/files/report/2017/TheSustainable DevelopmentGoalsReport2017.pdf. (accessed 2020 January 26).

Vaux, H., 2011. Groundwater under stress: the importance of management. *Environmental Earth Sciences*, *62*, pp.19-23.

Vizzari, M., 2022. PlanetScope, Sentinel-2, and Sentinel-1 data integration for object-based land cover classification in Google Earth Engine. *Remote Sensing*, *14*(11), p.2628.

Wada, Y., Van Beek, L.P., Van Kempen, C.M., Reckman, J.W., Vasak, S. and Bierkens, M.F., 2010. Global depletion of groundwater resources. *Geophysical research letters*, *37*(20).

Walter, H., 1973. *Vegetation of the earth in relation to climate and the eco-physiological conditions* (p. 237pp).

Wang, Q., Dong, S., Wang, H., Yang, J., Zhao, C., Dong, X. and Wang, T., 2020. Effects of groundwater table decline on vegetation transpiration in an arid mining area: a case study of the Yushen mining area, Shaanxi Province, China. *Mine Water and the Environment*, *39*(4), pp.839-850.

Wattendorf, P., Niederberger, J., Ehrmann, O. and Konold, W., 2010. Consequences of climate change on the water balance of fen peatlands in Baden-Wuerttemberg. *Hydrologie und Wasserbewirtschaftung*, *54*(5), pp.293-303.

Weih, R.C. and Riggan, N.D., 2010. Object-based classification vs. pixel-based classification: Comparative importance of multi-resolution imagery. *The International Archives of the Photogrammetry, Remote Sensing and Spatial Information Sciences*, *38*(4), p.C7.

Werstak, C.E., Housman, I., Maus, P., Fisk, H., Gurrieri, J., Carlson, C.P., Johnston, B.C., Stratton, B. and Hurja, J.C., 2012. Groundwater-dependent ecosystem inventory using remote sensing. *United States Department of Agriculture: Washington, DC, USA*.

Wessels, K.J., Pretorius, D.J. and Prince, S.D., 2008. *Reality of rangeland degradation mapping with remote sensing: the South African experienc*e. 14th Australasian Remote Sensing and Photogrammetry Conference, Darwin, Australia, 29 September - 3 October 2008, pp 7.

Williams, S., 2018. Perceptions of wetland ecosystem services in a region of climatic variability.

Wu, Y., Liu, T., Paredes, P., Duan, L. and Pereira, L.S., 2015. Water use by a groundwater dependent maize in a semi-arid region of Inner Mongolia: Evapotranspiration partitioning and capillary rise. *Agricultural Water Management*, *152*, pp.222-232.

Xia, P., Yin, S. and Jiang, J., 2012. Pinus aiwanensis tree-ring chronology and its response to climate. *Procedia Environmental Sciences*, *13*, pp.307-315.

Xu, W. and Su, X., 2019. Challenges and impacts of climate change and human activities on groundwater-dependent ecosystems in arid areas–A case study of the Nalenggele alluvial fan in NW China. *Journal of Hydrology*, *573*, pp.376-385.

Xu, Y. and Beekman, H.E. eds., 2003. *Groundwater recharge estimation in Southern Africa* (Vol. 64). Unesco.

Yates, M.J., Anthony Verboom, G., Rebelo, A.G. and Cramer, M.D., 2010. Ecophysiological significance of leaf size variation in Proteaceae from the Cape Floristic Region. *Functional Ecology*, *24*(3), pp.485-492.

Zhang, G., Su, X. and Singh, V.P., 2020. Modelling groundwater-dependent vegetation index using Entropy theory. *Ecological Modelling*, *416*, p.108916.

Zhang, K., Zhu, G., Ma, N., Chen, H. and Shang, S., 2022. Improvement of evapotranspiration simulation in a physically based ecohydrological model for the groundwater–soil–plant–atmosphere continuum. *Journal of Hydrology*, *613*, p.128440.

Zhao, X., Zhou, D. and Fang, J., 2012. Satellite-based studies on Large-Scale vegetation changes in China F. *Journal of integrative plant biology*, *54*(10), pp.713-728.

Zhaoming, W., 2020. A theoretical review of vegetation extraction methods based on UAV. In *IOP Conf Ser: Earth Environ Sci* (Vol. 546, p. 032019).

Zhou, B., Okin, G.S. and Zhang, J., 2020. Leveraging Google Earth Engine (GEE) and machine learning algorithms to incorporate in situ measurement from different times for rangelands monitoring. *Remote Sensing of Environment*, *236*, p.111521.

APPENDICES

Appendix A: List of Publications

1. Msesane, Q, Gxokwe S, and Dube T. 2025. Groundwater modelling applications coupled with Space-based observations in groundwater-dependent assessments: A review on applications, challenges, and future research directions. *Physics and Chemistry of the Earth, Parts A/B/C*. 103860.
2. Dalu T, Chiloane C, Dondofema F, Dube T, Leshaba EN, Masina FM and Munyai LF. 2024. Application of remote sensing techniques to monitor climate variability effects on groundwater-dependent ecosystems. In: Dube T, Shekede MD, Shoko C and Mushore T (eds) *Remote Sensing of Climate*. Elsevier, Cambridge.
3. Leshaba EN, Dube T, Dondofema F, Munyai LF, Keates C, Riddell E, Khosa D and Dalu T. 2025. Macroinvertebrate diversity within pan wetlands in relation to geological type and hydroperiod in a protected subtropical Austral national park. *Chemistry and Ecology*. DOI: 10.1080/02757540.2025.2470974.

Appendix B: List of Conference Presentations

1. Leshaba EN, Dube T, Dondofema F, Munyai LF, Dalu T. 2024. Macroinvertebrates diversity within pan wetlands in relation to geological type and hydroperiod in a protected subtropical national park. NRF-SAEON Graduate Student Network Indibano 2024. 16 September 2024. Gqeberha, South Africa

Appendix C: List of Graduated Students and Post-Doctoral Fellows

Name	Degree Programme	University	Year
Elsie Nomcebo Leshaba	MSc	University of Mpumalanga	2024
Qawekazi Msesane	MSc	University of the Western Cape	2024
Chantel Nthabiseng Chiloane	PhD	University of the Western Cape	2025
Dr Siyamthanda Gxokwe	Postdoctoral Fellow	University of the Western Cape	2024